

ENCAPSULATION OF METAL HYDRIDE NANOPARTICLES

GEOFF PARR

Ph.D. Thesis

2021



University of
Salford
MANCHESTER

Encapsulation of Metal Hydride Nanoparticles

Geoff Parr

School of Science, Engineering and Environment

University of Salford, Salford, UK

A thesis submitted in partial fulfilment of the requirements for the degree of

Doctor of Philosophy

March 2021

Contents

Contents	i
List of Figures	iii
List of Tables	x
List of Abbreviations, Symbols and Nomenclature	xi
Abstract	xvii
1 Introduction and Background	1
1.1 Nanoparticles and Applications.....	2
1.2 Characterisation of Nanoparticles	5
1.2.1 Introduction.....	5
1.2.2 Light Microscopy.....	6
1.2.3 Scanning Electron Microscopy	7
1.2.4 Transmission Electron Microscopy.....	8
1.2.5 Dynamic Light Scattering.....	9
1.2.6 Laser Diffraction	11
1.2.7 Coulter Counting.....	11
1.2.8 Acoustosizing.....	12
1.2.9 Resonant Mass Measurement.....	12
1.3 Motivation for the Current Research.....	14
1.3.1 Categories of Metal Hydrides.....	15
1.3.2 Characterisation of Lithium Amide Particles.....	16
1.4 Research Aims and Objectives.....	18
1.4.1 Research Aims	18
1.4.2 Research Objectives	18
1.5 Organisation of the Thesis.....	19
2 Microencapsulation.....	20

2.1	Microencapsulation	21
2.1.1	Introduction	21
2.1.2	Categories of microcapsules.....	21
2.1.3	Microcapsule Release Mechanisms.....	23
2.1.4	Microencapsulation Experimental Design.....	24
2.1.5	Gaps in the Literature	26
3	Materials and Methods	30
3.1	Materials and Methods	30
3.2	Methodology	31
3.3	Characterisation	53
3.3.1	Instrumentation used for Research.....	53
3.3.2	Light Microscopy.....	53
3.3.3	Scanning Electron Microscopy (SEM)	54
3.3.4	Energy Dispersive X-ray Analysis (EDX)	57
3.3.5	Transmission Electron Microscopy (TEM)	59
4	Results and Discussion	62
4.1	Encapsulation of Titanium Dioxide (TiO₂)	63
4.1.1	Encapsulation of TiO ₂ within Cellulose Acetate Phthalate (CAP).....	63
4.1.2	Encapsulation with Polysulfone (PSF)	73
4.2	Encapsulation of Lithium Carbonate (Li₂CO₃)	85
4.3	Encapsulation of Lithium Phosphate (Li₃PO₄)	122
4.4	Encapsulating Moisture-Sensitive Lithium Amide (LiNH₂)	137
4.5	Encapsulation of Sodium Borohydride (NaBH₄)	146
4.5.1	Characterisation of Sodium Borohydride Primary Particles.....	155
4.5.2	Preparation Chamber Facilitating Sample Manipulation Under Vacuum.....	163
4.6	An Investigation into the Stability of Sodium Borohydride (NaBH₄)	248
5	Conclusions and Future Work	255
	References	260

List of Figures

Figure 1.1 TEM micrograph of titanium dioxide nanoparticles ex Aldrich	3
Figure 1.2 TEM micrograph of lithium amide particles	17
Figure 2.1 Single-Core microcapsule	22
Figure 2.2 Coated Core-Shell microcapsule	22
Figure 2.3 Multiple-Core microcapsule	23
Figure 2.4 Matrix microcapsule	23
Figure 3.1 FEI Quanta FEG 250 Scanning Electron Microscope	54
Figure 3.2 Philips XL30 SFEG Scanning Electron Microscope	55
Figure 3.3 Atomic model of X-ray generation	58
Figure 3.4 JEOL JEM-2100 Transmission Electron Microscope	59
Figure 3.5 Cross-section of JEOL JEM-2100 column	60
Figure 4.1 SEM micrographs of 1:1 CAP-TiO ₂ microcapsules	64
Figure 4.2 TEM micrographs of TiO ₂ primary particles and 1:1 ratio microcapsule	65
Figure 4.3 Light micrograph of 2:1 ratio microcapsule	66
Figure 4.4 SEM micrographs of 2:1 ratio microcapsule	66
Figure 4.5 Light micrograph of 1:2 ratio microcapsules	67
Figure 4.6 SEM micrograph of 1:2 ratio microcapsule	67
Figure 4.7 SEM micrographs from fractured 1:2 microcapsules	68
Figure 4.8 TEM micrographs from a cross-section of 1:2 ratio microcapsules	69
Figure 4.9 Light micrograph of 1:2 ratio of CAP-TiO ₂ using THF	70
Figure 4.10 Light micrograph of 1:4 ratio using THF	71
Figure 4.11 Light micrograph of 1:4 ratio using acetonitrile	72
Figure 4.12 Image of 1:4 ratio using acetone	72
Figure 4.13 Light micrograph of 1:4 ratio microcapsules	73
Figure 4.14 Structure of cellulose acetate phthalate – Sigma-Aldrich	74
Figure 4.15 Structure of polysulfone - Sigma-Aldrich	74
Figure 4.16 Image of PSF polymer TiO ₂ precipitate	75
Figure 4.17 Image of liquid paraffin - PSF polymer	76
Figure 4.18 Image of PSF polymer microcapsules	78

Figure 4.19 SEM micrographs from cross-sectioned PSF-TiO ₂ microcapsule	78
Figure 4.20 SEM cross-sectioned PSF-TiO ₂ microcapsule - acetonitrile/hexane 70:30	79
Figure 4.21 SEM-cross-sectioned PSF-TiO ₂ microcapsule - acetonitrile/hexane 50:50	81
Figure 4.22 SEM surface micrographs- PSF-TiO ₂ microcapsule - acetonitrile/hexane 50:50	82
Figure 4.23 EDX spectrum overlay from areas 'A' and 'B'	83
Figure 4.24 SEM micrographs from cross-sectioned PSF-TiO ₂ microcapsule	84
Figure 4.25 SEM micrographs of surface PSF Li ₂ CO ₃ microcapsule - sample 1	86
Figure 4.26 SEM micrographs of cross-sectioned PSF Li ₂ CO ₃ microcapsule - sample 1	87
Figure 4.27 SEM micrographs of cross-sectioned PSF Li ₂ CO ₃ microcapsule - sample 2	88
Figure 4.28 SEM micrographs of cross-sectioned PSF Li ₂ CO ₃ microcapsule - sample 3	89
Figure 4.29 SEM micrographs of surface PSF Li ₂ CO ₃ microcapsule - sample 3	90
Figure 4.30 SEM micrographs of surface PSF Li ₂ CO ₃ microcapsule - sample 4	91
Figure 4.31 SEM micrographs of cross-sectioned PSF Li ₂ CO ₃ microcapsule - sample 4	91
Figure 4.32 SEM micrographs of surface PSF Li ₂ CO ₃ Microcapsule - sample 5	94
Figure 4.33 SEM micrographs of cross-sectioned PSF Li ₂ CO ₃ microcapsule - sample 5	94
Figure 4.34 Light micrograph of PSF-Li ₂ CO ₃ microcapsules - sample 6	95
Figure 4.35 SEM micrographs of surface PSF Li ₂ CO ₃ microcapsule - sample 7	96
Figure 4.36 SEM micrographs of cross-sectioned PSF Li ₂ CO ₃ microcapsule - sample 7	97
Figure 4.37 SEM micrographs of surface PSF Li ₂ CO ₃ microcapsule - sample 8	98
Figure 4.38 SEM micrographs of cross-sectioned PSF Li ₂ CO ₃ microcapsule - sample 8	98
Figure 4.39 SEM micrographs of surface PSF Li ₂ CO ₃ microcapsule - sample 9	99
Figure 4.40 SEM micrographs of cross-sectioned PSF Li ₂ CO ₃ microcapsule - sample 9	100
Figure 4.41 SEM micrographs of surface PSF Li ₂ CO ₃ microcapsule - sample 10	100
Figure 4.42 SEM micrograph of cross-sectioned PSF Li ₂ CO ₃ microcapsule - sample 10	101
Figure 4.43 SEM micrographs of surface PSF Li ₂ CO ₃ microcapsule - sample 11	102
Figure 4.44 SEM micrographs of cross-sectioned PSF Li ₂ CO ₃ microcapsule - sample 11	103
Figure 4.45 SEM micrographs of surface PSF Li ₂ CO ₃ microcapsule - sample 12	104
Figure 4.46 SEM micrographs of cross-sectioned PSF Li ₂ CO ₃ microcapsule - sample 12	104
Figure 4.47 SEM micrographs of surface PSF Li ₂ CO ₃ microcapsule - sample 13	105
Figure 4.48 SEM micrographs of cross-sectioned PSF Li ₂ CO ₃ microcapsule - sample 13	105
Figure 4.49 SEM micrographs of surface PSF Li ₂ CO ₃ microcapsule - sample 14	106
Figure 4.50 SEM micrographs of cross-sectioned PSF Li ₂ CO ₃ microcapsule - sample 14	106

Figure 4.51 SEM micrographs of surface PSF Li ₂ CO ₃ microcapsule - sample 15	107
Figure 4.52 SEM micrographs of cross-sectioned PSF Li ₂ CO ₃ microcapsule - sample 15	108
Figure 4.53 SEM micrographs of surface PSF Li ₂ CO ₃ microcapsule – sample 16	108
Figure 4.54 SEM cross-sectioned micrographs of PSF Li ₂ CO ₃ microcapsule – sample 16	109
Figure 4.55 SEM micrographs of lithium carbonate particles ex Sigma-Aldrich	110
Figure 4.56 Light micrograph of PSF Li ₂ CO ₃ microcapsules - sample 17	111
Figure 4.57 Light micrograph of PSF-Li ₂ CO ₃ microcapsule - sample 18	112
Figure 4.58 Light micrograph of PSF Li ₂ CO ₃ microcapsule - sample 19	113
Figure 4.59 Light micrograph of PSF Li ₂ CO ₃ microcapsule - sample 20	114
Figure 4.60 Light micrograph of PSF Li ₂ CO ₃ microcapsule - sample 21	115
Figure 4.61 Light micrograph of PSF Li ₂ CO ₃ microcapsule - sample 22	116
Figure 4.62 Light micrograph of PSF Li ₂ CO ₃ microcapsule - sample 23	117
Figure 4.63 Light micrograph of PSF Li ₂ CO ₃ microcapsule - sample 24	118
Figure 4.64 Light micrograph of PSF Li ₂ CO ₃ microcapsule - sample 25	118
Figure 4.65 Light micrograph of PSF Li ₂ CO ₃ microcapsules - sample 26	120
Figure 4.66 SEM micrograph of cross-sectioned PSF Li ₂ CO ₃ microcapsule - sample 26	120
Figure 4.67 Light micrograph of microcapsules from different solvent ratios	121
Figure 4.68 Light micrograph of PSF Li ₂ CO ₃ microcapsules - sample 27	122
Figure 4.69 Light micrograph of PSF Li ₃ PO ₄ microcapsules - sample 28	124
Figure 4.70 SEM micrographs of cross-sectioned PSF Li ₃ PO ₄ microcapsule - sample 28	124
Figure 4.71 EDX spectrum overlay from PSF polymer and Li ₃ PO ₄ particles - sample 28	125
Figure 4.72 Light micrograph of PSF Li ₃ PO ₄ microcapsules - sample 29	126
Figure 4.73 SEM micrographs of surface PSF Li ₃ PO ₄ microcapsule - sample 29	127
Figure 4.74 SEM micrographs of cross-sectioned PSF Li ₃ PO ₄ microcapsule - sample 29	127
Figure 4.75 EDX spectrum of surface particles - sample 29	128
Figure 4.76 Light micrograph of PSF Li ₃ PO ₄ microcapsules - sample 30	129
Figure 4.77 Light micrograph of PSF Li ₃ PO ₄ microcapsules - sample 31	130
Figure 4.78 Light micrograph of PSF Li ₃ PO ₄ microcapsules - sample 32	131
Figure 4.79 Light micrograph of PSF Li ₃ PO ₄ microcapsule - sample 33	132
Figure 4.80 SEM micrograph of cross-sectioned PSF Li ₃ PO ₄ microcapsule - sample 33	132
Figure 4.81 Light micrograph of PSF Li ₃ PO ₄ microcapsule - sample 34	134
Figure 4.82 SEM micrograph of cross-sectioned PSF Li ₃ PO ₄ microcapsule - sample 34	134

Figure 4.83 EDX spectra overlay PSF surface against Li_3PO_4 particles - sample 34	135
Figure 4.84 SEM micrograph of surface PSF Li_3PO_4 microcapsule - sample 35	136
Figure 4.85 SEM micrograph of cross-sectioned PSF Li_3PO_4 microcapsule - sample 35	137
Figure 4.86 Light micrograph of PSF LiNH_2 microcapsules - sample 36	139
Figure 4.87 SEM micrograph of cross-sectioned PSF LiNH_2 microcapsule - sample 36	139
Figure 4.88 EDX spectra overlay PSF polymer against LiNH_2 particles - sample 36	140
Figure 4.89 Light micrograph of PSF LiNH_2 microcapsule - sample 37	141
Figure 4.90 SEM micrograph of cross-sectioned PSF LiNH_2 microcapsule - sample 37	142
Figure 4.91 EDX-spectra overlay PSF polymer against LiNH_2 particles - sample 37	142
Figure 4.92 Light micrograph of PSF- LiNH_2 microcapsule - sample 38	143
Figure 4.93 SEM micrographs of PSF LiNH_2 microcapsules - sample 38	144
Figure 4.94 Light micrograph of PSF LiNH_2 microcapsule - sample 39	144
Figure 4.95 SEM micrographs of cross-sectioned PSF NaBH_4 microcapsule - sample 40	147
Figure 4.96 EDX spectra overlay PSF polymer against NaBH_4 particles - sample 40	147
Figure 4.97 Light micrograph of PSF NaBH_4 microcapsules - sample 41	148
Figure 4.98 Light micrograph of PSF NaBH_4 microcapsule - sample 42	149
Figure 4.99 Light micrograph of PSF NaBH_4 microcapsules - sample 43	150
Figure 4.100 Light micrograph of PSF NaBH_4 microcapsules - sample 44	151
Figure 4.101 Light micrograph of PSF NaBH_4 microcapsules - sample 45	152
Figure 4.102 Light micrograph of PSF NaBH_4 microcapsules - sample 46	152
Figure 4.103 SEM micrograph of cross-sectioned PSF NaBH_4 microcapsule - sample 46	153
Figure 4.104 EDX spectra overlay PSF polymer against NaBH_4 particles - sample 46	154
Figure 4.105 Light micrograph of PSF NaBH_4 microcapsules - sample 47	155
Figure 4.106 SEM micrographs of NaBH_4 particles ex Sigma-Aldrich	156
Figure 4.107 EDX Spectrum from NaBH_4 particles ex Sigma-Aldrich	156
Figure 4.108 SEM micrograph of NaBH_4 particles ex Acros Organics before grinding	157
Figure 4.109 SEM micrograph of NaBH_4 particles ex Acros Organics after grinding	158
Figure 4.110 EDX Spectrum from ground NaBH_4 particles ex Acros Organics	158
Figure 4.111 Light Micrograph of PSF NaBH_4 microcapsules - sample 48	159
Figure 4.112 Light micrograph of PSF NaBH_4 microcapsules - sample 49	160
Figure 4.113 Light micrograph of PSF NaBH_4 microcapsules - sample 50	161
Figure 4.114 Light micrograph of PSF NaBH_4 microcapsules - sample 51	162

Figure 4.115 Light micrograph of PSF NaBH ₄ microcapsules - sample 52	163
Figure 4.116 - Preparation Stage for direct manipulation of microcapsules	165
Figure 4.117 Light micrograph of a glued microcapsule onto a brass rivet - sample 46	166
Figure 4.118 SEM micrograph of cross-sectioned microcapsule - sample 46-Revisited	167
Figure 4.119 EDX spectra overlay of PSF/NaBH ₄ particle - sample 46-Revisited	168
Figure 4.120 SEM micrograph of internal area showing particles - sample 50-Revisited	169
Figure 4.121 EDX spectra overlay of PSF polymer/NaBH ₄ particle - sample 50-Revisited	170
Figure 4.122 Light micrograph of microcapsules glued onto a rivet using Loctite	171
Figure 4.123 SEM micrographs of internal area showing particles - sample 52-Revisited	172
Figure 4.124 EDX spectra overlay NaBH ₄ particle/PSF polymer - sample 52-Revisited	173
Figure 4.125 SEM micrograph of internal area showing particles - sample 52-Revisited	174
Figure 4.126 EDX spectra overlay NaBH ₄ particle/PSF polymer - sample 52-Revisited	174
Figure 4.127 SEM micrograph of internal area showing particles - sample 53	175
Figure 4.128 EDX spectra overlay NaBH ₄ particle/PSF polymer - sample 53	176
Figure 4.129 SEM micrograph of internal area showing particles - sample 53	177
Figure 4.130 EDX spectrum from particles shown in figure 4.129 - sample 53	177
Figure 4.131 SEM micrograph of internal area showing NaBH ₄ particles - sample 53	178
Figure 4.132 EDX spectrum from particles shown in figure 4.131 - sample 53	178
Figure 4.133 SEM micrograph of internal area - sample 55	181
Figure 4.134 SEM micrograph of internal area showing small particles - sample 55	181
Figure 4.135 EDX spectrum from particles shown in figure 4.134 - sample 55	182
Figure 4.136 SEM micrograph of internal area showing NaBH ₄ particles - sample 55	182
Figure 4.137 EDX spectra overlay NaBH ₄ particle/PSF polymer - sample 55	183
Figure 4.138 SEM micrograph of internal area - sample 57	184
Figure 4.139 SEM micrograph of internal area - sample 58	185
Figure 4.140 EDX spectrum from particle shown in figure 4.139 - sample 58	185
Figure 4.141 SEM micrograph of particle within the microcapsule - sample 58	186
Figure 4.142 EDX spectrum from particle shown in figure 4.141 - sample 58	186
Figure 4.143 SEM micrograph of particle within the microcapsule - sample 65	188
Figure 4.144 EDX spectrum from particle shown in figure 4.143 - sample 65	189
Figure 4.145 EDX spectrum from PSF polymer substrate - sample 65	189
Figure 4.146 SEM micrograph of surface particles on the microcapsule - sample 65	190

Figure 4.147 EDX spectra overlay from 3 separate particles figure 4.146 - sample 65	191
Figure 4.148 SEM micrograph of internal structure - sample 70	192
Figure 4.149 SEM micrograph of external structure - sample 70	193
Figure 4.150 EDX spectrum from particles shown in figure 4.149 - sample 70	193
Figure 4.151 EDX spectrum from polymer substrate shown in figure 4.149 - sample 70	194
Figure 4.152 SEM micrograph of internal structure - sample 62	195
Figure 4.153 EDX spectrum from particles shown in figure 4.152 - sample 62	196
Figure 4.154 EDX spectrum from polymer substrate figure 4.152 - sample 62	197
Figure 4.155 SEM micrograph of internal structure - sample 62	197
Figure 4.156 EDX spectrum from particles figure 4.155 - sample 62	198
Figure 4.157 SEM micrograph of internal structure - sample 63	199
Figure 4.158 EDX spectrum from particles figure 4.157 - sample 63	199
Figure 4.159 SEM micrograph of internal structure - sample 64	200
Figure 4.160 EDX spectrum from particles figure 4.159 - sample 64	201
Figure 4.161 SEM micrograph of internal structure - sample 66	202
Figure 4.162 EDX spectra overlay PSF polymer against particles figure 4.161 - sample 66	203
Figure 4.163 SEM micrograph of internal structure - sample 66	203
Figure 4.164 EDX spectrum from crystallites figure 4.163 - sample 66	204
Figure 4.165 EDX spectrum from polymer substrate figure 4.158 - sample 66	205
Figure 4.166 SEM micrograph of internal structure - sample 68	206
Figure 4.167 EDX spectrum from particles figure 4.166 - sample 68	206
Figure 4.168 EDX spectrum from polymer substrate figure 4.166 - sample 68	207
Figure 4.169 SEM micrograph of internal structure - sample 68	207
Figure 4.170 EDX spectrum from particles - sample 68	208
Figure 4.171 SEM micrograph of internal structure-XL30 - sample 68	209
Figure 4.172 EDX spectra overlay PSF polymer against NaBH ₄ particles - sample 68	209
Figure 4.173 SEM micrographs of particles from internal structure-XL30 - sample 68	210
Figure 4.174 EDX spectra overlay PSF polymer against NaBH ₄ particles - sample 68	211
Figure 4.175 SEM micrograph of particles from internal structure-XL30 - sample 69	212
Figure 4.176 EDX spectrum from particles - sample 69	213
Figure 4.177 SEM micrograph of particles from internal structure-XL30 - sample 69	213
Figure 4.178 EDX spectrum from particles figure 4.177 - sample 69	214

Figure 4.179 SEM micrograph of particles from internal structure - sample 73	215
Figure 4.180 EDX spectrum from particles figure 4.179 - sample 73	216
Figure 4.181 SEM micrograph of particles/phase from internal structure - sample 73	216
Figure 4.182 EDX spectrum from particles figure 4.181 - sample 73	217
Figure 4.183 SEM micrograph of particles from internal structure - sample 75	218
Figure 4.184 EDX spectrum from particles figure 4.183 - sample 75	219
Figure 4.185 EDX spectrum from polymer substrate near particles - sample 75	219
Figure 4.186 NMR spectrum obtained from THF solvent ex Fisher	220
Figure 4.187 SEM micrograph of particles from internal structure - sample 76	222
Figure 4.188 SEM micrograph of particles from internal structure - sample 76	223
Figure 4.189 EDX spectrum from particles figure 4.188 - sample 76	223
Figure 4.190 EDX spectrum from polymer substrate near particles - sample 76	224
Figure 4.191 SEM micrograph of particles from the outer surface - sample 77	225
Figure 4.192 EDX spectra overlay from surface particles - sample 77	226
Figure 4.193 SEM micrograph of molecular sieve particle - ex acetonitrile	226
Figure 4.194 EDX spectrum from molecular sieve particle - ex acetonitrile	227
Figure 4.195 SEM micrograph of particles from internal structure - sample 78	228
Figure 4.196 EDX spectrum from particles figure 4.195 - sample 78	228
Figure 4.197 EDX spectrum from polymer substrate near particles - sample 78	229
Figure 4.198 SEM micrograph of particles from internal structure - sample 80	231
Figure 4.199 EDX spectrum from particle figure 4.198 - sample 80	232
Figure 4.200 EDX spectrum from particle figure 4.194 - sample 80	232
Figure 4.201 SEM micrograph of particles from internal structure - sample 81	234
Figure 4.202 EDX spectrum from particle figure 4.197 - sample 81	234
Figure 4.203 EDX spectrum from polymer substrate near particles - sample 81	235
Figure 4.204 SEM micrograph of particles from internal structure - sample 82	236
Figure 4.205 EDX spectrum from large particle figure 4.204 - sample 82	236
Figure 4.206 EDX spectrum from polymer substrate near the particles - sample 82	237
Figure 4.207 EDX spectrum from small particle figure 4.200 - sample 82	238
Figure 4.208 SEM micrographs of surface particles - sample 83	239
Figure 4.209 EDX spectrum from surface of large particles figure 4.208 - sample 83	240
Figure 4.210 SEM micrograph of particles from internal structure - sample 84	241

Figure 4.211 EDX spectrum overlay from internal particle/ PSF figure 4.210 - sample 84	242
Figure 4.212 SEM micrograph of particles from internal structure - sample 84	242
Figure 4.213 EDX spectrum overlay from internal particle/ PSF figure 4.212 - sample 84	243
Figure 4.214 SEM micrographs of surface particles - sample 84	243
Figure 4.215 EDX spectrum from surface particles figure 4.214 - sample 84	244
Figure 4.216 SEM micrographs of surface particles - sample 85	246
Figure 4.217 EDX spectrum from surface particles figure 4.213 - sample 85	246
Figure 4.218 SEM micrographs of NaBH ₄ after grinding under nitrogen	248
Figure 4.219 EDX spectrum obtained from NaBH ₄ particles shown in figure 4.222	249
Figure 4.220 SEM micrographs of NaBH ₄ particles left overnight in air	249
Figure 4.221 EDX spectrum obtained from hexagonal particle shown in figure 4.224	250
Figure 4.222 NaBH ₄ particles uncoated - 8.27am	251
Figure 4.223 NaBH ₄ particles uncoated - 11.45am	251
Figure 4.224 NaBH ₄ particles uncoated at 3.45pm	252
Figure 4.225 EDX spectrum obtained from NaBH ₄ particle at 8.27am	253
Figure 4.226 EDX spectrum obtained from NaBH ₄ particle at 3.45pm	254

List of Tables

Table 1.1: Current methods available for particle size analysis	6
Table 3.1 Summary of Experimental Methods Used	31
Table 3.2 Structure of Materials and Solvents Utilised - Sigma-Aldrich	51
Table 4.1 NMR results from THF analysis	221

List of Abbreviations, Symbols and Nomenclature

Abbreviations

LM	Light Microscopy
SEM	Scanning Electron Microscopy
TEM	Transmission Electron Microscopy
EDX	Energy Dispersive X-ray Analysis
XRD	X-ray Diffraction
VP	Variable Pressure
SE	Secondary Electron Detection
BSE	Back Scattered Electron Detection
LFD	Large Field Detection
DLS	Dynamic Light Scattering
ESA	Electrokinetic Sonic Amplitude
RMM	Resonant Mass Measurement
MEMS	Microelectromechanical Systems
PSS	Polystyrene Sulfonate
PAH	Poly(allylamine hydrochloride)
CAP	Cellulose Acetate Phthalate
PSF	Polysulfone
ESE	Emulsion Solvent Evaporation
ENSA	Emulsion Non-Solvent Addition
MESE	Modified Emulsion Solvent Evaporation
THF	Tetrahydrofuran
DMF	Dimethylformamide

NMP	1-Methyl-2-Pyrrolidone
ACN	Acetonitrile
DMSO	Dimethyl sulfoxide
DCM	Dichloromethane
NMR	Nuclear Magnetic Resonance
PDMS	Polydimethylsiloxane
HPLC	High Performance Liquid Chromatography

Symbols

μm	Micrometre
nm	Nanometre
Pa.s	Pascal-second
Wh/L	Watt-hour per litre
Wh/Kg	Watt-hour per kilogram
M+	Metal cation
H-	Hydride anion
ml/min	Millilitre per minute
Rpm	Revolutions per minute
ml	millilitre
g	Gram
mbar	Millibar
mm	Millimetre
kV	Kilovolt

Nomenclature

Ti	Titanium
O	Oxygen
N	Nitrogen
C	Carbon
P	Phosphorus
S	Sulfur
H	Hydrogen
B	Boron
Pt	Platinum
Pd	Palladium
Li	Lithium
Si	Silicon
Mg	Magnesium
Na	Sodium
K	Potassium
Al	Aluminium
Cl	Chlorine

Acknowledgements

This PhD would not have come together if it were not for the support and guidance I have received from both my supervisors, Dr Dan Bull and Professor Neil Boag. I am extremely grateful to both for the help they have given me throughout the term of this PhD.

I am also thankful to Professor Ian Morrison, Dr Richard Pilkington, and Dr Stuart Astin for reading and listening to my internal assessments and to Professor Nigel Mellors for recommending I complete a PhD.

In addition, I am indebted to Salford University for allowing me to complete this PhD as a part-time project during my employment.

Many thanks are also extended to my good friends and colleagues Kirit Amin for his NMR spectroscopy analysis and support, together with Joe McMahon for his encouragement throughout my PhD.

Finally, I would like to express my sincere gratitude to my wife, Lindsay, for her encouragement and help throughout this PhD. I am forever thankful for her patience in helping to proof-read this thesis. Also, to my two boys Callum and Liam – I could never have completed this PhD without their understanding about the many hours I had to devote to this project rather than spending time with them.

Many thanks to all of you and those I might have forgotten.

Declaration

This thesis has been written by Geoff Parr (the author) and contains only experimental work that has been done by the author, with necessary assistance of Prof Neil Boag and Dr Dan Bull.

All data has been directly collected by the author.

I, Geoff Parr, confirm that the work presented in this thesis is my own.

Abstract

Hydrogen is likely to play a significant role in future low and zero carbon energy infrastructures. Alkali metal hydride nanoparticles could provide a route to an efficient lightweight hydrogen storage technology for automotive applications. However, a particular issue with alkali metal hydrides is their sensitivity to air/moisture, making their characterisation extremely difficult. In addition to unwanted changes to the materials on contact with air/moisture, reaction products that can be released such as hydroxides and ammonia, could cause significant damage to expensive analytical instrumentation. To address these issues, a method for encapsulating metal hydride nanoparticles in spherical polysulfone microcapsules has been developed, offering an environment for both safe storage and handling of moisture-sensitive nanoparticles.

A methodology for producing spherical polysulfone microcapsules with a typical diameter between 1-2mm is presented. Microcapsules are produced with a solid outer wall structure, preventing moisture permeation, but being soft enough to allow easy access to the internal structure for characterisation of the nanoparticle morphology. In addition to the design of the microcapsules, a robust preparation technique to allow the study of their internal structure, without exposing the nanoparticles to moisture, using high-resolution Scanning Electron Microscopy (SEM) is defined. The established technique allows the microcapsules to be cross-sectioned under vacuum with an additional option of purging the reactive particles with argon gas. In order to examine the encapsulated nanoparticles, Energy Dispersive X-ray Analysis (EDX) was used, for which lithium-containing hydrides are not suited. Therefore, the main focus of the research presented involves the encapsulation of sodium borohydride (NaBH_4) nanoparticles. In addition, this technology could be considered for the storage of other air/moisture sensitive materials.

1 Introduction and Background

Chapter Contents

1.1	Nanoparticles and Applications	2
1.2	Characterisation of Nanoparticles	5
1.2.1	Introduction.....	5
1.2.2	Light Microscopy.....	6
1.2.3	Scanning Electron Microscopy	7
1.2.4	Transmission Electron Microscopy.....	8
1.2.5	Dynamic Light Scattering.....	9
1.2.6	Laser Diffraction	11
1.2.7	Coulter Counting.....	11
1.2.8	Acoustosizing.....	12
1.2.9	Resonant Mass Measurement.....	12
1.3	Motivation for the Current Research	14
1.3.1	Categories of Metal Hydrides.....	15
1.3.2	Characterisation of Lithium Amide Particles.....	16
1.4	Research Aims and Objectives	18
1.4.1	Research Aims	18
1.4.2	Research Objectives	18
1.5	Organisation of the Thesis	19

1.1 Nanoparticles and Applications

The simple definition of a 'nanoparticle' is a particle with a size range between 1 to 100 nanometres (nm). Standard authorities, ISO and ASTM, have conflicting views about the definition of a nanoparticle based on the number of dimensions required to define one. Given that particles are 3 dimensional, ISO specifies that an object with one or more external dimensions in the nanoscale can be classified as a nanoparticle. However, ASTM cite that a particle is required to have two or three dimensions greater than 1nm and less than 100nm in size to be categorised as a nanoparticle.

Nanoparticles have a larger surface area when compared with coarser particles of the same volume. This has a significant effect on the properties of the material. As many chemical reactions occur at the surface, nanoparticles can offer improved reaction kinetics.

Nanoparticles are used in numerous applications and are present in various commercial products. Some of the major industrial sectors that make use of nanoparticles are petroleum, cosmetics, food, textiles, pharmaceutical, renewable energy, printing, and colourants.

An example of a versatile, well-known nanomaterial that has been used since the 20th century is titanium dioxide (TiO₂). The bright white nanoparticles of TiO₂ were discovered in 1821. In 1916, the Titanium Pigment Corporation in America and the Titan Co. AS, of Norway, started commercial production of the white pigment for industrial applications. The pigment was later formulated into a white oil in 1921 in America, making it suitable to be used as a white paint. Leading paint manufactures still use titanium dioxide nanoparticles in many commercial products as a bright white pigment (Douma, 2021).

Using high resolution Transmission Electron Microscopy (TEM), the shape and size of the primary particles can be studied. The example given in Figure 1.1 represents a TEM micrograph obtained from small primary particles of titanium dioxide ex Aldrich. The micrograph clearly demonstrates that the morphology of the particles exists as a

combination of lath- and irregular-shaped nanoparticles with a particle size range below 100nm.

The TEM micrograph was obtained using the JEOL JEM-2100 Transmission Electron Microscope. The microscope settings utilised an accelerating voltage of 200kV and system magnification of 12,000x.

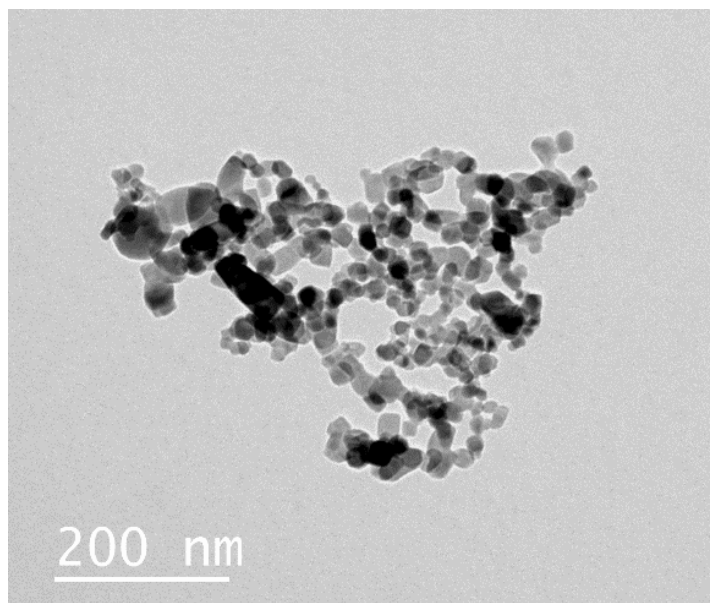


Figure 1.1 TEM micrograph of titanium dioxide nanoparticles ex Aldrich

Titanium dioxide nanoparticles are also renowned for the ability to absorb harmful ultraviolet light. This property makes the nanoparticles perfect in the cosmetics industry for formulating commercial sunscreens (Dréno et al., 2019). As the particles are extremely small, typically less than 100nm, they produce an invisible protective barrier from harmful UV light on the surface of the skin.

Titanium dioxide nanoparticles are used in the food industry for many commercial products as a whitening agent, and are referred to as E171 on the food packaging label. E171 is readily used to whiten toothpastes or improve the look of food products such as icing and chewing gum - achieving a uniform, bright white colouration. Also due to the UV-absorbing properties of these nanoparticles, they are used in food packaging materials to increase the shelf-life of consumer products.

The use of E171 is a controversial issue, as food science experts are very concerned about the long-term health issues these nanoparticles could have on the body (Blaznik et al., 2021). The primary particles are small enough to be trapped in skin pores and within the stomach lining. Some European countries such as France are considering banning the use of E171 in all food products (Askew, 2021).

1.2 Characterisation of Nanoparticles

1.2.1 Introduction

This is a brief overview to cover some of the analytical instrumentation available today that would allow particle size information to be obtained from nanoparticles. Specific references are made towards the characterisation of moisture-sensitive particles.

Many different methodologies are commercially available, allowing information relating to the particle size of materials to be obtained. However, each individual technique has its issues concerning sample preparation and interpretation of the data. This review outlines the different systems available and explores their viability when working with moisture-sensitive materials.

To determine the particle size of small, finely divided primary particles, it is worth considering the different technologies available. If all particles were spheres, then their primary particle size would simply be defined by the diameter. If the particles were cubical, then the measurement of the length along one edge would be satisfactory to represent the primary particle size. This type of measurement is appropriate when the particle shape is uniform or exists as a regular shape (as appropriate dimensions can be chosen). However, if a particle shape is non-uniform, then particle size can only be thought of as a general definition.

In commercial industrial sectors, solid materials such as pharmaceutical excipients, food grains and ceramics usually exist at some point as a powder or granular form. These particles would be present in many different shapes and sizes. To define the average particle size, many primary particles would require measurements to achieve credible data.

When measuring primary particles, the data generated can be subjective, as it is often difficult to differentiate between one or many particles that can be present as aggregates.

Is the true definition of particle size the individual primary particle or the non-dispersible aggregate?

Many particle size measurement techniques define the size of a particle as an equivalent spherical diameter. This allows data to represent non-uniform particle morphologies. The equivalent spherical diameter assigned to an irregular-shaped particle has the same diameter of a sphere behaving identically when both are exposed to that same process (Washington, 1992).

Table 1.1 represents a general summary of the current methods available today, with the corresponding range of particle size measurements.

Table 1.1: Current methods available for particle size analysis

Method	Size Range
Light Microscopy (1.2.2)	0.2µm – 30mm
Scanning Electron Microscopy (1.2.3)	1nm – 10mm
Transmission Electron Microscopy (1.2.4)	0.1nm - 50µm
Dynamic Light Scattering (1.2.5)	1nm – 10µm
Laser Diffraction (1.2.6)	10nm - 3.5mm
Coulter Counting (1.2.7)	0.4µm - 1600µm
Acoustosizing (1.2.8)	20nm - 10µm
Resonant Mass Measurement (1.2.9)	50nm - 5µm

1.2.2 Light Microscopy

Light Microscopy is a very good method for quickly investigating particle morphology. As a technique, it allows the user to instantly look at the sample with minimum preparation. It benefits from visualisation of the particles and image capture for storage of data, allowing accurate size measurements. Due to the visual aspects, it is an excellent technique for the

study of particle shape and size. However, for the characterisation of nanoparticles, light microscopy is limited in its ability to resolve fine detail. The best achievable resolving range is approximately $0.2\mu\text{m}$ because of the wavelength of the white light source (Sanderson, 2019).

Light microscopy could be a very useful technique for the study of larger air/moisture-sensitive particles existing above $1\mu\text{m}$. Preparation of the sample would benefit from the use of a hydrophobic, non-protic liquid. An example would be the use of liquid paraffin oil to encase the particles, reducing any exposure to moisture from air. The liquid paraffin would provide a vehicle into which the particles could be dispersed, thereby reducing any clusters. Securing the particles between a glass slide and cover glass would help prevent exposure to air.

1.2.3 Scanning Electron Microscopy

Scanning Electron Microscopy (SEM) is an improved technique over Light Microscopy for obtaining high resolution images of fine nanoparticles (Goldstein et al., 1992).

. It benefits from the use of an electron beam to illuminate the particles, significantly improving the resolving capability of the microscope (Nanakoudis, 2019).

The sample chamber in a traditional SEM is held under high vacuum in the order of 4.0×10^{-7} Torr. The high vacuum restricts the use of oils as previously outlined in the light microscopy section to help stabilise air/moisture-sensitive materials. However, once the sample is held under high vacuum within the microscope, it is essentially free from exposure to moisture from the atmosphere, providing a more stable environment for the analysis of air/moisture-sensitive materials.

Preparation of metal hydrides for SEM analysis is a major problem. Moisture-sensitive materials are affected by electron beam charging issues as they tend to be non-conductive. This build-up of electrostatic charge at the surface of the sample hinders the imaging process. To overcome this issue, one option is to deposit several nanometres of a suitable

metal such as platinum onto the surface of the particles. For best results, this is achieved using a sputter coating device, rather than evaporation. This process creates an added sequence, exposing the sample to moisture from the atmosphere.

More recent improvements in Scanning Electron Microscopy have led to the development of variable pressure microscopes (VP-SEM). These microscopes offer the user the capability to adjust the internal pressure in the sample chamber. The chamber pressure is typically adjusted using water vapour, but the microscope can operate using an external inert gas supply such as nitrogen. Using VP-SEM could help inhibit any degradation of air/moisture-sensitive materials, as the sample can be continuously purged with an inert gas. However, when operating the microscope in VP mode, it is not possible to utilise high spatial resolution secondary electron detection (SE). Alternative detection systems such as Back Scattered Electron detection (BSED) or Large Field Detection (LFD) are available, but these restrict the resolution capability of the microscope. The preferred detection mode when working with air/moisture-sensitive nanoparticles would be SE, as this offers outstanding spatial resolution of the small particles.

The work presented in this thesis is a unique methodology for the study of moisture-sensitive materials. This novel approach enables air/moisture sensitive materials to be safely transferred and prepared for high-resolution SEM studies, minimising exposure to moisture.

1.2.4 Transmission Electron Microscopy

Transmission Electron Microscopy (TEM) utilises a completely different method of electron beam interaction with the sample. The sample is located in the base of the objective lens and in the path of the electrons, which then pass through the particles. Due to this, it is essential that the thickness of the sample is maintained below several hundred nanometres. It is imperative that the preparation method generates well-dispersed dry particles onto the surface of a carbon TEM support grid.

The advantage of using TEM for the study of small nanoparticles is its ability to generate high spatial resolution images of the primary particles. Unlike with the SEM, it is not possible to purge the particles with an inert gas. However, once the sample is held within the column of the microscope, it is thought that the high vacuum will keep air/moisture-sensitive particles stable.

Preparation, as with the SEM, can be difficult when working with moisture-sensitive materials. Techniques involving the use of non-protic solvents could help generate a dispersion of nanoparticles.

The standard method for preparing a dispersion for TEM analysis is to allow a droplet of the sample to dry down onto a carbon-based TEM grid. When working with moisture-sensitive samples, this procedure could be done within an inert gas environment but would be extremely difficult. Transferring the prepared TEM grid to the microscope would be problematic as even if this procedure were done quickly, it still allows some exposure of the particles to moisture from the air. This is the same issue as discussed previously with the SEM. Transferring particles from one device to another could be enough for the particles to react.

1.2.5 Dynamic Light Scattering

Dynamic light scattering (DLS) is sometimes referred to as Photon Correlation Spectroscopy or Quasi-Elastic Light Scattering (Malvernpanalytical, 2021).

DLS is a well-established technique for measuring the size distribution of molecules and particles typically in the submicron region down to 1nm.

It is an extremely useful technique for obtaining size information from direct measurement of particles, emulsions, or molecules, which have been dispersed in a liquid. The basic principle of DLS is based on the scattering of laser light at different intensities by the Brownian motion of particles or molecules in suspension. The difference in intensity

measurements is a direct relationship to the speed of particle motion. Using the Stokes-Einstein relationship, it is possible to obtain values for particle size.

In theory, the larger the particle, the slower the Brownian motion. Smaller particles move more rapidly and further due to the solvent molecules. The DLS technique requires knowledge of some parameters such as viscosity, refractive index, and temperature of the cell. During measurements, the temperature of the sample is required to be constant to minimise potential convection currents that would cause non-random movements influencing the true size measurement.

DLS would be an extremely interesting technique for the characterisation of moisture-sensitive samples. If the particles could be dispersed into an inert solvent, then in principle this would be a very good technique to obtain size information only. This would only work if the relative details could be obtained to help satisfy the Stokes-Einstein equation. The sample could be prepared under an inert gas and, once dispersed into a suitable solvent, the particles should be stable within the sealed glass sample holder - allowing suitable measurements to take place.

The upper size limit can be an issue with this technique; therefore, it would be essential to minimise any aggregation of the particles before analysis. If the dispersion had many large particles and/or aggregates, then this would fill the number of particles in the scattering volume and mask the number of smaller particles being measured.

Sample preparation would very much be a development process based on the size and type of nanoparticles being measured. It is essential to optimise the sample concentration, to prevent poor light scattering from dilute samples and multiple scattering from concentrated samples.

1.2.6 Laser Diffraction

Laser diffraction is a widely used particle-sizing technique for materials ranging from 10nm to several millimetres in size (Horiba, 2021).

This technique generates particle size distributions by measuring the angular variation in intensity of light scattered as a laser beam passes through a dispersion of small particles (Malvern, 2021). It uses the Mie theory of light scattering to calculate the particle size distribution. The particle size is reported as a volume equivalent sphere diameter.

In order to satisfy the Mie theory, information such as refractive index of the sample being measured, together with the refractive index of the dispersant, is required.

A more simplified approach would be to generate size data using the Fraunhofer approximation. This does not require any knowledge of the refractive index properties of the sample or dispersant. The Fraunhofer methodology can provide good data from large particles only. It does not generate good data for transparent materials or particles existing below 50 μm .

The Fraunhofer technique would not be suitable for nanoparticles.

1.2.7 Coulter Counting

Coulter counting is a non-optical method for counting and sizing particles based on a technique that uses electrical impedance to measure the volume of particles as they individually pass through an aperture of defined size. Particle size measurements can be obtained in the range from 0.4 μm up to 1600 μm in diameter (Beckman, 2021).

The principle of the technique requires the sample to be dispersed within a dilute conducting liquid, and electrodes are introduced on both sides of the aperture. As particles are pulled through an aperture, they displace a volume of conductive liquid equivalent to their size. This generates measurable pulses which can be analysed. The Coulter counting

technique is different from light scattering techniques as it can also provide additional information such as sample concentration.

1.2.8 Acoustosizing

Acoustosizing is a technique that can measure particle size together with zeta potential based on the use of Electrokinetic Sonic Amplitude (ESA), (Delgado et al., 2007).

This is a non-optical technique which uses an oscillating electric field to produce acoustic compression waves. The sound waves force the particles in suspension to move at the frequency of excitation. The dynamic mobility can be expressed as a function of particle size and zeta potential.

The technique can generate size information for particles existing between 20nm to 10 μ m. It can measure particle size distributions and zeta potential in both aqueous and non-aqueous suspensions. This would be an interesting technique to evaluate for moisture-sensitive materials as it allows the use of a non-aqueous medium. To minimise air/moisture exposure, it would be good practice to minimise the sample volume. This technique allows the user to work with a small sample volume such as 20ml and concentrations down to 1%.

One slight issue that could affect the use of non-aqueous solvents and/or light oils is the maximum allowed viscosity of 0.5 Pa·s.

1.2.9 Resonant Mass Measurement

Resonant Mass Measurement (RMM) delivers true particle size distributions based on the floating mass of particles that pass through a resonating flow path. As well as mass and size distributions, the technique can also distinguish between differences in the type of particle morphology (Newey-Keane, 2021)

The principle of RMM is that the particles are drawn in their suspensions through MEMS (Microelectromechanical Systems). The presence of a particle in the sensor changes the total mass and shifts the sensor resonant frequency. The shifts are measured as each individual particle passes through the sensor, and particle mass is obtained with a resolution of 1 femtogram.

From these mass measurements, the corresponding size distributions are derived by translating the mass of each particle to equivalent circular diameter using the density of the particles measured.

The practical size range depends on the density of the analysed particles and is approximately 50nm to 5 μ m. This would be a useful technique if it allowed the use of non-aqueous and/or light oils for the dispersant.

Technology, in the form of the instrumentation discussed above, is available that could be suitable to support the characterisation of moisture-sensitive nanoparticles. It would be interesting to compare data generated from visual techniques, such as microscopy, directly with some of the alternative technologies outlined. Microscopy has many advantages as it offers the user direct visualisation of the particles. This is extremely useful for characterisation, as the micrographs clearly show particle shape and size, together with any aggregation. With many of the alternative techniques, it is not possible to view the primary particles, making it difficult to comment on the sample morphology. Any aggregation in a sample would only be represented as a single particle due to limitations in the modes of detection. Alternative techniques, such as DLS, can offer faster data acquisition times and may generate good particle size data, but could be a difficult technique to develop for moisture-sensitive materials.

1.3 Motivation for the Current Research

Hydrogen is likely to play a significant role in future low and zero carbon energy infrastructures (Childs, 2020). Key to facilitating this are efficient storage technologies. In terms of transportation, a high energy density both volumetrically (Wh/L) and gravimetrically (Wh/kg) is required. Transition metal hydrides (Jacobsen, 2008) offer high volumetric density, but have too low a gravimetric density. Alkali metal hydrides and other complex hydrides (Orimo et al., 2007) formed from low mass elements could provide a solution. However, they are typically sensitive to air/moisture (Keller & Klebanoff, 2012).

These metal hydrides can be extremely useful compounds for the storage and controlled release of flammable hydrogen gas (Gislon et al., 2009). This could be an effective means for generating hydrogen for a fuel cell (Kwon et al., 2019), (Fernandes et al., 2010). Hydrogen fuel cells combine hydrogen and oxygen to produce electricity. Fuel cells offer a means of generating electricity but require a continuous supply of hydrogen (Galli et al., 2010).

If the particle size of the alkali metal hydride were reduced, this would increase the specific surface area thus improving the reaction kinetics (Yang et al., 2022).

Metal hydrides exist as compounds that can contain either a single or several metal cations (M⁺) together with a single or several hydride anions (H⁻). The metal cation is often covalently bonded to the hydrogen anion to form the metal hydride.

Some examples of familiar metal hydrides contain the metal cation: lithium, sodium, or potassium, together with elements that include boron and calcium. An example is sodium borohydride (NaBH₄). Other metal hydrides may incorporate lithium as the cation, such as lithium aluminium hydride (LiAlH₄) and lithium borohydride (LiBH₄), (Schueth et al., 2005).

1.3.1 Categories of Metal Hydrides

Binary Metal Hydride

The most common example of a metal hydride is a metal cation bonded to the hydride anion, labelled as a simple binary metal hydride (Bourgeois et al., 2017). A typical example of a binary metal hydride is lithium hydride (LiH), which is a colourless solid. This hydride is generally insoluble but is known to react with protic solvents. It reacts violently with water to form H₂ gas and the corresponding hydroxide (Leckey et al., 1996).

Ternary Metal Hydride

A ternary metal hydride contains either an alkali metal or alkaline earth metal and a transition metal (Guegan, 2010). A typical example of a ternary metal hydride is sodium borohydride (NaBH₄). This can be effective as a reducing agent in chemical reactions (Ward & Rhee, 1989). It can be used to reduce aldehydes and ketones to alcohols. Another example of a ternary metal hydride is lithium aluminium hydride LiAlH₄. This metal hydride acts as a more powerful reducing agent than NaBH₄ as it can reduce carboxylic acids and esters to alcohols (Wang et al., 2021). The Al-H bond is weaker than the B-H bond, making the NaBH₄ more stable and LiAlH₄ more reactive.

Co-ordination Complexes

These transition metal hydrides are different as they contain other ligands, forming a complex with a single bond between the transition metal and the hydride anion.

A well-known example of a co-ordination complex is cobalt tetracarbonyl hydride (HCo(CO)₄), (Veillard et al., 1990).

This organometallic compound exists as a yellow liquid and forms a colourless, toxic vapour. This co-ordination complex was used in industry as a catalyst for the conversion of alkenes to aldehydes.

Cluster Hydrides

Hydride clusters are complex, containing both transition metals and rare earth metals (Shima et al., 2011). Many clusters have a single bond between the metal and the hydride anion, but other examples demonstrate the hydride ligand to bridge between the two metals. Metal hydride clusters are very difficult to generate and characterise. Because of this, these heterometallic hydrides have not been studied to a great degree.

An example of a cluster hydride is decacarbonyldihydridotriosmium ($\text{H}_2\text{Os}_3(\text{CO})_{10}$).

1.3.2 Characterisation of Lithium Amide Particles

Researchers at the University of Salford synthesised pure lithium amide nanoparticles by treating ammonia gas with alkyl lithium reagents affording the desired product as a free flowing very fine powder, (Baldissin et al., 2013). The characterisation of the primary particles of lithium amide was undertaken by the thesis author using a Philips 410 Transmission Electron Microscope (TEM).

Due to the extreme reactivity of the particles, the results generated required rapid analysis. This was essential to overcome the effects of lithium amide reacting with moisture from the air and generating corrosive lithium hydroxide and ammonia.

To minimise any exposure to moisture, the sample preparation involved dusting the particles onto a holey, carbon-coated copper square mesh TEM support grid in a glove box under argon gas. The sample held under argon was rapidly introduced to the goniometer stage of the microscope and quickly pumped to high vacuum. There was optimism that the high vacuum of the TEM would prevent moisture reaching the nanoparticles, thus retarding any unwanted hydrolysis. One concern was that any vigorous reactions taking place within the microscope column could damage the instrument, so only a very fine dusting of material was used for analysis on a very old microscope. The sample was removed immediately after the TEM micrographs were obtained. The preparation technique was extremely basic and not the usual protocol followed for sample preparation for TEM analysis.

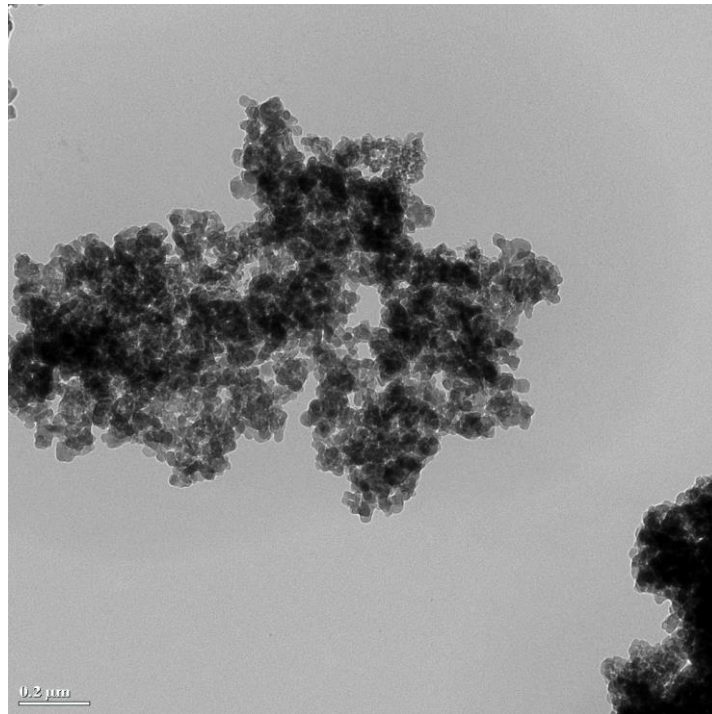


Figure 1.2 TEM micrograph of lithium amide particles

The resulting TEM micrograph shown in figure 1.2 shows many small primary particles tightly aggregated together, thought to be lithium amide. It is possible to see that individual primary particles exhibit an irregular shape and particle size below 100nm. The aggregation is thought to be the result of the limited sample preparation. The preparation simply involved dusting the particles onto a suitable support grid. Usually for TEM analysis, small nanoparticles are dispersed into a suitable liquid vehicle to allow sonication for separation of the primary particles.

For materials subject to excessive aggregation, it is often preferential to examine the particles using high resolution SEM. As SEM is a surface-imaging technique, it can generate good quality micrographs from clusters of primary particles. However, it was not possible to utilise SEM as the complex sample preparation would have exposed the sample to moisture from the atmosphere, thus promoting a chemical change.

1.4 Research Aims and Objectives

1.4.1 Research Aims

This research will investigate the development of a novel procedure for the controlled study of reactive metal hydride primary particles. The methodology is based on designing a suitable system which encapsulates moisture-sensitive particles into soft polymer microcapsules. This new approach will allow the study of moisture-sensitive reactive materials to be examined using high-resolution Scanning Electron Microscopy (Goldstein et al., 1992).

This research could have additional interests as the generated microcapsules may lead onto an effective vehicle for both controlled release and storage of metal hydrides (Fakioğlu et al, 2004), (Pinto, et al, 2006). Potentially, the microcapsules could provide a means for producing controlled levels of hydrogen. This unique idea will hopefully generate interest in the area of renewable energy storage (Liu et al., 2020).

1.4.2 Research Objectives

The objective is to develop a microcapsule that will allow metal hydride particles to be sealed into an airtight polymer capsule. This controlled method of storage would allow the capsules to be broken open in an inert environment, minimising exposure to moisture from the air, retarding any violent reactions. Once the microcapsules are cut open, micrographs of the primary particles can be produced using high-resolution SEM in a controlled manner.

1.5 Organisation of the Thesis

This PhD thesis is structured as follows:

Chapter 2 delivers background information on microencapsulation. In addition, it covers a literature review of encapsulation with specific reference to metal hydrides.

Chapter 3 covers the methodology from the start of the encapsulation process together with an outline of the instrumentation used for characterisation.

Chapter 4 describes the specific experimental details used to develop the microcapsules and provides results from the analysis and discussions of the research.

Chapter 5 illustrates some conclusions and directions for future work.

2 Microencapsulation

Chapter Overview

This chapter covers some background about microencapsulation and how this methodology could be applicable for both controlled analysis and storage of metal hydride particles.

Chapter Contents

2.1	Microencapsulation	21
2.1.1	Introduction.....	21
2.1.2	Categories of Microcapsules	21
2.1.3	Microcapsule Release Mechanisms.....	23
2.1.4	Microencapsulation Experimental Design.....	24
2.1.5	Gaps in the Literature.....	26

2.1 Microencapsulation

2.1.1 Introduction

Microencapsulation is defined as a procedure for capturing particles or a liquid within a small, sealed capsule (Pasha et al., 2021), (Galogahi et al., 2020). Microcapsules, often made from a polymer, are effective for holding active materials in a safe, controlled environment until release is required (Peanparkdee et al., 2016). They are generally classified based on the size range. A microcapsule has a size range generally below 1mm. Any capsules with a size range less than 1 μ m can be referred to as nanocapsules.

This technology has been used for many years for the controlled release of active ingredients for industrial sectors such as agrochemicals, (Li et al., 2021), pharmaceuticals (Singh et al., 2010), (Bansode et al., 2010), foods (Choudhury et al., 2021), (McClements, 2017), (Oberoi et al., 2019), textiles (Salaün, 2016), (Ghayempour & Montazer, 2016) and cosmetics (Tekin et al., 2013), (Goldstein & Duchi, 2019).

Microencapsulation is effective for protecting materials from degradation and the safe handling of catalyst or toxic materials (Poe et al., 2007).

2.1.2 Categories of Microcapsules

This section gives a brief overview of the different categories of microcapsules. A more detailed description can be found in (Mishra, 2016).

Single Core Microcapsule

Figure 2.1 is a schematic of a single core microcapsule holding many nanoparticles. This is a basic design comprising of a single outer wall with a hollow centre (Bewernitz et al., 2020), (Li et al., 2016). This design of microcapsule would offer the most appropriate structure for this research project.

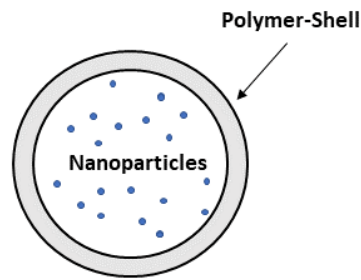


Figure 2.1 Single-Core microcapsule

The use of a single core microcapsule would allow uncomplicated access to the metal hydride particles for high resolution Scanning Electron Microscopy studies.

Coated Core-Shell Microcapsule

This is a single core microcapsule with a second external coating, often made from a different material for extra stability (Kang et al., 2015).

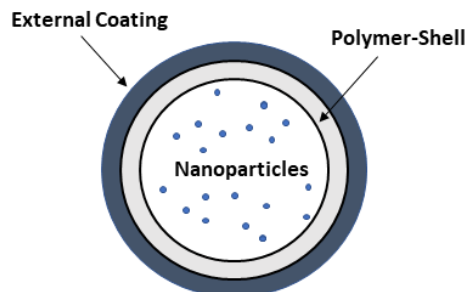


Figure 2.2 Coated Core-Shell microcapsule

This type of microcapsule can be utilised in agrochemical applications to target a specific insect and prevent unnecessary harm to other creatures (Feng et al., 2021).

Multiple-Core Microcapsule

An alternative microcapsule to the single core is a capsule containing many cores enclosed within the shell (Eqbal & Gundabala, 2017).

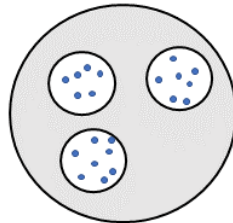


Figure 2.3 Multiple-Core microcapsule

Matrix Microcapsule

This type of encapsulation has a simple structure that allows the particles or small cores to be dispersed throughout the whole of the microcapsule (Jeannot et al., 2018). The particles within the microcapsule can be present at the surface. It is possible to have a coated matrix capsule if required, as the additional outer layer can protect surface particles.

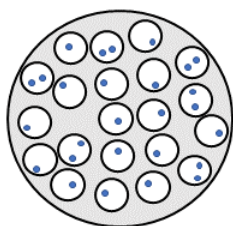


Figure 2.4 Matrix microcapsule

2.1.3 Microcapsule Release Mechanisms

The active material can be released from micro-encapsulation using a variety of techniques. Some examples of popular release mechanisms are as follows:

Mechanical Breakage - An example of this type of microcapsule application is the cosmetics industry. Perfumes can be released from small silicone co-polymer microcapsules by a simple mechanical breakage. This is based on a shear mechanism, initiated by gentle rubbing of the skin or the garment, resulting in the release of an encapsulated fragrance (Peña et al., 2012).

Enzymatic Hydrolysis and pH Switch - An alternative release mechanism is based on pH changes (Luz & Wenyan, 2006) or enzymatic hydrolysis (Huang et al., 2018). Both can lead to erosion of the outer layer, slowly releasing the internal active material. This type of release mechanism is often associated with both the pharmaceutical (Ahmad et al., 2021) and agrochemical sectors (Alonso et al., 2013). Microcapsules are used in pharmaceuticals for controlled drug delivery (Mankar and Shaikh, 2020).

Microencapsulation is key in the agrochemical sector for holding active pesticides that can target specific insects (Yu et al., 2021). By encapsulating active chemicals into a sealed vessel, it can minimise exposure to skin contact for humans when dealing with toxic insecticides (Tsuji, 2001).

For the purpose of this PhD, the release mechanism for accessing the metal hydride particles involves cutting open the polysulfone microcapsule using a sharp blade. Initially, this procedure was performed with the aid of a stereo microscope in the open lab. A procedure utilising a preparation chamber was later developed. This enabled the microcapsules to be cross sectioned under vacuum with the option to purge the chamber using argon gas, which minimises exposure to air/moisture.

2.1.4 Microencapsulation Experimental Design

The criteria for choosing a specific microcapsule are based on the chemical structure and physical morphology of both the active material and the outer wall coating. Many different procedures have been created over the years for both research and industrial applications. Some of the encapsulation processes used today include controlled precipitation, in situ

polymerisation, centrifugal suspension separation, and freeze/spray drying (Guo et al., 2020).

The objective for this PhD was to design and produce a microcapsule to allow the safe handling of moisture-sensitive metal hydrides. The fundamental issue when designing a microcapsule for the storage and release of metal hydrides was to consider the physiochemical characteristics of the nanoparticles and the polymer system, with the knowledge that metal hydride particles react violently with protic solvents. Many aspects of the experimental procedure had to be carefully selected to prevent unwanted reactions.

When considering the structure of the microcapsule, it was essential that the wall strength should be enough to hold the spherical structure intact, preventing collapsing issues. The porosity of the polymer surface had to be kept to a minimum, ensuring the capsule would provide resistance from external moisture. The mechanism of release for the metal hydride particles was also an important factor, as easy access to the inner core was a crucial requirement.

The single core polysulfone microcapsule was designed to stabilise the particles, to allow controlled storage. It was expected to allow easy release/access to the particles from a direct mechanical cutting action using a razor blade.

This novel technique could develop into a robust system for stabilising moisture-sensitive metal hydride particles for characterisation studies.

The initial procedure used for this project was an emulsion non-solvent addition technique (ENSA). The ENSA method was a good starting point as it offered practical experience in the principle of producing polymer microcapsules (Nokhodchi and Farid, 2002).

A brief explanation of the process of generating microcapsules using a non-solvent addition technique can be explained as follows: the chosen polymer for encapsulation is added to a suitable solvent and agitated to dissolve the polymer, forming a solution. The nanoparticles chosen for encapsulation are then added to liquid paraffin together with a few drops of a

dispersing agent and anti-foaming agent. The nanoparticles are subject to continuous agitation with the liquid paraffin to generate a dispersion. The polymer solution is then slowly added to the dispersion using a dropping funnel. Microcapsules are created by the addition of a non-solvent, that can be defined as a solvent incapable of dissolving the polymer. The addition of the non-solvent is achieved by the slow release of small droplets from a dropping funnel into the emulsion at an approximate rate of 1ml/min. The emulsion is under a constant agitation during the addition of the non-solvent.

Due to incompatibilities with polysulfone and liquid paraffin, the process for generating microcapsules was changed. The modified procedure involved allowing small droplets of the polymer dispersion to drip slowly from the needle of a syringe (at an approximate rate of one droplet every 5 seconds) into the non-solvent to generate the microcapsules. To improve on the microcapsule morphology, the non-solvent was modified from a single solvent system to a blend of different solvents. This research demonstrated that a small change to the ratio of the chosen non-solvents had a direct effect on the internal morphology of the generated microcapsules.

2.1.5 Gaps in the Literature

At the very start of the PhD in January 2014, there were no reports of research involving microencapsulation of metal hydride materials.

No papers were available at that time relating to metal hydride encapsulation by the formation of a genuine mononuclear single core capsule. This is a microcapsule containing a hollow core for the encapsulation of the metal hydride particles with a single outer shell. The nearest research to this area was published in a paper reporting the protection of hydrogen storage materials using polymer systems (Dobbins et al., 2007). This research does not utilise microencapsulation but simply protects the metal hydride particles by forming a polymer film.

The paper demonstrates that sodium aluminium hydride was protected with a polymer film using a layer-by-layer electrostatic self-assembly coating of nano-films, using formamide as the working medium.

This is a novel approach for the protection of metal hydrides but would not be considered a useful approach for this PhD as the research simply stabilises the metal hydride particles.

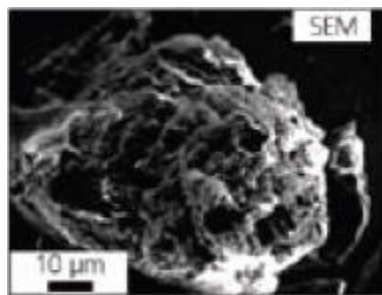


Figure 2.2: (NaAlH_4 bilayer of PSS/PAH)

The SEM micrograph, as shown in figure 2.2, represents the coated particles. The bilayer of polystyrene sulfonate (PSS) and poly(allylamine hydrochloride) (PAH) is effectively a solid bulk particle. Any attempts to cut the particles open to access the nanoparticles would be difficult and result in the polymer film smearing. This would mask the metal hydride particles, making it extremely difficult to obtain good SEM micrographs for the purpose of characterising the primary particle morphology.

A second paper written later (Borodina et al., 2010) was concerned with the formation of micro-containers of sodium borohydride and polystyrene. This experimental work involved the formation of a non-aqueous emulsion of dimethylformamide and soybean oil. The sodium borohydride and polystyrene were dissolved in dimethylformamide. The dimethylformamide was evaporated, allowing the sodium borohydride to crystallise and the polystyrene to precipitate on the crystal surface, resulting in the formation of a solid particle.

This technique may again be useful to allow characterisation of the metal hydrides using

X-ray Diffraction (Bunaciu et al., 2015) but, as discussed from the previous paper, it would have limitations for the characterisation of the primary particle shape and size. In addition, the fact that the metal hydride was dissolved then recrystallized in the dimethylformamide would impede specific control of the primary particle size formation and could lead to potential polymorphism issues.

The methods outlined from the literature searches are based on generating a solid polymer particle. They do not produce a core-shell microcapsule, and the resulting polymer phase produces a rough coating as shown above in figure 2.2. Both examples suggest that the moisture-sensitive particles are stabilised, but these methods would not be suitable for primary particle shape and size studies using Scanning Electron Microscopy.

The design of the microcapsules for this PhD ensures that access to the particles will be obtained with minimum masking from the surrounding polymer phase. This is based on the hypothesis that the core of the microcapsule can be easily opened when the microcapsule is placed under vacuum within a controlled environment. The nanoparticles will be free from polymer, allowing good quality SEM micrographs to be obtained from the moisture-sensitive primary particles for characterisation studies.

The literature available on microencapsulation was based on studies designed for the entrapment of active ingredients for pharmaceutical (D'onofrio et al., 1979), agrochemical (Scher et al., 1998) food (Arenas-Jal et al., 2020) and cosmetics (Ashraf et al., 2015) applications. A paper entitled 'Microencapsulation of Paracetamol by Various Emulsion Techniques using Cellulose Acetate Phthalate' (Nokhodchi and Farid, 2002) was extremely useful for background information on microencapsulation methods. It demonstrated various emulsion techniques used to encapsulate paracetamol using CAP (Cellulose Acetate Phthalate). The techniques of interest were emulsion solvent evaporation (ESE), emulsion non-solvent addition (ENSA) and modified emulsion solvent evaporation (MESE). The ENSA methodology was modified initially for this PhD to determine the suitability for generating a microcapsule that could encapsulate titanium dioxide nanoparticles. The process and results from this initial starting point are covered in greater detail in Chapter 4, Results and Discussions, of this thesis.

A similar paper written some 12 years earlier (Sprockel and Prapaitrakul, 1990), was based on the microencapsulation of paracetamol by various emulsion techniques using CAB (Cellulose Acetate Butyrate) as the polymer. This was an interesting read, but it was decided to start the experimentation studies utilising CAP as the polymer to initially encapsulate TiO₂ as a moisture-stable test system.

3 Materials and Methods

This chapter covers the methodology from the start of the encapsulation process together with an outline of the instrumentation used for characterisation.

Chapter Contents

3.1	Materials and Methods	30
3.2	Methodology	31
3.3	Characterisation	53
3.3.1	Instrumentation used for Research.....	53
3.3.2	Light Microscopy.....	53
3.3.3	Scanning Electron Microscopy (SEM).....	54
3.3.4	Energy Dispersive X-ray Analysis (EDX)	57
3.3.5	Transmission Electron Microscopy (TEM).....	59

3.2 Methodology

Table 3.1 Summary of Experimental Methods Used

Method Number	Description	Page Number
1	1:2 Ratio of TiO ₂ / CAP in Acetone	32
2	1:2 Ratio of TiO ₂ / CAP in THF	33
3	1:4 ratio of TiO ₂ / CAP in THF	34
4	1:4 ratio of TiO ₂ / CAP in Acetonitrile	35
5	1:4 ratio of TiO ₂ / CAP in Acetonitrile	36
6	1:4 ratio of TiO ₂ / CAP in Acetone	37
7	Generation of TiO ₂ - PSF Microcapsules	38
8	PSF Microcapsules	39
9	Microcapsule formation using PSF	40
10	Generation of TiO ₂ microcapsules using PSF	41
11	Encapsulation of Li ₂ CO ₃	42
12	Encapsulation of Li ₂ CO ₃	43
13	Encapsulation of Li ₃ PO ₄	44
14	Encapsulation of Li ₃ PO ₄	45
15	Encapsulation of LiNH ₂	46
16	Generation of a PSF NaBH ₄ Dispersion	47
17	Encapsulation of NaBH ₄	48
18	Encapsulation of NaBH ₄	49
19	Generation of a PSF NaBH ₄ Dispersion using THF	50

Method 1 (1:2 Ratio of TiO₂ / CAP in Acetone)

Materials:

1. Titanium Dioxide 20nm primary particle size, Sigma-Aldrich
2. Paraffin Oil, Sigma-Aldrich
3. Cellulose Acetate Phthalate, Fluka
4. Simethicone, KCL Basildon
5. Tween 80, Sigma-Aldrich
6. Acetone, Fisher Scientific
7. Cyclohexane, Sigma-Aldrich

Using a balance, 25 g of CAP was weighed out and dissolved into 200 ml of acetone with the aid of an IKA yellow line magnetic stirring unit. Next, 11.5 g of TiO₂ was weighed out and put directly into a 1 litre beaker. 230 g of liquid paraffin was then added to the TiO₂ together with a couple of drops of Tween 80 and Simethicone. The TiO₂ dispersion was agitated using an IKA RW 20 digital overhead stirrer with 90mm centrifugal stirrer blades at an agitation speed of 1050rpm. The polymer solution was added to the TiO₂ dispersion very slowly using a 250ml pressure equalising dropping funnel. Once the addition of the polymer solution was complete, the dispersion was further agitated for 5 minutes. Then 300 ml of cyclohexane, the non-solvent, was dripped slowly into the mixture over 15 minutes using a 500ml pressure equalising dropping funnel. The mixture was then agitated for an additional 20 minutes. The liquid paraffin was decanted from the flask and the resulting microcapsules were washed 3 times with 100 ml of cyclohexane each time. The microcapsules were air dried overnight.

Method 2 (1:2 Ratio of TiO₂ / CAP in THF)

Materials:

1. Titanium Dioxide 20nm primary particle size, Sigma-Aldrich
2. Paraffin Oil, Sigma-Aldrich
3. Cellulose Acetate Phthalate, Fluka
4. Simethicone, KCL Basildon
5. Tween 80, Sigma-Aldrich
6. THF, Fisher Scientific
7. Cyclohexane, Sigma-Aldrich

Using a balance, 2.5g of CAP was weighed out and dissolved into 20 ml of THF with the aid of an IKA yellow line magnetic stirring unit on spin setting 4. Next, 1.2g of TiO₂ was put directly into a 250ml, 3-neck round bottomed flask. 23g of liquid paraffin was then added to the TiO₂ with a couple of drops of Tween 80 and Simethicone. The TiO₂ dispersion was agitated using an IKA RW 20 digital overhead stirrer with 90mm centrifugal stirrer blades at 937rpm. The polymer solution was then added to the TiO₂ dispersion very slowly using a 250ml pressure equalising dropping funnel with an agitation speed of 466rpm. Once the polymer solution had been completely added to the dispersion, it was further agitated for 5 minutes at 630rpm. Then 30ml of cyclohexane, a non-solvent, was added to the mixture slowly over 20 minutes using the 250ml pressure equalising dropping funnel. The mixture was stirred for an additional 20 minutes with an agitation speed of 630rpm. The liquid paraffin was then decanted, and the residue was washed with 10ml of cyclohexane.

Method 3 (1:4 ratio of TiO₂ / CAP in THF)

Materials:

1. Titanium Dioxide 20nm primary particle size, Sigma-Aldrich
2. Paraffin Oil, Sigma-Aldrich
3. Cellulose Acetate Phthalate, Fluka
4. Simethicone, KCL Basildon
5. Tween 80, Sigma-Aldrich
6. THF, Fisher Scientific
7. Cyclohexane, Sigma-Aldrich

Using a balance, 2.5g of CAP was weighed out and dissolved into 20ml of THF with the aid of an IKA yellow line magnetic stirring unit on spin setting 4. Next, 0.5g of TiO₂ was weighed out and put directly into a 250ml, 3-neck round bottomed flask. 23g of liquid paraffin was then added to the TiO₂ with a couple of drops of Tween 80 and Simethicone. The TiO₂ dispersion was agitated using a stirring speed of 990rpm utilising an IKA RW 20 digital overhead stirrer connected to 90mm centrifugal blades. The polymer solution was then added to the TiO₂ dispersion slowly, using a 250ml pressure equalising dropping funnel with an initial agitation speed of 900rpm, slowing to 622rpm halfway through the addition period. Once all the polymer solution had been added to the dispersion, it was allowed to agitate for a further 5 minutes at 622rpm. Then 30ml of cyclohexane, the non-solvent, was added to the mixture slowly over 20 minutes using a 250ml pressure equalising dropping funnel. The mixture was then allowed to agitate for an additional 20 minutes with an agitation speed of 500rpm. The liquid paraffin was decanted, and the residue was washed with 10ml of cyclohexane.

Method 4 (1:4 ratio of TiO₂ / CAP in Acetonitrile)

Materials:

1. Titanium Dioxide 20nm primary particle size, Sigma-Aldrich
2. Paraffin Oil, Sigma-Aldrich
3. Cellulose Acetate Phthalate, Fluka
4. Simethicone, KCL Basildon
5. Tween 80, Sigma-Aldrich
6. Acetonitrile, 99.8%, for HPLC Acros Organics
7. Chloroform, Fisher Scientific

Using a balance, 2.5 g of CAP was weighed out and dissolved into 20ml of acetonitrile with the aid of an IKA yellow line magnetic stirring unit on spin setting 4. Next, 0.5g of TiO₂ was weighed out and put directly into a 250ml, 3-neck round bottomed flask. 23g of liquid paraffin was then added to the TiO₂ with a couple of drops of Tween 80 and Simethicone. The TiO₂ dispersion was agitated using an IKA RW 20 digital overhead stirrer connected to 90mm centrifugal blades with a speed setting of 990rpm. The polymer solution was then added to the TiO₂ dispersion very slowly using a 250ml pressure equalising dropping funnel with an agitation speed of 750rpm. Once the addition of the polymer solution was complete, the dispersion was agitated for an additional 5 minutes at 750rpm. Then 30ml of chloroform was added to the mixture slowly over 20 minutes with the aid of a pressure equalising dropping funnel using an agitation speed of 535rpm.

Method 5 (1:4 ratio of TiO₂ / CAP in Acetonitrile)

Materials:

1. Titanium Dioxide 20nm primary particle size, Sigma-Aldrich
2. Paraffin Oil, Sigma-Aldrich
3. Cellulose Acetate Phthalate, Fluka
4. Simethicone, KCL Basildon
5. Tween 80, Sigma-Aldrich
6. Acetonitrile, 99.8%, for HPLC Acros Organics
7. Cyclohexane, Sigma-Aldrich

Using a balance, 2.6 g of CAP was weighed out and dissolved into 20ml of acetonitrile with the aid of an IKA yellow line magnetic stirring unit on spin setting 4. Next, 0.5g of TiO₂ was weighed out and put directly into a 250ml, 3-neck round bottomed flask. 23g of liquid paraffin was then added to the TiO₂ together with a couple of drops of Tween 80 and Simethicone. The TiO₂ dispersion was agitated using an IKA RW 20 digital overhead stirrer connected to 90mm centrifugal blades at 1170rpm. The polymer solution was then added to the TiO₂ dispersion very slowly using a 250ml pressure equalising dropping funnel, with an agitation speed of 750rpm. Once the addition of the polymer solution was complete, the dispersion was then allowed to agitate for a further 5 minutes at 750rpm. 30ml of cyclohexane, the non-solvent, was added to the mixture slowly over 20 minutes with the aid of the pressure equalising dropping funnel, using an agitation speed of 636rpm.

Method 6 (1:4 ratio of TiO₂ / CAP in Acetone)

Materials:

1. Titanium Dioxide 20nm primary particle size, Sigma-Aldrich
2. Paraffin Oil, Sigma-Aldrich
3. Cellulose Acetate Phthalate, Fluka
4. Simethicone, KCL Basildon
5. Tween 80, Sigma-Aldrich
6. Acetone, Fisher Scientific
7. Chloroform, Fisher Scientific

Using a balance, 2.5 g of CAP was weighed out and dissolved into 20ml of acetonitrile with the aid of the IKA yellow line magnetic stirring unit. Next, 0.5g of TiO₂ was weighed out and placed into a 250ml, 3-neck round bottomed flask. 23g of liquid paraffin was then added to the TiO₂ together with a couple of drops of Tween 80 and Simethicone. The TiO₂ dispersion was agitated using 40mm stirrer blades (cut down from 90mm blades) at 650rpm for 30mins. The polymer solution was then added to the TiO₂ dispersion very slowly using a 250ml pressure equalising dropping funnel with an agitation speed of 640rpm. Once the addition of the polymer solution was completely added to the dispersion, it was then allowed to agitate for a further 5 minutes. The non-solvent addition involved slowly adding 30ml of chloroform into the mixture over 20 minutes at a rate of 1-2ml per/min using a 250ml pressure equalising dropping funnel with an agitation speed of 640rpm.

Method 7 (Generation of TiO₂ - PSF Microcapsules)

Materials:

1. Titanium Dioxide 20nm primary particle size, Sigma-Aldrich
2. Paraffin Oil, Sigma-Aldrich
3. Polysulfone (PSF), Sigma-Aldrich
4. Simethicone, KCL Basildon
5. Tween 80, Sigma-Aldrich
6. Dimethylformamide (DMF), Fisher Scientific
7. Chloroform, Fisher Scientific

Using a balance, 2.5 g of PSF was weighed out and dissolved into 20ml of DMF with the aid of an IKA yellow line magnetic stirring unit. Next, 0.5g of TiO₂ was weighed out and put directly into a 250ml, 3-neck round bottomed flask. 23g of liquid paraffin was then added to the TiO₂ together with a couple of drops of Tween 80 and Simethicone. The TiO₂ dispersion was agitated using an IKA RW 20 digital overhead stirrer connected to 40mm centrifugal blades for 30mins at 450rpm. The polymer solution was added slowly utilising a 250ml pressure equalising dropping funnel with a lower agitation speed of 300rpm.

Once the addition of the polymer solution was completely added to the dispersion, it was then allowed to agitate for a further 5 minutes. Using the pressure equalising dropping funnel, 30ml of chloroform was then slowly dripped into the mixture over 20 minutes using an agitation speed of 300rpm.

Method 8 (PSF Microcapsules)

Materials:

1. Paraffin Oil, Sigma-Aldrich
2. Polysulfone, Sigma-Aldrich
3. DMF, Fisher Scientific

Using a balance, 2.5 g of PSF was weighed out and dissolved into 20ml of DMF with the aid of an IKA yellow line magnetic stirrer. The polymer solution was added slowly to 23g of liquid paraffin within a 250ml, 3-neck round bottomed flask using a 250ml pressure equalising dropping funnel. The mixture was agitated during the polymer addition using an IKA RW 20 digital overhead stirrer connected to 40mm centrifugal blades set at an agitation speed of 300rpm.

Using a 250ml pressure equalising dropping funnel, 30ml of chloroform was then slowly dripped into the mixture over 20 minutes with an agitation speed of 300rpm.

Method 9 (Microcapsule formation using PSF)

The following experiment was performed using a high concentration of PSF solution with TiO₂ nanoparticles.

Materials:

1. Polysulfone (PSF), Sigma-Aldrich
2. 1-Methyl-2-Pyrrolidone (NMP), Honeywell
3. Titanium Dioxide 20nm primary particle size, Sigma-Aldrich
4. Acetonitrile, 99.8%, for HPLC Acros Organics

Using a balance, 4g of PSF was weighed out directly into a 50ml conical flask. Using a small measuring cylinder, 20ml of NMP was added directly to the flask. With the aid of an IKA yellow line magnetic stirrer the PSF was dissolved, forming a solution polymer. Next, 0.1g of TiO₂ was weighed out and put directly into the polymer solution. The mixture was then stirred for 60 minutes using the magnetic stirrer and a speed setting of 3, to allow the TiO₂ particles to disperse. The polymer dispersion was then dripped very slowly at an approximate rate of 1 droplet every 5 seconds, using a glass pipette, into a conical flask containing 30ml of acetonitrile.

Method 10 (Generation of TiO₂ microcapsules using PSF)

Materials:

1. Titanium Dioxide 20nm primary particle size, Sigma-Aldrich
2. Polysulfone (PSF), Sigma-Aldrich
3. Simethicone, KCL Basildon
4. Tween 80, Sigma-Aldrich
5. 1-Methyl-2-Pyrrolidone (NMP), Honeywell
6. Acetonitrile, 99.8%, for HPLC Acros Organics
7. Hexane, Sigma-Aldrich

Using a balance, 8g of PSF was weighed out directly into a 100ml conical flask. Then 30ml of NMP was measured using a small measuring cylinder, and added to the PSF. The mixture was stirred for 2 hours with the aid of an IKA yellow line magnetic stirrer on a speed setting of 3. Once the PSF had completely dissolved, 2 drops of Tween 80 and 1 drop of simethicone was added to the polymer solution. Next, 0.1g of TiO₂ was weighed out and put directly into the flask containing the polymer solution. The TiO₂ mixture was then agitated using the magnetic stirrer for 2 hours to generate a good dispersion. A mixture comprising of 35ml of acetonitrile and 15ml of hexane was placed directly into a 250ml round bottomed flask. Using an IKA RW 20 digital overhead stirrer connected to 40mm centrifugal blades, the solvent mix was agitated at 350rpm. Using a plastic 10ml syringe and a metal needle, small droplets of the polymer dispersion were slowly allowed to plunge into the non-solvent blend at an approximate rate of 1 droplet every 5 seconds. Once the addition was complete, the product was left to stir at 350rpm for 1 hour.

Method 11 (Encapsulation of Li_2CO_3)

The PSF polymer- Li_2CO_3 dispersion was prepared using the following method:

Materials used:

1. Lithium Carbonate, Honeywell
2. Polysulfone (PSF), Sigma-Aldrich
3. Acetonitrile, 99.8%, for HPLC Acros Organics
4. 1-Methyl-2-Pyrrolidone (NMP), Honeywell

Using a balance, 2g of PSF was weighed out directly into a 50ml conical flask. 10ml of NMP was measured using a measuring cylinder and the solvent was added to the polymer in the conical flask. The mixture was agitated using an IKA yellow line magnetic stirring unit set at speed 3 for 4 hours until the polymer had completely dissolved. 0.1g of Li_2CO_3 was weighed out and added directly to the polymer solution. The Li_2CO_3 dispersion was agitated for 60 minutes utilising the yellow line magnetic stirrer with a chosen speed setting of 3.

The polymer- Li_2CO_3 dispersion was slowly dripped into a 250ml round bottomed flask containing 30ml of acetonitrile utilising a 10ml plastic syringe and a metal needle at an approximate rate of 1 droplet every 5 seconds. The acetonitrile was agitated during the droplet addition using an IKA RW 20 digital overhead stirrer and 40mm centrifugal blades with a speed setting of 235rpm.

Method 12 (Encapsulation of Li_2CO_3)

Materials used:

1. Lithium Carbonate, Sigma-Aldrich
2. Polysulfone (PSF), Sigma-Aldrich
3. Acetonitrile, 99.8%, for HPLC Acros Organics
4. 1-Methyl-2-Pyrrolidone (NMP), Honeywell

Using a balance, 2g of PSF was weighed out directly into a 50ml conical flask. 10ml of NMP was measured out using a measuring cylinder and added to the polymer. The mixture was stirred using an IKA yellow line magnetic stirrer using heat setting 1 and agitation speed 3 for 2.5 hours until the polymer had fully dissolved.

Next, 0.1g of Li_2CO_3 was weighed out and added to the 50ml conical flask containing the polymer solution. The mixture was agitated using a magnetic stirrer for 60 minutes to generate a good dispersion.

The polymer- Li_2CO_3 dispersion was slowly allowed to drip, at an approximate rate of 1 droplet every 5 seconds, using a 10ml plastic syringe and a metal needle into a 250ml round bottomed flask containing 30ml of acetonitrile. The acetonitrile was stirred using a IKA RW 20 digital overhead stirrer connected to 40mm centrifugal blades at 235rpm.

Method 13 (Encapsulation of Li_3PO_4)

Materials used:

1. Lithium Phosphate, Sigma-Aldrich
2. Polysulfone (PSF), Sigma-Aldrich
3. 1-Methyl-2-Pyrrolidone (NMP), Honeywell
4. Acetonitrile, 99.8%, for HPLC Acros Organics
5. Chloroform, Fisher Scientific

Using a balance, 2 g of PSF was weighed out directly into a 100ml conical flask. 10ml of NMP was measured using a measuring cylinder and added to the polymer. The mixture was stirred using an IKA yellow line magnetic stirring unit on speed setting 4 and heater setting number 1 for 2 hours until the polymer had dissolved.

0.1g of Li_3PO_4 was weighed out and put directly into the 100ml conical flask. The Li_3PO_4 dispersion was agitated using the yellow line magnetic stirrer for 60 minutes on speed setting number 3 with a 20mm magnetic stir bar.

Method 14 (Encapsulation of Li_3PO_4)

Materials used:

1. Lithium Phosphate, Sigma-Aldrich
2. Polysulfone (PSF), Sigma-Aldrich
3. Dimethylformamide (DMF)
4. Acetonitrile, 99.8%, for HPLC Acros Organics
5. Chloroform, Fisher Scientific

Using a balance, 1.5g of PSF was weighed out directly into a 50ml conical flask. 10ml of DMF was measured out using a measuring cylinder and added to the polymer. The mixture was stirred using an IKA yellow line magnetic stirrer using speed 2 and heat setting 1 for a total of 4 hours until the polymer had dissolved. The polymer was then left overnight stirring, with the heat setting off. The following morning, an additional 0.5g of PSF was added to the polymer solution that was then allowed to stir using the yellow line unit with speed setting 2 and heat setting 1 for an additional 2 hours. It was clear that a smaller quantity of the PSF needed more time to dissolve into the DMF compared with the NMP.

Li_3PO_4 was then ground to a fine powder using a pestle and mortar to reduce the primary particle size of the nanoparticles further and to break up any aggregates.

Using a balance, 0.1g of the ground Li_3PO_4 was weighed out and put directly into the PSF solution in a 50ml conical flask. The PSF polymer- Li_3PO_4 dispersion was agitated using the yellow line magnetic stirrer for 60 minutes on a speed setting of 4 with a 20mm magnetic stir bar.

Method 15 (Encapsulation of LiNH_2)

Materials used:

1. Lithium Amide, Sigma-Aldrich
2. Polysulfone (PSF), Sigma-Aldrich
3. 1-Methyl-2-Pyrrolidone (NMP), Honeywell
4. Acetonitrile, 99.8%, for HPLC Acros Organics
5. Chloroform, Fisher Scientific

Using a balance, 2g of PSF was weighed out directly into a 100ml conical flask. 10ml of NMP was measured using a measuring cylinder, before adding to the polymer. The mixture was agitated using an IKA yellow line magnetic stirrer with 20mm stir bar with speed setting 4 and heat setting 1 for 3 hours until the polymer had dissolved.

Next, using a nitrogen glove box, a small quantity ($\sim 0.1\text{g}$) of LiNH_2 was added to the PSF solution in the 100ml conical flask, under a flow of nitrogen, together with a 20mm magnetic stir bar.

A glass stopper was then put onto the conical flask to ensure the mixture was held within a nitrogen environment. The conical flask was taken out of the glove box, then placed directly onto the yellow line magnetic stirrer and agitated for 60 minutes using speed setting 4 with a 20mm magnetic stir bar.

Method 16 (Generation of a PSF NaBH₄ Dispersion)

Materials used:

1. Sodium Borohydride, Sigma-Aldrich
2. Polysulfone (PSF), Sigma-Aldrich
3. 1-Methyl-2-Pyrrolidone (NMP), Honeywell
4. Acetonitrile, 99.8%, for HPLC Acros Organics/Extra Dry Acetonitrile, ACROS Organics
5. Chloroform, Fisher Scientific

Using a balance, 2g of PSF was weighed out directly into a 50ml conical flask. 10ml of NMP was measured using a measuring cylinder, before adding to the Polysulfone polymer. The mixture was stirred using an IKA yellow line magnetic stirrer with 20mm stir bar. The unit was set using at speed 4 and heat setting 1 for 3 hours until the polymer had dissolved.

The conical flask was filled with nitrogen using a rotaflo side arm that allows nitrogen to enter the flask before sealing by closing the valve.

Next, using a nitrogen glove box, a small quantity (~0.1g) of NaBH₄ was added to the PSF solution in the 50ml conical flask, under a flow of nitrogen, together with a magnetic stirring pellet.

A stopcock adapter with rotaflo side arm was put onto the conical flask to ensure the mixture was held within a nitrogen environment. The conical flask was taken out of the glove box then placed directly onto the yellow line magnetic stirrer and agitated using a speed setting of 10 for 60 minutes. The use of the stopcock adapter with rotaflo side arm allowed additional nitrogen into the conical flask when required.

Method 17 (Encapsulation of NaBH₄)

Using a fume cupboard, apparatus was assembled that initially involved clamping a 100ml round-bottomed 2-neck flask to a retort stand. Then 24ml of acetonitrile and 6ml of chloroform were carefully added to the flask directly from a measuring cylinder. A small cross-shaped stirring pellet was then added to the flask. The flask was held over a yellow line magnetic stirrer set for agitation of the non-solvent blend.

A glass extension with a separate side arm was fixed into the top neck of the round-bottomed flask. Nitrogen connections were then secured to both the round-bottomed flask and the glass extension. The top of the extension was left free to allow the polymer dispersion to be pipetted into the non-solvent.

Under nitrogen, a small amount of the polymer dispersion was extracted (using a glass pipette) from the conical flask, then allowed to slowly drip, at an approximate rate of one droplet every 5 seconds, under a flow of nitrogen into the non-solvent blend held within the 100ml round bottomed flask.

Method 18 (Encapsulation of NaBH_4)

Using a fume cupboard, apparatus was assembled that initially involved clamping a 100ml round-bottomed 3-neck flask to a retort stand. Then 25ml of acetonitrile and 5ml of chloroform were carefully added to the flask directly from a measuring cylinder. A small 10mm cross-shaped stirring pellet was then added to the flask. The flask was held over a yellow line magnetic stirrer set for agitation of the non-solvent blend.

Nitrogen connections were then secured to both the side and top necks of the flask using a stopcock adapter with rotaflo side arm. The 2nd side neck was covered in a Suba-Seal that allowed the needle to pass through whilst minimising contact of the dispersion with moisture.

The 1ml syringe was used to extract the PSF- NaBH_4 dispersion held under nitrogen from the conical flask. The syringe was connected to a Microlance needle that was injected through the Suba-Seal, allowing small droplets to drip slowly (at an approximate rate of one droplet every 5 seconds) under a flow of nitrogen into the non-solvent blend held within the 100ml round bottomed flask.

Method 19 (Generation of a PSF NaBH₄ Dispersion using THF)

Materials used:

1. Sodium Borohydride, Sigma-Aldrich
2. Polysulfone (PSF), Sigma-Aldrich
3. THF, Fisher Scientific / THF (Anhydrous 99.9%) Sigma-Aldrich

Using a balance, 2g of PSF was weighed out directly into a 50ml conical flask. 10ml of THF was measured using a measuring cylinder, before adding to the Polysulfone polymer. The mixture was stirred using an IKA yellow line magnetic stirring unit with a speed setting of 4 and heat setting 2 for 3 hours until the polymer had dissolved.

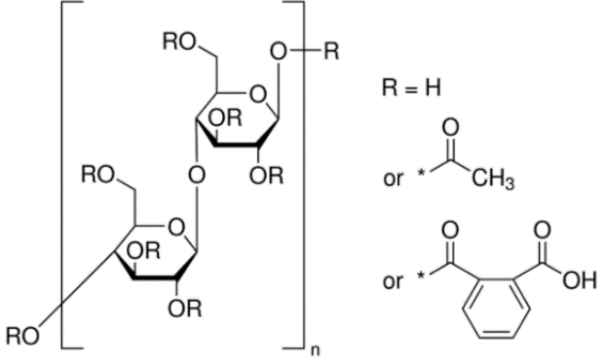
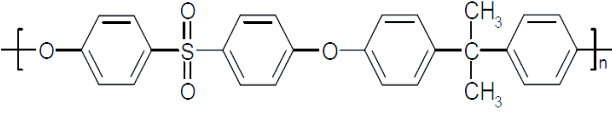
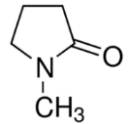
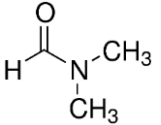
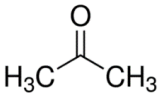
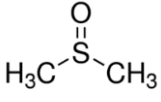
The conical flask was filled with nitrogen using a side rotaflo side arm that allowed nitrogen to enter the flask before being sealed by closing the valve.

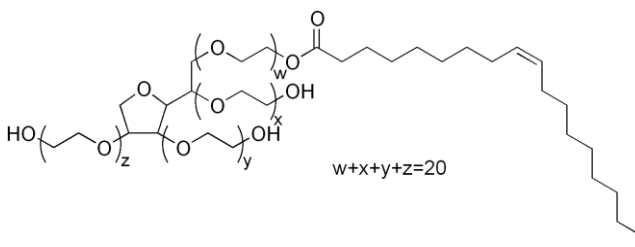
Next, using a nitrogen glove box, a small quantity (~0.1g) of NaBH₄ was added to the PSF solution in the 50ml conical flask, under a flow of nitrogen, together with a magnetic stirring pellet.

A stopcock adapter with rotaflo side arm was put onto the conical flask to ensure the mixture was held within a nitrogen environment. The conical flask was taken out of the glove box then placed directly onto the magnetic stirrer and agitated using a speed setting of 10 for 60 minutes. The use of the stopcock adapter with rotaflo side arm allowed additional nitrogen into the conical flask when required.

Table 3.2 represents a summary of the materials and solvents used for the research.

Table 3.2 Structure of Materials and Solvents Utilised - Sigma-Aldrich

Name	Synonyms	Structure
Cellulose Acetate Phthalate	CAP	
Polysulfone	PSF	
Tetrahydrofuran	THF	
Chloroform		CHCl ₃
Acetonitrile	ACN	CH ₃ CN
1-methyl-2-Pyrrolidone	NMP	
Dimethylformamide	DMF	
Acetone		
Dichloromethane		CH ₂ Cl ₂
Dimethyl sulfoxide	DMSO	
Cyclohexane		

<p>Simethicone</p>		$\text{H}_3\text{C} - \text{Si} \begin{array}{c} \\ \text{CH}_3 \\ \\ \text{CH}_3 \end{array} - \left[\text{O} - \text{Si} \begin{array}{c} \\ \text{CH}_3 \\ \\ \text{CH}_3 \end{array} \right]_n - \text{CH}_3 + \text{SiO}_2$
<p>Tween 80</p>	<p>Polysorbate 80</p>	 <p>The structure shows a central sorbitol ring with three hydroxyl groups. Each hydroxyl group is substituted with a polyoxyethylene chain of length x, y, or z. The chain of length w is further substituted with a palmitic acid chain (16 carbons, including one double bond). The equation $w+x+y+z=20$ is provided below the structure.</p>

3.3 Characterisation

3.3.1 Instrumentation used for Research

The analytical instrumentation used to characterise the generated microcapsules involved a combination of Light Microscopy (LM), Scanning Electron Microscopy (SEM) interfaced to Energy Dispersive X-ray Analysis (EDX) and Transmission Electron Microscopy (TEM).

Light microscopy was employed to obtain a general overview of the shape and size of the microcapsules together offering some information regarding the internal morphology. High resolution electron microscopy was crucial providing an in-depth overview of both the surface structure and internal morphology of the microcapsules. High resolution SEM interfaced to EDX was useful to identify nanoparticles encapsulated within the polymer microcapsules.

3.3.2 Light Microscopy

Light Microscopy is a simple but extremely useful bench top instrument that provided a fast assessment of the structure of the microcapsules (Sanderson, 2019). As a technique, it offered a means to evaluate both the external and internal surfaces of the microcapsules with minimum sample preparation. The light microscope utilised for this research project was the Zeiss stereo SV8.

This stereo microscope is a low resolving microscope but benefits from the large working distance between the binocular head and the sample stage. This microscope was extremely useful for inspecting the general morphology of the microcapsules, allowing digital micrographs to be recorded (Zeiss, 2021). The stereo microscope was essential for this research as it provided a means of viewing the small microcapsules whilst facilitating any manipulation. Using the microscope at a low zoom setting enabled sections to be cut through the microcapsule using a sharp razor blade. The cross-sections provided vital information from the internal features of the microcapsules.

The light microscope is an excellent tool for quickly visualising materials but is limited in its ability to resolve fine detail. Most conventional light microscopes utilise a white light source to illuminate the area of interest. They have limitations to the extent of resolving small features existing below $0.2\mu\text{m}$ in size because of the optics and the wavelength of light.

3.3.3 Scanning Electron Microscopy (SEM)

Scanning Electron Microscopy (SEM) is the preferred technique for obtaining high resolution images of small nanoparticles. It benefits from the use of an electron beam to illuminate the particles, significantly improving the resolving capability down to 1nm (Goldstein et al., 1992).

The useful advantage of the high vacuum sample chamber is that moisture-sensitive samples would be expected to be stable, once under vacuum.

The two Scanning Electron Microscopes used for this research are the FEI Quanta FEG 250 figure 3.1 and the Philips XL30 SFEG figure 3.2.



Figure 3.1 FEI Quanta FEG 250 Scanning Electron Microscope



Figure 3.2 Philips XL30 SFE Scanning Electron Microscope

The photographs from both microscopes demonstrate the general components of a fully functional SEM. The SEM has an electron optical column that is mounted on top of a sample chamber, complete with eucentric position stage for moving the sample around the chamber. The sample chamber is positioned on top of a cabinet that houses some electronics and the vacuum system. The Quanta 250 FEG SEM utilises a turbomolecular pumping system and the older Philips XL30 SFE employs an oil diffusion pumping system, both backed by a rotary pre-vacuum pump.

The electron gun for both microscopes used for this research is a Schottky - Field Emission Gun (FEG), that emits high energy electrons with small angular spread at a selectable energy range (Ilitchev, 2019). The beam can be focused to a fine spot, several nm in diameter on the surface of the sample. This is achieved by passing the beam through a series of electromagnetic lenses. A scan generator is utilised to scan the electron beam across the surface of the sample in a raster motion.

Different interactions of the electron beam with the sample surface will generate distinctive signals, based on the sample structure and topography. The sample surface will emit secondary electrons (SE) due to inelastic scattering. Elastic scattering involving the reflection of the primary electron beam generates backscattered electrons (BSED). The sample can

also emit characteristic X-rays as described in more detail in section 3.3.4 Energy Dispersive X-ray Analysis.

Secondary electron detection offers enhanced spatial resolution, so the particles examined appear well resolved. BSED detection is extremely useful, even though the resolution capability is reduced. It can demonstrate differences in atomic number based on direct contrast variation.

The initial stages for this research project involved preparing samples by fixing them directly onto a standard aluminium stub. This was achieved using a carbon adhesive pad. Because the samples are non-conducting materials, it was necessary to coat the surface with several nanometres of platinum / palladium to prevent electron beam charging issues. This was achieved using the Cressington 208 sputter coating unit (Cressington, 2021).

Principles of the Cressington 208 sputter coating unit

The sample is placed into a high vacuum chamber and pumped using a turbo-drag / rotary pump combination. Once the vacuum is better than 10^{-3} mbar, argon gas is leaked into the chamber. A potential is then applied between the Anode stage and the platinum/palladium Cathode, causing the argon gas to ionise, generating a plasma. The ionised argon gas interacts with the surface of the metal target, eroding small nanoparticles from the surface. Sputter coating is defined as a process that enables the deposition of a thin uniform coating onto the surface of the sample. Many metal targets are available depending on the user's specific requirements and budget such as silver, gold, gold/palladium, chromium, iridium platinum and platinum/palladium. For this research, platinum/palladium was chosen because it generates a uniform fine grain structure perfect for high resolution studies.

When working with moisture-sensitive materials, care had to be taken during the preparation to minimise exposure to air. The preparation involved cutting the microcapsule under the stereo microscope before quickly fixing to the SEM stub using a carbon adhesive pad. The sample was then transferred to the coating unit, and later to the microscope. This

procedure worked reasonably well, but the timescales of exposure to air would cause potential problems when working in the later stages with moisture-sensitive materials.

Part of this research involved designing a chamber that would allow the sample preparation for SEM analysis to be achieved, minimising any exposure to moisture from the atmosphere. In order to do this, a preparation device was fixed directly onto the side of the SEM sample chamber. This research would allow direct access to the microscope stage, minimising any exposure to air/moisture.

This involved fixing a used Oxford CT1500 cryo-preparation stage directly onto a high vacuum port hole of the Philips XL30 SFEG microscope chamber. The preparation stage allowed manipulation of the microcapsules whilst maintaining a dry vacuum environment. The chamber was fitted with a needle valve, allowing argon gas to be purged into the chamber whilst still under vacuum. The preparation chamber contained a scalpel knife that enabled the microcapsules to be cut open to allow access to the encapsulated particles. The preparation chamber was fitted with a sputter coating unit enabling the fractured microcapsule to be coated with a suitable metal such as platinum/palladium.

The prepared sample was transferred directly under vacuum into the high-vacuum microscope stage chamber for high resolution imaging. More details of this procedure will be given in section 4 of this thesis.

This research will hopefully demonstrate an effective and safe mechanism for preparing and transferring air-sensitive materials, avoiding any unwanted reactions due to moisture from the atmosphere.

3.3.4 Energy Dispersive X-ray Analysis (EDX)

This technique is associated with both SEM and TEM microscopes. It allows the user to obtain both qualitative and quantitative elemental information extremely quickly from the sample surface. The principle of EDX analysis is that the primary electron beam interacts

directly with the sample surface, producing X-ray photons. The generated X-rays have a characteristic energy (KeV) that enables peak identification based on respective X-ray energy levels (Bell & Garratt-Reed, 2003)

A greater understanding of the principles of EDX analysis is explained as follows:

A high energy electron beam can have enough energy to excite an inner electron from the atom. For the atom to return to a stable lower energy state, an outer electron from a greater energy shell will replace the vacant lower energy shell. This process generates a characteristic X-ray photon. The characteristic X-rays are linked directly to the energy generated based on the shell structure (Thermo Fisher Scientific, 2021). If an electron is ejected from a K-shell and is replaced from an L-shell electron, this generates a K-alpha photon. If a vacant K-shell is replaced by an M-shell electron, this would generate a K-beta photon.

Figure 3.3 is a simple schematic showing the process of X-ray generation. This technique was utilised extensively during this PhD to verify that the observed nanoparticles correlated with the materials put into the microcapsules.

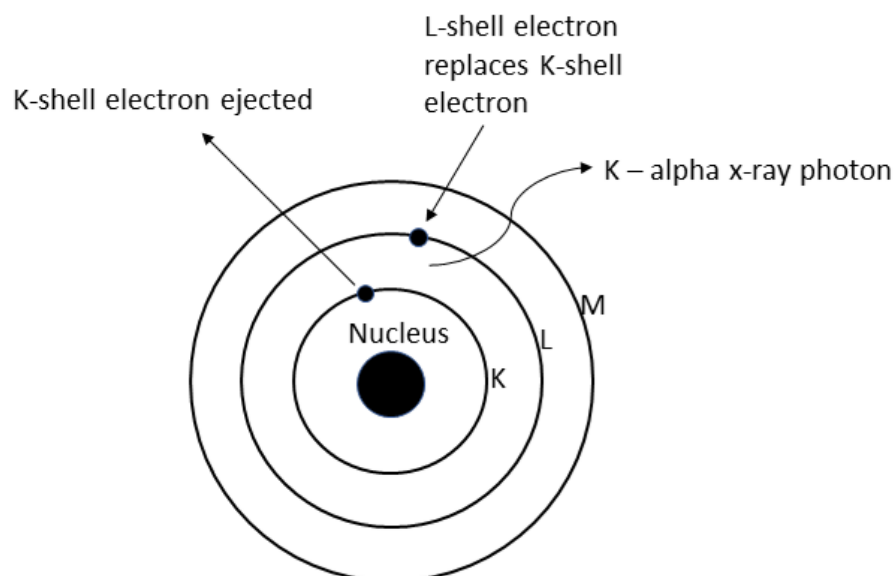


Figure 3.3 Atomic model of X-ray generation

3.3.5 Transmission Electron Microscopy (TEM)

The TEM utilised to examine samples for the purpose of this research was the JEOL JEM-2100 as shown in figure 3.4.

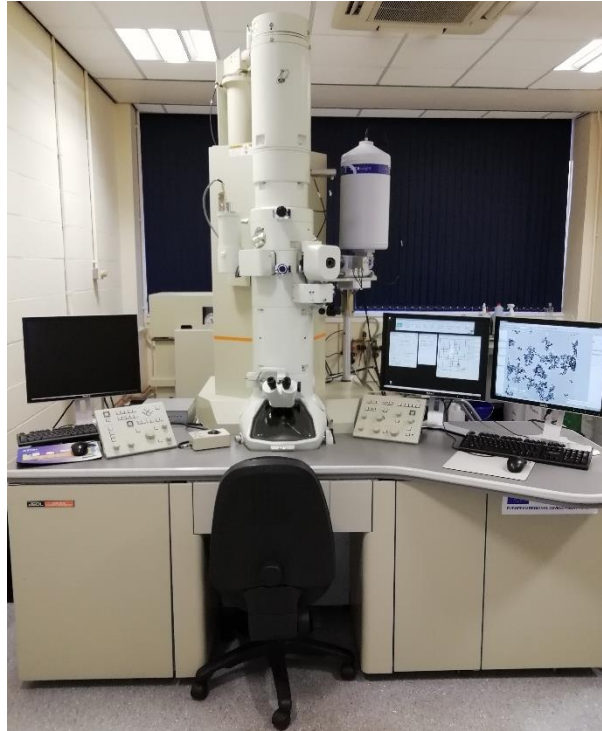


Figure 3.4 JEOL JEM-2100 Transmission Electron Microscope

Transmission Electron Microscopy (TEM) utilises a completely different method of electron beam interaction with the sample and detection system. The sample is located in the base of the objective lens in the path of the electron beam which passes through the sample. Subsequent magnification is achieved using a projector lens that produces an image which is viewed on a fluorescent screen (Chescoe & Goodhew, 1990). TEM micrographs traditionally were recorded directly onto photographic film, which produced excellent micrographs but was very time consuming. The JEOL JEM-2100 incorporates a GATAN Orius cooled CCD camera that allows instant capture allowing digital storage of the micrographs (Gatan, 2021)

A schematic of the cross-section of the JEOL JEM-2100 column is given in figure 3.5 demonstrating the complex array of electromagnetic lenses and coils that are used to obtain a suitable TEM micrograph (JEOL, 2021).

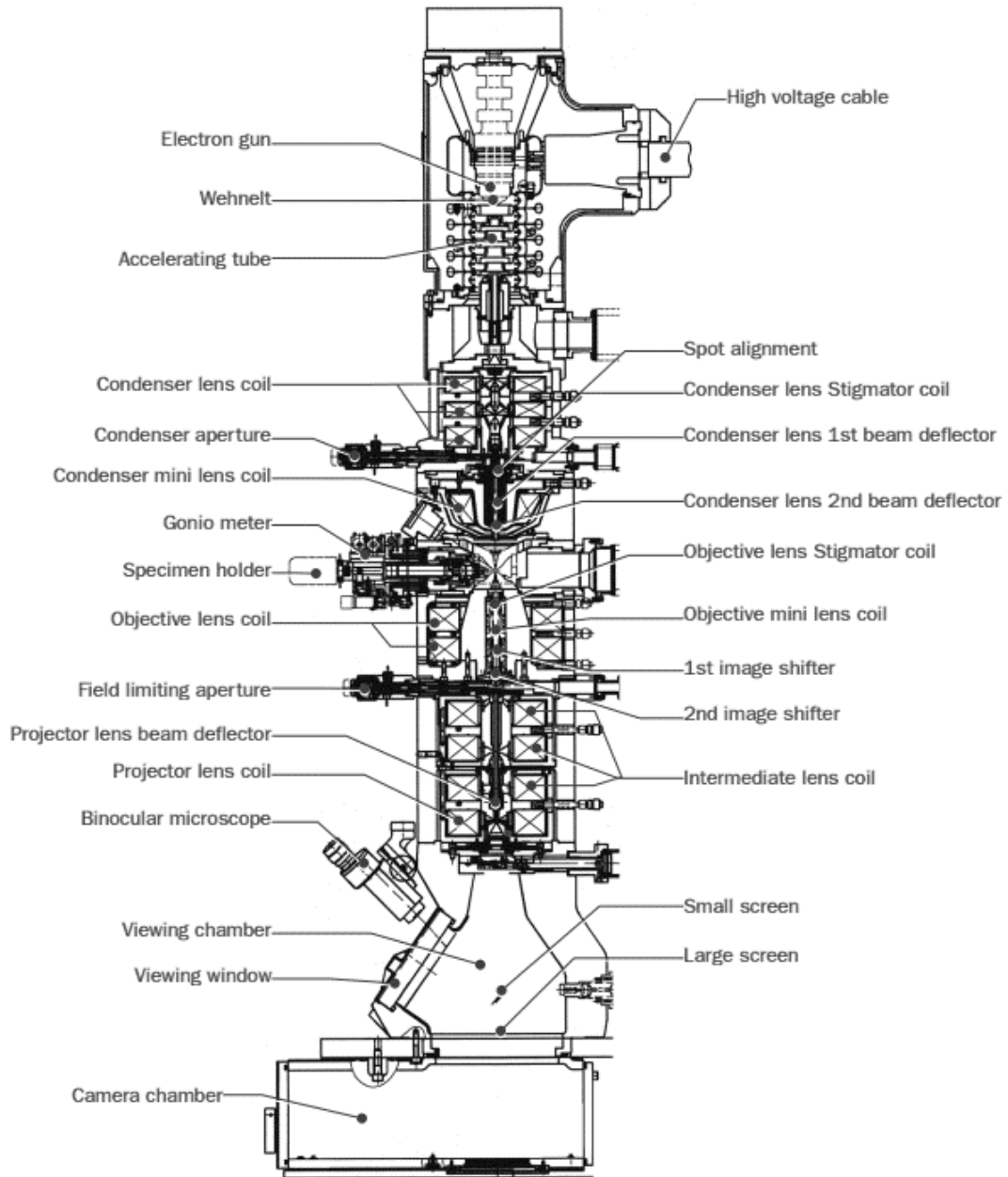


Figure 3.5 Cross-section of JEOL JEM-2100 column

A limitation to the use of TEM is the difficulty of sample preparation techniques. Samples need to have a thickness (preferably less than 100nm) to allow the electron beam to penetrate through the sample in order to generate an image. Using the TEM for the characterisation of nanoparticles is challenging as the particles would need to be well dispersed with limited aggregates to maintain the required sample thickness to allow good imaging. Any materials examined would also need to withstand the high vacuum conditions within the microscope column.

One advantage of using TEM for the study of small nanoparticles is that the instrumentation has the capability of generating high quality micrographs which demonstrate both shape and size of primary nanoparticles. Unlike the SEM, it does not allow the sample to be purged with an inert gas. However, once the sample is held in the column, it is thought that the high vacuum should help keep air/moisture-sensitive materials stable.

Preparation, as with the SEM, can be difficult with moisture-sensitive materials. Techniques involving the use of non-aqueous solvents can help generate uniform dispersions of the particles. In general, basic sample preparation involves allowing a small droplet of the dispersion to dry down onto a carbon coated TEM grid. Ideally, for moisture-sensitive samples, this would be best performed within a nitrogen glove box. To do this using a glove box would be difficult as it requires a great deal of dexterity. The TEM grid would then require fixing to the holder and this would have to be completed outside of the glove box due to the small screws that require tightening to hold the grid in-place. Transfer of the prepared TEM grid should be completed as quickly as possible to minimise contact with moisture from the air.

The sample preparation for moisture-sensitive materials would always be very difficult. Preparation is invariably going to leave doubt as no matter how quickly the material is transferred, the particles will still be subject to moisture from the air.

Due to this reason, it was decided that TEM would not be suitable for moisture-sensitive samples prepared during this project. Utilising the preparation chamber interfaced to the SEM was clearly the best approach for characterising moisture-sensitive nanoparticles.

4 Results and Discussion

Chapter Overview

The specific experimental details used to develop the microcapsules are presented in this chapter.

Chapter Contents

4.1	Encapsulation of Titanium Dioxide (TiO₂)	63
4.1.1	Encapsulation of TiO ₂ within Cellulose Acetate Phthalate (CAP).....	63
4.1.2	Encapsulation with Polysulfone (PSF)	73
4.2	Encapsulation of Lithium Carbonate (Li₂CO₃)	85
4.3	Encapsulation of Lithium Phosphate (Li₃PO₄).....	122
4.4	Encapsulating Moisture-Sensitive Lithium Amide (LiNH₂).....	137
4.5	Encapsulation of Sodium Borohydride (NaBH₄).....	146
4.5.1	Characterisation of Sodium Borohydride Primary Particles.....	155
4.5.2	Preparation Chamber Facilitating Sample Manipulation Under Vacuum.....	163
4.6	An Investigation into the Stability of Sodium Borohydride (NaBH₄).....	248

4.1 Encapsulation of Titanium Dioxide (TiO₂)

4.1.1 Encapsulation of TiO₂ within Cellulose Acetate Phthalate (CAP)

The initial objective was to demonstrate that it was viable to encapsulate nanoparticles of TiO₂ within a polymer microcapsule. Once this had been achieved, the research was developed further towards working with lithium salts and reactive metal hydrides such as lithium amides and sodium borohydride.

As a benchmark, the initial experimental conditions were analogous to those outlined in the non-solvent addition technique, as described in the encapsulation of paracetamol (Nokhodchi and Farid, 2002).

Different ratios of TiO₂ to CAP polymer were evaluated from 1:1, 1:2, 1:4 and 2:1. It was found that the experimental conditions which produced the best microcapsules were those used for the 1:2 ratio of TiO₂ to CAP as outlined in method 1, section 3.2.

1:1 Ratio of TiO₂ to CAP Polymer in Acetone

The first synthesis was based on using an equal ratio of CAP polymer to inorganic TiO₂ nanoparticles. The procedure for the experiment is outlined in method 1, except the concentration of TiO₂ was increased.

The SEM micrographs as shown in figure 4.1 were obtained using the FEI Quanta 250. The micrographs demonstrate that the polymer morphology was non-uniform, existing as clumps of polymer / TiO₂ rather than spherical microcapsules.

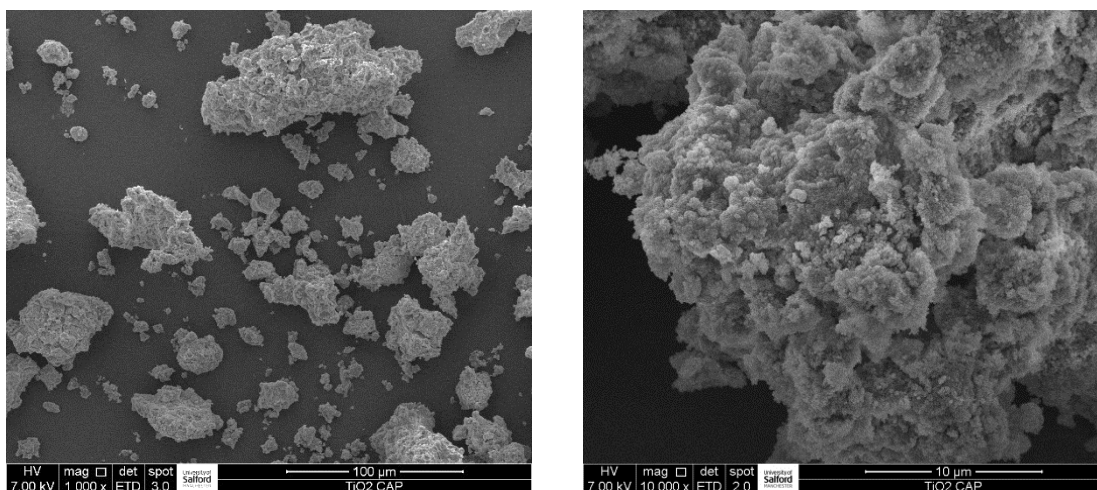


Figure 4.1 SEM micrographs of 1:1 CAP-TiO₂ microcapsules

In order to assess if any titanium dioxide nanoparticles had been encapsulated by the CAP, the internal structure of the polymer system was examined using high resolution TEM. To achieve this, a very thin cross-section $\sim 100\text{nm}$ of the CAP/TiO₂ particle was required. The thickness of the cross-section is very important, to enable the high energy electron beam to penetrate through the sample.

Sample preparation involved initially embedding a small amount of the generated polymer microcapsule into Loctite 358 UV curing resin. The resin was cured under UV light and washed with IPA solvent to clean off any residual monomer. The resin block was trimmed using a razor blade, then cut using the Reichert Ultracut E microtome to generate 100nm wafer-thin cross-sections of the CAP-TiO₂ microcapsule (Ranner and DeRose, 2022). The cross-sections were floated onto water and collected using a formvar-carbon 200 mesh copper TEM grid.

Figure 4.2 represents the resulting TEM micrographs obtained from both the initial primary particles of TiO₂ ex Aldrich together with the cross-sectioned CAP-TiO₂ microcapsule.

The micrographs were generated using the JEOL JEM 2100 TEM and captured using a GATAN Orius SC200 Digital Camera. The conditions of analysis utilised an accelerating voltage of 200kV together with a system magnification of 20,000x.

The Aldrich TiO_2 primary particles are seen to exist as irregular-shaped particles, with the majority having a size range below 50nm.

The TEM micrograph obtained from the cross-sectioned CAP- TiO_2 demonstrates that the TiO_2 nanoparticles are encapsulated by the polymer, as a coating is seen to exist around the particles. These results, however, do not represent a spherical capsule containing a shell wall with an internal core shell (Vasisht, 2014).

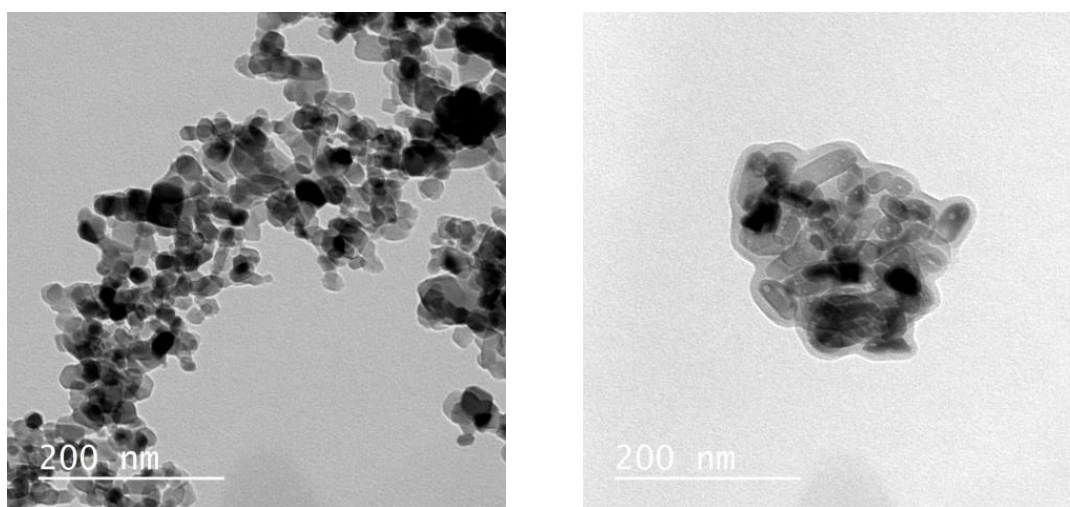


Figure 4.2 TEM micrographs of TiO_2 primary particles and 1:1 ratio microcapsule

2:1 Ratio of TiO_2 to CAP Polymer in Acetone

In an attempt to improve on the generation of spherical microcapsules, the mass ratio of the TiO_2 to polymer was changed. The experimental conditions involved using a 2:1 ratio of TiO_2 to CAP polymer. These changes were based on experimental trial and error. Figure 4.3 represents a light micrograph obtained from the resulting CAP- TiO_2 microcapsules using the Zeiss ZV8 stereo microscope (Zeiss, 2021). The light micrograph shows that the resulting microcapsules exist as elongated particles.



Figure 4.3 Light micrograph of 2:1 ratio microcapsule

The higher magnified SEM micrographs, figure 4.4, were obtained using the FEI Quanta 250 with system magnifications of 150x and 10,000x respectively. These micrographs demonstrate that the surface of the polymer is not continuous - exposing many of the TiO_2 nanoparticles. These results suggest that the 2:1 ratio is not ideal and would cause problems if the TiO_2 nanoparticles were substituted by reactive metal hydrides.

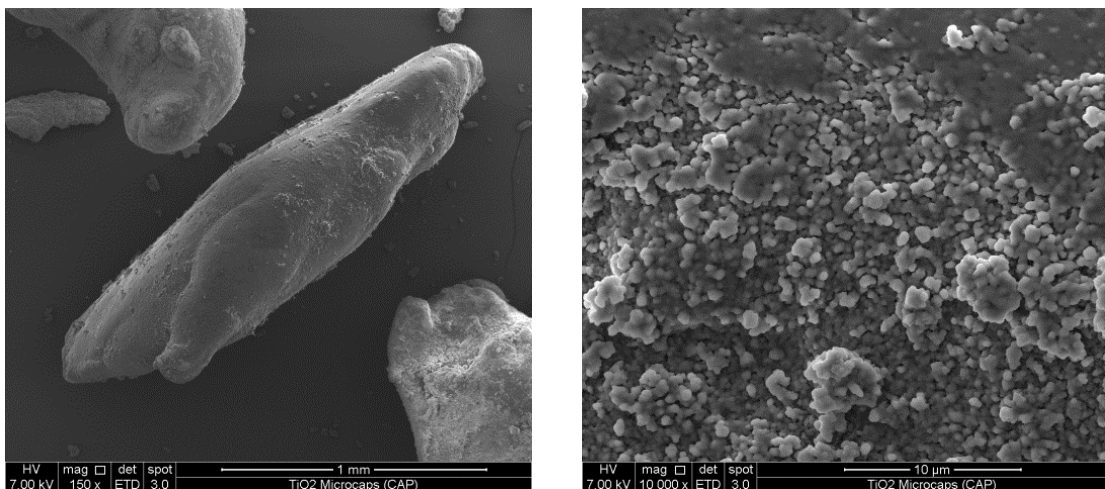


Figure 4.4 SEM micrographs of 2:1 ratio microcapsule

1:2 Ratio of TiO_2 to CAP Polymer in Acetone

Increasing the polymer concentration significantly improved the morphology, generating excellent spherical microcapsules. Figure 4.5 shows a light micrograph obtained from the spherical microcapsules, created using a 1:2 ratio of TiO_2 / CAP.



Figure 4.5 Light micrograph of 1:2 ratio microcapsules

The microcapsules are seen to exist as spheres with a particle size range between 100-400 μm.

The microcapsules were further examined using the FEI Quanta 250 Scanning Electron Microscope to obtain high resolution micrographs of the surface structure. Figure 4.6 demonstrates that the TiO₂ nanoparticles have been encapsulated within the spherical polymer structure.

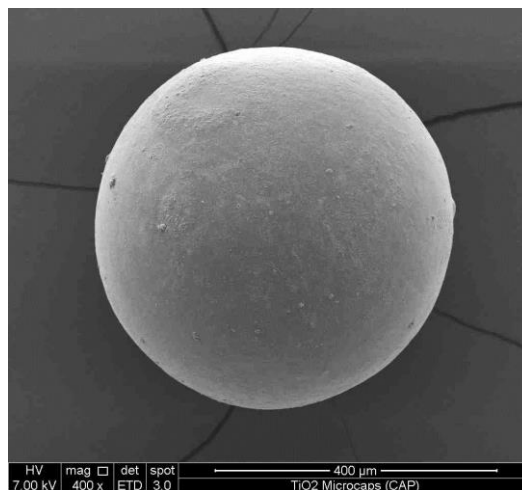


Figure 4.6 SEM micrograph of 1:2 ratio microcapsule

The internal structure of the microcapsule was examined using high resolution SEM to obtain information relating to the polymer wall structure and position of the TiO₂ nanoparticles.

To examine the internal structure, a microcapsule was initially exposed to liquid nitrogen. The microcapsule was then fractured open by applying shear to the surface. The SEM micrographs figure 4.7 represent the fractured internal structure. They clearly display that the polymer wall is solid and the TiO₂ nanoparticles are clustered together within the core of the microcapsule.

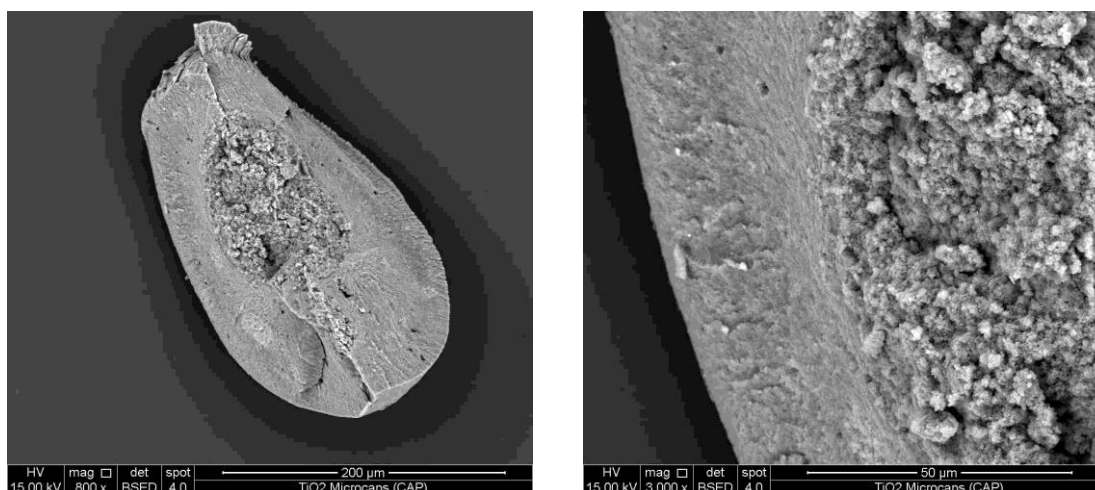


Figure 4.7 SEM micrographs from fractured 1:2 microcapsules

In addition to fracturing the polymer, the sample was embedded into Buehler epoxy resin. The resin was allowed to cure for 24 hours in an oven set at 40°C. Once the resin had cured, 100nm cross-sections of the microcapsules were obtained using the Reichert Ultracut E microtome.

The cross-sections were collected onto formvar/carbon 200 mesh copper TEM grids. The resulting TEM micrographs as shown below in figure 4.8 were obtained using the JEOL 2100 TEM - using a system magnification of 2000x and an accelerating voltage of 200kV. The resulting TEM micrographs verify that the bulk of the TiO₂ particles are encapsulated mainly within the polymer. A polymer wall is seen to be present with a thickness of approximately 2μm. These results indicate that the CAP polymer completely encapsulated the TiO₂ nanoparticles.

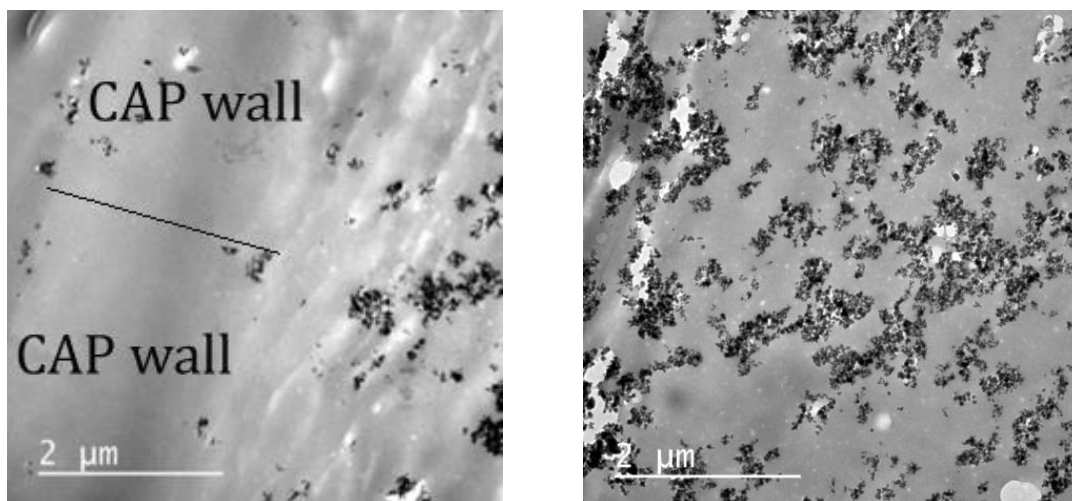


Figure 4.8 TEM micrographs from a cross-section of 1:2 ratio microcapsules

Substituting Acetone for THF

The initial concept to encapsulate small nanoparticles of titanium dioxide within a polymer microcapsule was proven to be successful. The results from the method using a 1:2 ratio produced very good microcapsules. When examined using both TEM and SEM, the resulting micrographs verified that a solid polymer wall had encapsulated the TiO₂ nanoparticles.

However, changes to the experimental conditions were necessary to prepare for the encapsulation of moisture-sensitive metal hydrides. The initial solvent acetone (used to dissolve CAP) can contain water and is very difficult to dry, so it was crucial to find an alternative non-protic solvent to replace the acetone. Due to the high reactivity of metal hydrides with moisture, the quantity of material used in the experimental procedure was also scaled down by a factor of 10.

1:2 Ratio of TiO₂ to CAP Polymer in THF

Acetone was replaced by the non-protic solvent THF, and the quantity of material used was scaled down by a factor of 10 as outlined in method 2.

The light micrograph, figure 4.9, shows that the procedure did not work. The final product did not form spherical microcapsules but existed as a large deposit of an irregular-shaped polymer cluster.



Figure 4.9 Light micrograph of 1:2 ratio of CAP-TiO₂ using THF

At this stage of the project, it was not possible to justify why the experimental conditions did not generate spherical microcapsules. The new conditions involved substituting the PET solvent from acetone to THF and the materials used in the experiment were scaled down by a factor of 10. In an attempt to improve the microcapsule formation, the experimental conditions were changed, incorporating a greater ratio of polymer to inorganic.

1:4 Ratio of TiO₂ to CAP Polymer in THF

The light micrograph as shown below in figure 4.10 represents the final product. Only a string-like precipitate can be seen, with no formation of small spherical microcapsules.

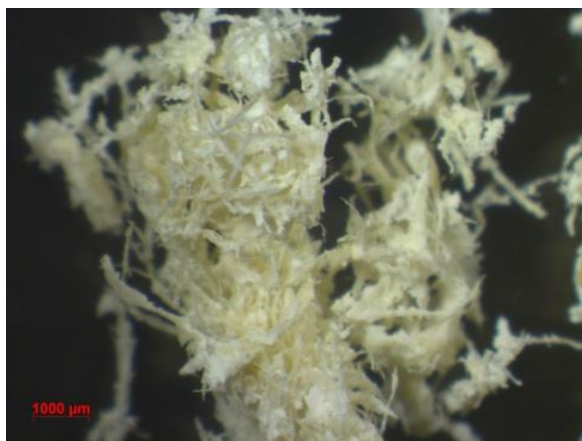


Figure 4.10 Light micrograph of 1:4 ratio using THF

These results outline that THF (as a replacement for acetone) was not the right solvent for this experimental procedure. In an endeavour to find a more robust/suitable solvent system, different combinations of both non-solvent and polymer solvent were sought.

Substituting THF by Acetonitrile

1:4 Ratio of TiO₂ to CAP Polymer in Acetonitrile

To improve on the generation of microcapsules, some modifications were made in this experimental procedure. The THF used to dissolve the CAP was substituted by acetonitrile, and cyclohexane was substituted for chloroform as the non-solvent. The same experimental conditions were performed with a ratio of 1:4 as outlined in method 4. After the addition of the non-solvent, cyclohexane, the mixture rapidly formed a precipitate and - after air drying - produced a hard, flat block of polymer as shown below in figure 4.11.



Figure 4.11 Light micrograph of 1:4 ratio using acetonitrile

Back to the Initial Starting Materials

1:4 Ratio of TiO₂ to CAP Polymer in Acetone

In order to understand what was causing the continuous failure during the experimental procedure, it was thought best to return to the original solvents as outlined in method 5. However, using a mixture of 1:4 CAP in acetone with cyclohexane as the non-solvent also produced poor results.

The end-product was an amorphous clump that was mainly fixed to the sides of the 250ml round-bottomed flask as shown below in figure 4.12.



Figure 4.12 Image of 1:4 ratio using acetone

The new scaled-down experimental conditions were not generating microcapsules whatever the combination of solvents. Because the quantities used were scaled down by a factor of 10, it was thought that too much energy was being generated from the agitation stirrer paddles. The hypothesis was that the stirrer paddles were too large for the flask, and the high speeds used for agitation were causing the polymer to degrade.

1:4 Ratio of TiO₂ to CAP using Acetone and Smaller Stirring Paddles

In an attempt to resolve this issue, the 90mm stirrer paddles were cut down to a smaller size of 40mm. The 1:4 ratio of TiO₂ to CAP experiment was carried out again using a slower agitation speed of 640rpm, and the non-solvent cyclohexane was substituted for chloroform as outlined in method 6.

The results were very good as the new experimental conditions created small spheres as shown below in figure 4.13.

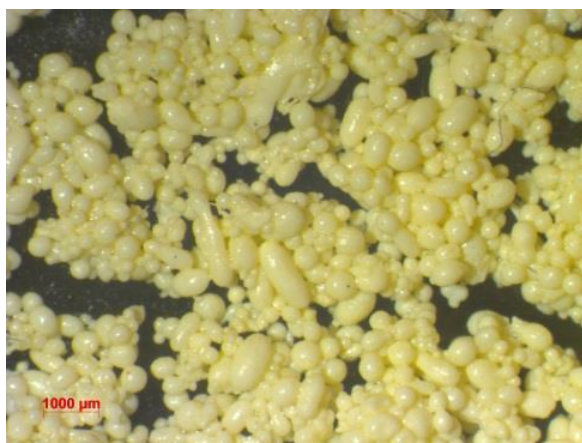


Figure 4.13 Light micrograph of 1:4 ratio microcapsules

4.1.2 Encapsulation with Polysulfone (PSF)

One concern with using CAP as the main polymer is that the structure contains some free hydroxyl groups. CAP is effectively a cellulose-based polymer, where approximately half of

the hydroxyls are esterified with acetyl groups. In addition, approximately a quarter are esterified with carboxyl groups of a phthalic acid as shown in figure 4.14.

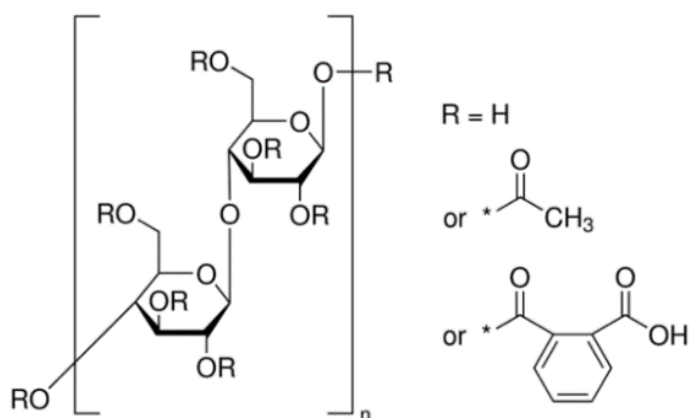


Figure 4.14 Structure of cellulose acetate phthalate – Sigma-Aldrich

As metal hydrides react with hydroxyl groups, on reflection it was necessary to change the CAP polymer. After careful consideration and research into different polymer structures, it was decided that Polysulfone (PSF) would be a more useful polymer for the encapsulation of metal hydrides, as it does not contain any hydroxyl or amine groups - as shown in figure 4.15.

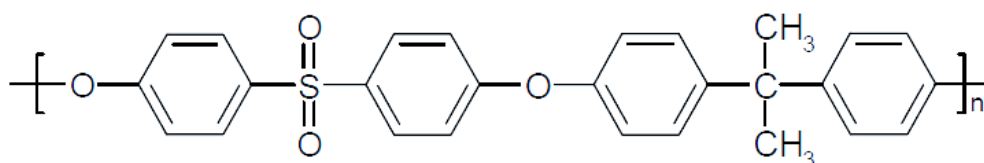


Figure 4.15 Structure of polysulfone - Sigma-Aldrich

Consultation with the literature together with some preliminary experimentation revealed that the best solvents for the dissolution of PSF were dimethylformamide (DMF), (Guillen et al., 2013) and 1-methyl-2-pyrrolidone (NMP), (Kim et al., 2000).

The same experimental procedure was executed as previously outlined in method 6, but this time the CAP polymer was substituted for PSF and acetone was replaced with DMF.

1:4 Ratio of TiO₂ to PSF Polymer in DMF

Problems occurred in following the method as outlined in method 7. It was observed that upon addition of the non-solvent chloroform, the polymer formed the amorphous precipitate, as shown below in figure 4.16.



Figure 4.16 Image of PSF polymer TiO₂ precipitate

Polymer Solution Addition to Liquid Paraffin

To understand the effect of the liquid paraffin on the behaviour of the PSF solution, the procedure as given in method 8 was followed, excluding the TiO₂ nanoparticles.

The polymer solution was added slowly to the liquid paraffin only. It appeared that the PSF remained in solution.

To expand on the understanding of the experimental design, 20ml of the non-solvent - chloroform - was slowly added to the mixture over 20 minutes with an agitation speed of 300rpm.

Initially the polymer appeared to show signs of forming capsules as shown in figure 4.17, but on further addition of the 30ml of chloroform, the polymer crashed out of solution.



Figure 4.17 Image of liquid paraffin - PSF polymer

The above experiment demonstrates that PSF does not appear to follow the same behaviour as CAP. On consideration, it was thought that perhaps the PSF polymer may be incompatible with the use of liquid paraffin. To confirm this assumption, a new experiment was designed removing liquid paraffin from the procedure.

New Procedure to Generate Microcapsules in the Absence of Liquid Paraffin

In addition, after completing some basic dissolution studies appeared to demonstrate that PSF was slightly more soluble in 1-methyl-2-pyrrolidone (NMP) than DMF so NMP was used from this point on as the polymer-soluble solvent.

To understand the formation of spherical microcapsules in greater detail, a simple experiment was performed. 1g of PSF was dissolved into 20ml of NMP using a 50ml conical flask and an IKA yellow line magnetic stirrer on spin setting 4. Once the PSF had fully dissolved, small droplets of the polymer solution were introduced into a beaker containing water using a glass pipette. Water was the chosen non-solvent at this stage of the experiment as it was recognised that PSF instantly dropped out of solution when exposed to water. It was thought that the insoluble nature of the PSF solution with water was linked to the high polarity of water (Hořda & Vankelecom, 2015). Water would never be acceptable for the encapsulation of metal hydride particles but was utilised in this instance to aid with the study of the generation of spherical microcapsules (Torras et al., 2006).

It was observed that when the PSF solution entered the water, the polymer did not form a sphere but simply dropped out of solution, forming a flat thin layer.

To understand the interaction of the polymer solution with water and improve the generation of spherical microcapsules, changes to the experimental design were necessary. Different concentrations of PSF solutions were generated using NMP as the solvent. Using a glass pipette, small droplets of the various concentrations of PSF solution were dripped into small vials containing water. The results from this simple experiment showed that the higher concentrated polymer solutions formed small spheres almost immediately upon entering the water, that was acting as the non-solvent.

This was very interesting as the question arose of why the higher concentration of PSF would generate a perfect sphere on entering the non-solvent (Gong et al., 2006). Perhaps this could be a surface tension and/or cohesion effect?

To move forward with this new approach, an alternative non-solvent was required for this research as water is protic and known to react violently with metal hydrides. After experimenting with different solvent systems, it was ascertained that acetonitrile was a good substitute for water because it is aprotic and generated small spheres from the addition of droplets of PSF polymer solution.

Acetonitrile is a solvent that has a polarity index of 5.8 and a density of 0.781(g/mL). It appears to generate spheres in the same way as water which has a relative polarity of 10.2 and a density of 1(g/mL), (Fischer Scientific, 2021). It is an aprotic solvent so will not cause unnecessary reactions when exposed to metal hydrides.

Microcapsule Formation Using PSF

The procedure given in method 9 involved slowly adding small droplets of the PSF-TiO₂ dispersion into a small conical flask containing 30ml of acetonitrile. This simple method produced promising results. Figure 4.18 displays the spherical structure of the generated microcapsules.



Figure 4.18 Image of PSF polymer microcapsules

The internal morphology of a microcapsule was examined using high resolution SEM. A cross-section of a single microcapsule was obtained by initially cooling the particle under liquid nitrogen. Once frozen, the polymer was sliced into 2 parts using a cold razor blade. The cross-sections were then mounted onto a standard aluminium SEM stub using a double-sided carbon adhesive pad. The surface of the cross-sectioned sample was coated with 4nm of platinum/palladium using the Cressington 208 sputter coating unit. SEM micrographs were obtained using the FEI Quanta 250. The resulting SEM micrographs, figure 4.19, were obtained using system magnifications of 100x and 1000x respectively. The micrographs reveal that the internal morphology of the microcapsule has a solid outer wall, with a honeycomb inner structure. Using Back Scattered Electron Detection (BSED), the TiO_2 nanoparticles are represented on the micrographs as the bright high-contrast regions.

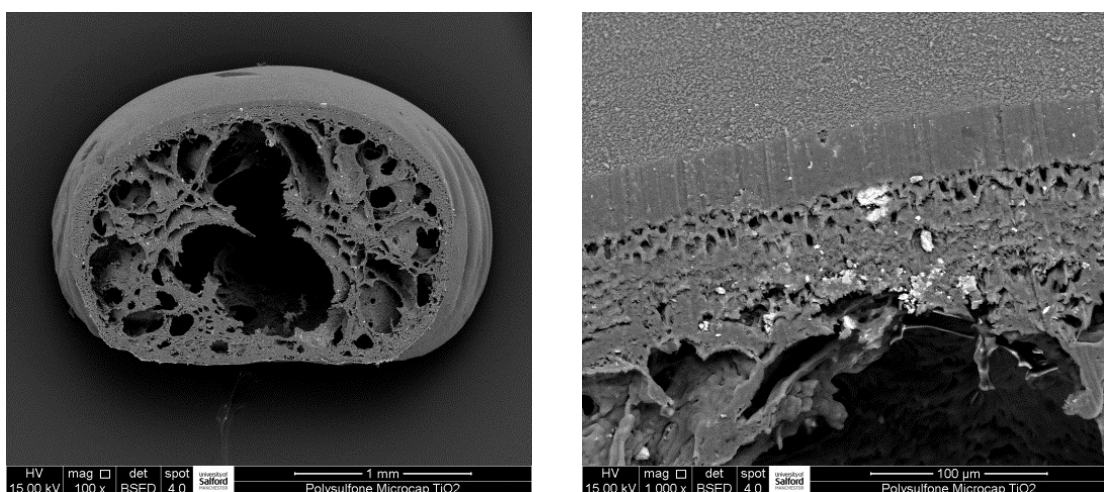


Figure 4.19 SEM micrographs from cross-sectioned PSF- TiO_2 microcapsule

These results suggest that most of the TiO_2 particles appear within the inner region of the microcapsule. Further efforts to improve the quality of the microcapsules required changes to the methodology. This included changing the concentration of the polymer and experimenting with different non-solvent blends. The target was to achieve a microcapsule with a robust non-porous outer wall structure and a porous internal structure. The ideal microcapsule would encapsulate all the metal hydride particles within the sealed polymer capsule.

Generation of TiO_2 Microcapsules Using PSF

The parameters as outlined in method 10 are a modification to the initial experimental design described in the previous method 9. These modified changes were aimed at improving the structure of the microcapsule.

The generation of spherical microcapsules involved slowly releasing small droplets of the PSF- TiO_2 dispersion into a non-solvent blend of acetonitrile/hexane 70:30 using a metal needle and plastic syringe. The use of different solvents would hopefully allow the microcapsules to be modified by varying the ratio of the non-solvent blend.

The generated microcapsules were examined using the FEI Quanta 250 and the micrographs obtained from a cross-sectional area are presented in figure 4.20.

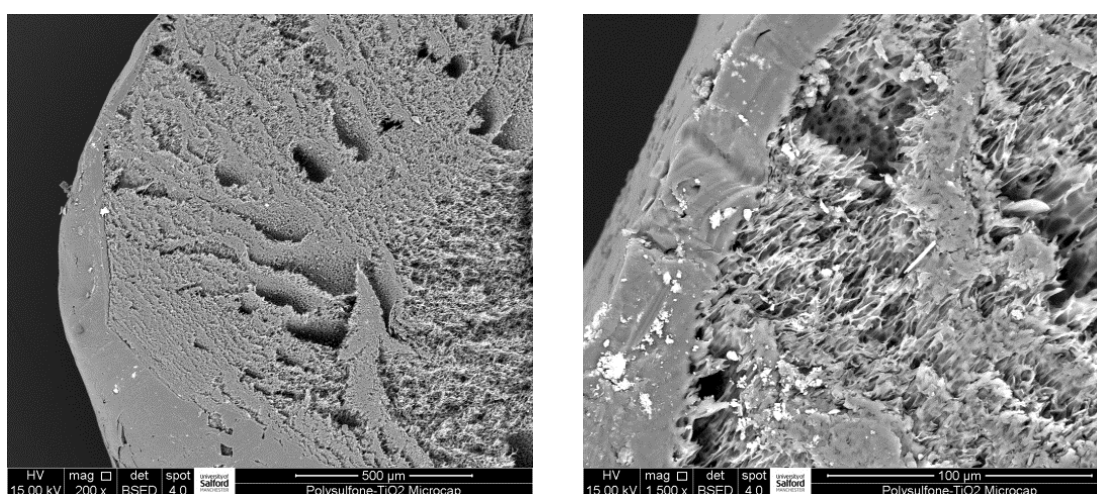


Figure 4.20 SEM cross-sectioned PSF- TiO_2 microcapsule - acetonitrile/hexane 70:30

The SEM micrographs were obtained using system magnifications of 200x and 1500x respectively. They demonstrate that the PSF-TiO₂ microcapsules have a solid outer wall with a very fine porous internal morphology. Many TiO₂ particles are seen to exist within the outer wall structure of the microcapsule.

This type of internal microcapsule structure is not ideal as it would cause issues when looking for small, encapsulated particles. The ideal target would be to produce a hollow internal microcapsule structure. The particles seen to exist within the outer wall could be due to a smearing issue from the cut. If the TiO₂ nanoparticles were present in the outer wall, this would not be an ideal situation for metal hydride materials.

Changing the Non-Solvent Blend to a Mixture of Acetonitrile/Hexane 50:50

To evaluate the suitability of using hexane as part of the non-solvent blend, the concentration was increased to a 50:50 mixture of acetonitrile/hexane.

The same PSF-TiO₂ polymer dispersion used for the previous sample was placed into a 10ml plastic syringe and connected to a metal needle. Small droplets of the dispersion were released into a 250ml flask containing 20ml acetonitrile and 20ml hexane. During the addition of the dispersion, the solvent blend was agitated using a drill speed setting of 350rpm.

After formation, the microcapsules were then stirred for an additional hour before the solvent was decanted off and the microcapsules air-dried.

The generated microcapsules were characterised using the high-resolution FEI Quanta 250.

Preparation involved initially slicing a microcapsule into 2 parts using a razor blade. The cross-sections were then mounted onto a standard SEM stub using a carbon adhesive pad. The surface of the cross-sectional area of the microcapsule was coated with 4nm of platinum/palladium using the Cressington 208 coating unit.

The resulting SEM micrographs, figure 4.21, illustrate that the microcapsule has a semi-porous internal structure enclosed within a thin outer wall. The cut from the razor blade has caused some smearing of the polymer due to the soft and delicate nature of the microcapsules. Clusters of the TiO_2 nanoparticles are seen to be present towards the outer edge of the microcapsule.

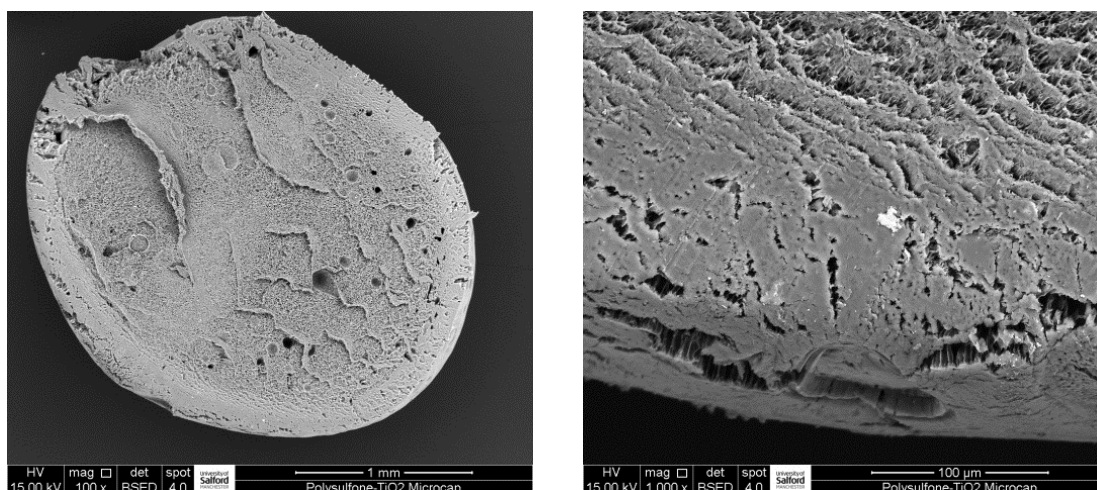


Figure 4.21 SEM-cross-sectioned PSF- TiO_2 microcapsule - acetonitrile/hexane 50:50

The surface of a microcapsule was also examined using high resolution SEM. Preparation involved placing the microcapsule directly onto a double-sided carbon adhesive pad. The particles were then sputter-coated with 4nm of platinum/palladium.

The surface SEM micrographs, figure 4.22, were acquired using system magnifications of 100x and 10,000x respectively. The micrographs demonstrate that the surface is porous, exhibiting many cracks.

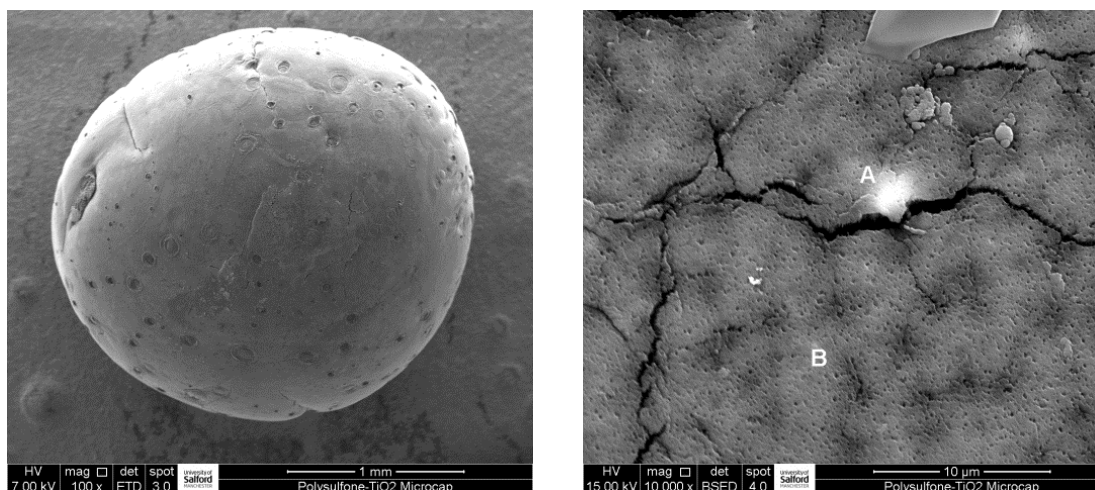


Figure 4.22 SEM surface micrographs- PSF-TiO₂ microcapsule - acetonitrile/hexane 50:50

The micrograph obtained using a system magnification of 10,000x displays an area of high contrast annotated with the letter 'A' and a low contrast area - marked as 'B'. The micrograph was acquired using BSED detection, which allows differences in atomic number to be observed based on direct contrast variation. The high contrast area 'A' was thought to represent a cluster of TiO₂ nanoparticles present at the surface. Both annotated areas were examined using the EDAX Genesis - Energy Dispersive X-ray analysis (EDX). The EDX microanalysis detector is interfaced directly onto the Quanta FEG 250 microscope. Figure 4.23 represents an overlay of the subsequent EDX spectra obtained from the analysis of each designated area. These results confirm that area 'A' is a cluster of TiO₂ nanoparticles, as the results revealed an increase in the levels of oxygen together with the detection of titanium.

These results denote that the experimental conditions chosen to generate the microcapsule would not be appropriate for air/moisture-sensitive metal hydride samples.

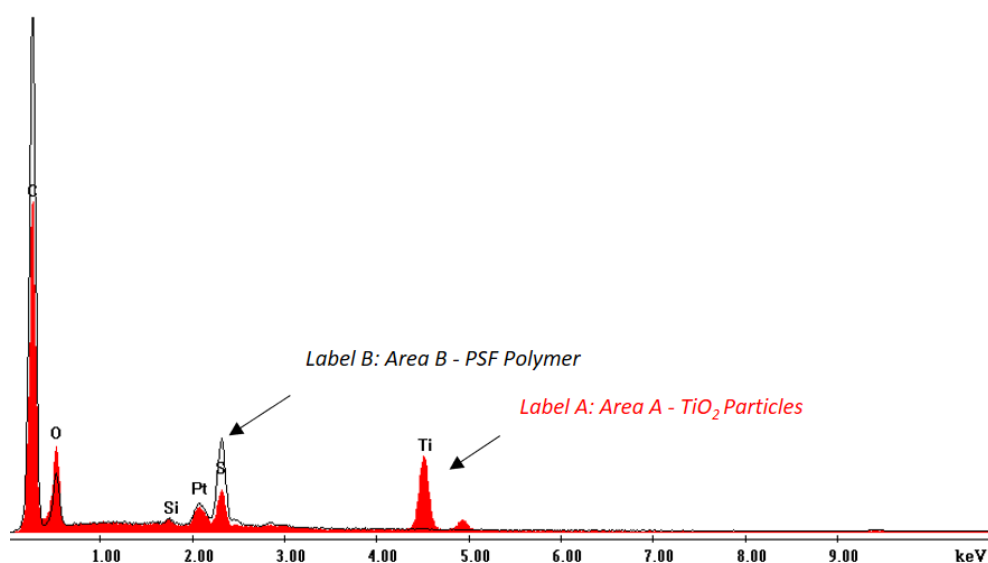


Figure 4.23 EDX spectrum overlay from areas 'A' and 'B'

Changing the Ratio of the Non-Solvent to 30:70 Acetonitrile/Hexane

To further understand the effects of introducing non-polar hexane into the non-solvent blend, the levels of hexane were increased to 30:70 acetonitrile/hexane. The same experimental procedure was followed using the higher concentration of hexane.

The microcapsules generated were stirred for a further 60 minutes before the solvent was decanted and the microcapsules air-dried.

Using the FEI Quanta 250, SEM micrographs were obtained for the internal structure of a microcapsule, prepared by slicing open with a razor blade.

The SEM micrographs, figure 4.24, were obtained from the internal structure of a microcapsule using system magnifications of 1000x and 10,000x respectively. They reveal a porous honeycomb internal morphology. The pore size of the honeycomb structure is seen to reduce towards the outer edge of the microcapsule. Interestingly, the outer regions of the microcapsules display an array of narrow channels that are present in a variety of sizes up to 100 μ m in length.

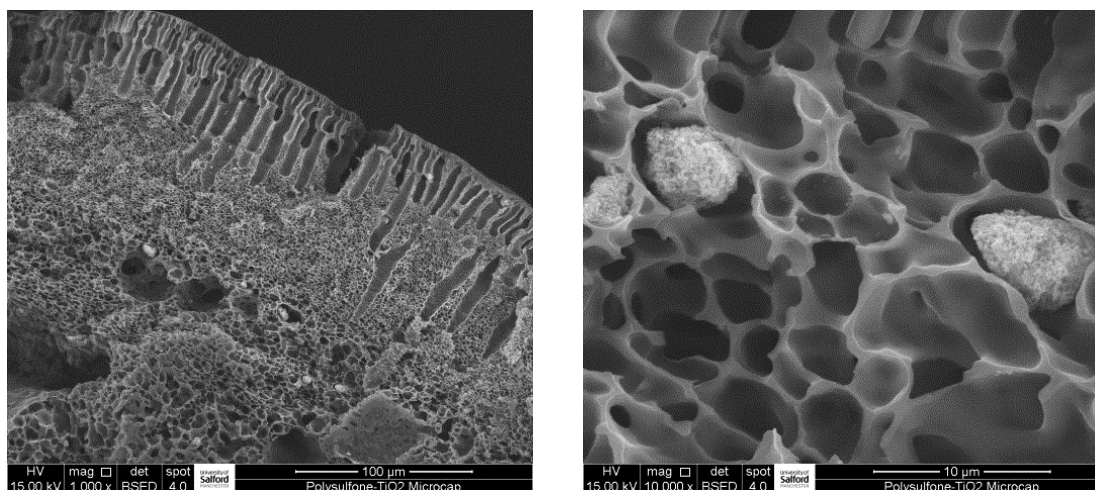


Figure 4.24 SEM micrographs from cross-sectioned PSF-TiO₂ microcapsule

The SEM micrograph obtained at 10,000x displays clusters of TiO₂ nanoparticles to be present within the internal pores of the microcapsule.

These SEM micrographs support the theory that modifying the non-solvent blend can have a dramatic effect on the internal morphology of the generated microcapsules.

The formation of the microcapsule is based on a phase inversion process. This involves a diffusion process between the PSF polymer solution and the non-solvent. When droplets of the PSF polymer solution enter the non-solvent of the polymer, a diffusion process takes place. The concentration of the PSF solvent decreases, while the concentration of the non-solvent increases. The PSF solution reaches a thermodynamically unstable region which ultimately causes the polymer to precipitate (Pena and Gumi, 2013).

Polysulfone has been widely used as a polymer for producing microfiltration and ultrafiltration membranes, based on the process of phase inversion by means of immersion precipitation. Interestingly, the observed internal membrane morphology is analogous to the internal structure of the microcapsules produced for this research (Hotda & Vankelecom, 2014).

The formation of the porous internal structure containing the larger conical-shaped voids are often referred to as macrovoids. These are regularly observed in diffusion induced phase

separation membranes. The mechanism of formation of the macrovoids has long been a controversial subject (Wienk et al., 1996). It is thought that the internal porous structure is initiated by surface tension gradients or mechanical stresses. However, other researchers (Broens et al., 1980) suggested that the internal structure is formed by the abnormal growth of nuclei, because the influx of the non-solvent is so small, that the growth of the macrovoid can keep pace with the phase separation induced by the non-solvent.

The internal structure of the cross-sectioned PSF microcapsules have an appearance that is analogous to the membranous structures associated with the rapid freezing process as part of the preparation for cryo-SEM. If a polymer gel is plunged into a slush of liquid nitrogen, the rapid freezing can generate a structure that is observed after fracturing and sublimation of the water phase under vacuum (Sriamornsak et al., 2008).

4.2 Encapsulation of Lithium Carbonate (Li_2CO_3)

The objective for this research was to generate a polymer microcapsule that would be capable of encapsulating reactive metal hydride particles. One area of interest was to encapsulate LiNH_2 as this would extend the previous documented research (Baldissin et al., 2013).

This new experimental method was designed to study the behaviour of non-reactive salts with similar properties to LiNH_2 . This experimental procedure involved substituting TiO_2 nanoparticles for lithium carbonate (Li_2CO_3), Sigma-Aldrich.

The aim was to continue with the research of evaluating different combinations of non-solvent mixtures to achieve the best conditions for generating the microcapsules and determine the effect of changing the material to be encapsulated.

This section of the thesis covers a series of experiments that involved encapsulating Li_2CO_3 into a PSF polymer microcapsule. Many changes needed to be made to the non-solvent system, with the aim of improving the final microcapsule structure.

A new, improved, quality system was introduced that allowed traceability of the created microcapsules. Therefore, from this stage in the project, all samples generated are classified numerically, starting at 1.

The PSF polymer was dissolved into NMP followed by the addition of Li_2CO_3 as outlined in method 11 to generate a suitable PSF- Li_2CO_3 dispersion.

Encapsulating Li_2CO_3 in PSF – Acetonitrile – Sample 1

The PSF- Li_2CO_3 dispersion was dripped slowly using a 10ml plastic syringe and a metal needle into a 250ml round bottomed flask containing 30ml of acetonitrile. The acetonitrile was stirred using an agitation speed of 235rpm.

The resulting microcapsules generated from this experiment were examined using the FEI Quanta 250. The SEM micrographs, figure 4.25, were obtained using an accelerating voltage of 3kV and secondary electron detection to show the surface morphology.

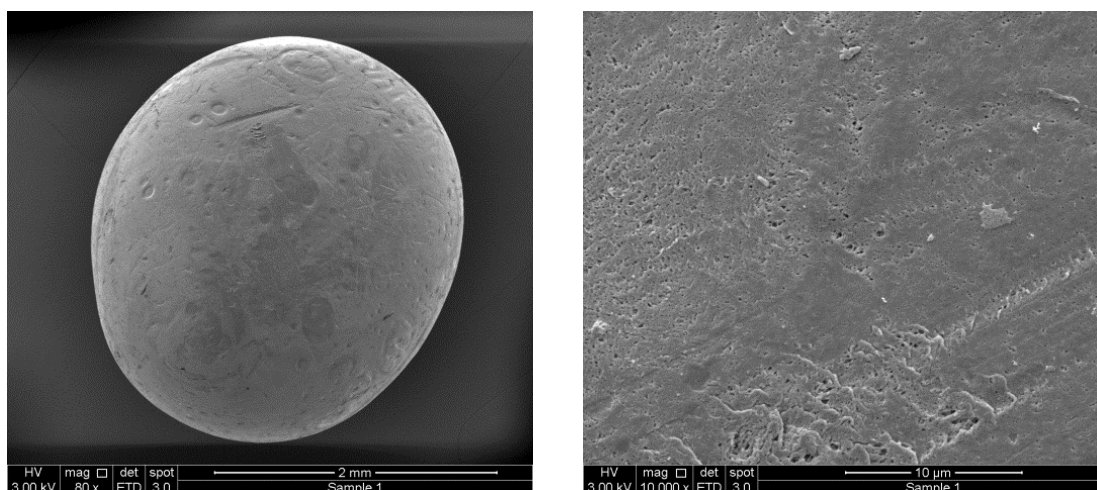


Figure 4.25 SEM micrographs of surface PSF Li_2CO_3 microcapsule - sample 1

The SEM micrographs were obtained using system magnifications of 80x and 10,000x respectively. They illustrate that the generated microcapsules are slightly off-spherical, possessing a relatively smooth surface structure. The higher magnified SEM micrograph shows some evidence of micro-porosity to be present in selected regions.

The SEM micrographs given in figure 4.26 represent the internal structure of a microcapsule after it had been sliced open using a razor blade. The inner core of the microcapsule is shown to exist as a porous honeycomb structure, surrounded by a solid polymer wall. The thickness of the outer wall was determined to be approximately 40 μ m.

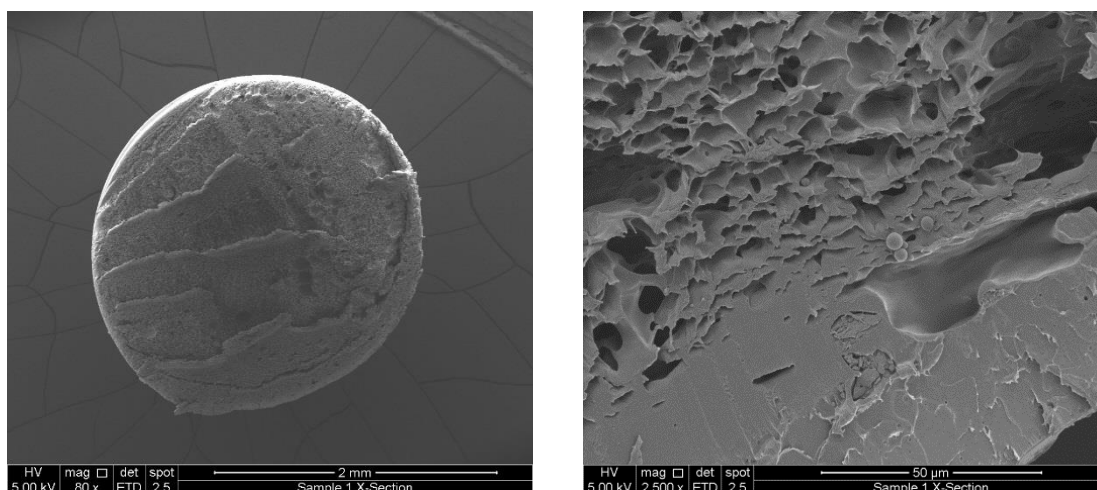


Figure 4.26 SEM micrographs of cross-sectioned PSF Li_2CO_3 microcapsule - sample 1

The honeycomb internal structure of these microcapsules would make it difficult to find encapsulated particles. A more desired design of the microcapsules would be to increase the internal porosity, creating a hollow structure. In an effort to modify the internal morphology of the generated microcapsules, the non-solvent was changed as outlined in sample 2.

Encapsulating Li_2CO_3 in PSF – Acetonitrile/Chloroform 80:20 – Sample 2

The methodology chosen for this experiment was to utilise the same batch of PSF-polymer- Li_2CO_3 dispersion outlined in method 11, but to change the non-solvent system to a blend of 20% chloroform and 80% acetonitrile.

The assumption of adding chloroform to acetonitrile is based on changing the density and therefore the surface tension of the non-solvent (Gong, Lu, Xiang and Luo, 2008). In addition, this will also alter the polarity of the non-solvent. At this stage of the project, changes were based only on research and development. Acetonitrile has a polarity index of

5.8 and density of 0.781(g/mL). Chloroform has a polarity index of 4.1 with a density of 1.489(g/mL) (Fischer Scientific, 2021).

The polymer dispersion was slowly released using a 10ml syringe and metal needle into the non-solvent blend. The generated microcapsules were left over the weekend in the non-solvent mixture before removing and air drying.

After drying, the microcapsules appeared transparent, extremely hard, dehydrated, and non-spherical. The SEM micrographs shown in figure 4.27 represent a cross-sectional area from the microcapsules - generated by slicing open using a razor blade.

The morphology of the microcapsules was completely different from any of the microcapsules previously examined. These microcapsules had an extremely hard solid outer wall with very little evidence of a porous honeycomb structure. However, these microcapsules did have a completely hollow centre.

The ideal structure for a microcapsule would be a solid outer wall with a hollow internal cavity. Unfortunately, the generated microcapsules were distorted and difficult to cut because of the tough outer-wall structure. The internal structure was a step in the right direction, but the consolidated shape and hardness would not be suitable for metal hydride encapsulation.

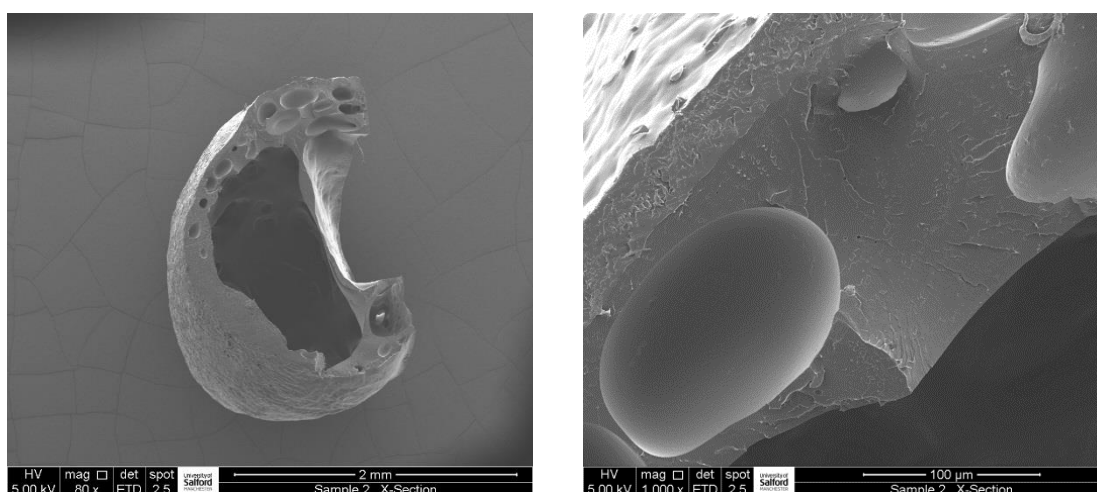


Figure 4.27 SEM micrographs of cross-sectioned PSF Li_2CO_3 microcapsule - sample 2

Encapsulating LiCO_3 in PSF - Acetonitrile/Chloroform/DCM 80:10:10 – Sample 3

This experiment was designed to maintain the hollow cavity as demonstrated in sample 2 but improve on the general morphology of the microcapsules. The chloroform concentration was reduced from 20% to 10% as the previous microcapsules were not ideal. The addition of 10% dichloromethane was based on using a solvent of similar density to chloroform as dichloromethane has a density of 1.324(g/mL) and a polarity index of 3.1.

The resulting SEM micrographs as shown in figure 4.28 indicate a slight improvement in the microcapsule shape whilst retaining some of the open structure as displayed in sample 2 using 20% chloroform. However, the general shape of the microcapsule is seen to be distorted.

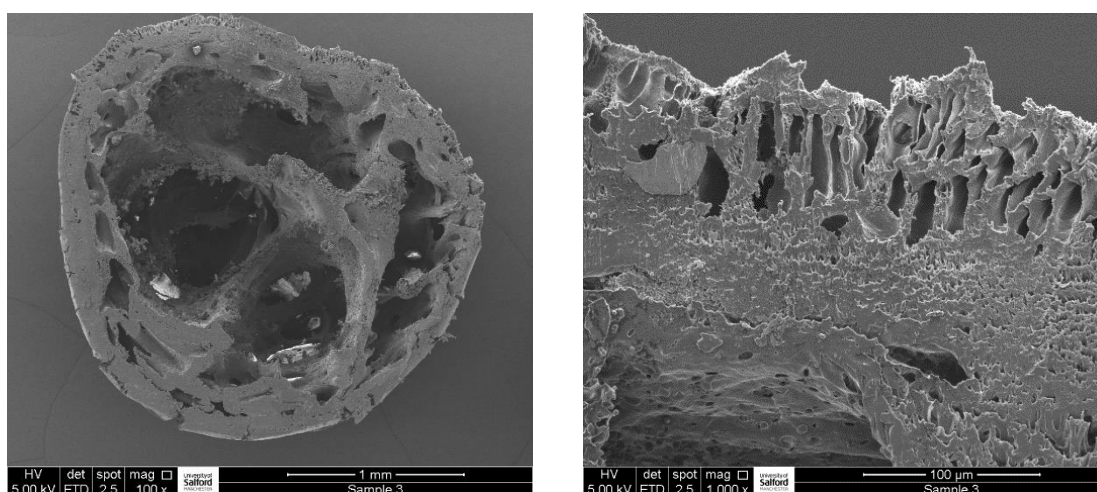


Figure 4.28 SEM micrographs of cross-sectioned PSF Li_2CO_3 microcapsule - sample 3

The surface micrographs figure 4.29 illustrate a very poor structure with severe cracking. This procedure generated microcapsules that would not be suitable to retain metal hydrides in a stable form.

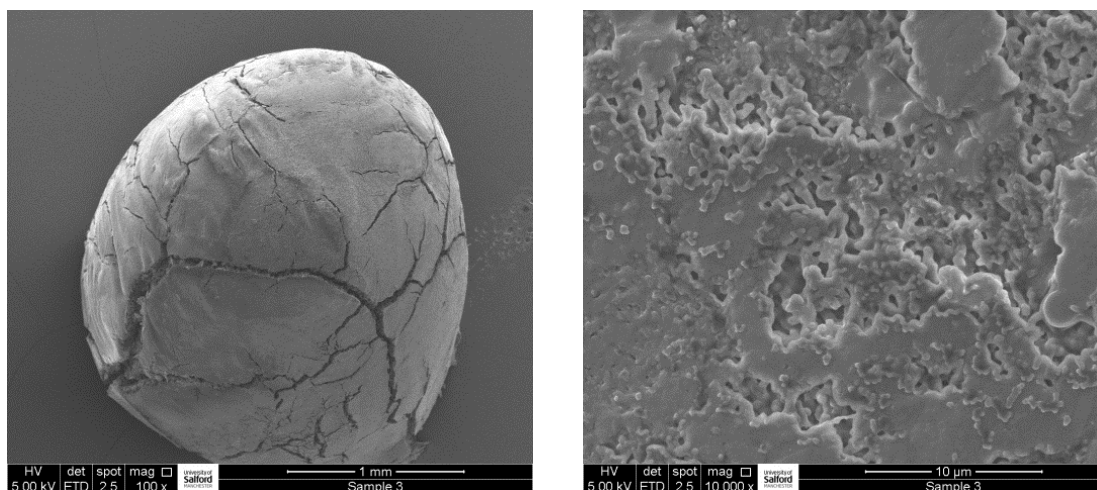


Figure 4.29 SEM micrographs of surface PSF Li_2CO_3 microcapsule - sample 3

Encapsulating LiCO_3 in PSF – Acetonitrile/DMSO 75:25 – Sample 4

A fresh new batch of PSF polymer and Li_2CO_3 dispersion was generated using the methodology as described in method 12. This involved some slight modifications made to the dissolution of the polymer using an IKA yellow line magnetic stirrer with heat setting of 1 and an agitation speed of 3 for 2.5 hours. The non-solvent blend used in this experiment was changed to 25% DMSO and 75% acetonitrile.

The process for generating a microcapsule involved the use of a 10ml syringe and a fine metal needle. The non-solvent blend was agitated using the IKA RW 20 digital overhead stirrer connected to 40mm centrifugal blades at 450rpm whilst the polymer dispersion was slowly introduced. Once the microcapsules had formed, the agitation speed was reduced to 235rpm, and the microcapsules remained stirring in the non-solvent for an additional 10 minutes. The excess non-solvent was then removed, and the microcapsules air-dried.

Figure 4.30 illustrates the surface SEM micrographs using system magnifications of 80x and 10,000x respectively. The microcapsules are off-spherical and have a porous surface structure, containing many cracks.

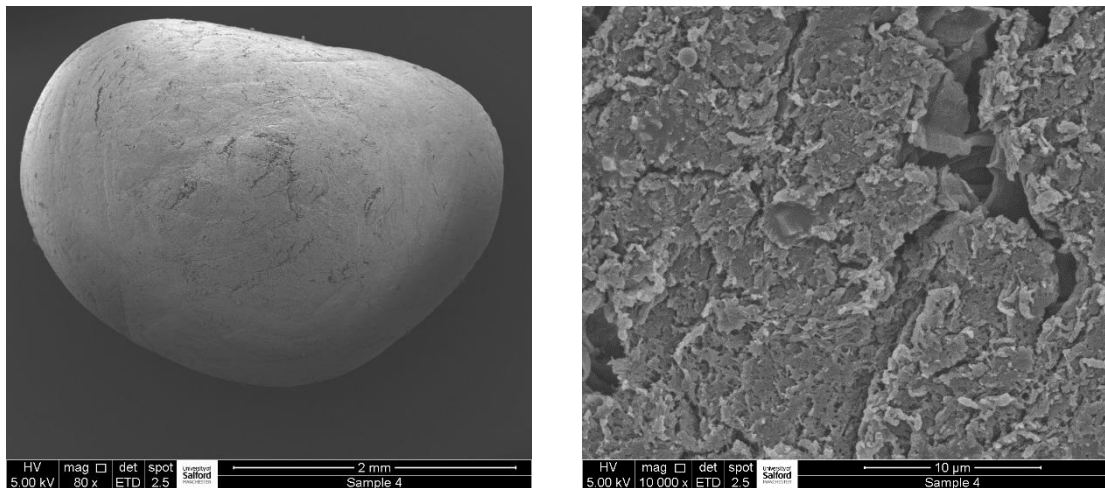


Figure 4.30 SEM micrographs of surface PSF Li_2CO_3 microcapsule - sample 4

Figure 4.31 shows the SEM micrographs obtained from a cross-sectional area of a typical microcapsule. The internal morphology is seen to be porous, forming channels towards the outer wall. This effect was observed from previously generated microcapsules (as displayed in figure 4.24).

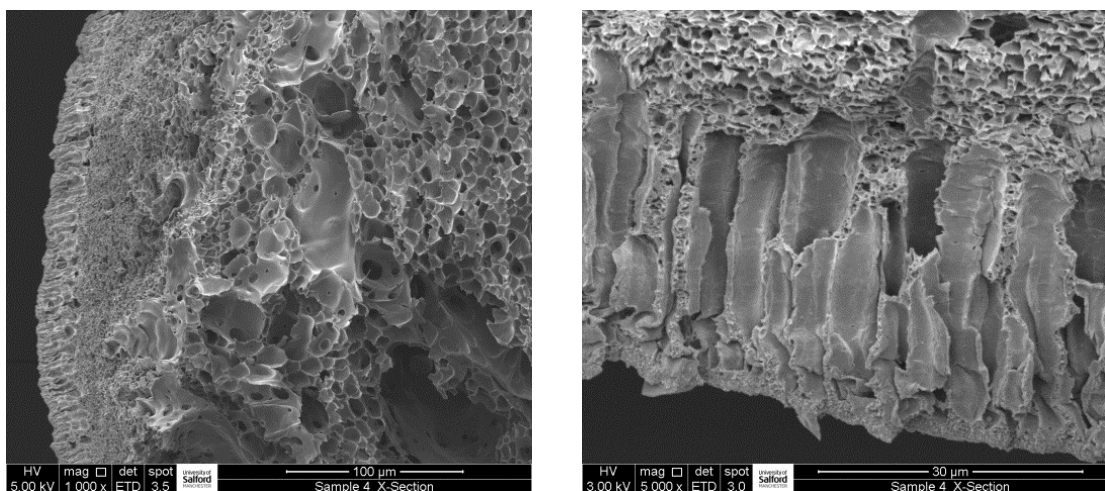


Figure 4.31 SEM micrographs of cross-sectioned PSF Li_2CO_3 microcapsule - sample 4

The non-solvent blend used in the experiment was clearly not suitable for this project. Any surface cracking would admit moisture into the capsule, causing issues for metal hydride encapsulation.

Many different influences are thought to contribute towards the formation of microcapsules based on this phase inversion process. The fundamentals of this technique involve the interaction of at least three compounds: the polymer, the solvent, and the non-solvent (Pena and Gumi, 2013).

The aim at this stage of the research was to produce a microcapsule containing a solid outer wall construction with a hollow internal morphology. The polarity of the non-solvent is thought to contribute towards the formation of the microcapsules. In addition to polarity, the density of the non-solvent can also influence the formation as density changes will modify the surface tension (Gong et al., 2008).

It was previously demonstrated that the addition of 20% chloroform to the acetonitrile non-solvent significantly changed the physical properties of the microcapsules generating a smooth outer surface with a hollow internal structure; however, the microcapsules were very hard and distorted.

At this stage of the research, the changes were based on trial and error but with an awareness that polarity and changes to the density of the non-solvent contribute towards the final structure. Just using acetonitrile as the non-solvent is shown to generate microcapsules, but the internal structure is not ideal for encapsulating materials as it forms a tight honeycomb structure. To generate the ideal internal structure, retaining the solid outer wall morphology of a microcapsule, it is necessary to add a modifier to the acetonitrile non-solvent.

When chloroform was substituted for DMSO, a polar aprotic solvent with a polarity index of 7.2 and density of 1.1(g/mL) (Fischer Scientific, 2021), it was anticipated that the resulting microcapsules would have retained the porous internal structure but with a reduction of the hard, distorted shape. However, the resulting SEM micrographs, figure 4.3, demonstrated that the outer surface contained many cracks that would not be suitable for the encapsulation of air/moisture sensitive materials.

In an attempt to improve the outer surface cracking issues and retain a soft microcapsule, a combination of 20% chloroform and 20% DMSO in the non-solvent was chosen with the understanding that the blend of different solvents could improve the structure of the microcapsules.

The following experiments outlined for samples 5-7 involved following the same procedure for the generation of the microcapsules but the ratio of the non-solvent concentrations was modified.

Encapsulating Li_2CO_3 in PSF – Acetonitrile / Chloroform / DMSO 60:20:20 – Sample 5

From previous experimentation, it was established that the microcapsules generated for sample 2 had a hard, hollow, distorted morphology. This implied that the addition of 20% chloroform significantly changed the physical properties of the microcapsules.

This sample utilised a non-solvent blend containing 20% chloroform together with an additional 20% DMSO. This blend of solvents was used with the intention of generating an improved microcapsule morphology whilst maintaining a softer polymer structure.

Figure 4.32 represents the resulting SEM micrographs obtained from the surface of the generated microcapsules. The micrographs denote that a slight improvement had been achieved regarding the general smoothness of the outer polymer wall. Some holes were seen to be present on the surface as revealed from the higher magnified surface micrograph, obtained using a system magnification of 1000x.

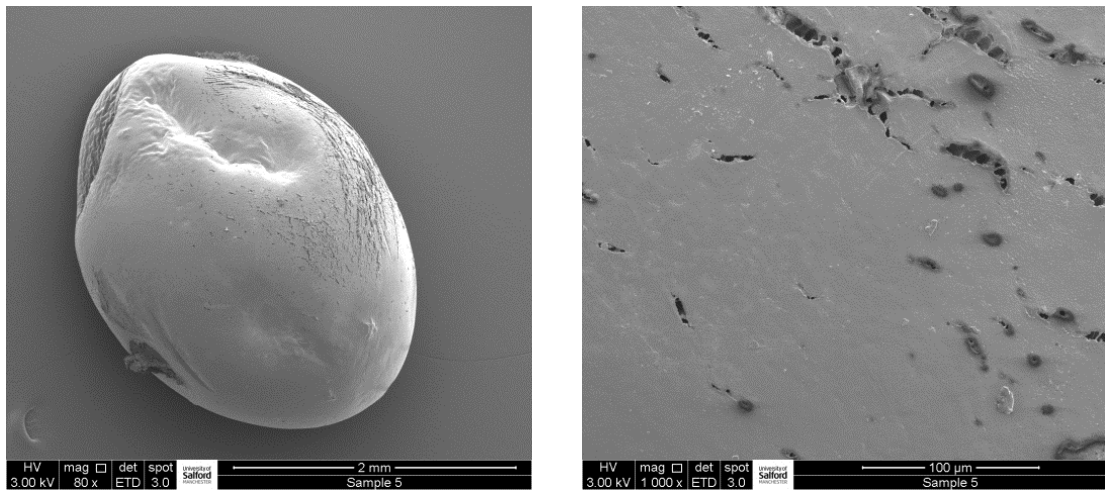


Figure 4.32 SEM micrographs of surface PSF Li_2CO_3 Microcapsule - sample 5

The microcapsule is off-spherical, showing signs of indentation - signifying a weak wall structure like the previously examined microcapsules in sample 3. The SEM micrographs obtained from a cross-section of a microcapsule, figure 4.33, show that the internal structure was porous, existing as a network of small holes with some larger hollow voids resulting in a very high pore volume (Gong et al., 2008). The outer wall was very thin, explaining the deformities seen in the general shape of the microcapsules.

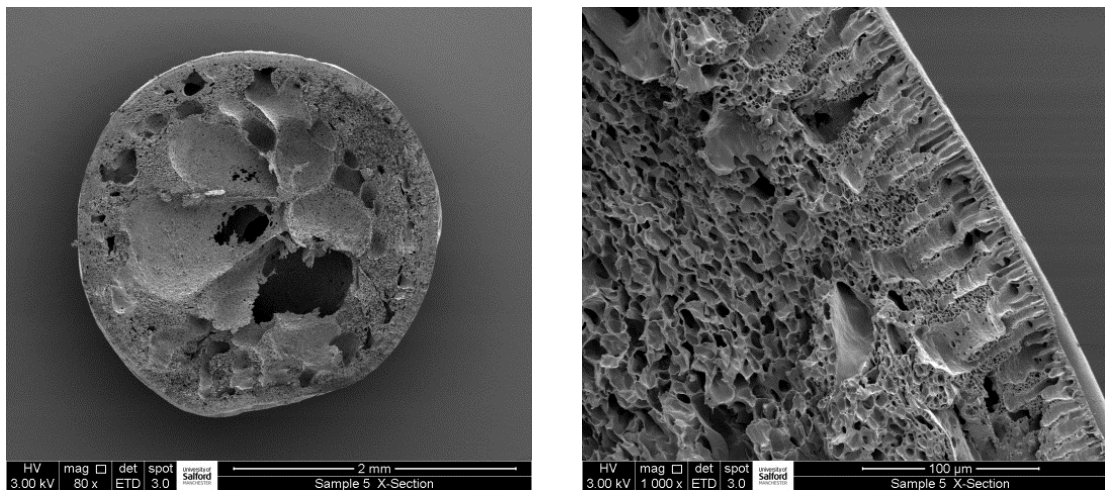


Figure 4.33 SEM micrographs of cross-sectioned PSF Li_2CO_3 microcapsule - sample 5

Encapsulating LiCO₃ in PSF – Acetonitrile / Chloroform / DMSO 66:27:7 – Sample 6

The blend of non-solvents used for sample 5 demonstrated an improved surface structure compared to sample 4, but the shape of the microcapsule was off-spherical and distorted. This experiment is designed to establish if the defects were associated with the use of 20% concentration of DMSO. The non-solvent blend involved a significant reduction in the concentration of DMSO and an increase in the chloroform levels. The polymer dispersion was dripped into a blend of 20ml of acetonitrile and 2ml of DMSO together with 8ml of chloroform as the non-solvent.

The results from this experiment were different from any of the previous microcapsules generated. The particles appeared soft, transparent, and distorted. When pressed with tweezers, they released a liquid phase, thought to be trapped non-solvent. The light micrograph figure 4.34, demonstrating the morphology of the microcapsule was obtained using the Zeiss SV8 stereo microscope.

It is not entirely clear why this procedure for generating microcapsules was unsuccessful. The use of 27% chloroform in the non-solvent blend may have caused problems. Chlorine has a high density of 1.489(g/mL) and this may have affected the surface tension of the non-solvent, preventing good microcapsule formation.

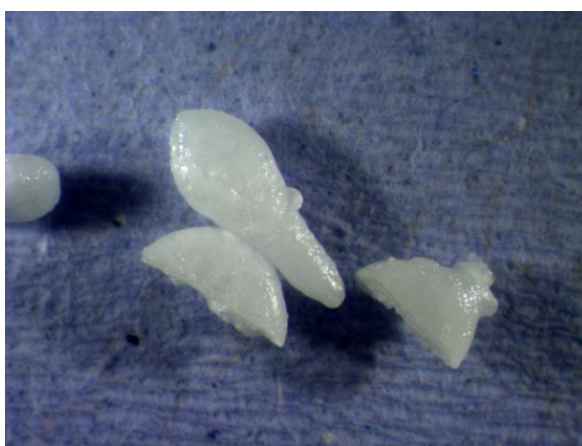


Figure 4.34 Light micrograph of PSF-Li₂CO₃ microcapsules - sample 6

Encapsulating Li_2CO_3 in PSF – Acetonitrile / Chloroform / DMSO 66:7:27 – Sample 7

This experiment was designed to further understand if the high levels of chlorine were contributing towards the poorly formed microcapsules as seen in sample 6. This experiment involved switching the ratios of DMSO and chloroform to the opposite concentrations as utilised for sample 6.

The polymer-dispersion was dripped into a non-solvent mix of 20ml acetonitrile, 8ml DMSO and 2ml of chloroform using an agitation speed of 450rpm with the IKA RW 20 digital overhead stirrer connected to 40mm centrifugal blades.

The SEM micrographs from the surface of the microcapsules, figure 4.35, were obtained using system magnifications of 80x and 10,000x respectively. They illustrate that the spheres have a moderately spherical shape. However, the higher magnified micrograph demonstrates a porous surface morphology. These results would suggest poor fusion when the polymer coalescence occurred.

However, the general shape and appearance of the microcapsule has significantly improved by changing the solvent ratios. The microcapsule is slightly off-spherical, but the shape has considerably improved when compared against both samples 5 and 6.

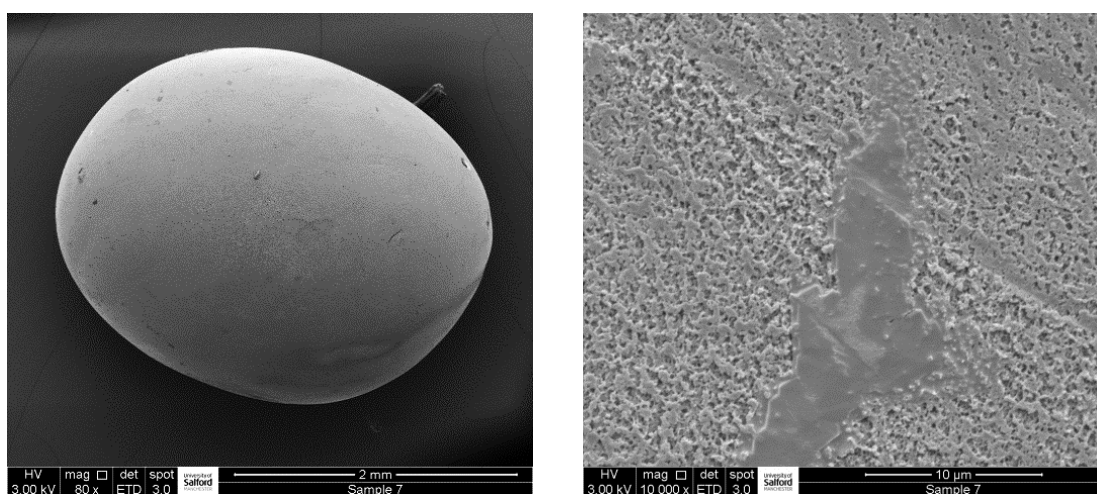


Figure 4.35 SEM micrographs of surface PSF Li_2CO_3 microcapsule - sample 7

The sample was cross-sectioned using a sharp blade and the internal structure is represented in figure 4.36. The SEM micrographs show a porous, honeycomb internal structure like many previously examined samples.

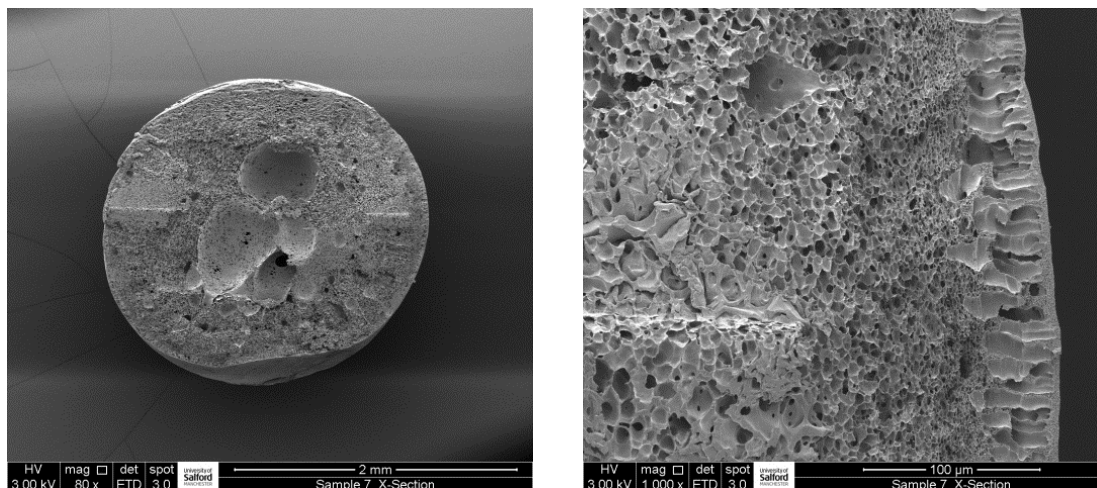


Figure 4.36 SEM micrographs of cross-sectioned PSF Li_2CO_3 microcapsule - sample 7

Encapsulating Li_2CO_3 in PSF – Acetonitrile 100% - 450rpm – Sample 8

The microcapsules generated in this procedure were the result of allowing small droplets of PSF polymer- Li_2CO_3 dispersion to slowly drip into 100% acetonitrile with the IKA RW 20 digital overhead stirrer set at an agitated speed of 450rpm. It is effectively the same procedure as used for Sample 1, but the agitation drill speed was increased to 450rpm rather than the slower speed of 235rpm.

The purpose for this experiment was to investigate if the higher spin rate would contribute towards the microcapsules forming an improved porous internal structure. Sample 1 had a honeycomb internal structure that would not be ideal for characterising encapsulated nanoparticles as they would be difficult to find.

The generated microcapsules were characterised using SEM and the resulting surface micrographs are shown in figure 4.37. The surface micrographs were acquired using system magnifications of 80x and 10,000x respectively. They show that the microcapsules had an off-spherical structure, containing some surface indentations. The higher magnified surface

micrograph illustrates the surface has a porous structure, coated with a crystalline phase thought to be Li_2CO_3 or crystalline PSF.

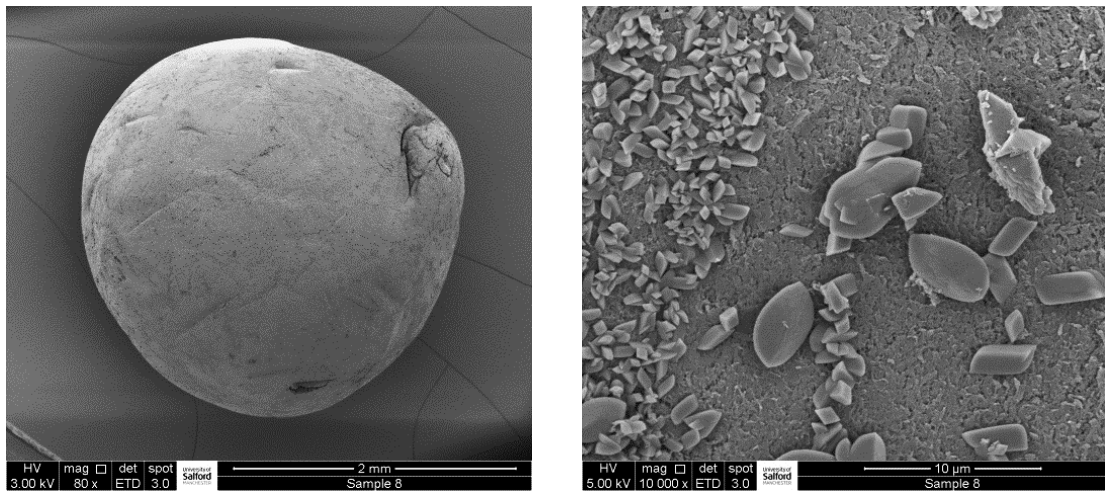


Figure 4.37 SEM micrographs of surface PSF Li_2CO_3 microcapsule - sample 8

Figure 4.38 displays the internal structure of a microcapsule after it had been cut open using a razor blade under liquid nitrogen. The low magnified micrograph shows that the sample had broken under the freezing and cutting action. However, the higher magnified micrograph demonstrates that the microcapsule has a porous centre with a honeycomb structure existing towards the outer regions. These results would suggest that the higher agitation speed has changed the internal morphology of the microcapsules but impeded the formation of a smooth, spherical outer structure.

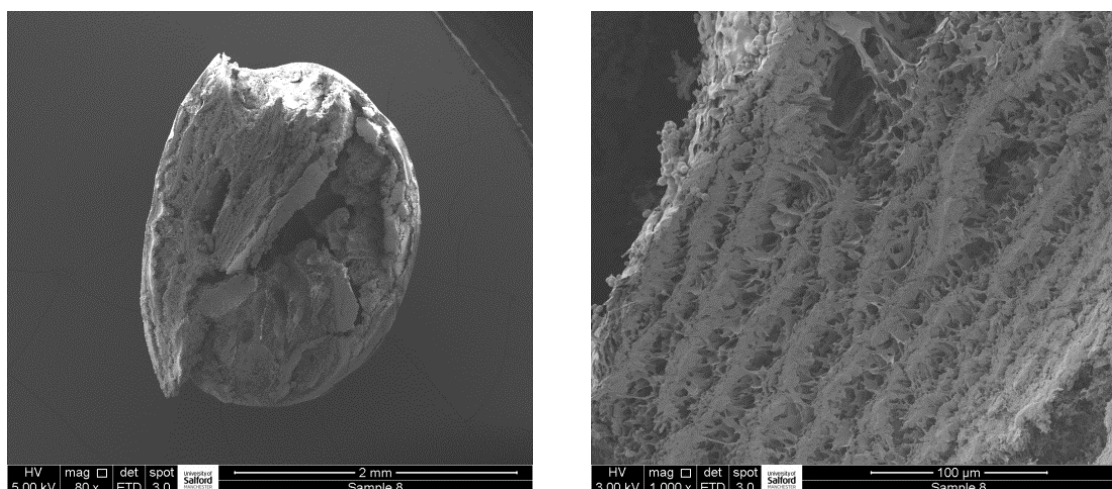


Figure 4.38 SEM micrographs of cross-sectioned PSF Li_2CO_3 microcapsule - sample 8

Encapsulating Li_2CO_3 in PSF – Acetonitrile/DMSO/DCM 66:17:17 – Sample 9

This experiment involved using a non-solvent blend consisting of 20ml acetonitrile, 5ml DMSO and 5ml DCM. The rationale for this procedure was based on modifying the conditions chosen for sample 3. The ratios of the non-solvent blend were slightly adjusted, increasing the concentration of both DMSO and DCM levels to 17% rather than 10% as specified in sample 3. The selected agitation drill speed was increased to 450rpm rather than the slower speed of 235rpm used for sample 3.

Figure 4.39 shows the SEM micrographs obtained from the surface of the microcapsules - displaying an off-spherical shape with a smooth surface appearance. The higher magnified micrograph demonstrates that the outer surface is solid, containing some small crystalline particles existing below $10\mu\text{m}$ that could represent crystalline PSF or Li_2CO_3 .

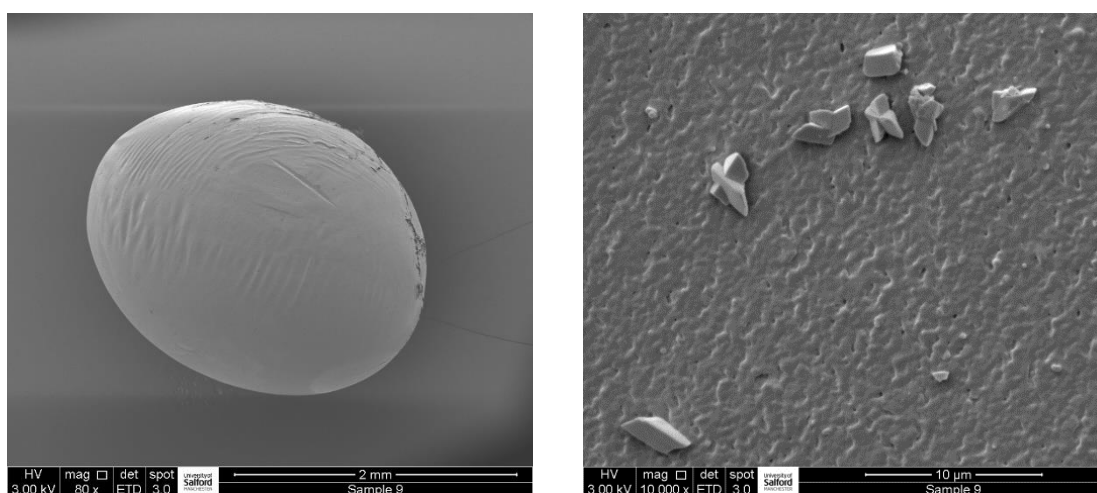


Figure 4.39 SEM micrographs of surface PSF Li_2CO_3 microcapsule - sample 9

Figure 4.40 represents the SEM micrographs obtained from the internal structure of a cut microcapsule. They show that the inner morphology consists of many pores of varying sizes within a honeycomb structure.

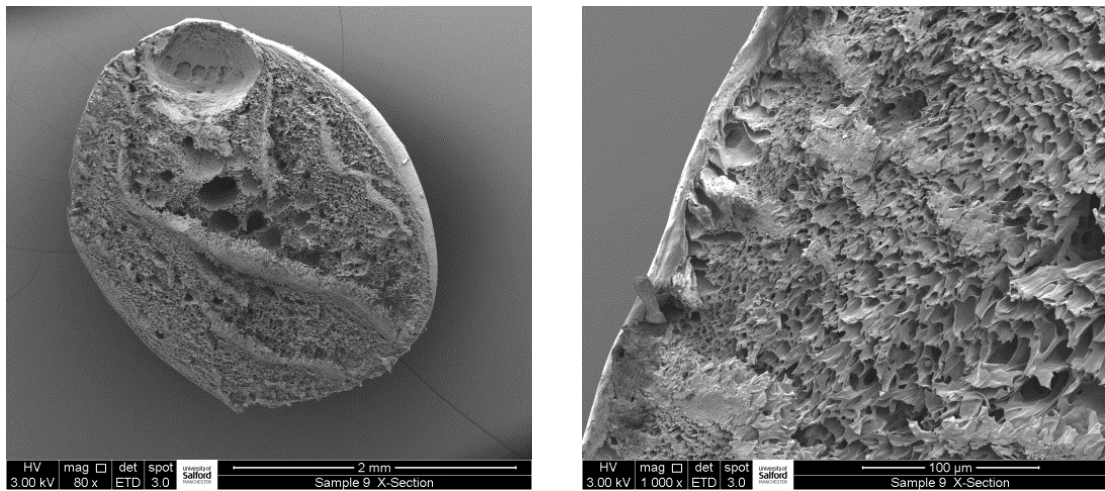


Figure 4.40 SEM micrographs of cross-sectioned PSF Li_2CO_3 microcapsule - sample 9

Encapsulating Li_2CO_3 in PSF – Acetonitrile/DMSO/DCM 66:27:7 – Sample 10

This experiment involved mixing 20ml of acetonitrile with 8ml of DMSO and 2ml of DCM. The surface SEM micrographs, figure 4.41, illustrate that the microcapsule exists as a slightly distorted sphere containing many surface cracks. This porous surface would not be suitable for the encapsulation of moisture-sensitive metal hydride particles.

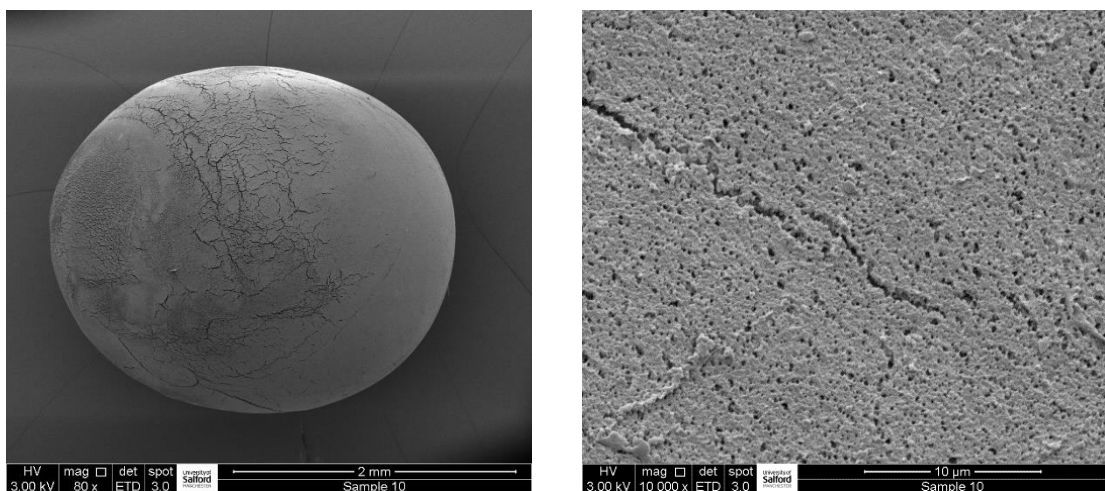


Figure 4.41 SEM micrographs of surface PSF Li_2CO_3 microcapsule - sample 10

Figure 4.42 represents an SEM micrograph obtained from a cross-sectioned microcapsule. The internal structure is seen to exist as a network of different sized pores present within a very thin outer wall.

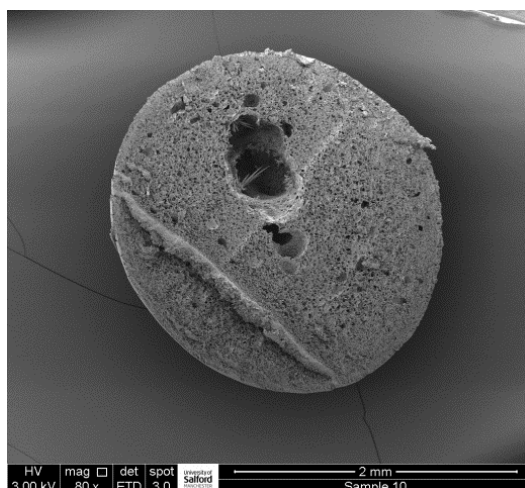


Figure 4.42 SEM micrograph of cross-sectioned PSF Li_2CO_3 microcapsule - sample 10

Encapsulating Li_2CO_3 in PSF in NMP/DMSO using the non-solvent Acetonitrile

In order to further evaluate the behaviour of the interaction of a solution of PSF with the non-solvent acetonitrile, the experimental method 12 was changed by including the addition of 5ml of DMSO to the 10ml of NMP. DMSO is known as a polar aprotic solvent with similar properties to NMP that can dissolve both polar and non-polar materials. This is analogous to the use of additives, often different solvents, that can change the polarity of the casting solution on PSF membrane formations (Chen et al., 2007).

An initial experiment was set up with the hope of dissolving PSF into 100% DMSO. However, after the initial addition of 2g of PSF in 10ml of DMSO followed by further additions of DMSO, it was established that DMSO is not a suitable solvent for the dissolution of PSF. However, it was determined that 2g of PSF would dissolve in a mixture of 5ml of DMSO and 10ml of NMP utilising the IKA yellow line magnetic stirrer on heat setting of 2 and an agitation of 3 for 2 hours. 0.1g of Li_2CO_3 was added to the polymer solution and stirred for 1 hour using an agitation setting of 3. This experiment was carried out to evaluate the use of DMSO as a co-solvent to the NMP (Maldonado-Lopez et al., 2021)

Encapsulating Li_2CO_3 in PSF – Acetonitrile 100% - 150rpm – Sample 11

The microcapsules were generated by introducing the polymer dispersion to the non-solvent acetonitrile with a drill agitation speed of 150rpm. The SEM micrographs at figure 4.43 were obtained from the surface of the microcapsules using system magnifications of 80x and 10,000x respectively. The results demonstrate that the morphology of the outer microcapsule is slightly off-spherical. The higher magnified surface micrograph shows signs of microporosity.

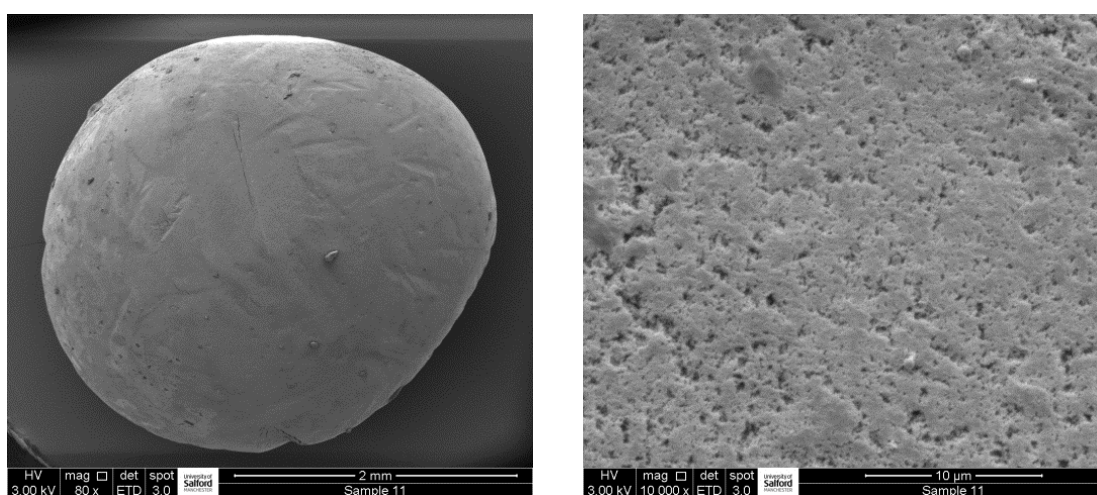


Figure 4.43 SEM micrographs of surface PSF Li_2CO_3 microcapsule - sample 11

The microcapsule was cross-sectioned using a new razor blade and the results are given in figure 4.44. The internal structure is seen to exist as various channels of hollows which become smaller towards the outer edge of the microcapsule.

This structure is analogous to the macrovoid as demonstrated in (Gong et al., 2006). This paper explains that when the polysulfone emulsion droplet contacts the non-solvent, the polymer solvent is diffused into the non-solvent. At the same time, the influx of the non-solvent is small. So, the macrovoid grew with the separating out of polysulfone.

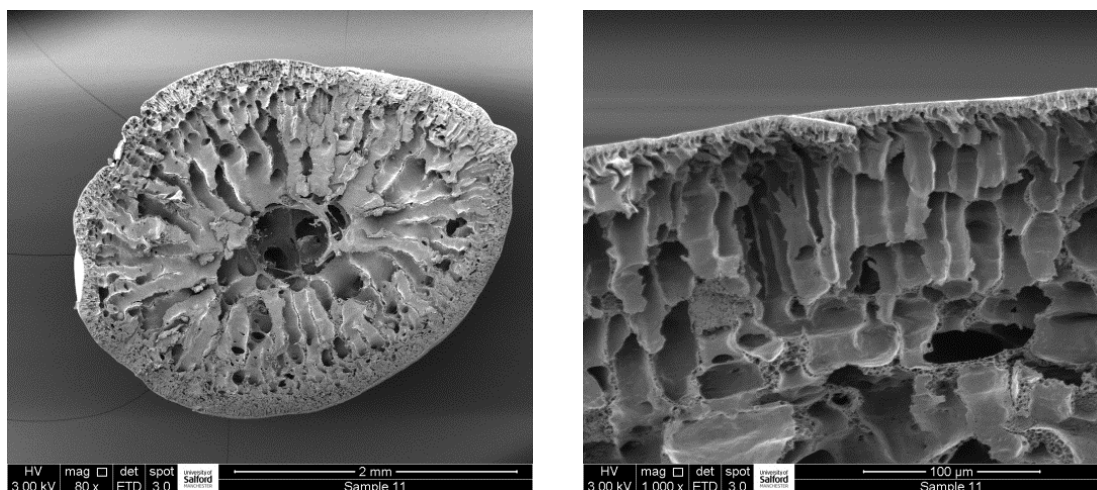


Figure 4.44 SEM micrographs of cross-sectioned PSF Li_2CO_3 microcapsule - sample 11

Interestingly, the addition of DMSO appears to have changed the internal structure as it is seen to exist as a mixture of channels coming from the centre of the microcap with a honeycomb structure around the outer edge. The surface micrographs, however, show an increased level of porosity that could allow moisture from the atmosphere to enter the microcapsule when switching to a metal hydride.

In order to further evaluate the effect of the addition of DMSO to the initial PSF solvent blend, the droplet formation was studied by further adjusting the speed of the drill agitation speed. This was based on the principle that increasing the shear on the agitation could change the final microcapsule structure both internally and externally. The following samples from 12 to 14 were generated as a direct result of using the same PSF- Li_2CO_3 dispersion but increasing the agitation speed.

Encapsulating Li_2CO_3 in PSF – Acetonitrile 100% - 340rpm – Sample 12

The SEM micrographs shown at figure 4.45 represent the results from the microcapsules generated using a faster agitation speed of 340rpm. The shape of the particles is seen to have deteriorated from spherical to off-spherical, showing signs of collapsing. The higher magnified micrograph shows the surface to be rough but relatively free from porosity. Small crystalline particles are also present at the surface - thought to be Li_2CO_3 or PSF.

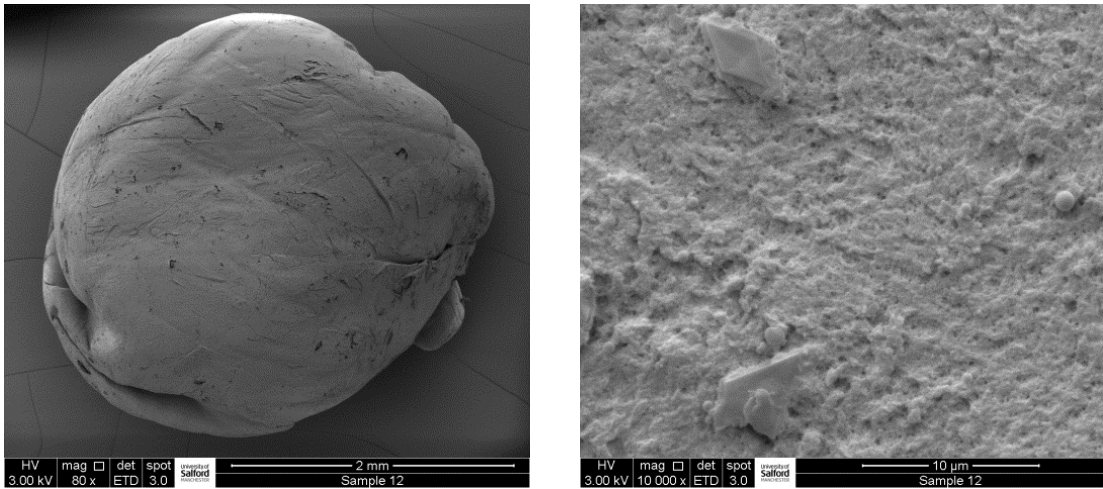


Figure 4.45 SEM micrographs of surface PSF Li_2CO_3 microcapsule - sample 12

After obtaining a suitable cross-section, the SEM micrographs obtained, figure 4.46, display a similar structure as observed from the previous sample 11. The inner region of the microcapsule has formed a series of channels that reduce to smaller pores towards the outer surface.

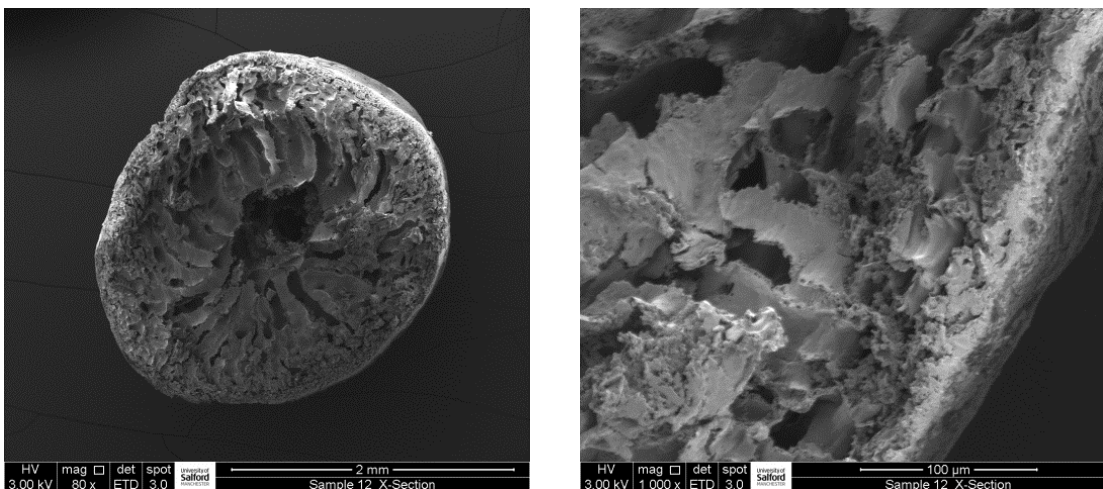


Figure 4.46 SEM micrographs of cross-sectioned PSF Li_2CO_3 microcapsule - sample 12

Encapsulating Li_2CO_3 in PSF – Acetonitrile 100% - 520rpm – Sample 13

The agitation speed was further increased to 520rpm and the results show a completely different microcapsule morphology. The microcapsule appears dehydrated and misshapen.

The higher magnified SEM micrograph illustrates that many crystalline particles are present at the surface of the microcapsule - thought to be Li_2CO_3 or PSF.

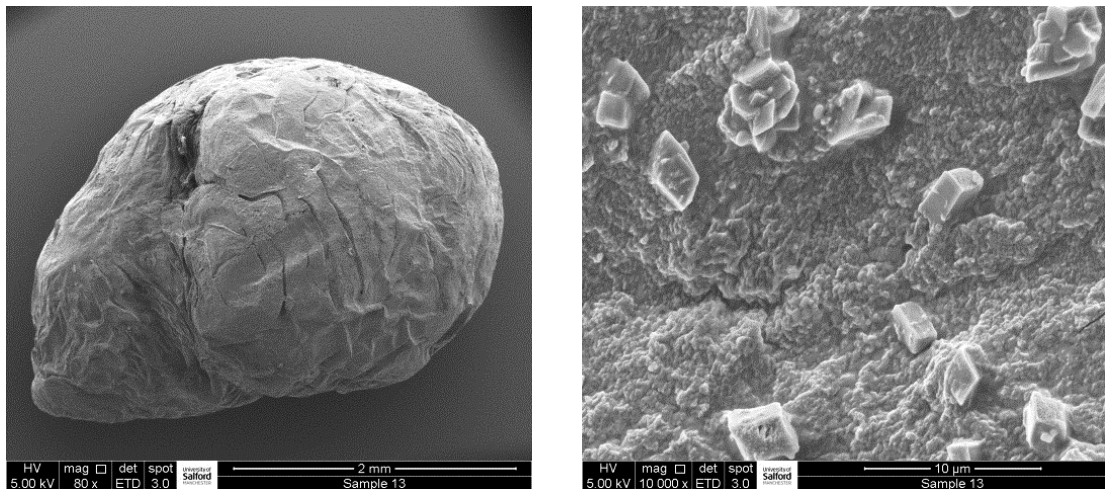


Figure 4.47 SEM micrographs of surface PSF Li_2CO_3 microcapsule - sample 13

The SEM micrographs shown in figure 4.48 represent a cross-section of the generated microcapsule. The internal morphology appears different from the previous samples examined in this agitation speed evaluation. The inner area is seen to exist as a hollow centre, becoming more solid towards the outer edge.

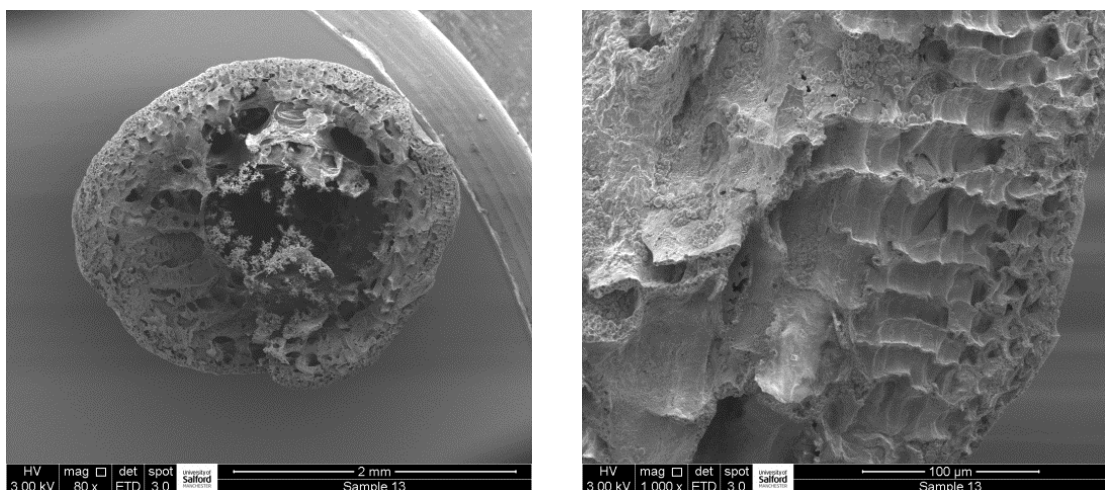


Figure 4.48 SEM micrographs of cross-sectioned PSF Li_2CO_3 microcapsule - sample 13

Encapsulating Li₂CO₃ in PSF – Acetonitrile 100% - 1660rpm – Sample 14

The same trend is seen from the results shown in figures 4.49 and 4.50. The extra shear has restricted the polymer from forming good microcapsules. The surface is seen to contain many cracks and has a rough, porous morphology containing crystalline particles that could be either Li₂CO₃ or PSF. The internal structure exists as a very porous structure that is loosely bound together. These results are positive, as they demonstrate that only a gentle agitation is required when the polymer dispersion is dropped into the non-solvent.

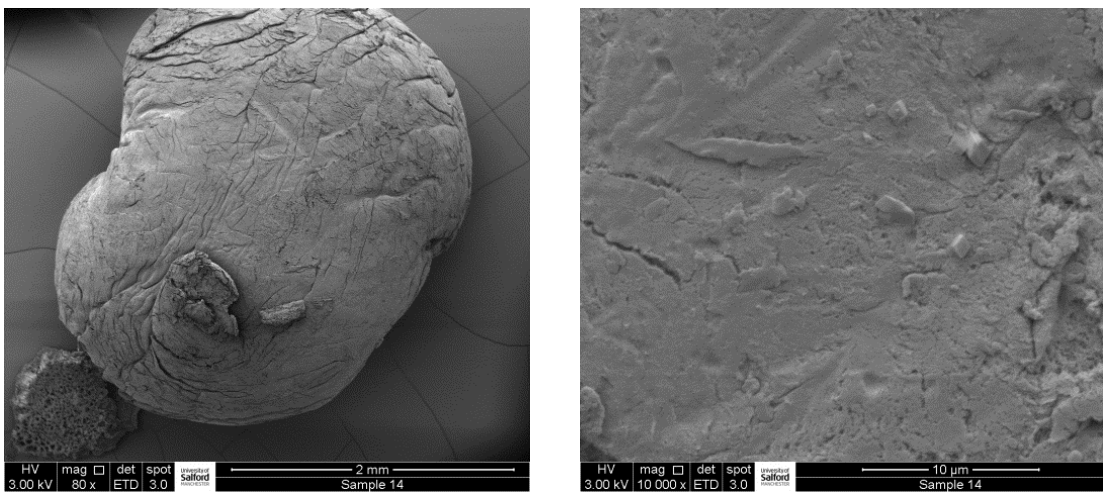


Figure 4.49 SEM micrographs of surface PSF Li₂CO₃ microcapsule - sample 14

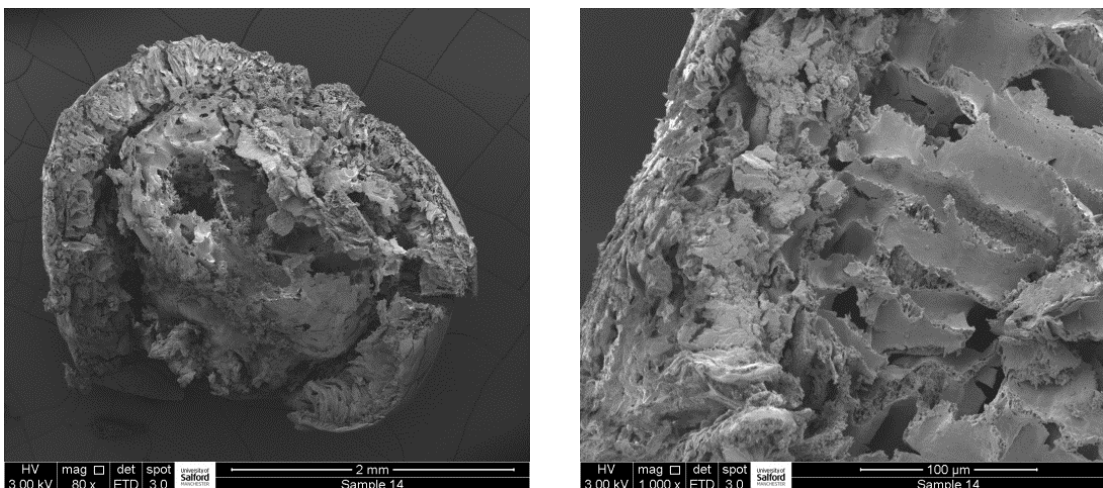


Figure 4.50 SEM micrographs of cross-sectioned PSF Li₂CO₃ microcapsule - sample 14

To support this evidence, the IKA RW 20 digital overhead stirrer unit was changed to the IKA Yellow Line Magnetic stirring unit. The polymer dispersion was dripped using a glass pipette into 30ml of acetonitrile in a 100ml conical flask. Samples 15 and 16 represent the resulting SEM micrographs from separate speed settings of 3 and 6 respectively.

Encapsulating Li_2CO_3 in PSF – Acetonitrile 100% - Speed Setting 3 – Sample 15

The SEM micrographs as shown below in figure 4.51 represent the surface of the resulting microcapsules generated with an agitation speed of 3. The micrographs were obtained using system magnifications of 80x and 10,000x respectively, using secondary electron detection. The low magnified micrograph illustrates that the polymer is not spherical and appears shrivelled. The higher magnified micrograph shows the surface is smooth, with little signs of porosity. Large crystals are observed that could be Li_2CO_3 or PSF.

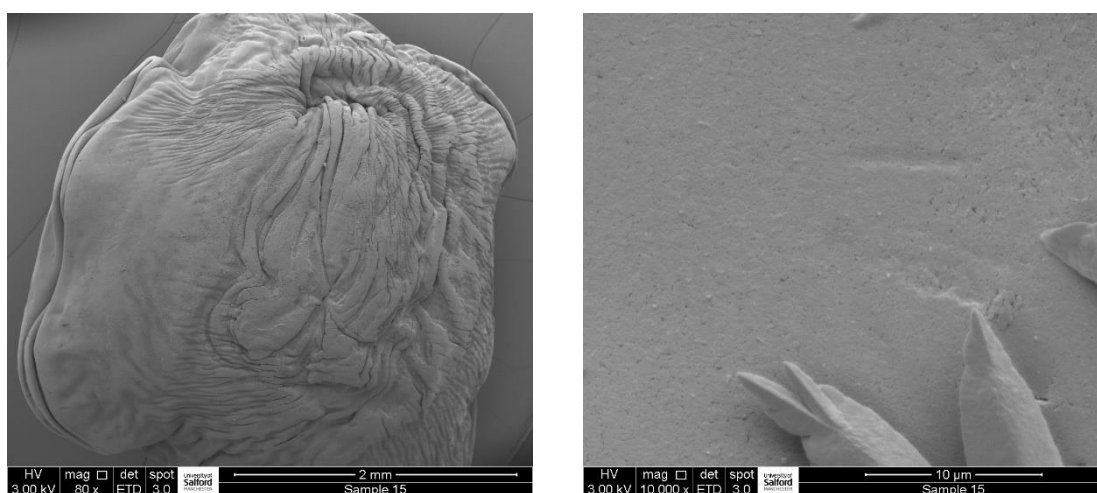


Figure 4.51 SEM micrographs of surface PSF Li_2CO_3 microcapsule - sample 15

The SEM micrographs as shown in figure 4.52 were obtained from a cross-section of a microcapsule after it had been frozen using liquid nitrogen. The internal morphology shows a honeycomb, porous structure that is less porous towards the outer edge. The higher magnified micrograph taken with a system magnification of 1000x shows many small spheres that did not fuse when the polymer coalesced.

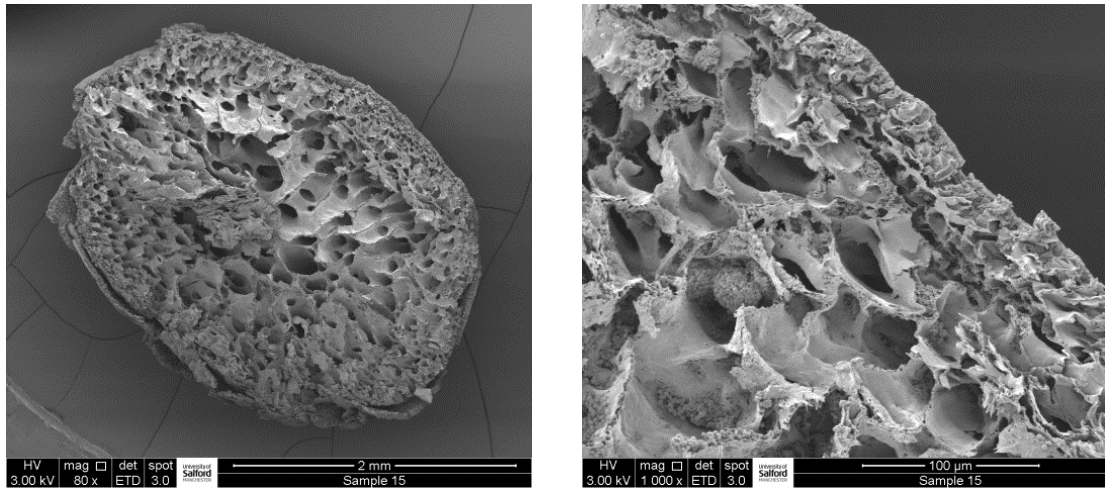


Figure 4.52 SEM micrographs of cross-sectioned PSF Li_2CO_3 microcapsule - sample 15

Encapsulating Li_2CO_3 in PSF – Acetonitrile 100% - Speed Setting No 6 – Sample 16

The speed of the magnetic stirrer was increased to 6 and the micrographs generated were examined following the same procedure as outlined from the previous sample. Figure 4.53 illustrates that the microcapsule is distorted and shrivelled. The SEM micrograph obtained using a system magnification of 10,000x displays an increased level of surface porosity when compared directly against the microcapsule generated with a lower speed setting of 3.

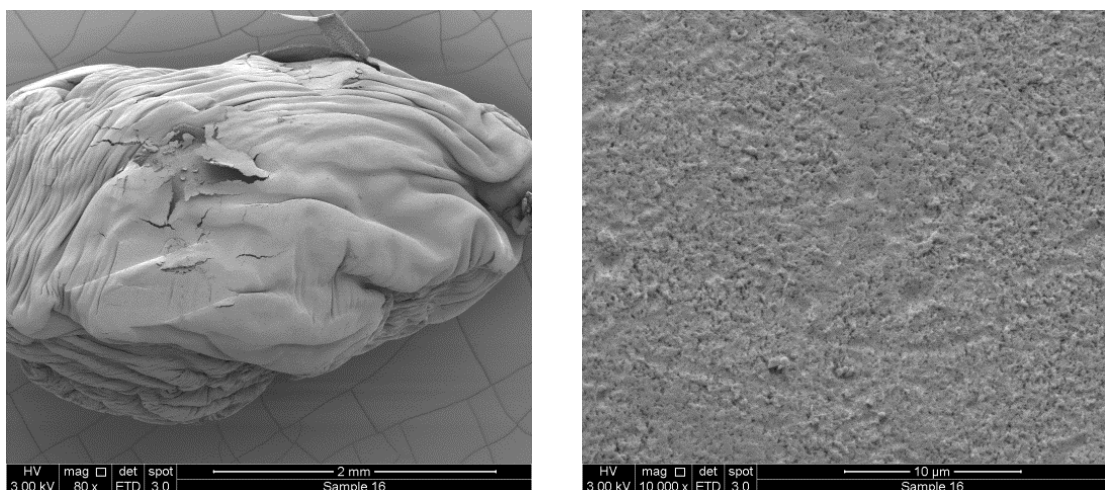


Figure 4.53 SEM micrographs of surface PSF Li_2CO_3 microcapsule – sample 16

The SEM micrographs shown in figure 4.54 were obtained from the internal structure after the microcapsule had been cross sectioned, following freezing with liquid nitrogen. The

internal morphology is seen to be very porous, as in previous samples. The general shape of the microcapsule is very poor, appearing distorted and shrivelled.

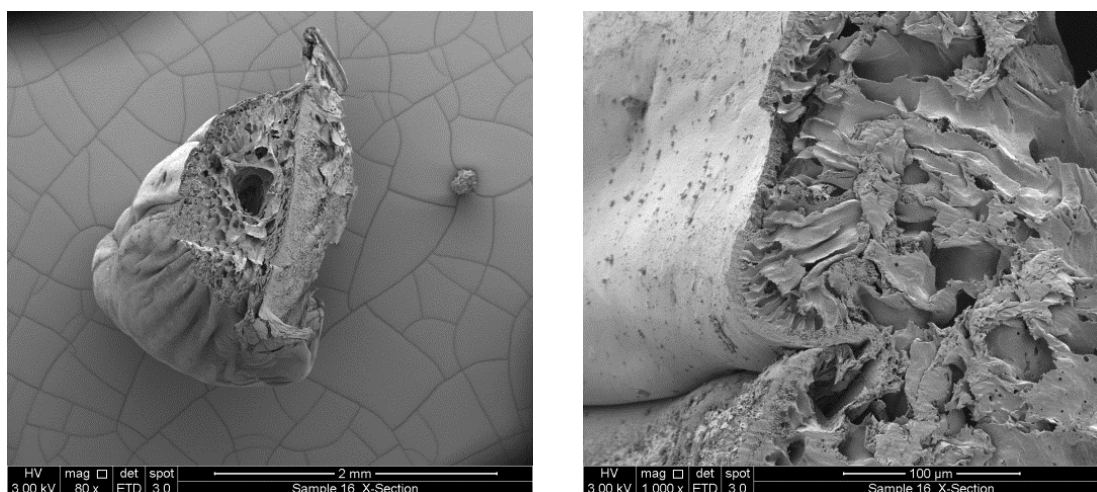


Figure 4.54 SEM cross-sectioned micrographs of PSF Li_2CO_3 microcapsule – sample 16

These findings are interesting as they suggest that increased shear can improve the internal porosity but destroys the general shape and structure of the microcapsule.

The addition of DMSO to the PSF has probably complicated the study by adding an extra element to the already complicated equation. The addition of DMSO has also changed the concentration of the polymer solution. At this point in the research, it was decided to maintain the 2g of PSF in 10ml of solvent.

Many of the comments made previously covering the characterisation of the surface structure of the microcapsules suggested that a crystalline phase was present at the surface, thought to be either Li_2CO_3 or PSF.

Figure 4.55 represents the SEM micrographs obtained from Li_2CO_3 particles ex Sigma-Aldrich using system magnifications of 500x and 2500x respectively. The preparation involved simply dusting the particles onto a carbon adhesive pad, then the particles were sputter coated with 4nm of platinum/palladium. The micrographs demonstrate that Li_2CO_3 exists as a well-crystalline material, forming many aggregates.

However, during the high shear required for generating the dispersion, these clusters may have broken down to form smaller, individual primary particles. The general morphology of the particles seen to exist on the surface of some microcapsules are not always similar in shape and size to the Li_2CO_3 particles shown in figure 4.55. EDX analysis cannot detect lithium - making it very difficult to confirm the presence of the inorganic salt or crystallisation from the PSF polymer.

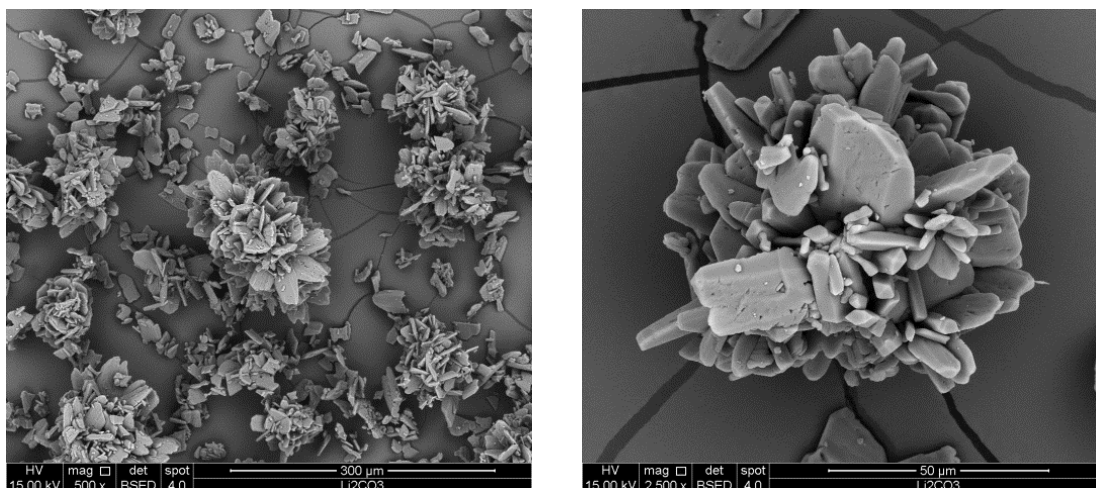


Figure 4.55 SEM micrographs of lithium carbonate particles ex Sigma-Aldrich

PSF Polymer- Li_2CO_3 in 100% Acetonitrile-220rpm – Sample 17

The research so far suggests that sample 1 formed one of the best structured microcapsules. The external morphology was spherical and generally smooth, with a honeycomb internal structure.

In order to improve on the methodology, a new batch of PSF- Li_2CO_3 dispersion was generated using method 12. The drill agitation speed used to generate the microcapsules was reduced slightly to 220rpm and a glass pipette was utilised to create the droplets of polymer dispersion. The dispersion droplets were dropped directly into 30ml of acetonitrile.

The microcapsules generated were then left in acetonitrile over the weekend. The solvent was decanted off, and the particles air-dried.

The light micrograph below, figure 4.56, was obtained using the Zeiss SV8 stereo microscope with a low zoom setting of 0.8x. The micrograph represents both surface and a cross-sectional area of the microcapsule.



Figure 4.56 Light micrograph of PSF Li_2CO_3 microcapsules - sample 17

From this low magnified stereo image, the surface appears smooth, and the general shape of the microcapsule is off-spherical - but that could be a reflection on the droplet formation. The internal morphology looks honeycomb, with some larger visible pores. This is interesting as when sample 2 - containing 20% chloroform - was left over the weekend in the non-solvent blend, the microcapsules were hard, clear, and distorted with a hollow internal structure.

PSF- Li_2CO_3 Dispersion in 80%-Acetonitrile, 10%-Chloroform, 10%-DCM – Sample 18

The purpose of this experiment was to investigate if an initial high agitation drill speed for the delivery of the polymer dispersion, followed by a reduction of the drill speed, would help improve the structure of the microcapsules. The non-solvent is the same composition as used for Sample 3, but the agitation mechanism is different.

The same polymer dispersion used for sample 17 was dropped slowly into a 250ml round-bottomed flask containing a non-solvent blend of 24ml acetonitrile, 3ml chloroform and 3ml DCM, using a glass pipette. The non-solvent was agitated with the IKA RW 20 digital overhead stirrer connected to 40mm centrifugal blades at 450rpm for 10 minutes then

reduced to 220rpm for 30 minutes. The microcapsules were then decanted from the non-solvent and allowed to air-dry. The reason for this increased shear for the addition was an attempt to improve the internal structure but retain the general microcapsule morphology by reducing it to 220rpm for the remaining stirring process.

The light micrograph at figure 4.57 represents both a cross-sectional area and the surface of the resulting microcapsule.



Figure 4.57 Light micrograph of PSF-Li₂CO₃ microcapsule - sample 18

The results demonstrate that the addition of 10% of both chloroform and dichloromethane helped change the morphology of both the internal and outer surface of the microcapsule structure. The internal morphology has an enhanced porous structure that would be favoured for the storage of metal hydride nanoparticles. The external surface, however, shows severe cracking. This methodology would not be suitable for storage of air/moisture-sensitive materials because of the surface cracking.

PSF-Li₂CO₃ Dispersion in 80%-Acetonitrile, 15%-Chloroform, 5%-DCM – Sample 19

The previous experiment, sample 18, generated microcapsules containing a good internal structure, but the external surface was poor showing cracking in many areas. The rationale for this experiment was based on the assumption that the 10% DCM may have influenced the surface cracking as no cracking was observed from sample 2 using 20% chloroform.

This experiment involved increasing the levels of chloroform to 15% and reducing the DCM content to 5% for the non-solvent. The speed of the drill stirrer and time allowed for agitation were identical to those outlined for the previous sample 18.

The resulting light micrograph in figure 4.58, obtained from the microcapsule surface and cross-sectional area, shows an improvement in the general morphology.

The internal structure appears relatively hollow, ideal for the storage of metal hydride particles. The surface is seen to show evidence of minor cracking; thought to be an improvement on sample 18. These results demonstrate that adjusting the ratio of the non-solvent mixture can change the morphology of the microcapsules. However, surface cracking is not ideal for this research.

These finding would suggest that a 5% difference in DCM has made a significant difference to the surface morphology of the microcapsules.



Figure 4.58 Light micrograph of PSF Li_2CO_3 microcapsule - sample 19

PSF- Li_2CO_3 Dispersion in 80%-Acetonitrile, 20%-Chloroform – Sample 20

This experiment was designed to completely eradicate the surface cracking as seen to exist in the 2 previous samples. It was demonstrated with sample 19 that reducing the DCM concentration by 5% made a significant change to the degree of surface cracking. This

involved taking the DCM out of the non-solvent completely and not leaving the samples in the non-solvent for a long period of time.

Sample 20 was obtained using the same conditions of analysis as used for sample 18, except that the DCM was removed from the non-solvent mixture. The non-solvent blend was 24ml of acetonitrile and 6ml of chloroform only.

The resulting light micrograph, obtained using the stereo microscope with a zoom of 0.8x, is encouraging as the cross-section shows a hollow internal structure. The general shape of the microcapsule is slightly off-spherical, and the outer surface appears smooth. The shape of the cross-section is slightly distorted, but this was caused during the cutting process. The sample was cut at room temperature with a sharp razor blade. Due to the delicate hollow structure, the shape of the microcapsule was easily distorted. However, the results demonstrate a good internal morphology as desired.



Figure 4.59 Light micrograph of PSF Li_2CO_3 microcapsule - sample 20

The next 2 samples - 21 and 22 respectively - are the result of changing the ratio of chloroform/acetonitrile.

PSF- Li_2CO_3 Dispersion in 90%-Acetonitrile, 10%-Chloroform – Sample 21

This sample is the result of reducing the levels of chloroform in the non-solvent blend by 10%. The settings for the drill agitation and stirring times remained the same as sample 18,

allowing a direct comparison. The non-solvent blend was 27ml of acetonitrile and 3ml of chloroform.

The resulting light micrograph, figure 4.60, exhibits a smooth outer surface structure with a honeycomb internal morphology, containing some hollow regions.



Figure 4.60 Light micrograph of PSF Li_2CO_3 microcapsule - sample 21

The ratio of chloroform was then increased to 30% to observe any noticeable changes in the structure of the final product for sample 22.

PSF- Li_2CO_3 Dispersion in 70%-Acetonitrile, 30%-Chloroform – Sample 22

The results from increasing the levels of chloroform generated clear microcapsules, which on drying were observed to collapse and appear dehydrated. The example shown in figure 4.61 demonstrates the poor structure of the microcapsules obtained from increasing the levels of chloroform to 30%. The shrivelled product developed a hard structure that was very difficult to cut.



Figure 4.61 Light micrograph of PSF Li_2CO_3 microcapsule - sample 22

Changing the levels of chloroform in the non-solvent blend had a major effect on the morphology of the microcapsule. This will hopefully enable the microcapsule to be designed to a desired structure for the encapsulation of metal hydride materials.

PSF- Li_2CO_3 Dispersion in 80%-Acetonitrile, 20%-Chloroform – Sample 23

A new batch of the PSF- Li_2CO_3 dispersion was prepared following the procedure as outlined in method 12. The results for sample 20 were very good so to be sure this was a genuine result, the same procedure was carried with a slight increase to the initial agitation speed.

Using a glass pipette, small droplets of the polymer-dispersion were released directly into a 250ml round-bottomed flask containing 24ml of acetonitrile and 6ml of chloroform. The non-solvent was agitated using an initial drill stirrer speed of 540rpm until all the polymer dispersion had been added to the non-solvent. The agitation speed was then reduced to 220rpm, and the microcapsules were stirred for an additional 30 minutes. The solvent was then decanted, and the microcapsules were air-dried at room temperature.

The light micrograph in figure 4.62 illustrates that the microcapsules have formed a spherical shaped structure with a relatively hollow internal structure. The outer surface morphology is seen to be slightly uneven and appears as a mixture of opaque and minor transparent regions. This could be a thickness effect as they differ to sample 20, generated using a

slower agitation speed of 450rpm, which appeared completely opaque. The cross-sectional area presents an internal structure that is relatively hollow.



Figure 4.62 Light micrograph of PSF Li_2CO_3 microcapsule - sample 23

PSF- Li_2CO_3 Dispersion in 75%-Acetonitrile, 25%-Chloroform – Sample 24

The same polymer dispersion was introduced using a glass pipette into a non-solvent blend of 75% acetonitrile and 25% chloroform.

The polymer dispersion was added using an agitation speed of 540rpm then reduced to 220rpm for 30mins.

The resulting microcapsules as shown in figure 4.63 present a good shape and have a hollow centre. However, the morphology of the polymer outer surface is a definite mix of clear and opaque structure, showing signs of a different topography that could represent surface cracking. These microcapsules do not appear as robust as the previous sample (23) generated using a 20% chloroform non-solvent mix.



Figure 4.63 Light micrograph of PSF Li_2CO_3 microcapsule - sample 24

PSF- Li_2CO_3 Dispersion in 80%-Acetonitrile, 20%-Chloroform – Sample 25

Some changes were introduced to this experiment to further comprehend the stability of the microcapsules in the non-solvent blend, together with an attempt to reduce the size of the microcapsule. The non-solvent mix was changed back to 80% acetonitrile and 20% chloroform, as this configuration was proven to form the most suitable microcapsules. To control the size of the generated microcapsules, the polymer dispersion was released into the non-solvent mix using a BD Microlance 3 20G(0.9mmx40mm) needle connected to a BD Plastipak 1ml syringe needle with an agitation speed of 450rpm. Once the initial addition of the dispersion was complete, the agitation speed was reduced to 220rpm for 1 hour. The microcapsules were left in the non-solvent overnight. The following morning, the solvent was decanted, and the microcapsules were air-dried at room temperature.



Figure 4.64 Light micrograph of PSF Li_2CO_3 microcapsule - sample 25

The microcapsules appeared as a mixture of both clear and opaque colouration. Little evidence was available to suggest they had collapsed. The light micrograph as shown in figure 4.64 suggests some evidence of outer surface cracking. The internal structure is good, displaying a hollow internal structure. Leaving the microcapsules overnight in the non-solvent had introduced issues with the morphology.

It was therefore necessary to evaluate the issues, as outlined, regarding the resting time in the non-solvent.

PSF-Li₂CO₃ Dispersion in 80%-Acetonitrile, 20%-Chloroform – Sample 26

This sample was prepared using the same conditions as sample 25 but the microcapsules were not left overnight in the non-solvent. The polymer-dispersion was introduced to the non-solvent using a 1ml syringe and a BD Microlance 3 20G(0.9x40mm) needle. The agitation speed for the initial addition of polymer dispersion to the non-solvent system was 450rpm, which was then reduced to 220rpm for an additional 45mins. After the agitation was complete, the non-solvent was immediately decanted, and the microcapsules were air-dried.

The results from this methodology are very good, as microcapsules were generated that display excellent morphology. Figure 4.65 represents a simple light micrograph obtained from both surface and cross-sectional area of the microcapsule. The slight distortion observed on the microcapsule is the result of cutting the hollow microcapsule without first freezing below the PSF glass transition temperature. The particle has an opaque, smooth surface and appears free from surface cracking. The internal structure is hollow with a uniform and solid outer wall. Clearly, these results confirm that leaving the microcapsules overnight in the non-solvent, as for sample 25, had caused issues to the general morphology of the PSF-Li₂CO₃ microcapsules.



Figure 4.65 Light micrograph of PSF Li_2CO_3 microcapsules - sample 26

The cross-sectioned microcapsules were further examined using high resolution scanning electron microscopy utilising the FEI Quanta 250. The SEM micrographs at figure 4.66 were obtained using BSED detection and system magnifications of 100x and 1000x respectively.

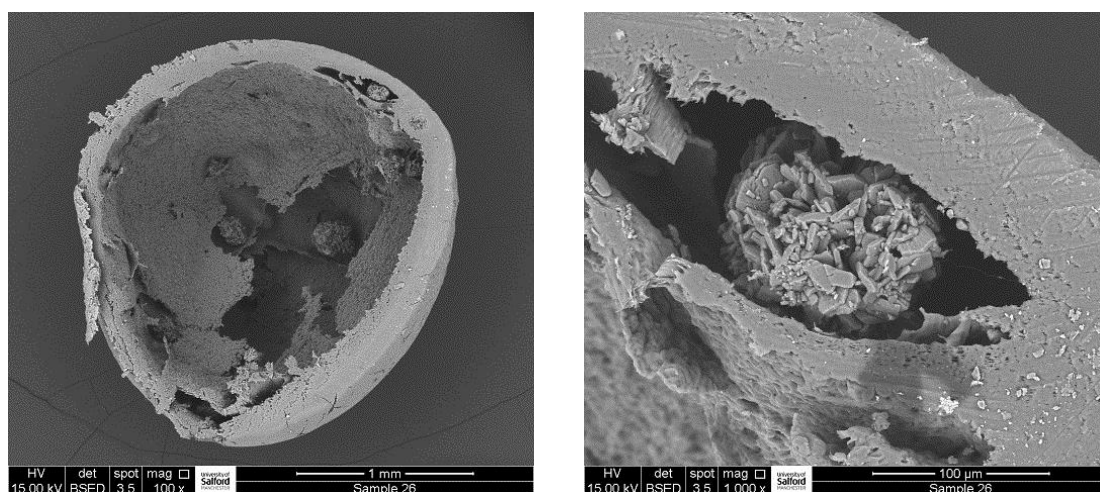


Figure 4.66 SEM micrograph of cross-sectioned PSF Li_2CO_3 microcapsule - sample 26

Both SEM micrographs clearly demonstrate that the microcapsule has a solid external wall with a hollow internal structure. These designed microcapsules have a polymer wall structure strong enough to maintain the spherical structure but soft enough to easily cross-section. Interestingly, clusters of Li_2CO_3 can be seen to be present within the centre of the microcapsule and encased around the inner wall structure. These results are excellent, presenting a microcapsule structure that would be ideal for the storage and safe characterisation of metal hydride particles.

Changing the ratio of Acetonitrile to Chloroform

The light micrograph, figure 4.67, presents the effect of changing the ratio of acetonitrile to chloroform. It was clearly observed that a 10% concentration of chloroform produced a solid microcapsule with a honeycomb internal structure. Increasing the concentration of chloroform to 20% changed the internal structure, generating microcapsules with a hollow internal morphology - ideal for the requirements of this project. When the concentration of chloroform was increased to 30%, the resulting microcapsules had a completely different morphology. They appeared transparent, existing as a hard, shrivelled shell. It is thought that the inclusion of solvent might cause softening as polysulfone is naturally brittle. Using 30% chloroform may have contributed to the complete drying of the polymer too quickly.



Figure 4.67 Light micrograph of microcapsules from different solvent ratios

PSF-Li₂CO₃ Dispersion in 80%-Acetonitrile, 20%-Chloroform reduced Agitation – Sample 27

This experiment was designed to study the influence of leaving the microcapsules in the non-solvent blend after the initial formation of the microcapsules.

A new batch of microcapsules was generated following the same experimental conditions as outlined for sample 26. However, shortly after the formation of the microcapsules, the

solvent was removed and the microcapsules were air-dried, thus preventing the additional agitation at 220rpm for 45 minutes in the non-solvent.

Figure 4.68 is a light micrograph demonstrating both the surface and a cross-sectioned internal structure of the microcapsule. The results illustrate that the strength of the outer wall was not enough to maintain a spherical structure, as the capsules collapsed upon drying. Interestingly, the cross-sectioned microcapsule shows a hollow centre, which would be ideal for the encapsulation of small metal hydride particles. This shows that the additional agitation for 45 minutes after the formation of the capsules is essential to strengthen the polymer structure.



Figure 4.68 Light micrograph of PSF Li_2CO_3 microcapsules - sample 27

4.3 Encapsulation of Lithium Phosphate (Li_3PO_4)

The limitation of EDX analysis as a technique is the ability to detect very light elements. The EDX detection systems used in this research utilise a polymer-based thin window to protect the sensitive silicon crystal. The polymer window allows for the detection of light elements down to boron.

Encapsulating Li_2CO_3 made it difficult to characterise the small particles using EDX analysis as the EDX detection system available could not detect lithium. Both PSF polymer and Li_2CO_3

contain carbon and oxygen so to help differentiate between the salt and the polymer, the Li_2CO_3 was substituted by Li_3PO_4 .

Phosphorus can be readily detected using EDX analysis, making it a good substitute for Li_2CO_3 to encapsulate within the PSF-polymer microcapsules.

PSF- Li_3PO_4 Dispersion in 80%-Acetonitrile, 20%-Chloroform – Sample 28

A batch of PSF- Li_3PO_4 dispersion was generated using the method as outlined in method 13.

Using a glass pipette, the polymer dispersion was slowly added to a non-solvent blend of 24ml acetonitrile and 6ml of chloroform. The addition was slow, over a 10-minute period, with an agitation speed of 450rpm, utilising the IKA RW 20 digital overhead stirrer connected to 40mm centrifugal blades. Once the addition was complete, the agitation speed was reduced to 216rpm for 45 minutes.

The solvent blend was then decanted from the flask and the microcapsules were air-dried at room temperature.

The light micrograph given below, figure 4.69, displays that the methodology used has generated a good spherical-shaped microcapsule. The surface of the microcapsule appears smooth, showing little signs of cracking. The light micrograph also displays a microcapsule that had been sliced open using a razor blade. The cross-sectioned particle reveals an outer wall containing a semi-hollowed inner core.



Figure 4.69 Light micrograph of PSF Li_3PO_4 microcapsules - sample 28

SEM-EDX was utilised to demonstrate the presence of encapsulated Li_3PO_4 particles. The resulting SEM micrographs, figure 4.70, were obtained using back scattered electron detection (BSED) from a cross-sectional area of a generated microcapsule. The SEM micrographs were obtained using system magnifications of 100x and 1000x respectively. The micrograph obtained using 1000x magnification displays patches of high contrast areas within the outer wall structure. These are thought to be clusters of the Li_3PO_4 nanoparticles.

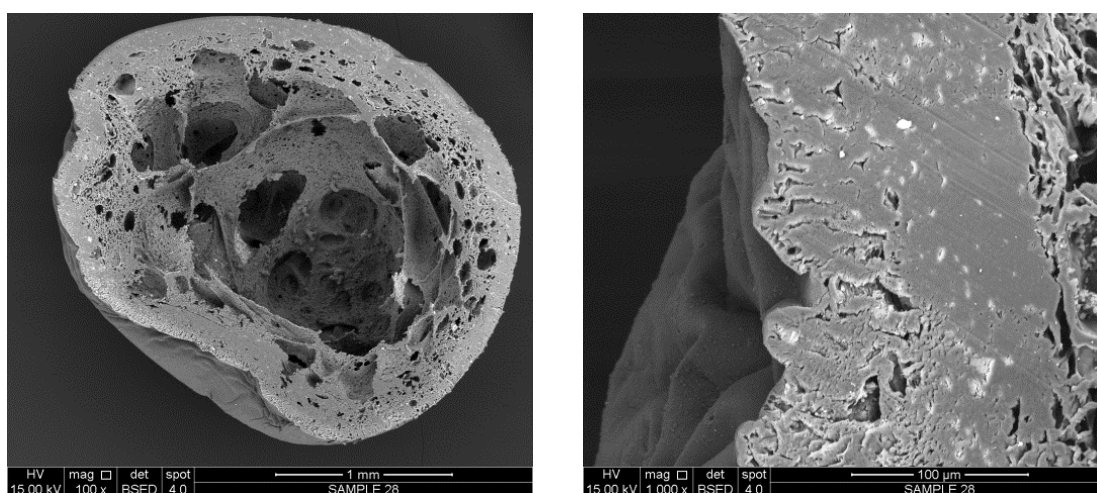


Figure 4.70 SEM micrographs of cross-sectioned PSF Li_3PO_4 microcapsule - sample 28

To identify the presence of Li_3PO_4 , an area showing high contrast together with a separate area displaying low contrast was examined using EDX analysis.

The EDX spectrum overlay, figure 4.71, verifies the presence of the Li_3PO_4 nanoparticles existing in the high contrast regions. The EDX spectra overlay is comprised of a spectrum obtained from a spot probe of a high contrast region, together with a second spectrum obtained from a low contrast area, representing the PSF polymer.

The EDX spectrum obtained from the PSF polymer displays high levels of carbon and oxygen together with lower levels of sulfur. Smaller peaks are observed that represent platinum and palladium used in the sample preparation. The spectrum obtained from the high contrast area is different - showing high levels of phosphorus and oxygen, with lower sulfur and carbon from the polymer - confirming the presence of Li_3PO_4 .

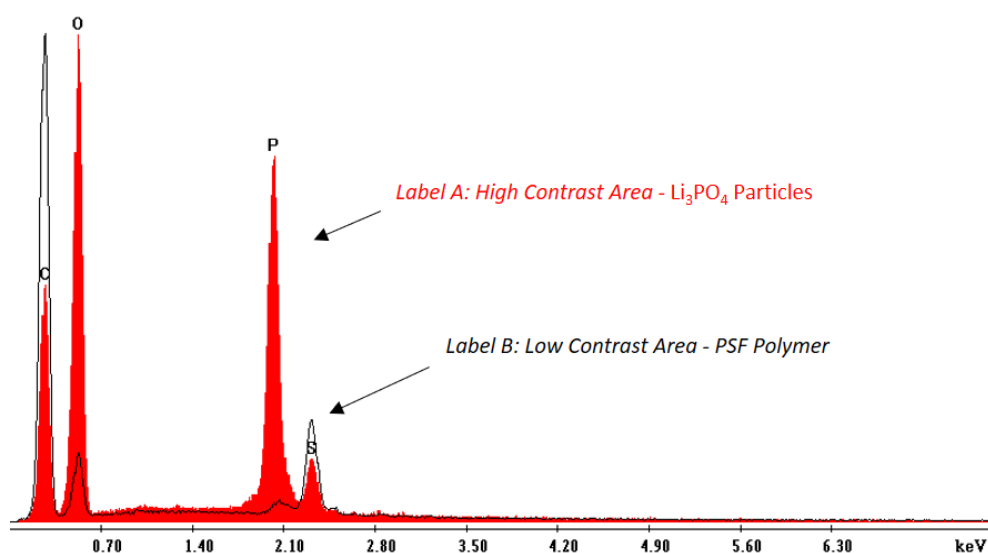


Figure 4.71 EDX spectrum overlay from PSF polymer and Li_3PO_4 particles - sample 28

PSF added to a Dispersion of Li_3PO_4 in 80%-Acetonitrile, 20%-Chloroform – Sample 29

This sample is the result of an experiment that involved pipetting droplets of the polymer solution directly into a dispersion of 0.1g of Li_3PO_4 in 24ml of acetonitrile and 6ml of chloroform.

The polymer solution was generated using the same experimental conditions as previously outlined for sample 28, but this time Li_3PO_4 was not dispersed into the PSF polymer.

The Li_3PO_4 salt dispersion was generated in a separate round-bottomed flask in the presence of 24ml of acetonitrile and 6ml of chloroform.

The Li_3PO_4 dispersion was agitated using an IKA RW 20 digital overhead stirrer with 40mm centrifugal stirrer blades at 640rpm for 20 minutes. Using a glass pipette, the polymer was slowly dripped into the salt dispersion in the non-solvent blend. The addition was carried out using an agitation speed of 450rpm. Once the addition of the polymer was complete, the agitation speed was reduced to 240rpm for 45 minutes.

The light micrograph figure, 4.72, represents the resulting microcapsule, showing a hollow internal structure together with a smooth outer surface.



Figure 4.72 Light micrograph of PSF Li_3PO_4 microcapsules - sample 29

When examined using high resolution SEM utilising back scattered electron detection, the surface of the microcapsule, shown at figure 4.73, appears to be coated in the Li_3PO_4 particles.

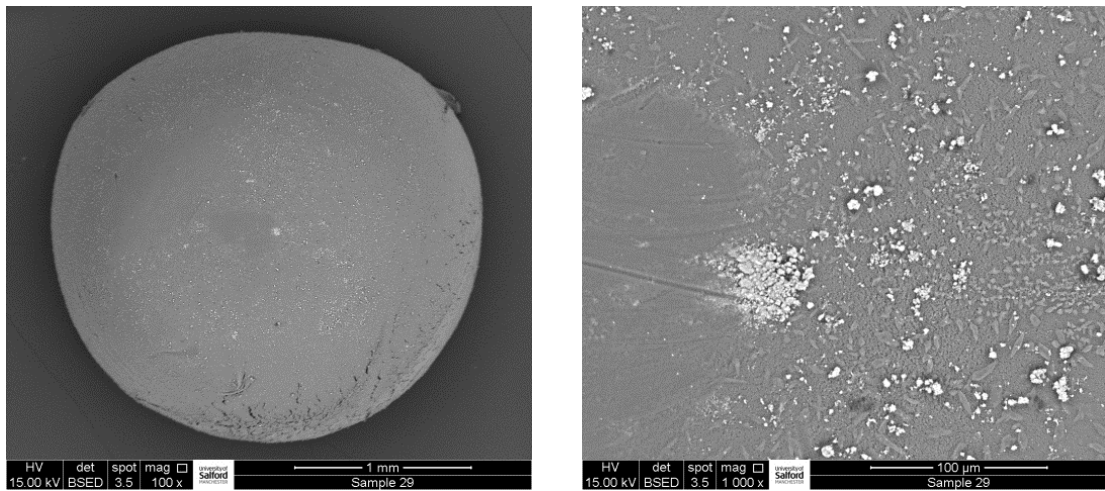


Figure 4.73 SEM micrographs of surface PSF Li₃PO₄ microcapsule - sample 29

The cross-sectioned microcapsule presented in figure 4.74 shows very little evidence of any Li₃PO₄ existing within the inner core or the wall of the microcapsule.

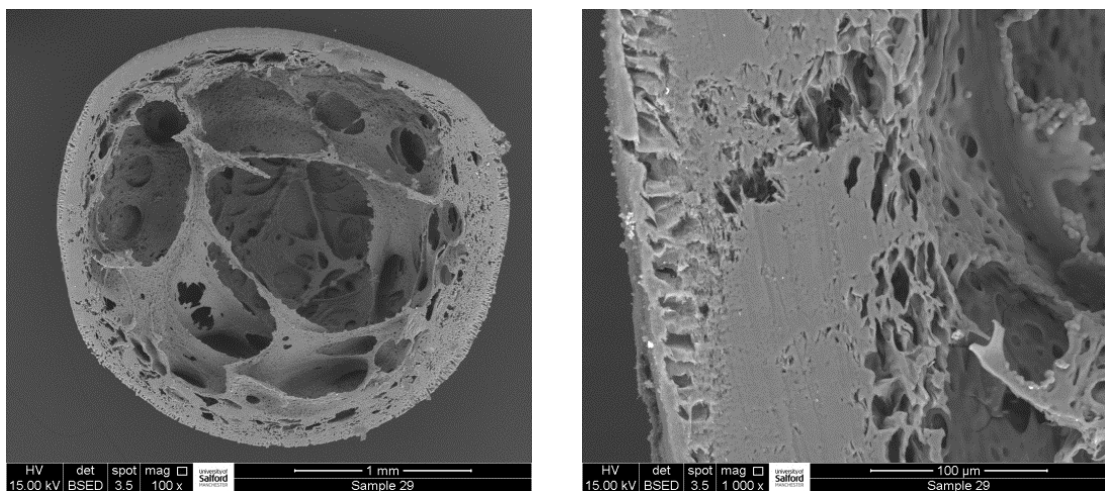


Figure 4.74 SEM micrographs of cross-sectioned PSF Li₃PO₄ microcapsule - sample 29

The small particles on the surface of the microcapsule were examined using EDX analysis and the results, as shown in figure 4.75, suggest the presence of Li₃PO₄. The EDX spectrum shows high levels of phosphorus and oxygen. This was not a suitable method for encapsulating Li₃PO₄ into PSF polymer.

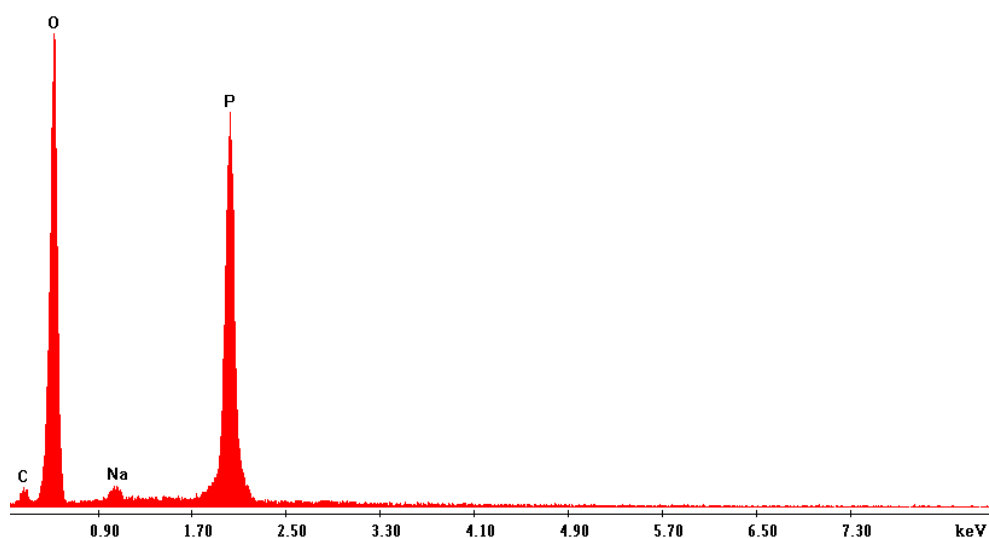


Figure 4.75 EDX spectrum of surface particles - sample 29

PSF-Li₃PO₄ Dispersion in 80%-Acetonitrile, 20%-Chloroform – Sample 30

A new batch of PSF-Li₃PO₄ dispersion was produced following the conditions as outlined in method 13. A slight modification involved grinding the Li₃PO₄ salt to a finer powder, using a pestle and mortar, before it was added to the PSF polymer solution. This procedure was used to minimise aggregation and reduce the primary particle size of the particles.

Using a BD Microlance 3 20G (0.9mm x 40mm) needle and a 1ml syringe, the polymer dispersion was slowly added to a non-solvent blend of 24ml acetonitrile and 6ml of chloroform. The addition was carried out over a 10-minute period using an agitation speed of 500rpm. Once the addition of the PSF-Li₃PO₄ dispersion was complete, the agitation speed was reduced to 240rpm, and the microcapsules were left to stir for an additional 45 minutes.

The solvent blend was then decanted from the flask and the microcapsules were air-dried at room temperature.

The light micrograph below, figure 4.76, illustrates that the microcapsules exist as a mixture of opaque and clear polymer beads, containing a hollow centre. The clear microcapsule shows patches of white regions, thought to be clusters of Li_3PO_4 . The particles are spherical but contain an additional extension - assumed to be the result of the polymer fusing as it leaves the syringe, generating a trailing section.



Figure 4.76 Light micrograph of PSF Li_3PO_4 microcapsules - sample 30

These results are not ideal as differences can be seen between the generated microcapsules. Sample 31 follows the same procedure, except the solvent for the PSF was changed from NMP to DMF.

PSF (DMF)- Li_3PO_4 Dispersion in 80%-Acetonitrile, 20%-Chloroform – Sample 31

This experiment was chosen to evaluate if DMF would offer a preferred alternative solvent for the PSF rather than NMP. The resulting micrographs from samples 28 and 30 show the LiPO_4 to be present in the wall of the microcapsules, which would not be ideal.

A new batch of PSF- Li_3PO_4 dispersion was generated by changing the initial solvent from NMP to DMF using the methodology as given in method 14.

Using a BD Microlance 3 20G (0.9mm x 40mm) needle and a 1ml syringe, the polymer dispersion was slowly added to a non-solvent blend of 24ml acetonitrile and 6ml of chloroform. This process took place over a 10-minute period, using an agitation speed of

500rpm. Once the addition of polymer dispersion was complete, the agitation speed was reduced to 240rpm for 45 minutes.

The light micrograph at figure 4.77 reveals that the generated microcapsules exist as non-spherical particles. The surface appears smooth, and the cross-sections show a semi-hollow inner core. The particles show evidence of a warped extension as previously observed from sample 30, and a slight mis-shape due to the polymer solidifying as it left the needle.



Figure 4.77 Light micrograph of PSF Li_3PO_4 microcapsules - sample 31

PSF in DMF- Li_3PO_4 Dispersion in 80%-Acetonitrile, 20%-Chloroform – Sample 32

This experiment is based on an attempt to move away from the drill agitation device. Metal hydrides are extremely moisture-sensitive, so it is essential to minimise any exposure to air. The drill agitation unit requires an open neck to allow the stirring pole to rotate. This is not an ideal situation for air/moisture-sensitive materials.

An alternative to the drill agitation unit is the use of the magnetic agitation unit. Using a suitable round-bottomed flask and the yellow line magnetic stirring unit, controlled agitation can be achieved in a sealed vessel, maintaining an airtight environment.

A new PSF- Li_3PO_4 dispersion was generated using the same method as outlined in method 14.

The polymer dispersion was slowly added to 24ml of acetonitrile and 6ml of chloroform using a small BD Microlance 3 20G (0.9mm x 40mm) needle connected to a 1ml syringe, utilising an agitation speed of 4. The generated microcapsules were removed from the non-solvent blend after 15 minutes.

The light micrograph as given below in figure 4.78 illustrates that the microcapsules are semi-transparent and have a poor morphology. A longer time was possibly required in the non-solvent blend to achieve stronger microcapsules.



Figure 4.78 Light micrograph of PSF Li_3PO_4 microcapsules - sample 32

PSF in DMF- Li_3PO_4 Dispersion in 80%-Acetonitrile, 20%-Chloroform – Sample 33

A new batch of polymer- Li_3PO_4 dispersion was generated following the same method as outlined in the previous sample 32. The PSF- Li_3PO_4 dispersion was then slowly added to 24ml acetonitrile and 6ml chloroform using a BD Microlance 3 20G (0.9mm x 40mm) needle and a 1ml syringe whilst stirring in a 250ml round-bottomed flask using a cross-shaped magnetic bead and an agitation speed setting of 4.

The generated microcapsules were then left for an additional 45 minutes, to allow the polymer to harden before the non-solvent was removed, allowing the microcapsules to air-dry. The light micrograph, figure 4.70, illustrates the effect of leaving the microcapsules longer in the non-solvent after the formation the spherical structure. These generated

microcapsules are spherical, with a smooth outer surface. The internal morphology is honeycomb, containing some larger hollows.



Figure 4.79 Light micrograph of PSF Li_3PO_4 microcapsule - sample 33

Improved resolution of the internal structure of the microcapsules was obtained using the Quanta 250 SEM. The micrographs as given in figure 4.80 were obtained using BSED detection and system magnifications of 100x and 1000x respectively.

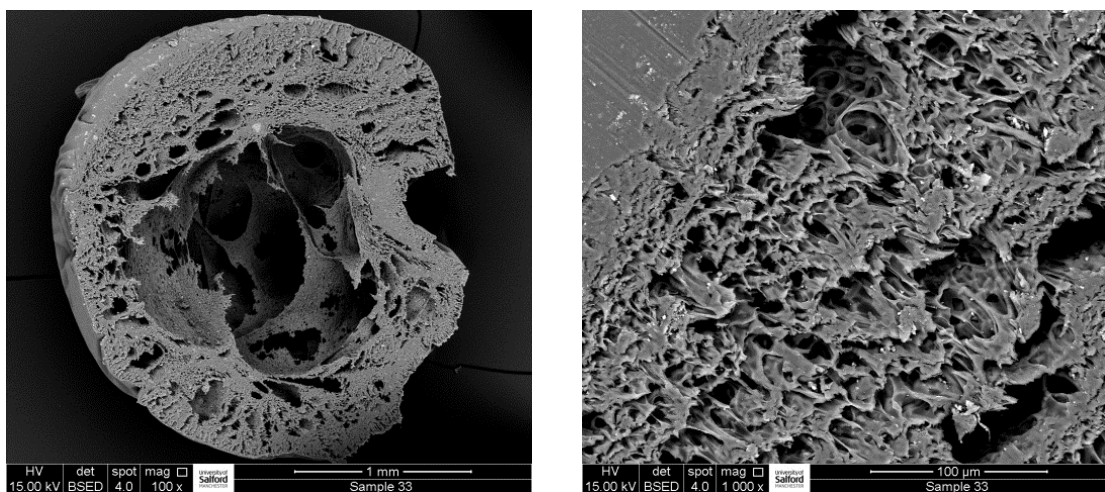


Figure 4.80 SEM micrograph of cross-sectioned PSF Li_3PO_4 microcapsule - sample 33

The internal structure is relatively hollow, surrounded by an outer honeycomb porous structure containing a variety of different pore sizes.

Due to the issues regarding solubility of PSF and reduced internal porosity of the microcapsule structure, it seemed logical to go back to the initial solvent system utilising NMP. For this research project, it was necessary to try many different solvent combinations with the aim of finding the best conditions to produce robust microcapsules.

PSF in NMP-Li₃PO₄ Dispersion in 80%-Acetonitrile, 20%-Chloroform – Sample 34

The preferred formation of a microcapsule for this research project would be a single outer wall as achieved for sample 26. Efforts to improve on the morphology of the microcapsules were continued with the aim of improving the internal structure. A fresh new batch of PSF-Li₃PO₄ dispersion was prepared utilising the method as defined in method 13.

Using a BD Microlance 3 20G (0.9mm x 40mm) needle coupled to a 1ml syringe, droplets of the PSF-Li₃PO₄ dispersion were gradually released into the non-solvent blend of 24ml acetonitrile and 6ml of chloroform within a 250ml round-bottomed flask. The addition was made over a 10-minute period, using an agitation speed of 8 with a small 12mm diameter disc-shaped magnetic stirring bar.

The microcapsules were stirred for an additional 40 minutes; the excess solvent was decanted, and the microcapsules were air-dried at room temperature overnight.

The light micrograph at figure 4.81 represents both surface and cross-sectioned areas of the generated microcapsules. These microcapsules present a perfect morphology, demonstrating a spherical particle with smooth outer surface. The internal structure displays good porosity throughout the microcapsule structure.



Figure 4.81 Light micrograph of PSF Li_3PO_4 microcapsule - sample 34

Further examination of the internal structure of a microcapsule was achieved using high resolution SEM. Figure 4.82 illustrates that the internal morphology is hollow with evidence of small particles existing within the pores, thought to be Li_3PO_4 .

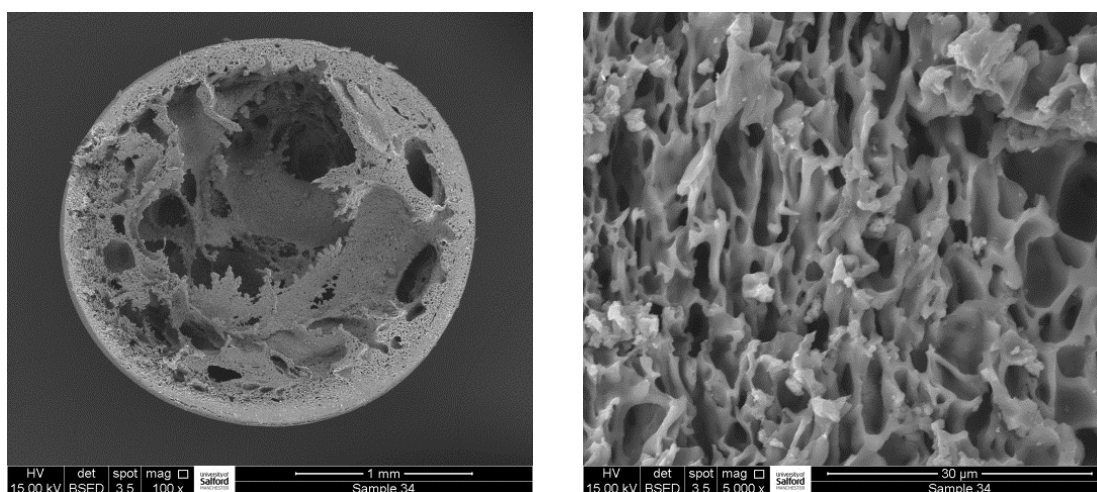


Figure 4.82 SEM micrograph of cross-sectioned PSF Li_3PO_4 microcapsule - sample 34

EDX analysis was utilised to examine the small particles present in clusters within the pores. The results confirm the presence of Li_3PO_4 as demonstrated in the EDX spectra overlay - figure 4.83.

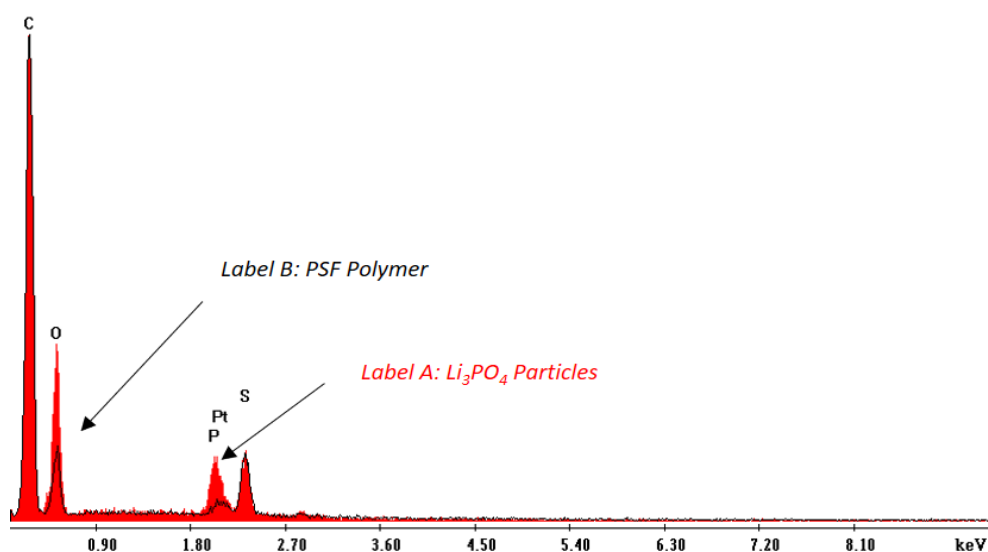


Figure 4.83 EDX spectra overlay PSF surface against Li_3PO_4 particles - sample 34

The EDX spectra overlay represents examination of both the nanoparticles thought to be Li_3PO_4 and the PSF polymer away from the particles. The EDX spectrum from the analysis of a cluster of particles shows the presence of phosphorus, sulfur, carbon and oxygen. The polymer background gave a spectrum showing only carbon, oxygen and sulfur as expected from the PSF polymer. The platinum and palladium peaks are associated with the sample preparation, as 4nm of Pt/Pd was sputter-coated onto the surface of the cross-section using the Cressington 208 coating unit to minimise electron charging issues.

Using NMP as the polymer solvent and increasing the agitation speed from 4 to 8 has shown an improvement in the microcapsule formation.

PSF in DMF- Li_3PO_4 Dispersion in 80%-Acetonitrile, 20%-Chloroform – Sample 35

This experiment was aimed at evaluating the effect of increasing the agitation speed to 8 during the polymer dispersion addition to the non-solvent blend.

Sample 34 generated an excellent microcapsule formation using the faster agitation rate of 8.

It was necessary to fully understand if the improved microcapsule structure was the result of increasing the agitation rate or changing from DMF to NMP solvent for the polymer dissolution. Therefore, this time the same experimental conditions as sample 34 were used, except NMP was substituted for DMF.

The resulting SEM micrographs, figure 4.84, were obtained using system magnifications of 200x and 10,000x from the outer surface of the microcapsule.

The low magnified SEM micrograph displays the surface morphology has very little cracking but does show some porosity. The higher magnified micrographs show clearly the microcapsule has a porous outer surface with some regions containing crystalline particles – that could represent Li_3PO_4 .

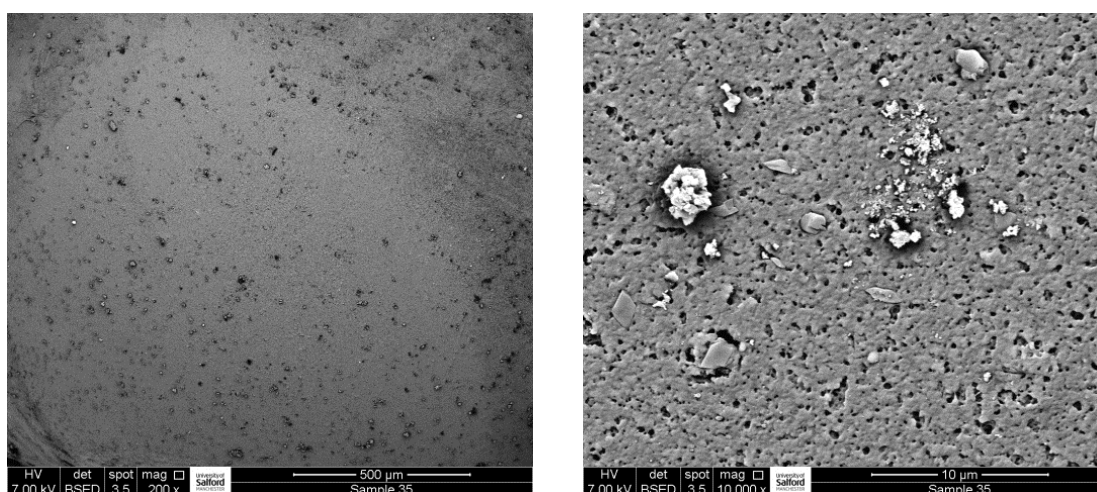


Figure 4.84 SEM micrograph of surface PSF Li_3PO_4 microcapsule - sample 35

The SEM micrographs obtained from a cross-sectioned microcapsule (figure 4.85) display a semi hollow morphology, with nanoparticles of Li_3PO_4 seen to exist within the outer wall.

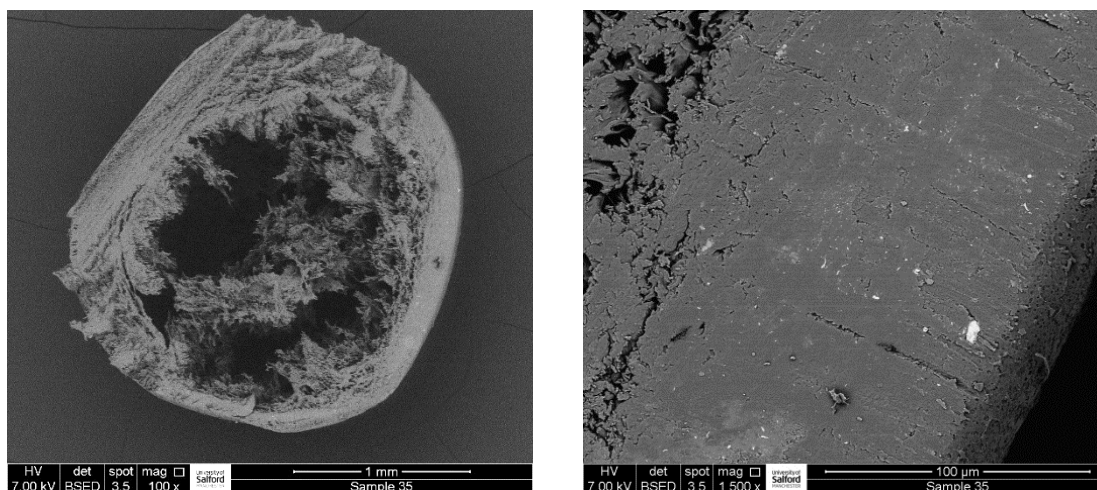


Figure 4.85 SEM micrograph of cross-sectioned PSF Li_3PO_4 microcapsule - sample 35

These results are an improvement on the internal structure observed for sample 33 using the lower agitation rate of 4. However, the general morphology of sample 34 achieved using NMP as the initial solvent for the PSF polymer is significantly better.

4.4 Encapsulating Moisture-Sensitive Lithium Amide (LiNH_2)

PSF in NMP – LiNH_2 Dispersion in 80%-Acetonitrile, 20%-Chloroform – Sample 36

This sample is the first attempt to work with a moisture-sensitive reactive material.

Lithium amide was chosen, as this nanomaterial follows on from the previous experimental work completed in 2013 (Baldissin et al., 2013).

Lithium amide is a flammable inorganic compound which reacts with moisture from the air to release flammable gases that can be harmful. To successfully encapsulate lithium amide, it was essential that the nanoparticles would not have any exposure to air/moisture. Lithium amide particles in contact with water will react, generating ammonia gas and corrosive lithium hydroxide.

A small glove box was used to allow the LiNH_2 container purchased from Sigma-Aldrich to be opened under nitrogen.

A batch of PSF polymer – LiNH_2 dispersion was prepared using the experimental conditions as outlined in method 15.

The apparatus was set up in the fume cupboard using a 100ml round-bottomed 2-neck flask containing 24ml acetonitrile and 6ml chloroform. A small 12mm diameter disc-shaped magnetic stir bar was added to the flask. The flask was then clamped over the IKA yellow line magnetic stirring unit to allow agitation of the non-solvent. A glass extension with a separate side arm was fixed into the top neck of the round-bottomed flask, and a stopcock adapter was secured to the other neck. Nitrogen connections were then fastened to both the round-bottomed flask and the glass extension. The top of the extension was left open to allow the polymer dispersion to be pipetted into the non-solvent.

Under nitrogen, a small amount of the polymer dispersion was taken (using a glass pipette) from the conical flask and pipetted under a flow of nitrogen into the non-solvent mix with an initial agitation speed setting of 4.

The generated microcapsules were stirred for an additional 45 minutes before the excess non-solvent was removed using a glass pipette under nitrogen. The microcapsules were dried overnight under a continuous nitrogen purge.

The light micrograph below in figure 4.86 shows the microcapsules to have a smooth outer surface, free from cracking, and a porous internal structure together with a visible outer wall structure.



Figure 4.86 Light micrograph of PSF LiNH₂ microcapsules - sample 36

To improve on the detail of the internal morphology, the cross-sectioned particles were examined using high resolution SEM, utilising the FEI Quanta 250.

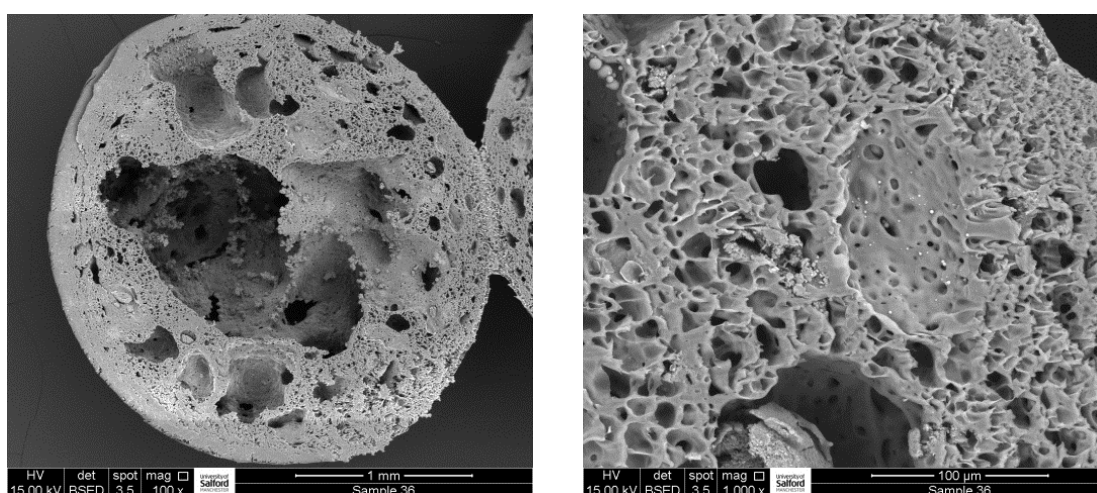


Figure 4.87 SEM micrograph of cross-sectioned PSF LiNH₂ microcapsule - sample 36

The SEM micrographs, figure 4.87, confirm that a good internal structure had been achieved. The internal morphology is porous, displaying clusters of particles within the pores - thought to be lithium amide. EDX analysis was utilised to characterise the nanoparticles.

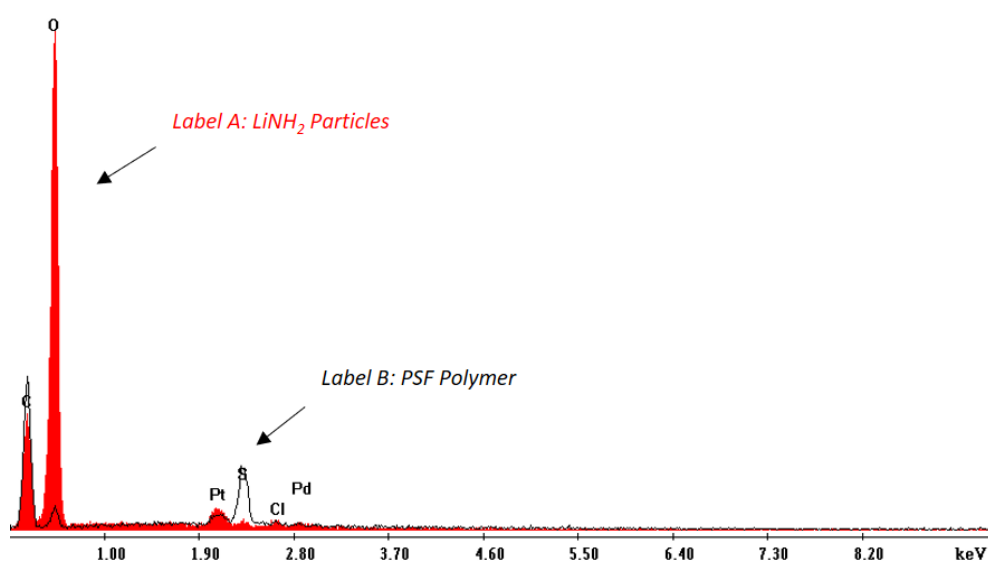


Figure 4.88 EDX spectra overlay PSF polymer against LiNH₂ particles - sample 36

The resulting EDX spectra overlay, figure 4.88, represents the analysis from both the observed nanoparticles, together with surrounding PSF polymer. The results illustrate that the particles analysed contain carbon with high levels of oxygen and trace levels of chlorine. When an area away from the particles was examined, the resulting EDX spectrum from the polymer substrate was consistent with the PSF polymer, displaying carbon, sulfur and lower levels of oxygen.

The lightest element that EDX analysis can detect is boron. Due to this, it is not possible to detect lithium using EDX. Because of the high levels of oxygen, the results would suggest that the LiNH₂ has reacted with moisture to form the hydroxide, LiOH. Future experimental work is required to allow the microcapsules to be cross-sectioned under nitrogen and transferred into the SEM chamber avoiding exposure to moisture. However, the results suggest that it has been experimentally possible to encapsulate LiNH₂, under a nitrogen atmosphere.

PSF in NMP – LiNH₂ Dispersion in 80%-Acetonitrile, 20%-Chloroform – Sample 37

To reduce the size of the generated microcapsules, the glass pipette was substituted for a BD Plastipak 1ml syringe connected to a BD Microlance 3 20G (0.9mm x 40mm) needle. The polymer dispersion was pipetted into the non-solvent blend utilising an agitation speed setting of 4.

The generated microcapsules were examined using light microscopy and the resulting microcapsules are presented in figure 4.89. The light micrograph reveals that substituting the glass pipette for the Microlance 3 needle has reduced the particle diameter of the microcapsules. The surface of the microcapsule is smooth and appears free from defects. The cross-section displays an internal porous structure, showing a satisfactory hollow centre that is surrounded by the porous honeycomb effect.

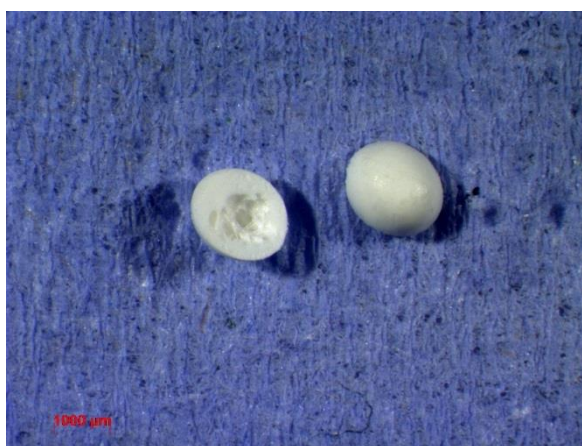


Figure 4.89 Light micrograph of PSF LiNH₂ microcapsule - sample 37

The sample was further examined using the FEI Quanta 250 utilising secondary electron detection for enhanced spatial resolution over back scattered electron detection. The resulting SEM micrographs shown in figure 4.90 were generated using system magnifications of 100x and 10,000x respectively. The higher magnified area reveals that many small nanoparticles are present within the pores of the cross-sectioned microcapsule. These are thought to represent clusters of LiNH₂ as seen in the previous sample 36.

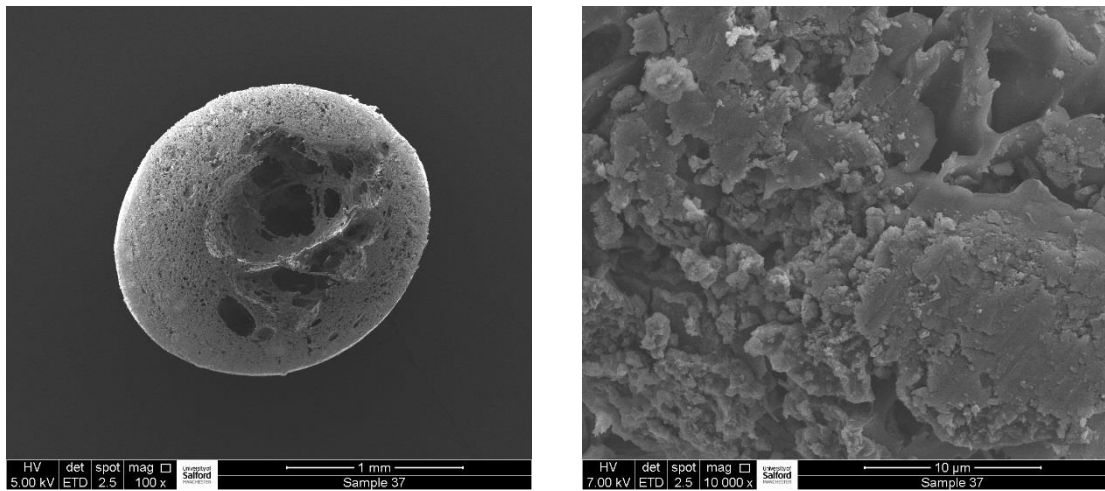


Figure 4.90 SEM micrograph of cross-sectioned PSF LiNH₂ microcapsule - sample 37

The EDX spectrum below (figure 4.91) replicates the same results as seen from the previous sample 36. The nanoparticles generated an EDX spectrum displaying high levels of oxygen with lower levels of carbon. When compared directly against a particle-free area of the polymer, only carbon and sulfur with low levels of oxygen were detected. These results would suggest that the LiNH₂ has again formed the hydroxide.

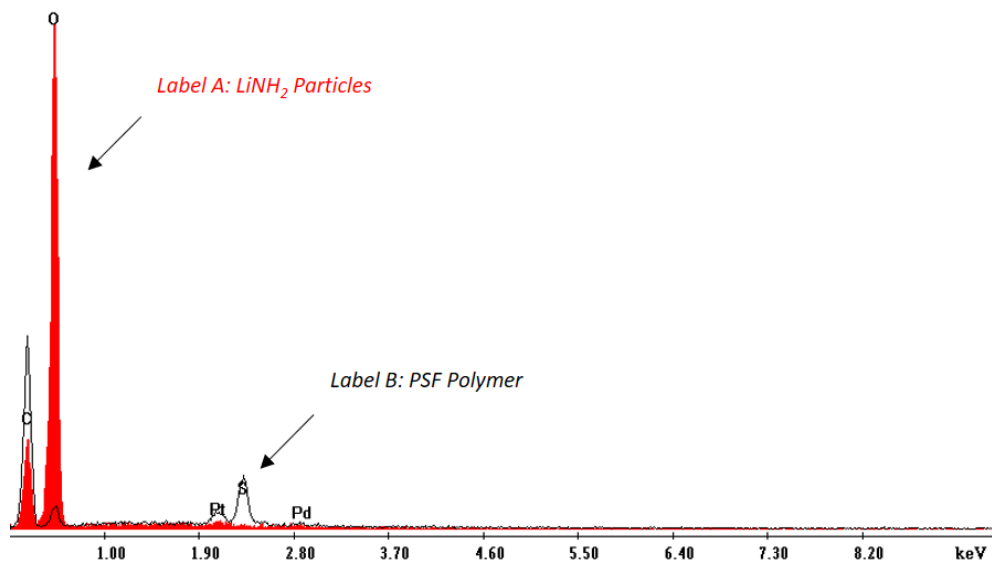


Figure 4.91 EDX-spectra overlay PSF polymer against LiNH₂ particles - sample 37

PSF in NMP – LiNH₂ Dispersion in 80%-Acetonitrile, 20%-Chloroform – Sample 38

The internal structure obtained from both samples 36 and 37 were good demonstrating a porous environment that was adequate for encapsulating small particles. This experiment is designed to improve the internal morphology by reducing the honeycomb structure. The procedure involved releasing the polymer dispersion into the non-solvent blend using an increased agitation speed of 8 as previously outlined for sample 34.

The resulting microcapsule as given in figure 4.92 shows a slight improvement to the internal porosity of the microcapsule.



Figure 4.92 Light micrograph of PSF-LiNH₂ microcapsule - sample 38

The SEM micrographs as shown in figure 4.93 confirm that increasing the agitation speed on delivery of the polymer dispersion droplets to the non-solvent blend has improved the internal structure. The spheres are slightly off-spherical so the method might benefit from reducing the agitation speed after the initial introduction of the polymer dispersion.

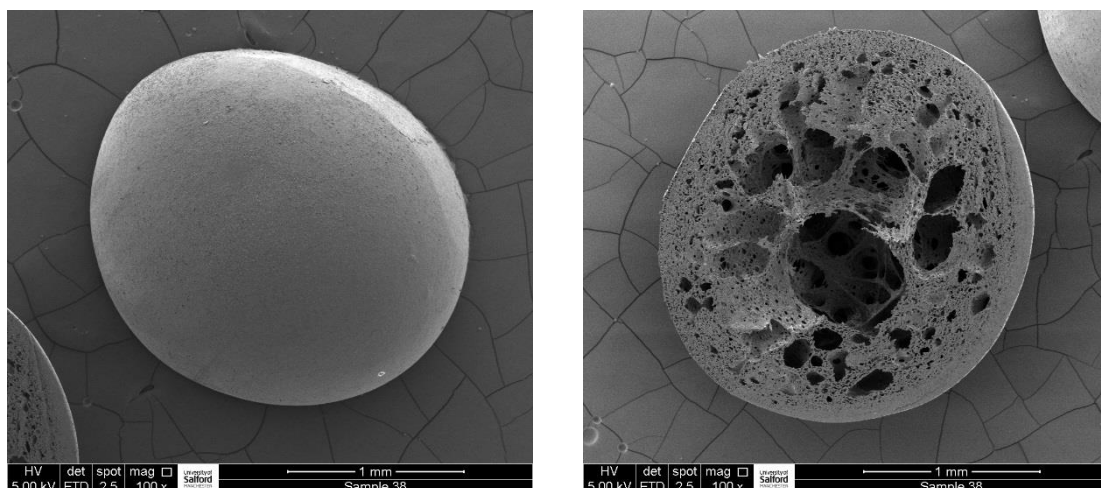


Figure 4.93 SEM micrographs of PSF LiNH₂ microcapsules - sample 38

PSF in NMP – LiNH₂ Dispersion in 80%-Acetonitrile, 20%-Chloroform – Sample 39

This sample preparation involved following the same procedure as outlined for the previous sample 38. However, the agitation speed after the initial addition of the polymer dispersion was reduced from 8 to 4 after a 5-minute time-period.

The resulting microcapsule, as shown in light micrograph figure 4.94, demonstrates an improved spherical shape. The microcapsules exist as a good spherical structure containing a porous internal morphology. Reducing the speed has improved the general microcapsule shape, maintaining an effective porous internal structure.



Figure 4.94 Light micrograph of PSF LiNH₂ microcapsule - sample 39

One of the issues at this stage of this research project was that the microcapsules had to be cut open on the bench in the lab then transferred to the sputter coating unit, followed by an additional transfer to the microscope. In this time, moisture could have reacted with the LiNH_2 producing the hydroxide. Another assumption could be that perhaps the purchased LiNH_2 had already reacted forming the hydroxide before the encapsulation process.

Although the project appeared to have been successful, proof of encapsulation of LiNH_2 could not be obtained because, at this stage of the project, there was no way of cutting and transferring the samples into the electron microscope under an inert atmosphere.

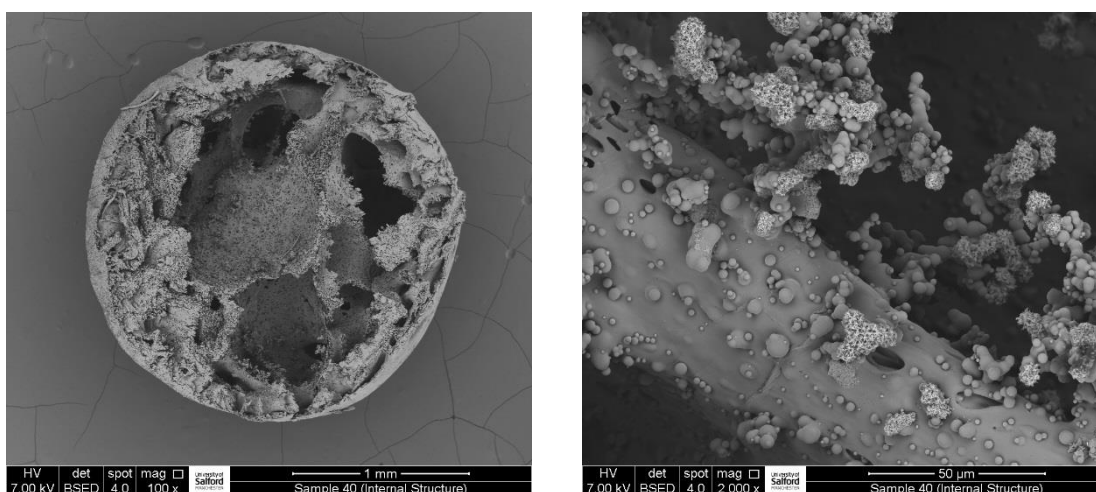
Accordingly, it was decided to encapsulate a less reactive metal hydride that consisted of elements suitable for detection using EDX analysis.

4.5 Encapsulation of Sodium Borohydride (NaBH_4)

PSF in NMP – NaBH_4 Dispersion in 80%-Acetonitrile, 20%-Chloroform – Sample 40

An initial batch of PSF- NaBH_4 dispersion was generated using the methodology as outlined in method 16. Under nitrogen, utilising a BD Microlance 3 20G (0.9x40mm) needle and a BD Plastipak 1ml syringe, the polymer dispersion was allowed to slowly drip into a blend of 24ml acetonitrile and 6ml of chloroform using an agitation speed of 8 for the initial introduction followed by a reduction of the agitation speed to 4 after 5 minutes. The addition utilised the same apparatus as described previously for sample 36. The non-solvent was removed using a pipette and the generated microcapsules were allowed to air-dry.

The microcapsules were sliced open with a razor blade and attached to a standard SEM stub using a 12mm carbon adhesive support tab. The cross-section was then coated with 4nm of platinum/palladium using the Cressington 208 sputter coating unit. The coated sample was then introduced into the Quanta 250 SEM for analysis. Figure 4.95 demonstrates that the internal morphology of the microcapsule is relatively hollow, containing clusters of small needle-shaped particles.



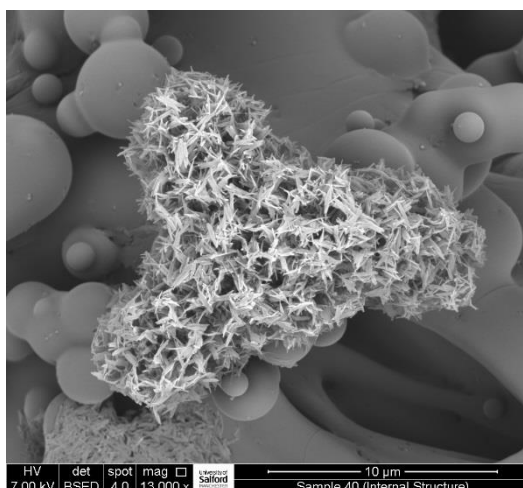


Figure 4.95 SEM micrographs of cross-sectioned PSF NaBH_4 microcapsule - sample 40

The thin needle-like particles were examined using EDX analysis. The resulting spectrum revealed the presence of high levels of sodium, oxygen, and lower carbon. Figure 4.96 represents an overlay of the EDX spectra obtained from the particles against a spectrum obtained from the polymer background.

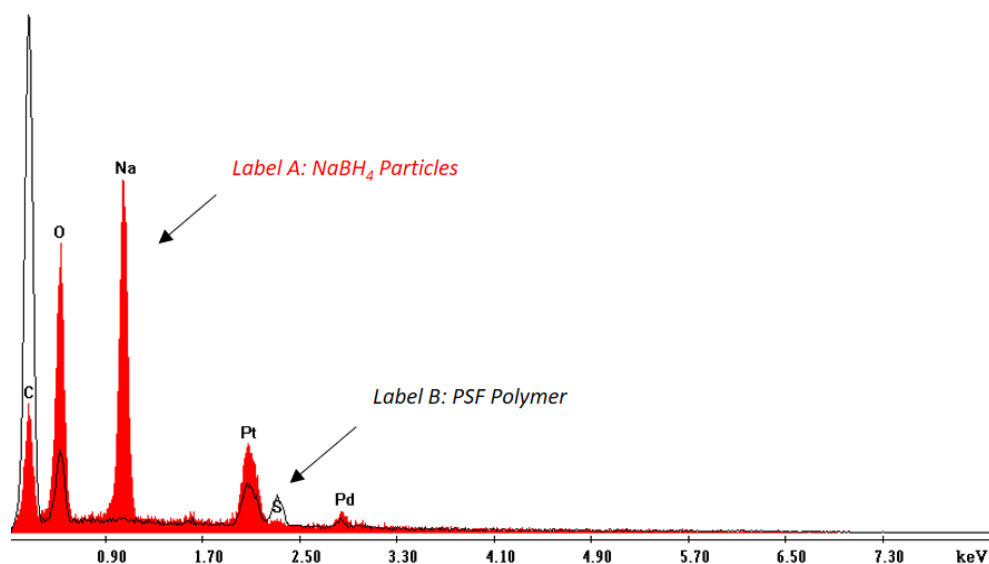


Figure 4.96 EDX spectra overlay PSF polymer against NaBH_4 particles - sample 40

The EDX spectrum obtained from the particles shows high levels of sodium and oxygen with a lower level of carbon and traces of sulfur. This spectrum would suggest that the NaBH_4 has hydrolyzed to form oxides.

The sample preparation for SEM analysis required initially obtaining a cross-section of the microcapsule. This procedure was executed in the open lab, exposing the particles to moisture from the air. The EDX results would suggest that this process may have caused the NaBH_4 to have hydrolyzed.

PSF in NMP – NaBH_4 Dispersion in 80%-Acetonitrile, 20%-Chloroform – Sample 41

This experiment was designed to further reduce the size of the microcapsule. The experimentation involved utilising the same conditions as used for sample 40 except the BD Microlance 3 20G needle was substituted for a BD precision glide needle 25Gx (0.5mm x 40mm).

The needle was connected to a 10ml Terumo syringe containing the polymer dispersion. It was extremely difficult to push the polymer dispersion through the syringe in order to form small droplets. The pressure involved using a 10ml syringe and the viscosity of the polymer dispersion was too high to allow a good flow of polymer through the narrow bore.

The light micrograph in figure 4.97 shows that the microcapsules had collapsed upon air-drying and formed a clear appearance rather than the usual opaque morphology. These results would suggest that the rheology for this experiment was not satisfactory.



Figure 4.97 Light micrograph of PSF NaBH_4 microcapsules - sample 41

PSF in NMP – NaBH₄ Dispersion in 80%-Acetonitrile, 20%-Chloroform – Sample 42

This sample involved using the same polymer dispersion as utilised for sample 41. The polymer dispersion was introduced into the non-solvent using a 10ml syringe connected to a BD Microlance 3 20G (0.9 x 40mm). The method was changed slightly by reducing the agitation speed to 6 for the initial introduction. The agitation was then allowed to continue for a further 2 hours at setting 6, in an effort improve the structure of the microcapsule wall.

The solvent was then removed using a glass syringe and the microcapsules were dried under nitrogen overnight.



Figure 4.98 Light micrograph of PSF NaBH₄ microcapsule - sample 42

The particles looked opaque and the light micrograph, figure 4.98, displays a good spherical microcapsule with a solid outer structure and a porous internal structure. The larger bore size of the needle allowed the flow of polymer under high pressure.

PSF in NMP – NaBH₄ Dispersion in 80%-Acetonitrile, 20%-Chloroform – Sample 43

The same procedure as outlined for sample 41 was applied again to sample 43 but the larger syringe was substituted for a 1ml plastic syringe utilising a BD precision glide needle 25G (0.5mm x 40mm). The smaller 1ml syringe made the process of pushing the polymer dispersion slowly through a fine bore needle easier as less pressure was generated.

The light micrograph at figure 4.99 demonstrates a solid outer wall microcapsule with a porous internal structure.



Figure 4.99 Light micrograph of PSF NaBH₄ microcapsules - sample 43

PSF in NMP – NaBH₄ Dispersion in 80%-Acetonitrile, 20%-Chloroform – Sample 44

A new batch of PSF solution was prepared following the same method as outlined in the experimental section 16. The solution polymer was then left for a week because of time restrictions.

Under nitrogen, 2 micro-spatulas of NaBH₄ were added to the PSF polymer solution. This amount was double the loading compared with previous polymer dispersions used for samples 40-43. The PSF-NaBH₄ dispersion was then stirred under nitrogen at an agitation rate of 8 for 1 hour.

As outlined in the procedure given in method 17, droplets of the dispersion were added to a non-solvent blend of 24ml acetonitrile and 6ml of chloroform using a BD Microlance 3 20G (0.9mm x 40mm) needle connected to a 1ml syringe with an agitation speed setting of 6.

An example of the created microcapsules is presented in light micrograph figure 4.100. The microcapsules are semi-transparent and have collapsed upon drying, developing a shrivelled appearance.



Figure 4.100 Light micrograph of PSF NaBH₄ microcapsules - sample 44

This outcome is thought to be associated with either the delay in using the prepared PSF solution as it had been left for a week prior to the addition of the NaBH₄ and perhaps could have picked up water, or, alternatively, it could be the result of using an increased loading of NaBH₄ as 2 micro-spatulas were used in the preparation rather than 1.

PSF in NMP – NaBH₄ Dispersion in 87%-Acetonitrile, 13%-Chloroform – Sample 45

To understand the problems associated with sample 44, the same polymer dispersion was slowly added to a modified non-solvent blend of 26ml acetonitrile and 4 ml of chloroform using the same needle and syringe. It was thought that the slight reduction in chloroform could stabilise the polymer, generating more opaque microcapsules that don't collapse on drying. The results as given in figure 4.101 show that the microcapsules are slightly more opaque but have collapsed upon drying.



Figure 4.101 Light micrograph of PSF NaBH₄ microcapsules - sample 45

PSF in NMP – NaBH₄ Dispersion in 87%-Acetonitrile, 13%-Chloroform – Sample 46

The PSF-NaBH₄ dispersion and the same non-solvent system used previously for sample 45 was utilised for this experiment. The speed of the agitation was increased to 8, then reduced to 4 after 10 minutes. The cross-sectioned microcapsule as shown in figure 4.102 presents an improved structure. The lower levels of chloroform compromised the internal structure, generating microcapsules that exhibited a reduction in the internal porosity.



Figure 4.102 Light micrograph of PSF NaBH₄ microcapsules - sample 46

The cross-sectioned sample was placed onto a carbon adhesive pad, on a standard SEM stub. The sample was then coated with 4nm of platinum/palladium using the Cressington 208 coating unit. Once coated, the sample was quickly introduced to the chamber of the FEI Quanta 250 SEM for analysis.

The SEM micrograph, figure 4.103, was obtained using a system magnification of 83x. The micrograph shows the internal structure of the microcapsule has a reduced porous structure. This is thought to be a direct result of the reduced concentration of chloroform in the non-solvent. The SEM micrograph obtained using a system magnification of 20,000x shows the presence of small, irregular-shaped particles to exist within the pores of the internal structure.

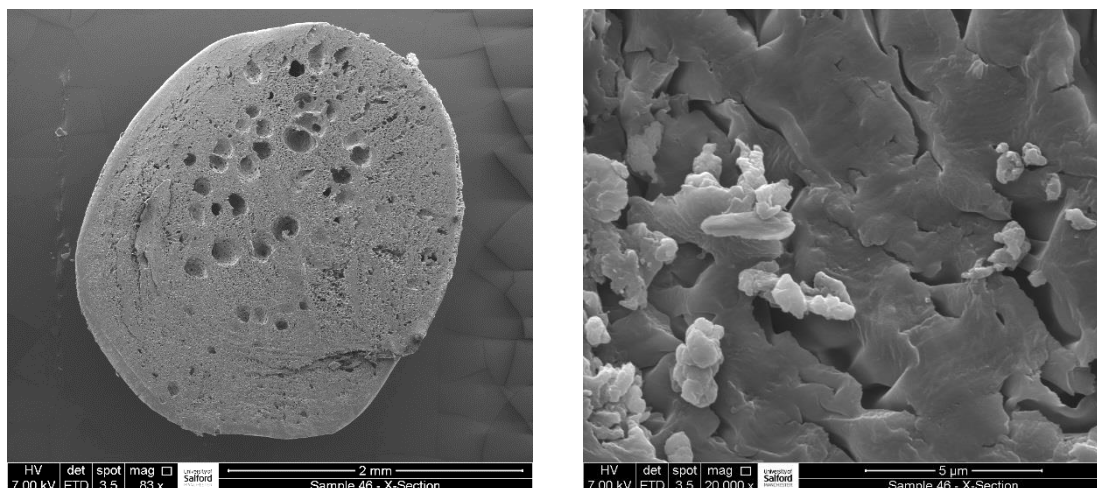


Figure 4.103 SEM micrograph of cross-sectioned PSF NaBH₄ microcapsule - sample 46

The particles were examined using EDX analysis, and the corresponding results are interesting. The EDX spectral overlay given in figure 4.104 represents the spectrum obtained from the particles, together with the spectrum obtained from the supporting PSF polymer.

The results show that the particles contain sodium with no additional elements detected other than those associated with the surrounding PSF polymer. The oxygen levels from the particles, although not quantitative, appear to be the same as the polymer. This would suggest that the NaBH₄ has not formed the oxide from unwanted reactions with moisture. The detection of boron in the presence of high levels of carbon is always compromised using EDX analysis, as the carbon tends to absorb the low energy signal associated with boron.

EDX analysis has limited spatial resolution, thus when small particles are examined the spectrum will always show elements from the surrounding area. These additional elements

will be generated from either beam penetration through the particle or electron scattering around the particles.

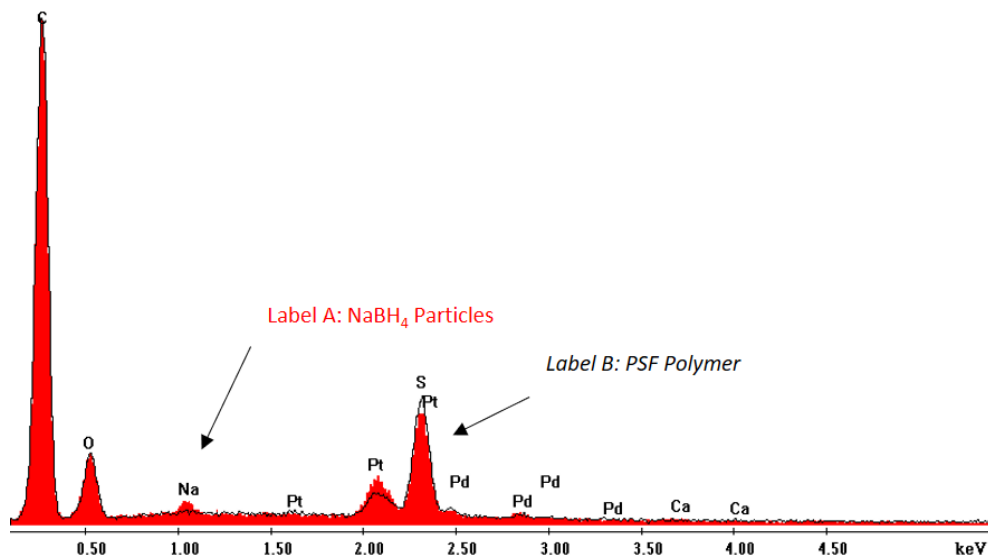


Figure 4.104 EDX spectra overlay PSF polymer against NaBH₄ particles - sample 46

PSF in NMP – NaBH₄ Dispersion in 87%-Acetonitrile, 13%-Chloroform – Sample 47

To investigate some of the issues associated with samples 44-46, a fresh PSF-NaBH₄ dispersion was generated following the procedure as outlined in method 16. Using a microspatula, a single quantity of NaBH₄ was added to the PSF polymer solution. The dispersion was agitated using the IKA yellow line magnetic stirring unit on speed setting 8 for 1 hour.

Using a BD Microlance 3 20G (0.9mm x 40mm) needle coupled to a 1ml syringe, droplets of the polymer dispersion were slowly released into a non-solvent blend of 4ml of chloroform and 26ml of acetonitrile.

The light micrograph, figure 4.105, displays both surface and internal morphology of the generated microcapsules. The surface is generally smooth; however, one microcapsule appears to show signs of surface cracking. Several spherical microcapsules appear to have

stuck together. The lower concentration of chloroform used in the non-solvent has significantly reduced the internal porosity of the microcapsules.



Figure 4.105 Light micrograph of PSF NaBH₄ microcapsules - sample 47

4.5.1 Characterisation of Sodium Borohydride Primary Particles

Further work is required to fully understand the morphology of the NaBH₄ particles. The NaBH₄ used so far for this research was initially purchased from Sigma-Aldrich, but little information is known regarding the particle shape and size of the individual primary particles. The description from Sigma-Aldrich only specified that the sample was a powder. At this stage of the research, it was fundamental that the morphology of the particles should be fully characterised.

Using a glove box under nitrogen, a small amount of the NaBH₄ as received was dusted onto a carbon adhesive pad fixed to a standard SEM stub.

The SEM stub was transferred under nitrogen quickly to the Cressington 208 series coating unit. Once under vacuum, the NaBH₄ particles were coated with 4nm of platinum/palladium. The sample was then quickly introduced to the FEI Quanta 250 for examination.

The SEM micrographs as displayed in figure 4.106 show the NaBH_4 particles are irregular in shape and exist as a mixture of primary particles from $35\mu\text{m}$ to $300\mu\text{m}$. This is a large particle size spread. These particles are not a perfect size distribution for encapsulation into small 1mm-sized microcapsules.

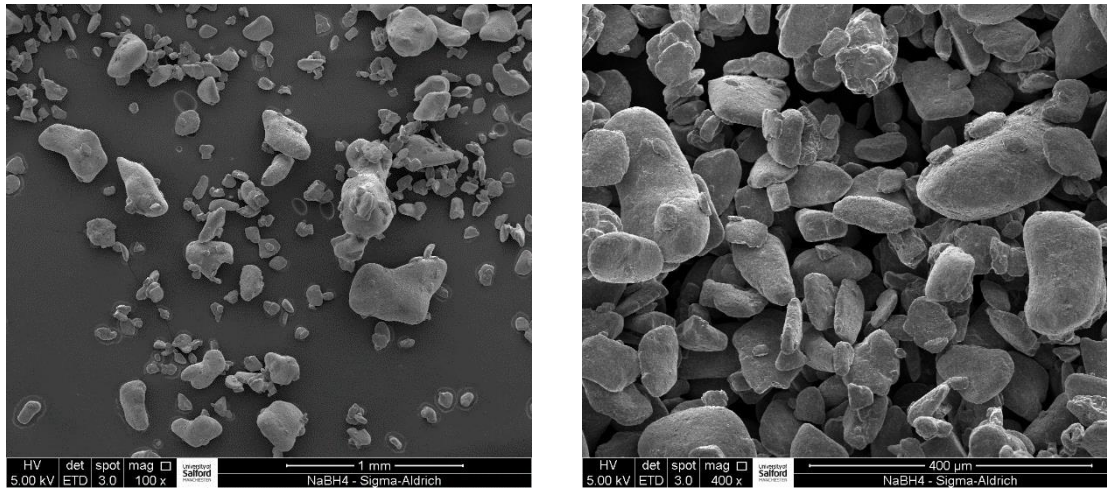


Figure 4.106 SEM micrographs of NaBH_4 particles ex Sigma-Aldrich

EDX analysis was executed on several particles and a typical spectrum was produced, as given in figure 4.107. The EDX spectrum shows high levels of sodium with lower levels of boron and oxygen, and trace magnesium.

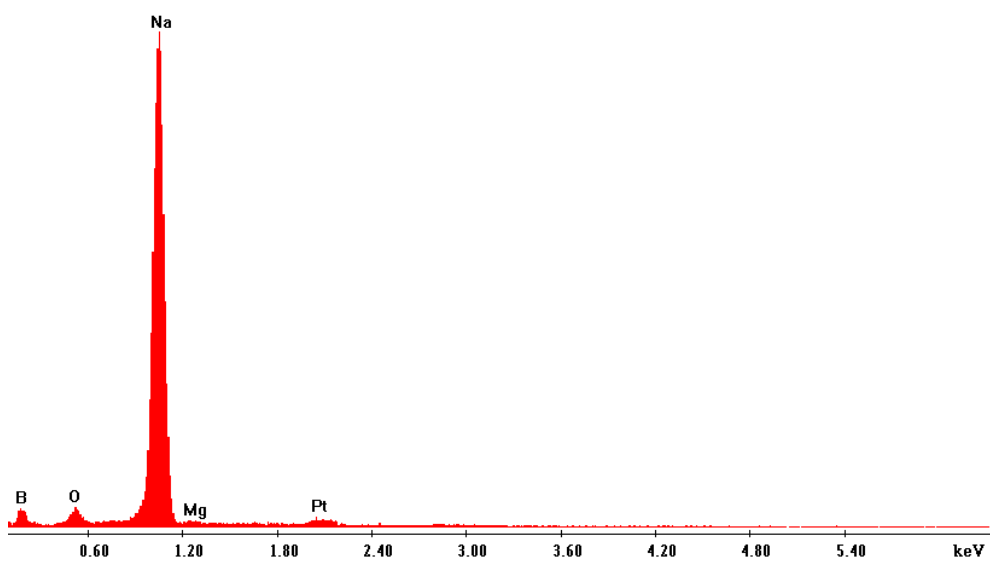


Figure 4.107 EDX Spectrum from NaBH_4 particles ex Sigma-Aldrich

A new batch of NaBH_4 was ordered from Acros Organics; the information relating to particle size is limited as it was defined only as a powder 98%+.

The particles were examined in the same manner as the previous NaBH_4 purchased from Sigma-Aldrich. The SEM micrographs as given in figure 4.108 represent the NaBH_4 primary particles as received. Particles can be seen to exist as various sizes up to $200\mu\text{m}$.

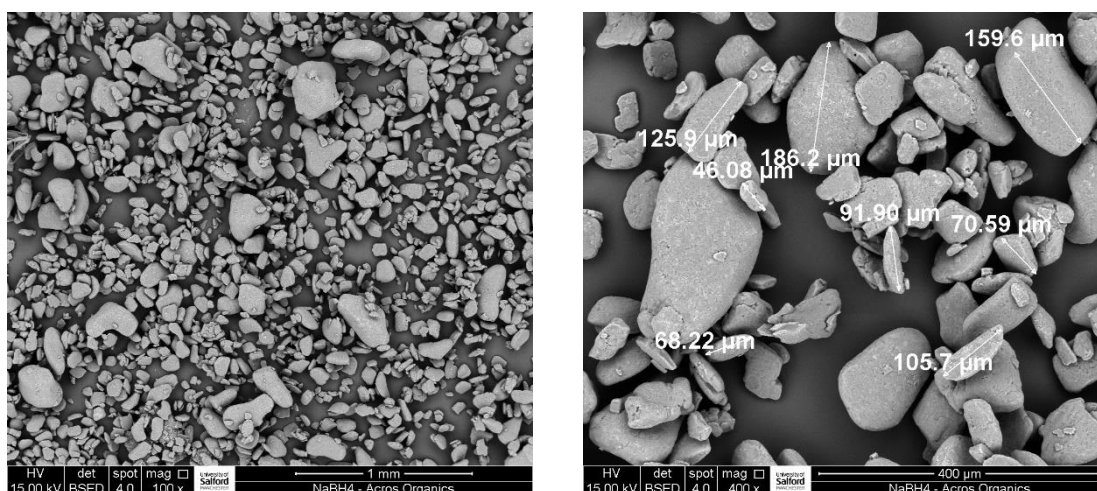


Figure 4.108 SEM micrograph of NaBH_4 particles ex Acros Organics before grinding

To break the particles down to a size more suitable for encapsulating into a small polymer microcapsule, the NaBH_4 was ground using a pestle and mortar within the glove box under a flow of nitrogen. Figure 4.109 represents the SEM micrographs obtained from the primary particles after grinding. The micrographs demonstrate a significant size reduction, signifying that the pestle and mortar grinding process was successful. Particles are seen to exist as showing an irregular shape with an average particle size around $30\mu\text{m}$.

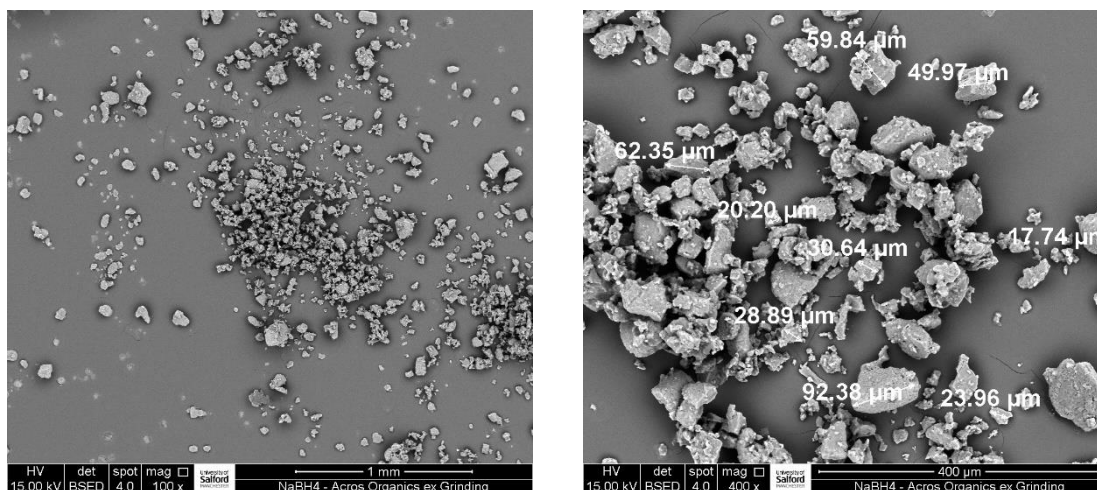


Figure 4.109 SEM micrograph of NaBH_4 particles ex Acros Organics after grinding

EDX analysis was performed on the ground particles and the resulting spectrum, as given in figure 4.110, displays high levels of sodium with lower levels of boron and trace oxygen. Boron is not a good element for EDX detection as it has a K-alpha energy of 0.18 KeV that exists on the very edge of what can be detected. The small oxygen peak was not expected; this could indicate that perhaps the NaBH_4 is starting to turn into the oxide forming a surface monolayer or perhaps as the NaBH_4 was only classified as 98%+, an impurity may be present at the surface of the particles.

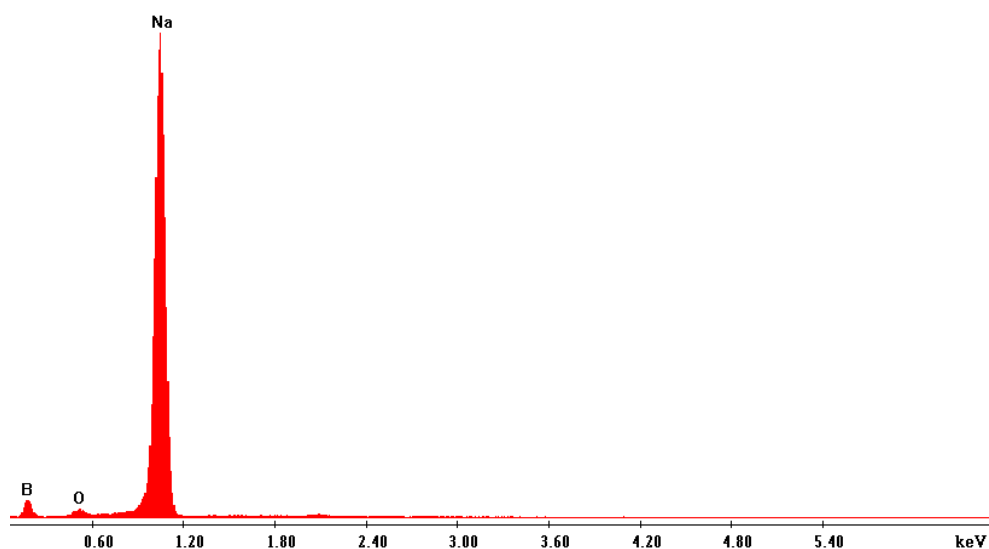


Figure 4.110 EDX Spectrum from ground NaBH_4 particles ex Acros Organics

PSF in NMP – NaBH₄ Dispersion in 80%-Acetonitrile, 20%-Chloroform – Sample 48

A fresh PSF solution was generated following the procedure outlined in method 16.

Using a nitrogen glove box, a fresh batch of ground NaBH₄ ex Acros Organics was prepared using a pestle and mortar to reduce the particle size. Several micro-spatula loadings of the ground NaBH₄ were added to the polymer solution. The glass stopper was put onto the flask and the flask was transferred to the fume cupboard under nitrogen. The polymer dispersion was then agitated for 1 hour using the IKA yellow line magnetic stirring unit on speed setting 8.

Small droplets of the PSF-NaBH₄ dispersion were slowly released into the non-solvent blend of 24ml acetonitrile and 6ml of chloroform using a Microlance 3 20G (0.9mm x 40mm) needle connected to a 1ml syringe with an agitation speed of 6. The fast agitation rate was continued for a further 10 minutes after the addition was complete, then reduced to a speed of 4 for 2 hours.

The experiment was not successful as the generated microcapsules appeared transparent and soft - as shown in light micrograph 4.111.



Figure 4.111 Light Micrograph of PSF NaBH₄ microcapsules - sample 48

The reason for the unsuccessful generation of microcapsules was not fully understood. The NaBH₄ after grinding would be more reactive as the surface area would have increased due

to the generation of smaller particles. This, together with the excess loading of NaBH_4 , could have increased the number of nucleation sites. As demonstrated below, by reducing the chloroform concentration the deposition was slowed.

PSF in NMP – NaBH_4 Dispersion in 83%-Acetonitrile, 17%-Chloroform – Sample 49

This sample was generated using the same polymer dispersion as sample 48, which was held under nitrogen for 2 days. Droplets of the dispersion were slowly released into a modified non-solvent blend of 5ml of chloroform and 25ml of acetonitrile. The polymer dispersion was introduced to the non-solvent using a Microlance 3 20G (0.9mm x 40mm) needle connected to a 1ml syringe. The addition of the polymer dispersion to the non-solvent blend was achieved using an increased agitation speed of 8 for 10 minutes. The agitation speed was then reduced to 4, and the particles were agitated for an additional 3 hours, followed by removal of the solvent using a pipette.

The resulting microcapsules show a significant improvement over the previously generated microcapsules (sample 48). The light micrograph, figure 4.112, illustrates that the particles are opaque with an off-spherical structure. The internal morphology of the cross-sectioned microcapsule is observed to exist as a honeycomb structure. This could be a direct result of leaving the capsules stirring for an extended time of 3 hours.



Figure 4.112 Light micrograph of PSF NaBH_4 microcapsules - sample 49

PSF in NMP – NaBH₄ Dispersion in 83%-Acetonitrile, 17%-Chloroform – Sample 50

In an effort to understand the reason for the reduced porosity associated with sample 49, changes were made to the experimental procedure. The final agitation time was reduced to 1 hour, using a stirring speed of 4 after the initial formation of the microcapsules.



Figure 4.113 Light micrograph of PSF NaBH₄ microcapsules - sample 50

The light micrograph, figure 4.113, demonstrates a much-improved porous internal structure. These results illustrate that the agitation time is critical for the generation of the desired internal structure.

PSF in NMP – NaBH₄ Dispersion in 83%-Acetonitrile, 17%-Chloroform – Sample 51

The apparatus used to introduce the polymer dispersion into the non-solvent was modified for this sample. In addition, the bore size of the needle was changed to a Microlance 3 20G (0.7mm x 30mm).

These changes included substituting the 2-neck 100 ml round bottomed flask for a 3-neck 100ml flask as outlined in method 18. This allowed greater control for the input of the polymer dispersion into the non-solvent. The 3rd neck contained a fitted Suba-Seal that allowed the needle containing the polymer dispersion to pass through, minimising contact of the dispersion with moisture from the atmosphere.

The light micrograph, figure 4.114, represents both the surface and internal structure of the generated microcapsules. The microcapsules are seen to be slightly off-spherical but display a smooth outer surface structure, free from cracks and indentations. The internal structure of the microcapsules is ideal, showing a good internal porosity. Using the 30mm needle length caused restricted travel of the syringe needle when using a Suba-Seal. The needle length was too short to allow the PSF dispersion to be dropped in at the optimum spot



Figure 4.114 Light micrograph of PSF NaBH_4 microcapsules - sample 51

PSF in NMP – NaBH_4 Dispersion in 83%-Acetonitrile, 17%-Chloroform – Sample 52

This sample was generated using the same experimental conditions as utilised for the previous sample 51, except the syringe needle was substituted for a Microlance 3 20G (0,9x40mm) as used in previous experiments.

Using the slightly longer syringe needle improved the delivery of the polymer dispersion into the non-solvent. The generated microcapsules were examined using light microscopy. The light micrograph figure 4.115 illustrates that the created microcapsules are perfectly spherical, retaining an excellent porous internal structure.



Figure 4.115 Light micrograph of PSF NaBH_4 microcapsules - sample 52

4.5.2 Preparation Chamber Facilitating Sample Manipulation Under Vacuum

The main issue when preparing the microcapsules for characterisation was that the cross-section work was being carried out in the open lab. Even though this procedure was performed as quickly as possible, the internal moisture-sensitive materials were still being exposed to moisture from the atmosphere.

An ideal scenario for the purpose of this research would be the introduction of a methodology that would allow manipulation of the microcapsules to be managed under vacuum with an additional option of introducing a purge of dry, inert gas.

In an attempt to develop an ideal system for the manipulation of microcapsules, an old Oxford CT1500 cryo-stage was utilised. The unit was modified to fit directly onto a high vacuum porthole of the Philips XL30 SFEG Scanning Electron Microscope.

The Oxford CT1500 was designed for use as a cryo-stage, allowing the examination of either liquid materials or samples that have delicate tissue. These materials would be easily damaged by either the high vacuum of the microscope chamber or the high energy electron beam.

Utilising the cryo-stage allowed liquid materials to be examined at high magnifications using electron microscopy after prior freezing under a slush of liquid nitrogen. Once the sample had frozen, it was quickly transferred to the preparation chamber held under high vacuum. Once the frozen sample was fixed within the preparation chamber it could be fractured before transferring directly under high vacuum into the SEM chamber using a 1-meter length transfer rod. Any ice from the fractured face of the sample could then be removed by a sublimation process, revealing fine detail within the sample.

This technology was thought to be ideal for the preparation of air/moisture-sensitive materials to be examined using the high-resolution SEM utilising microcapsules as the transfer vehicle.

Figure 4.116 represents photographs of the assembled Oxford CT1500 preparation stage. The stage is fixed onto the high vacuum porthole of the Philips XL30 SFEG. The preparation chamber has several portholes that allow the user to manipulate the sample before examination. The electronics - displayed in the rear of the photograph - allow the control of air into the chamber to release the porthole. The preparation unit is fitted with a pre-vacuum transfer chamber that allows samples to enter the preparation chamber without the need to let the full chamber down to air. Once the transfer chamber has reached high vacuum, the inner porthole can be opened allowing the microcapsules to be positioned onto the preparation stage using the transfer rod. Once the microcapsules are in position on the preparation stage, they are maintained within the airtight high vacuum environment by the turbo pumping system. Under vacuum, the microcapsules can be cross-sectioned using a razor blade and coated using the built-in sputter coating unit to prevent unnecessary electron beam charging.

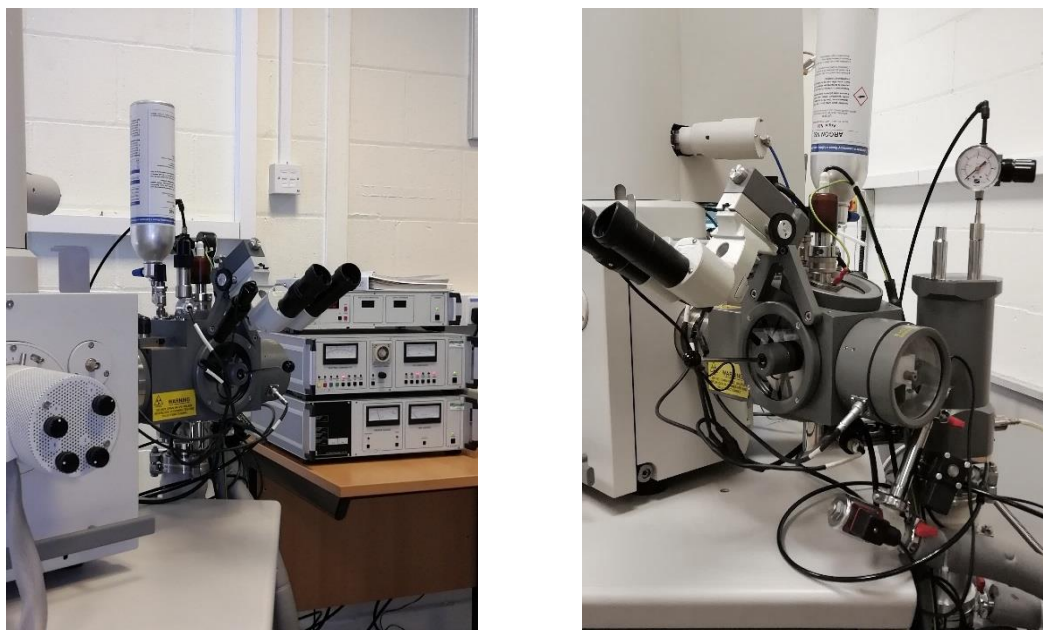


Figure 4.116 - Preparation Stage for direct manipulation of microcapsules

After coating with several nano-meters of platinum, the cross-sectioned microcapsules can be transferred under vacuum directly onto the SEM stage for examination - minimising unwanted reactions due to moisture from the atmosphere.

SEM micrographs can then be obtained from the air/moisture-sensitive nanoparticles in a controlled manner, restricting any unwanted reactions.

In addition to obtaining high resolution micrographs, the moisture-sensitive metal hydride particles can also be examined using Energy Dispersive X-ray Analysis (EDX). This technique is interfaced to the SEM and utilises the primary electron beam to generate characteristic X-rays from the particles, producing a spectrum of different X-ray energies - allowing the particles to be fully characterised.

Analysis of Previously Examined Samples using the Preparation Chamber

Rather than continuing with new preparations of microcapsules, it was decided at this point to revisit previous samples in order to test the suitability of the preparation chamber.

Analysis using the preparation stage - Philips XL30 SFEF - Sample 46-Revisited

This part of the research involved cutting a small microcapsule within the preparation chamber under vacuum. A system was initially required so that each spherically-shaped microcapsule could be held firmly in place, to allow the scalpel blade to slice through the polymer.

To test the validity of the new preparation chamber, sample 46 was first chosen for the initial experimental work. The polymer microcapsule was secured onto a small brass rivet using rapid-setting Araldite. The light micrograph, figure 4.117, illustrates the simplicity of the microcapsule that was glued onto a brass rivet. The rapid-setting Araldite appears to have had minimum reaction with the polymer microcapsule.



Figure 4.117 Light micrograph of a glued microcapsule onto a brass rivet - sample 46

The rivet was then clamped to the holder, which was designed to fit onto both the preparation chamber stage and the microscope stage. The sample holder was then attached to the end of the long transfer rod. Once the sample was fixed onto the stage of the preparation chamber, a sharp scalpel knife was used to cut open the microcapsule whilst under vacuum. The surface of the cross-sectioned microcapsule was then coated with platinum using the sputter coating unit present within the preparation chamber. After coating, the cross-sectioned microcapsule was transferred using the rod onto the stage of the XL30 SFEF microscope.

The microscope is fitted with a chamber camera, which allowed the positioning of the holder onto the stage with precision accuracy.

Figure 4.118 represents the resulting SEM micrographs obtained from the surface of the cross-sectional area, using system magnifications of 300x and 10,000x respectively.

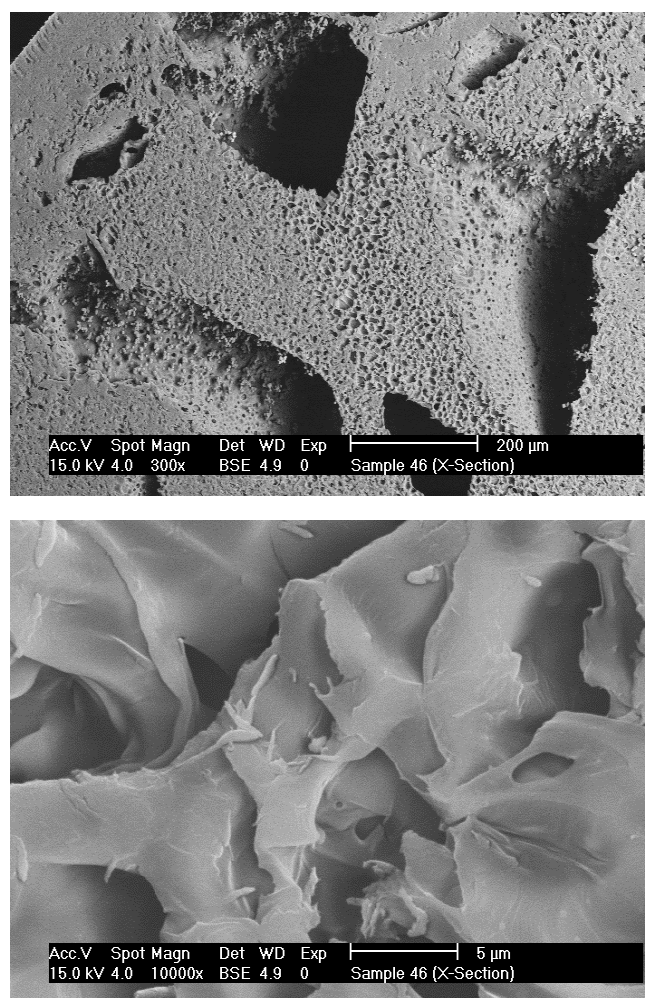


Figure 4.118 SEM micrograph of cross-sectioned microcapsule - sample 46-Revisited

The small particle was examined using EDX and the resulting spectra overlay is given in figure 4.119. The results are similar to the spectral overlay illustrated in figure 4.104, which represents sample 46 under examination using a different preparation technique.

The spectrum obtained from the polymer background shows high levels of carbon with lower levels of oxygen and sulfur. However, the spectrum obtained from the particle has an

additional sodium peak. The levels of oxygen are shown to be very similar to the background polymer.

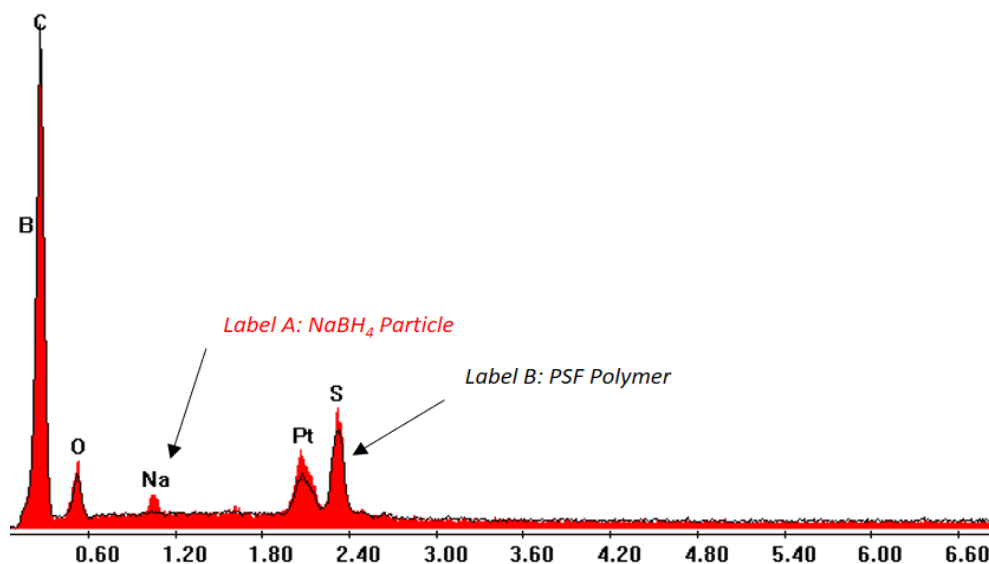


Figure 4.119 EDX spectra overlay of PSF/NaBH₄ particle - sample 46-Revisited

These results would suggest that the encapsulated NaBH₄ particle has not reacted with moisture to form the oxide. This data is different from the EDX spectrum obtained from the previously examined microcapsule - sample 40. The EDX spectrum shown at figure 4.96, obtained from the particles, displayed a significantly higher concentration of oxygen.

Analysis using XL30 SFEF – Oxford CT1500 preparation chamber - Sample 50-Revisited

The same experimental conditions were carried out for sample 50. The SEM micrographs at figure 4.120 represent the internal structure of a cross-sectioned microcapsule prepared under vacuum.

The low magnified micrograph obtained using a system magnification of 174x illustrates the very good internal porosity of the microcapsule. The higher magnified micrograph obtained using a system magnification of 4000x shows a cluster of particles existing within the pores of the cross-section - thought to represent NaBH₄.

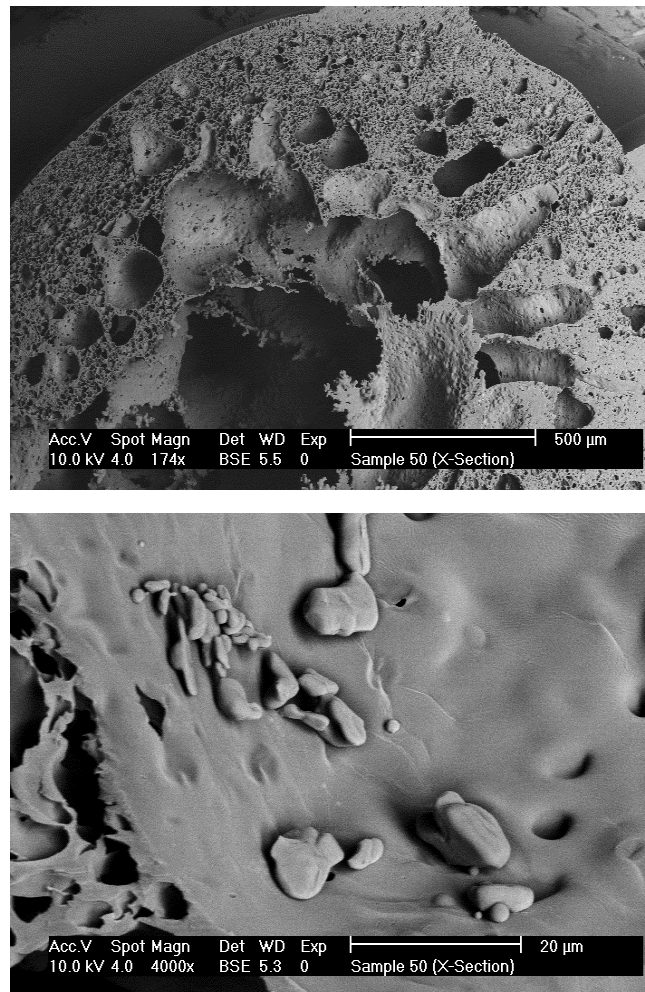


Figure 4.120 SEM micrograph of internal area showing particles - sample 50-Revisited

The particles were examined using EDX analysis and the resulting spectrum, figure 4.121, represents an overlay of examined particle against a spectrum obtained from the surrounding PSF polymer.

The particle shows high levels of sodium and oxygen, suggesting that the NaBH_4 has hydrolyzed. The conversion of NaBH_4 to the oxide leads to many questions, and many reasons could perhaps have been responsible for the conversion of the hydride to the oxide. Could the reaction have been initiated using rapid-setting Araldite? This could have been from the initial wet stage of gluing - perhaps a solvent from the Araldite had migrated into the microcapsule? A further factor could be that a small amount of water may have been generated during the process of Araldite setting. An alternative assumption could be that perhaps the curing process from the epoxy resin may have initiated an exotherm?

This is only an inference as the previous sample (46) appeared to produce good results. The light micrograph, figure 4.117, generated from the fixed microcapsule onto the brass rivet would suggest that very little external damage had occurred during the cure process, as the sphere was seen to be completely intact.

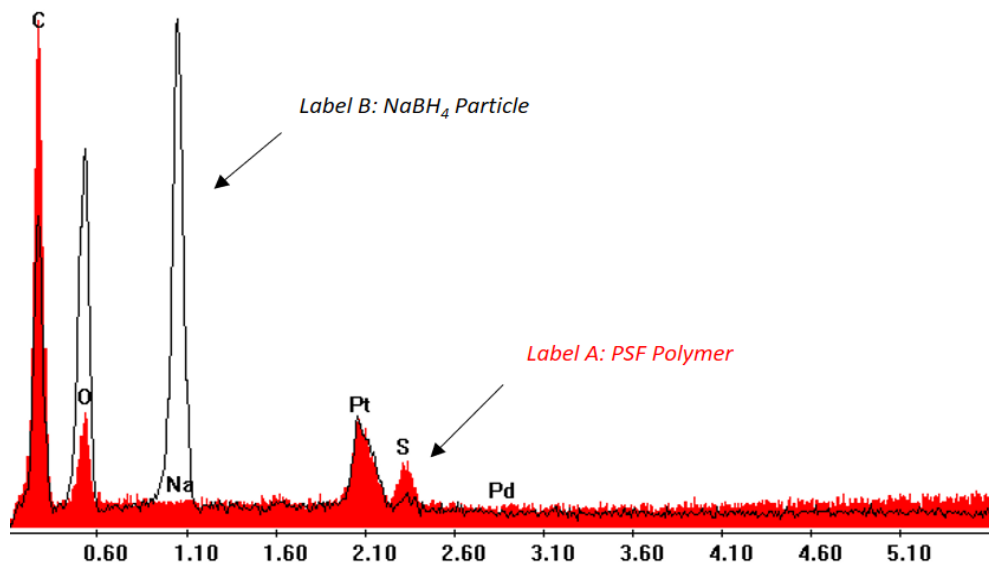


Figure 4.121 EDX spectra overlay of PSF polymer/ NaBH_4 particle - sample 50-Revisited

Alternative glues were considered to replace the rapid-setting Araldite. The light micrograph shown in figure 4.122 represents the results obtained from using a cyanoacrylate-based product. These results demonstrate that the glue had reacted with the microcapsule, damaging the structure.



Figure 4.122 Light micrograph of microcapsules glued onto a rivet using Loctite

Using the rivet initiative to support the microcapsules provided a good system for allowing cross-sections to be obtained by directly slicing through the microcapsule using a scalpel knife. Concern over the effect of the glue was always an issue.

An alternative to gluing the microcapsules onto rivets was to fix the microcapsules onto a carbon adhesive support pad. This system enabled the microcapsule to be cut in half, followed by suitable manipulation of the particle to position the sectioned face upwards. This was an extremely difficult procedure as the preparation chamber had limitations for easy manipulation.

Analysis using XL30 SFEG – Oxford CT1500 preparation chamber - Sample 52-Revisited

Sample 52 was cut under vacuum by slicing the microcapsule in half, followed by positioning the cut face so that the cross-sectional area was facing upwards. This procedure has a tendency to smear parts of the carbon adhesive glue onto the microcapsule. However, the procedure did allow particles to be examined while minimising the need for Araldite. The SEM micrographs, figure 4.123, represent both a low magnified area of the cut cross-sectional area together with a higher magnified region, utilising back scattered electron detection.

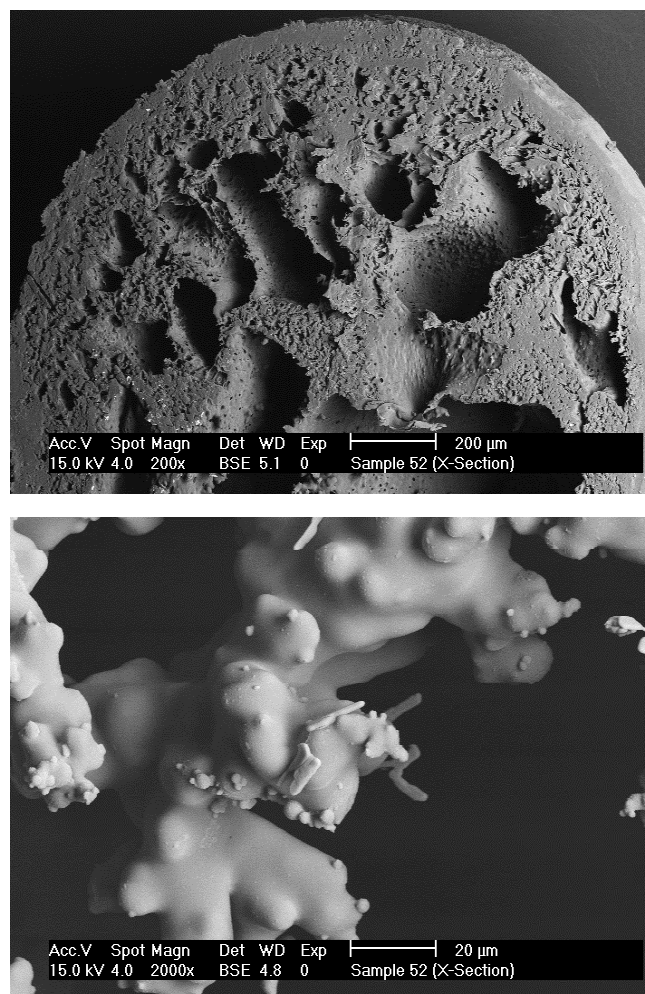


Figure 4.123 SEM micrographs of internal area showing particles - sample 52-Revisited

The low magnified micrograph shows that the microcapsule has a good internal porosity, ideal for accessing the small NaBH_4 particles. The higher magnified micrograph, obtained using a system magnification of 2000x, clearly shows the presence of some crystalline, irregular-shaped particles.

The small particles were examined using EDX analysis and the results are presented in figure 4.124. The EDX spectra overlay is the outcome of both the analysis of a small particle, together with the background polymer substrate. The results verify that the small particle contains high levels of sodium. The spectrum from the particle also shows carbon, oxygen and sulfur - but these are associated with the polymer. The overlay indicates that the levels of oxygen from the particle are the same as the background polymer. When examining small particles using EDX analysis, the electron beam will pick up elements from the

substrate by electron scatter or by penetrating through small, thin particles. The spatial resolution is limited to approximately $1\mu\text{m}$.

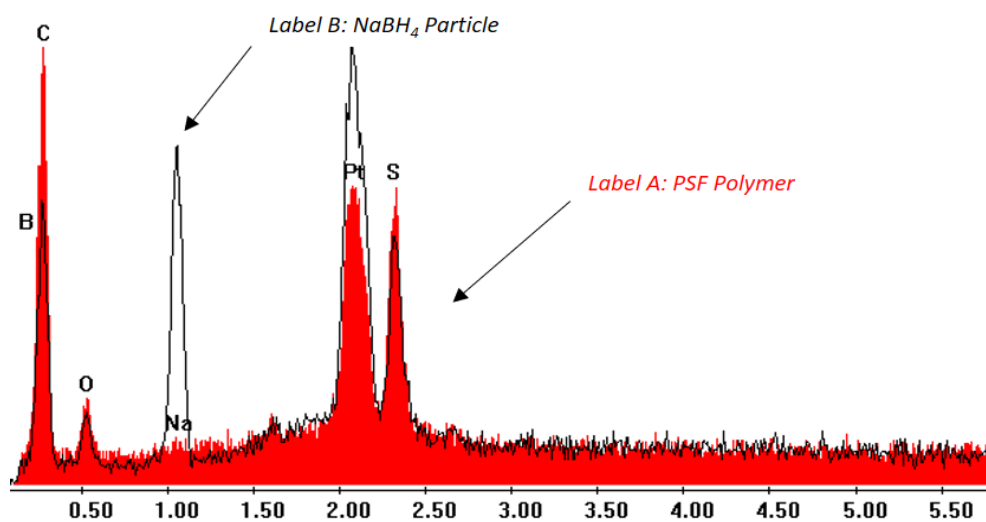


Figure 4.124 EDX spectra overlay NaBH₄ particle/PSF polymer - sample 52-Revisited

These results would suggest that the NaBH₄ has not hydrolyzed as a result of being encapsulated within the small microcapsule.

The SEM micrograph, figure 4.125, represents a different area within the cross-sectioned microcapsule. Irregular particles are seen to be present below $10\mu\text{m}$ in size, thought to represent the NaBH₄.

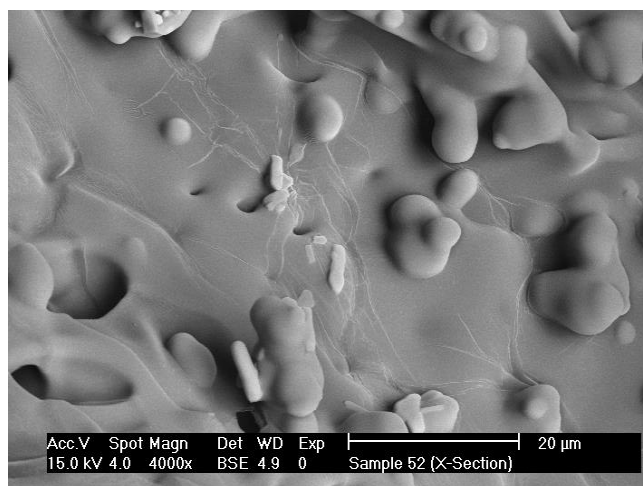


Figure 4.125 SEM micrograph of internal area showing particles - sample 52-Revisited

These particles are interesting as the corresponding EDX analysis, figure 4.126, shows that they contain sodium, however, the oxygen level is seen to be slightly higher than in the previous particles examined. This may suggest that the NaBH_4 has started to hydrolyse.

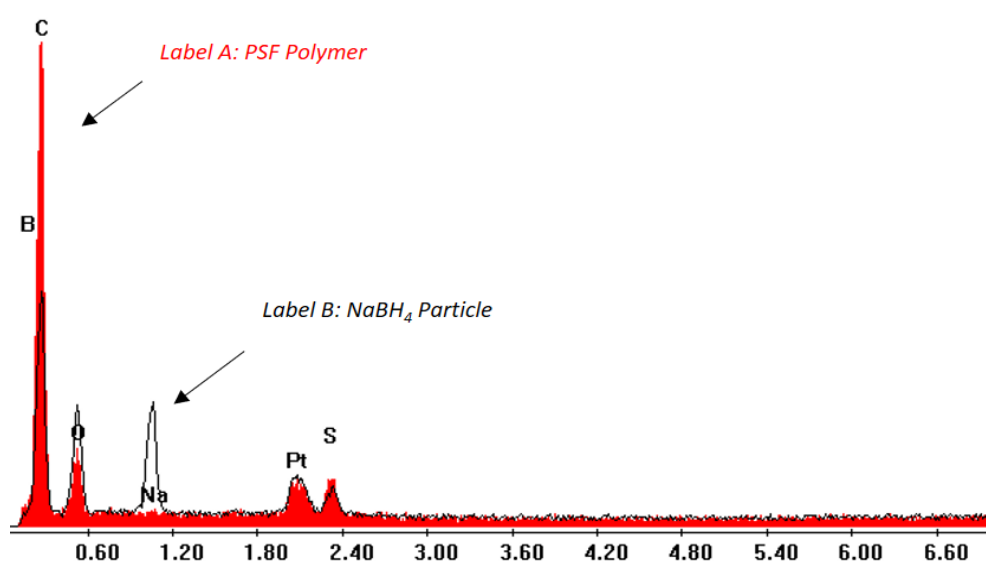


Figure 4.126 EDX spectra overlay NaBH_4 particle/PSF polymer - sample 52-Revisited

These results are interesting as they suggest that some of the encapsulated NaBH_4 particles have either hydrolyzed or started to react, and others have remained as the borohydride.

PSF in NMP – NaBH₄ Dispersion in 83%-Acetonitrile, 17%-Chloroform - Sample 53

This experiment followed the same procedure as outlined for sample 52. The time between the preparation of sample 52 and the EDX analysis was 16 days. This delay could have been enough for moisture to diffuse into the microcapsules, causing some of the NaBH₄ particles to oxidise or perhaps the experimental conditions have caused some oxidation.

A fresh batch of PSF-NaBH₄ dispersion was prepared following the same experimental conditions as outlined in method section 16.

Using a Microlance 3 20G (0.9mmx40mm) needle connected to a 1mm syringe, droplets of the PSF-NaBH₄ dispersion was slowly released into a 100ml round-bottomed flask, as outlined in method 18. After leaving to dry in nitrogen overnight, the microcapsules were seen to appear wet the following morning. Because of this, the microcapsules were placed into a petri-dish to air-dry.

A typical microcapsule was glued onto a rivet using rapid-setting Araldite. Once the glue had set, the microcapsule was cross-sectioned within the preparation chamber under vacuum. The micrograph as given in figure 4.127 displays that some small particles exist within an internal area approximately 10µm in size.

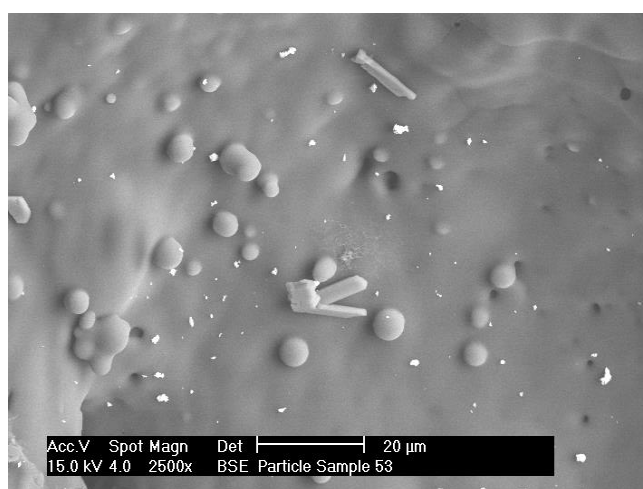


Figure 4.127 SEM micrograph of internal area showing particles - sample 53

The particles were examined using EDX and the resulting spectrum, figure 4.128, was superimposed over a spectrum obtained from the polymer background. The results imply that the NaBH_4 has not changed as the oxygen levels are lower than the background PSF polymer spectrum.

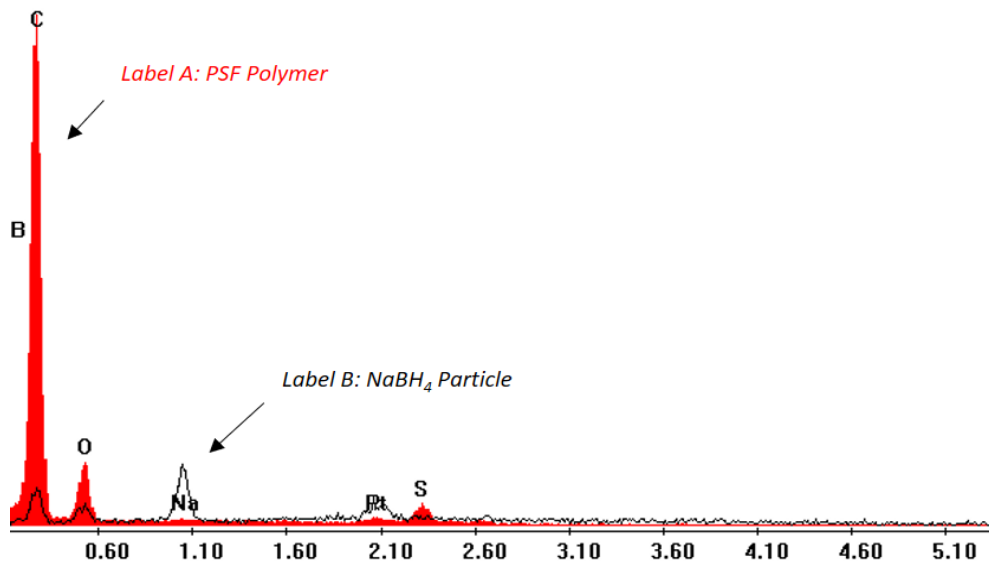


Figure 4.128 EDX spectra overlay NaBH_4 particle/PSF polymer - sample 53

However, when particles were examined from different regions within the cross-sectional area, the oxygen levels were high - suggesting that NaBH_4 had hydrolyzed.

To understand if the process of fixing the microcapsules onto the rivet using Araldite was causing the hydrolysis, a separate microcapsule from the same batch was fixed to a carbon adhesive pad, then cut open in the preparation chamber. The SEM micrograph at figure 4.129 shows a cluster of needle-shaped particles, together with a small irregular-shaped particle below the needles.

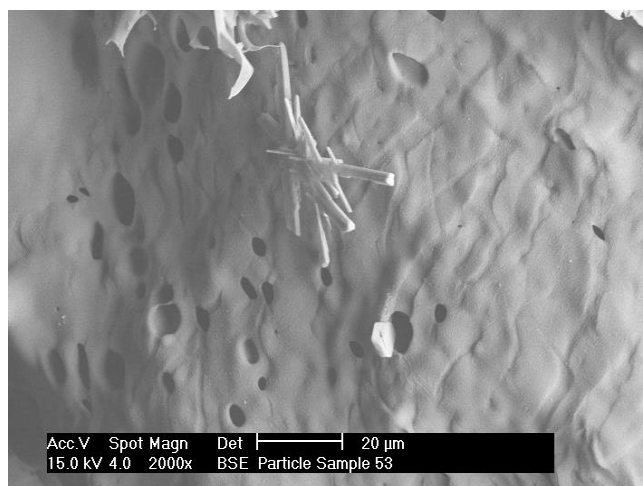


Figure 4.129 SEM micrograph of internal area showing particles - sample 53

The EDX spectrum from both particles show the oxygen levels to be greater than the polymer background, as shown in figure 4.130.

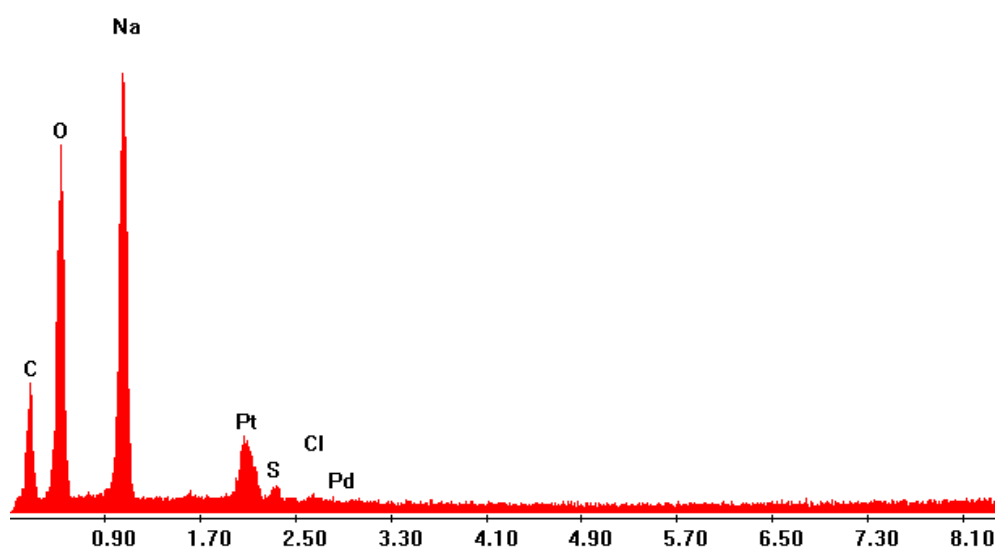


Figure 4.130 EDX spectrum from particles shown in figure 4.129 - sample 53

The micrograph shown below, figure 4.131, represents a particle from a different area of the cross-section. This particle generated an EDX spectrum (figure 4.132) showing low levels of oxygen, suggesting that the NaBH_4 had not hydrolyzed.



Figure 4.131 SEM micrograph of internal area showing NaBH_4 particles - sample 53

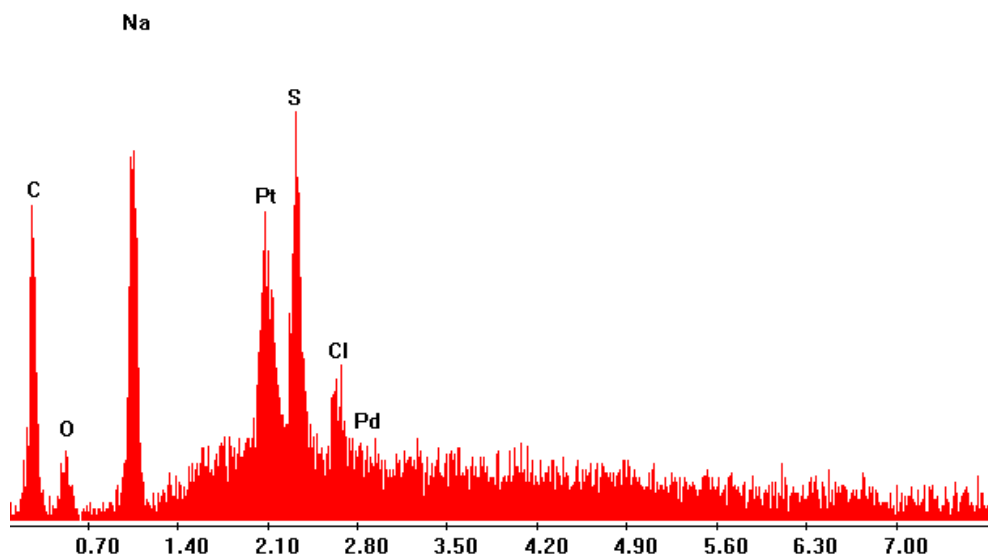


Figure 4.132 EDX spectrum from particles shown in figure 4.131 - sample 53

These results would suggest that the process of gluing the microcapsules onto rivets using Araldite had probably not induced any unwanted changes to the encapsulated metal hydride particles due to the heat generated from the curing process or residual solvents. The main concern is that many of the NaBH_4 particles are seen to have a needle-shaped morphology, rather than the irregular-shaped particles as shown in figure 4.109 (from the ground particles). Some of the larger crystalline particles appear to have maintained an irregular morphology. This would suggest that perhaps the larger particles are more stable and less prone to hydrolysis (Lo et al., 2007). The needle-shaped particles, however, suggest that the

NaBH₄ particles have re-crystallised. This re-crystallisation may have been associated with the particles remaining wet overnight even though they had a nitrogen purge.

PSF in NMP – NaBH₄ Dispersion in 83%-Acetonitrile, 17%-Chloroform - Sample 54

This sample was generated by reproducing the same experimental conditions as the previous sample 53. The generated microcapsules were also wet after they had been purged under nitrogen. After they were eventually dried, the microcapsules were cross-sectioned. The NaBH₄ particles had the same appearance as seen in sample 53 - suggesting they had re-crystallised.

Dissolution Test

The previous samples 53 and 54 have indicated that perhaps there was a dissolution issue with the solvents used and the NaBH₄ particles. This inference may also account for the results from previous samples demonstrating that some particles had reacted, forming the oxide, and others remained unchanged.

To identify whether the solvents used in the experimental procedure could be dissolving the NaBH₄, a basic dissolution experiment was performed. This procedure involved placing a small quantity of the ground NaBH₄ into 5 separate glass vials under nitrogen using the glove box. Equal volumes of chloroform, NMP, acetonitrile, THF and DMF were then placed into the separate vials and a sealed lid was put onto each glass vial. This dissolution test showed that chloroform and NMP dissolved the NaBH₄, as in both cases the particles completely disappeared and formed a clear solution. The DMF may have had some influence on the particles as the solvent was slightly cloudy, but many particles could still be seen to be present in the glass vial. The acetonitrile and THF, however, did not appear to dissolve the NaBH₄ particles as the solvent remained clear with the particles unaffected.

Due to this experiment showing that the NMP had dissolved the NaBH_4 particles, the procedure was changed - substituting NMP by DMF as this solvent had been used at previous stages of the research project.

PSF in DMF – NaBH_4 Dispersion in 83%-Acetonitrile, 17%-Chloroform - Sample 55

Using the procedure outlined in method 16, a new batch of PSF- NaBH_4 dispersion was generated after substituting NMP by DMF. At this stage in the project, it was thought best to leave the non-solvent blend the same as the previous sample 54. Chloroform, although seen to dissolve the NaBH_4 , was used to open the internal structure of the microcapsule. The process of the liquid polymer dispersion forming a microcapsule is very rapid so the assumption was that the particles would be protected within the polymer shell.

Using a Microlance 3 20G (0.9mmx40mm) syringe, droplets of the dispersion were introduced into a mixture of 5ml chloroform and 25ml acetonitrile following the same procedure as given in method 18.

The dried microcapsules were initially glued onto a rivet using rapid-setting Araldite then examined using the XL30 SFEG interfaced to the preparation chamber.

The SEM micrograph at figure 4.133 shows that the cross-sectioned microcapsule had formed a perfect structure with a solid outer wall and a hollow internal morphology.

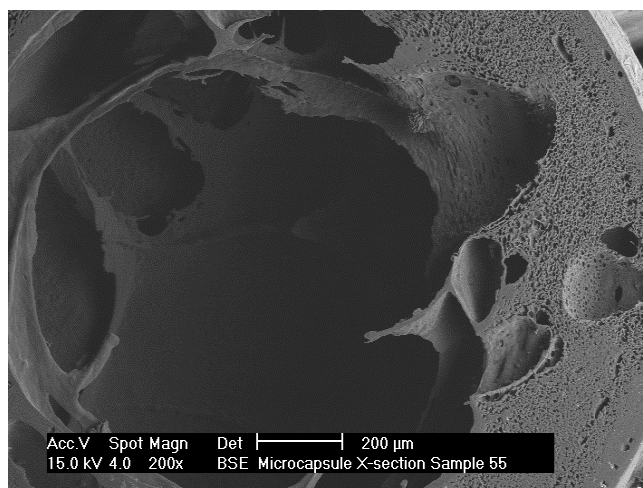


Figure 4.133 SEM micrograph of internal area - sample 55

The internal structure of the microcapsule was examined in detail to find encapsulated NaBH_4 particles. The SEM micrograph in figure 4.134 shows a cluster of small particles.

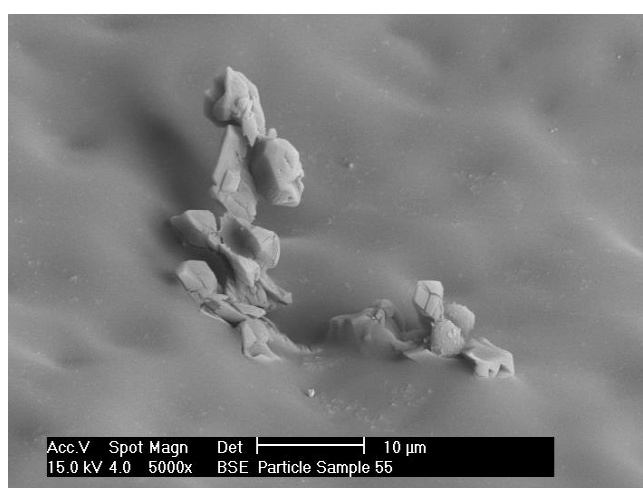


Figure 4.134 SEM micrograph of internal area showing small particles - sample 55

These particles appear irregularly shaped and display little evidence to suggest they had been subject to solvent dissolution, causing unwanted re-crystallisation issues as observed from the previous sample 53. However, the EDX spectrum, figure 4.135, obtained from the particles shows an increase in the oxygen levels, suggesting that the NaBH_4 had hydrolyzed.

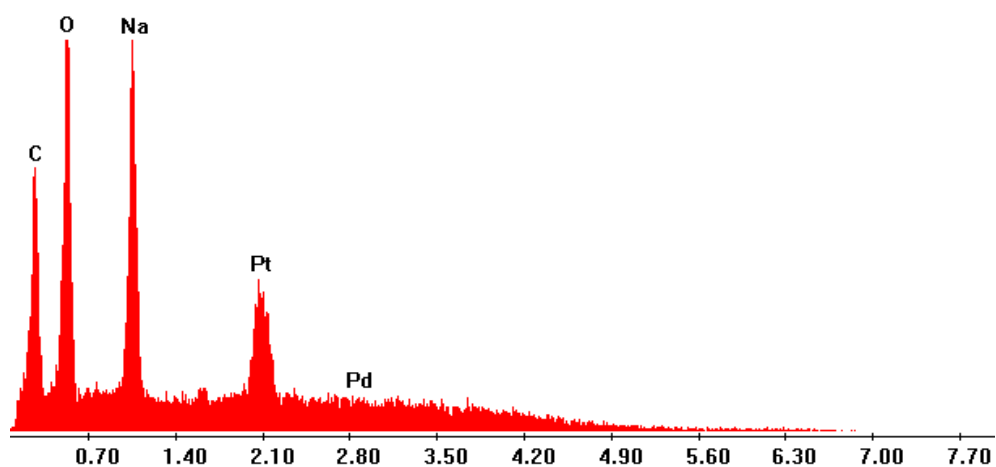


Figure 4.135 EDX spectrum from particles shown in figure 4.134 - sample 55

However, when a second microcapsule from the same generated batch was cross-sectioned, the particle as shown in figure 4.136 gave the corresponding EDX overlay figure 4.137, signifying that the NaBH_4 particles had remained unchanged. This is because the oxygen levels were seen to be the same as the background polymer.

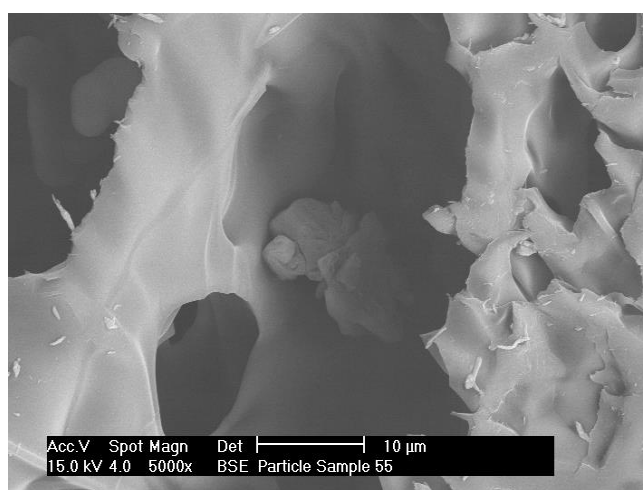


Figure 4.136 SEM micrograph of internal area showing NaBH_4 particles - sample 55

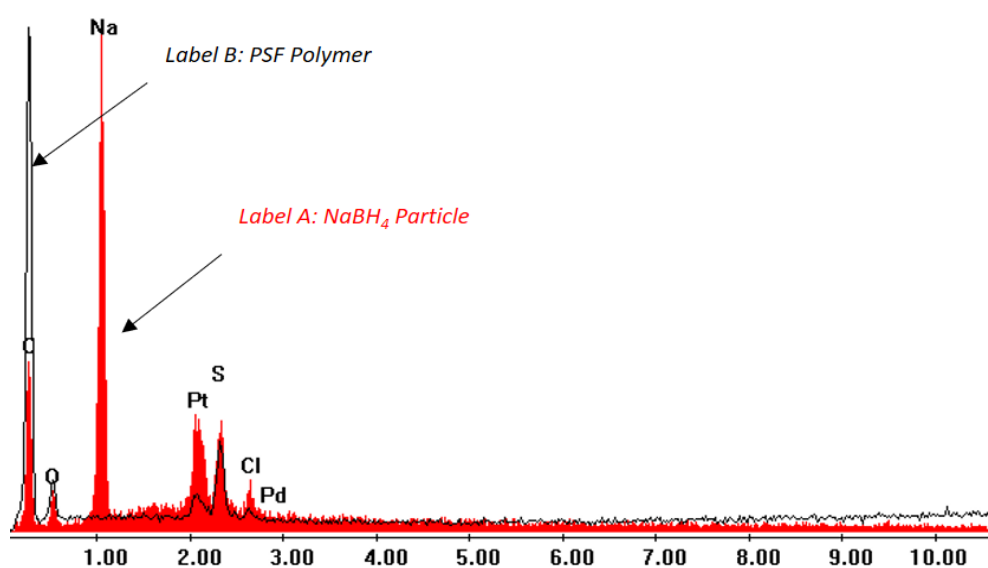


Figure 4.137 EDX spectra overlay NaBH₄ particle/PSF polymer - sample 55

PSF in DMF – NaBH₄ Dispersion in 83%-Acetonitrile, 17%-Chloroform - Sample 56

Further experiments were performed and the generated microcapsules, when examined using the XL30 SFEG interfaced to the preparation chamber, produced similar results to sample 55. Some of the encapsulated particles had remained as the hydride but others had hydrolyzed.

PSF in DMF – NaBH₄ Dispersion in 83%-Acetonitrile, 17%-Chloroform – Sample 57

One issue with the current experimental design was the drying procedure. It was feasible to infer that the microcapsules were slow to dry, and that the process may have allowed the hydride particles to change. Sample 57 involved increasing the nitrogen pressure during the addition of the PSF-NaBH₄ droplets using 2 necks of the reaction flask together with an increased purge for the drying process, with the hope that this may stop any unwanted hydrolysis.

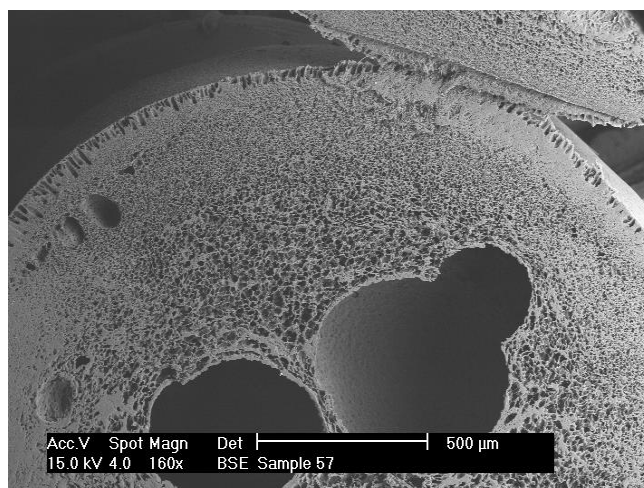


Figure 4.138 SEM micrograph of internal area - sample 57

The SEM micrograph in figure 4.138 shows a perfectly formed microcapsule with good internal porosity. However, the main issue was that it was extremely difficult to find any particles from the encapsulated NaBH_4 existing within the cross-sectional area.

PSF in DMF – Increased NaBH_4 Levels in the PSF Dispersion – Sample 58

Due to the difficulty of finding any encapsulated particles, sample 58 is the result of adding an extra micro-spatula of NaBH_4 to the dispersion initially created for sample 57.

The microcapsules were examined using the Quanta 250 to speed up the process of examining the internal structure. The nature of this exercise was to evaluate if adding extra NaBH_4 to the dispersion would increase the distribution of particles within the microcapsule. The SEM micrographs given in figure 4.139 show that the microcapsule has good internal morphology. However, it was still difficult to find many NaBH_4 particles to be present within the cross-sectioned area.

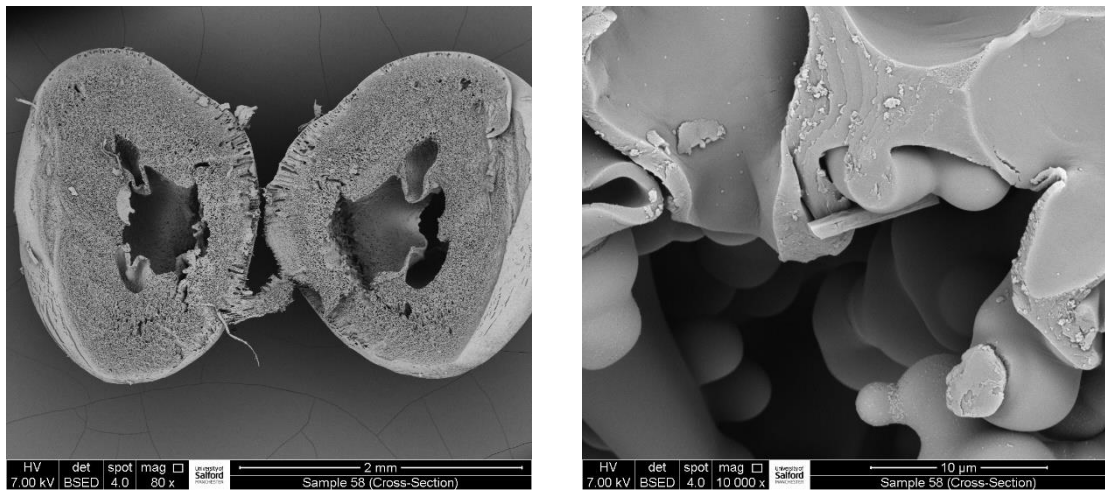


Figure 4.139 SEM micrograph of internal area - sample 58

The lath-shaped particles in the higher magnified micrograph (with a system magnification of 10,000x) were examined using EDX analysis. The consequent spectrum, figure 4.140, shows the presence of sodium with low levels of oxygen, implying that the NaBH_4 particle had not changed.

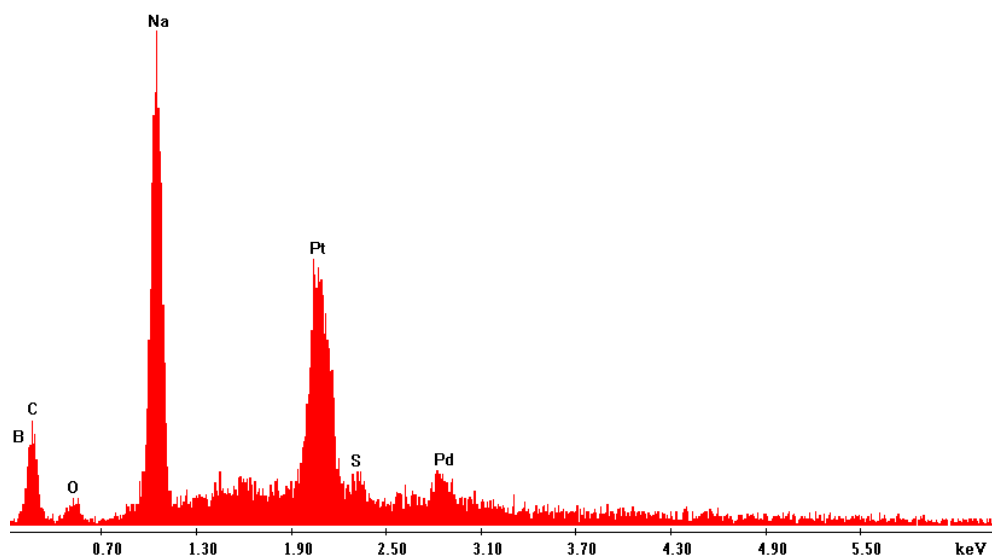


Figure 4.140 EDX spectrum from particle shown in figure 4.139 - sample 58

However, another particle examined from a different region of the cross-sectional area (figure 4.141) produced a different EDX spectrum (figure 4.142), which shows an increased level of oxygen – confirming that the NaBH_4 had hydrolyzed.

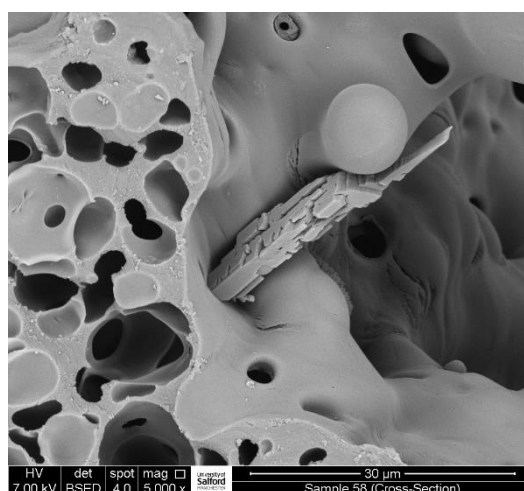


Figure 4.141 SEM micrograph of particle within the microcapsule - sample 58

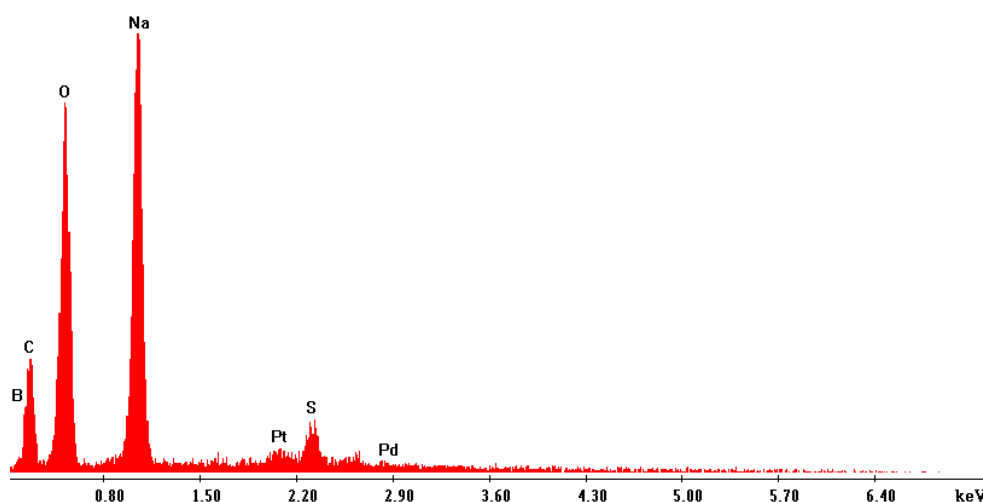


Figure 4.142 EDX spectrum from particle shown in figure 4.141 - sample 58

Samples 59-61 represent additional experiments using DMF as the solvent for PSF with the hope of developing a robust methodology for the study of encapsulating NaBH_4 within a polymer microcapsule. These efforts included changing the non-solvent blend ratio, and

finally working with 100% acetonitrile as the non-solvent. The results follow the same trend of showing only low concentrations of encapsulated particles. When the particles were examined using EDX, they either showed no change to the NaBH_4 or they revealed that the particles had hydrolyzed. The lack of concentrated particles of NaBH_4 within the microcapsules was initially believed to be the consequence of working with low concentrations of NaBH_4 within the dispersion. Alternatively, it could have been a solubility issue with the solvents used in the procedure, or perhaps they may have picked up low levels of water.

The sample numbering from this point onwards is not consecutive as additional microcapsules were generated using alternative solvent systems to DMF. This part of the thesis has been written to maintain continuance of the use of DMF.

PSF in DMF – Increased NaBH_4 Levels – 100% Acetonitrile – Sample 65

Using the same PSF- NaBH_4 dispersion utilised for samples 59-61, an additional micro-spatula of NaBH_4 was added to the dispersion using the nitrogen glove box.

The dispersion was agitated for 1 hour before the droplets were introduced slowly into 25ml of 100% acetonitrile using a Microlance 20G(0.9x40mm) needle coupled to a 1ml syringe. The initial agitation speed was 8, which was then reduced to 4 after 10 minutes; the generated microcapsules were dried under nitrogen overnight.

To check for an increase in the encapsulated NaBH_4 particles the microcapsules were quickly cut open using a razor blade and introduced to the Quanta 250 SEM for analysis.

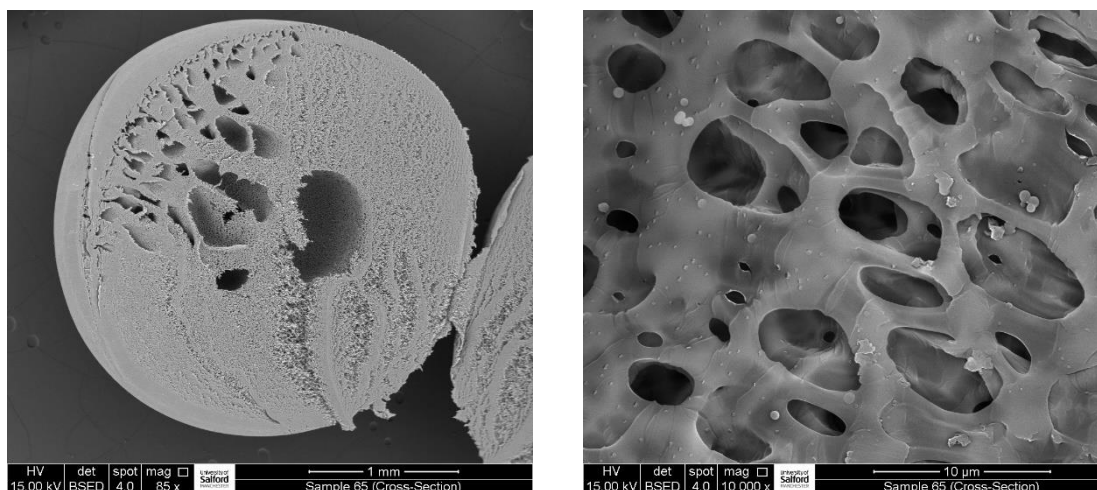


Figure 4.143 SEM micrograph of particle within the microcapsule - sample 65

The results using 100% acetonitrile as the non-solvent generated good, spherical microcapsules. The SEM micrographs obtained using system magnifications of 85x and 10,000x respectively (figure 4.143) illustrate that the internal structure had reduced porosity and formed a honeycomb structure.

The particles observed in the higher magnified SEM micrograph were examined using EDX analysis.

The results would suggest that the NaBH_4 has started to or completely converted to boron oxides.

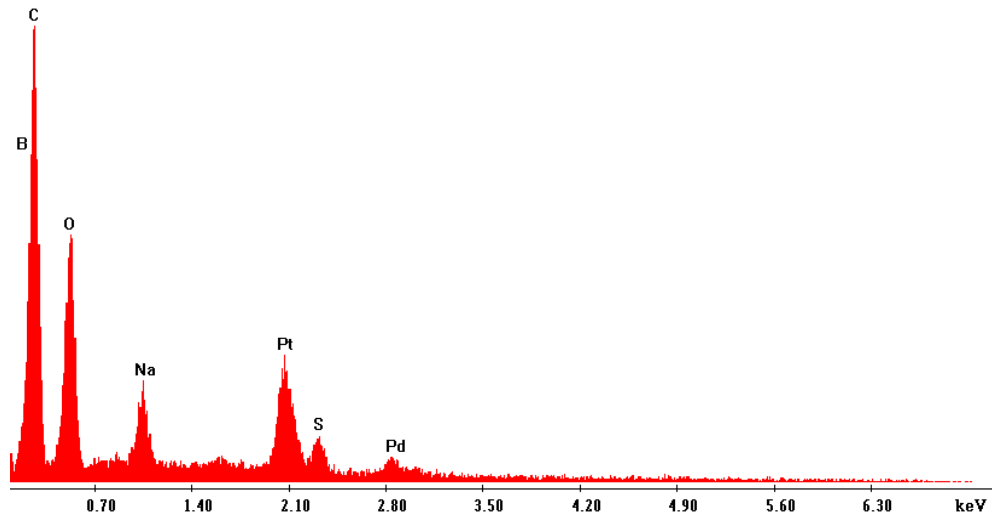


Figure 4.144 EDX spectrum from particle shown in figure 4.143 - sample 65

Figure 4.144 represents the spectrum obtained from the particles using an accelerating voltage of 7kV. The spectrum shows the presence of sodium, but the oxygen levels are seen to be significantly higher than the levels of oxygen obtained from the background polymer (figure 4.145).

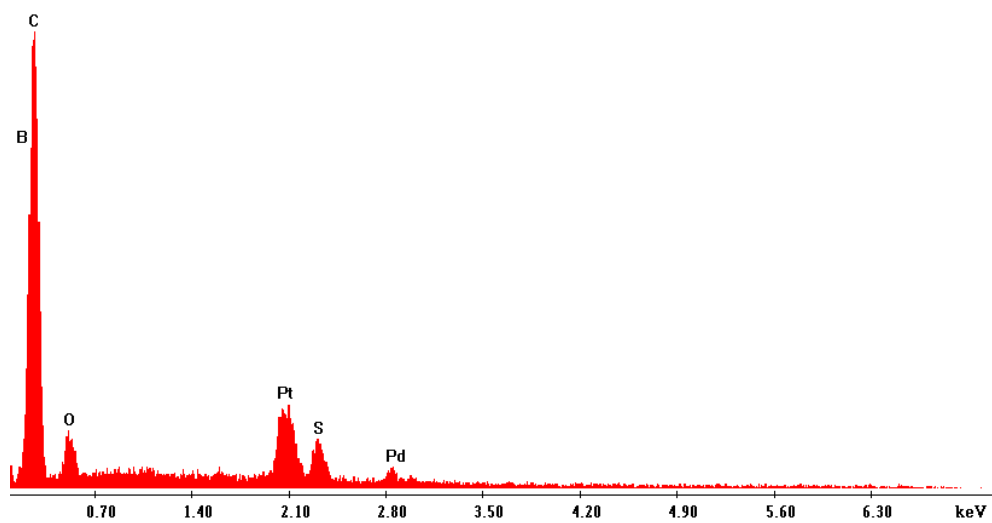


Figure 4.145 EDX spectrum from PSF polymer substrate - sample 65

Looking at a different region of the cross-section, another group of particles produced EDX spectra showing higher levels of sodium to oxygen - suggesting that the NaBH_4 had not hydrolyzed. However, the main concern is that very few particles appear to be present within the microcapsules.

Figure 4.146 represents the resulting SEM micrographs obtained from the surface of the microcapsules. The micrographs clearly show that irregular-shaped particles can be seen to exist on the surface of the microcapsule.

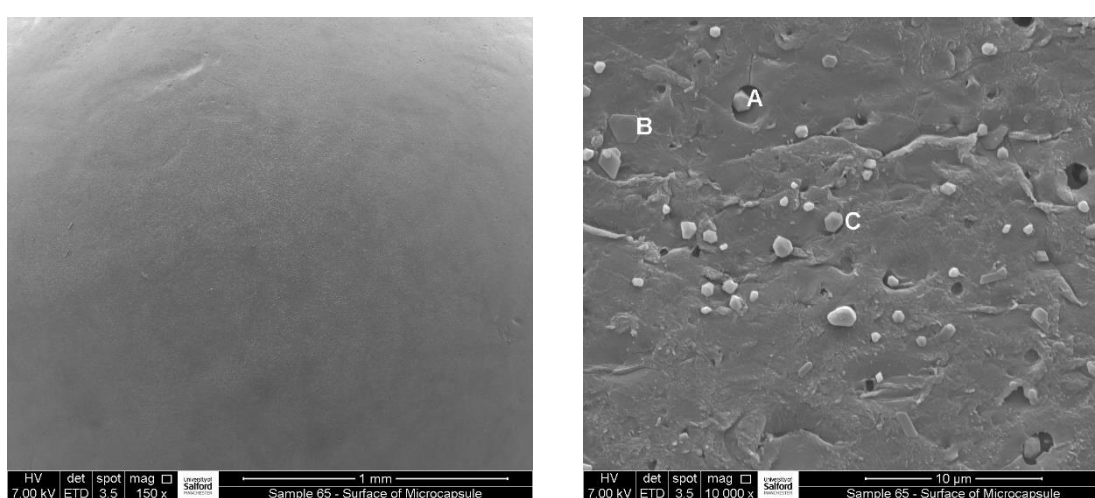


Figure 4.146 SEM micrograph of surface particles on the microcapsule - sample 65

The particles were annotated A-C and individually examined using EDX analysis with an accelerating voltage of 7kV.

Figure 4.147 represents the EDX spectra obtained from each annotated particle A-C presented as an overlay. All 3 particles examined show that the NaBH_4 had hydrolyzed, as the peak height for oxygen was significantly higher than the sodium peak. These surface NaBH_4 particles could be a direct result of increasing the concentration of NaBH_4 dispersion. An additional micro-spatula of NaBH_4 was added to the initial dispersion in an attempt to increase the loading of encapsulated metal hydride particles. This could have had the reverse effect as particles were seen to have deposited on the outer surface rather than the internal structure. Alternatively, this may be associated to the use of DMF as the solvent for the PSF polymer.

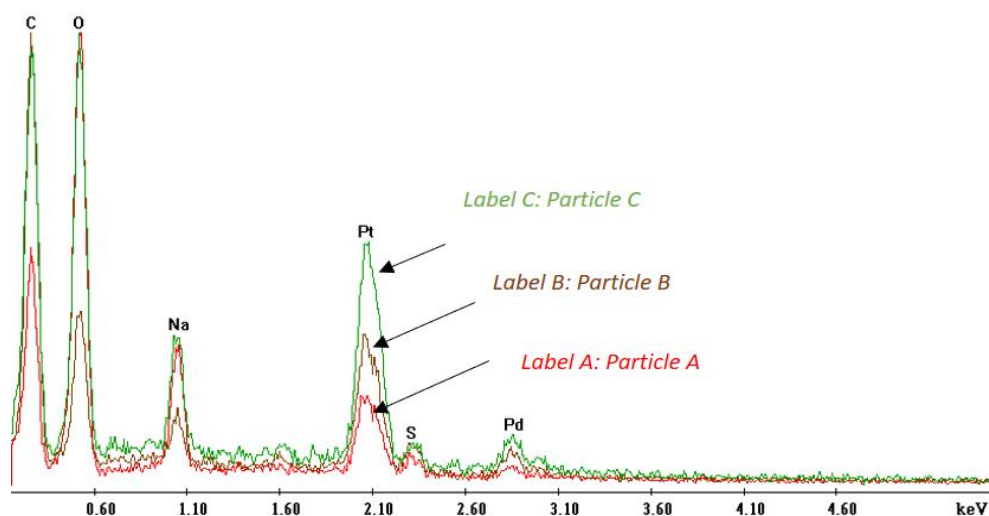


Figure 4.147 EDX spectra overlay from 3 separate particles figure 4.146 - sample 65

The conditions for EDX analysis involved using an accelerating voltage of 7kV to generate the electron beam. This was an attempt to try to increase the sensitivity of the lighter elements such as sodium and oxygen. The electron beam in contact with the surface of a sample produces an interaction volume which signifies electrons travelling into the surface of the sample. When the energy of the beam is reduced, the interaction volume (that can increase the sensitivity of the lighter elements) is also reduced.

PSF in DMF – Increased NaBH₄ Levels - Extra-Dry Acetonitrile – Sample 70

To verify the results seen for the previous sample 65, this sample was generated by following the same procedure, except the non-solvent acetonitrile was substituted by extra-dry acetonitrile to eliminate the possibility of hydrolysis in solution and a new batch of PSF-NaBH₄ dispersion was generated as outlined in method 16, substituting NMP by DMF. The level of concentration of NaBH₄ was increased by the addition of an extra micro-spatula of NaBH₄. The new dispersion was released into a non-solvent of 100% extra-dry acetonitrile, purchased from ACROS Organics, using a Microlance 3 20G (0.9mmx40mm) needle connected to a 1ml syringe.

SEM micrographs shown in figure 4.148 represent the internal morphology of the generated microcapsules.

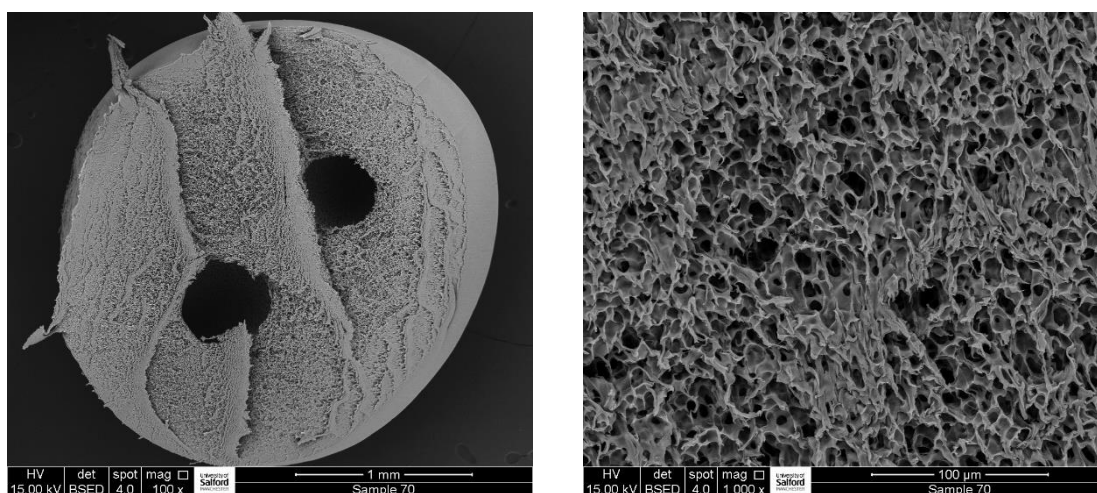


Figure 4.148 SEM micrograph of internal structure - sample 70

The internal structure is seen to have the same morphology as sample 65, existing as a honeycomb structure.

Several microcapsules were cut open and examined using the Quanta 250 SEM. The internal honeycomb structure was examined closely with the aim of finding clusters of NaBH_4 particles. However, the microcapsules did not show any evidence to suggest the encapsulation of NaBH_4 particles.

Figure 4.149 represents SEM micrographs obtained from the surface of the created microcapsules using system magnifications of 100x and 20,000x respectively. The low magnified micrograph shows the microcapsule to exist as a perfectly smooth sphere. The higher magnified micrograph illustrates that the surface is coated in clusters of very small particles existing between 0.1 μm to 0.5 μm in size.

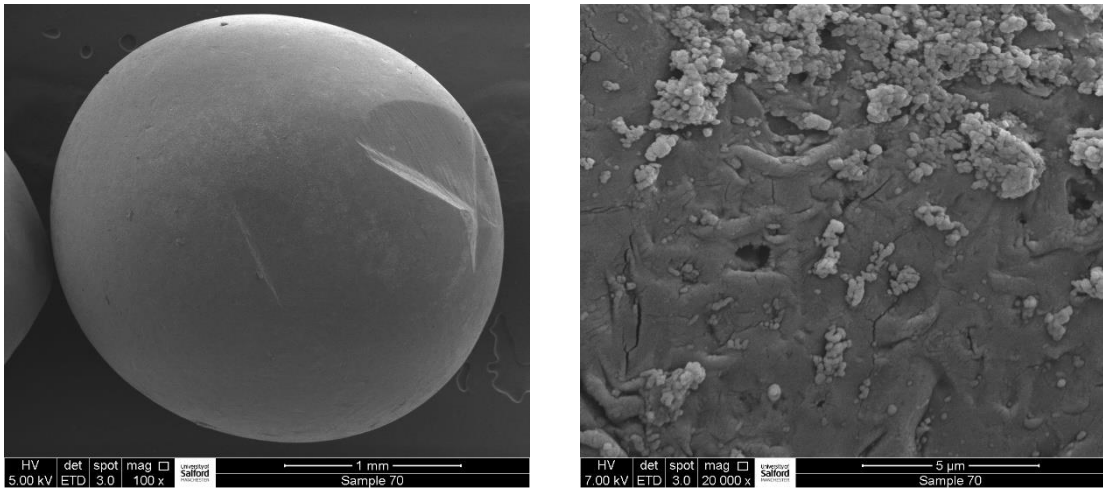


Figure 4.149 SEM micrograph of external structure - sample 70

EDX analysis of the particles produced the spectrum figure 4.150, showing high levels of carbon with lower levels of oxygen, sodium, sulfur and nitrogen.

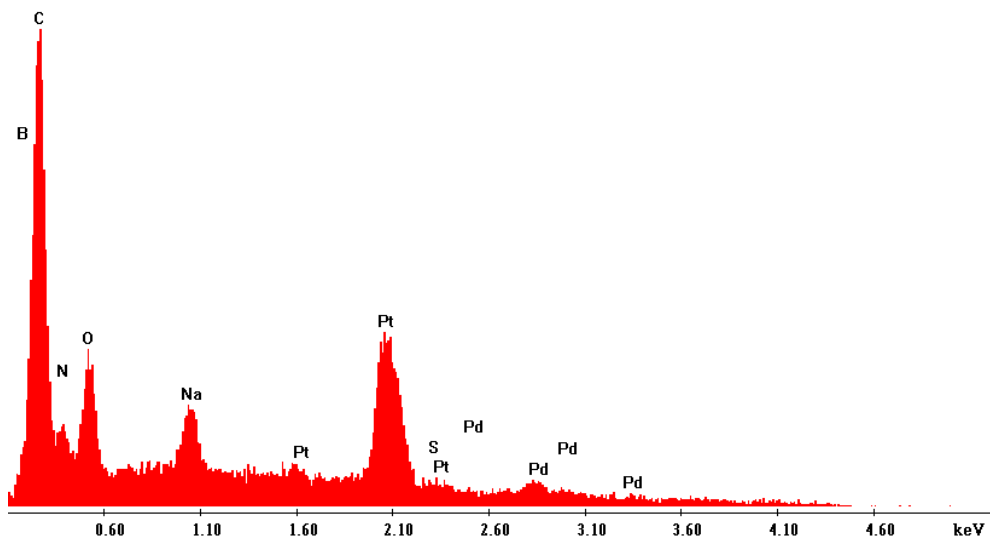


Figure 4.150 EDX spectrum from particles shown in figure 4.149 - sample 70

The EDX spectrum given in figure 4.151 was obtained from the polymer surface, near the small particles. The ratio of carbon and oxygen appear similar with trace levels of sodium.

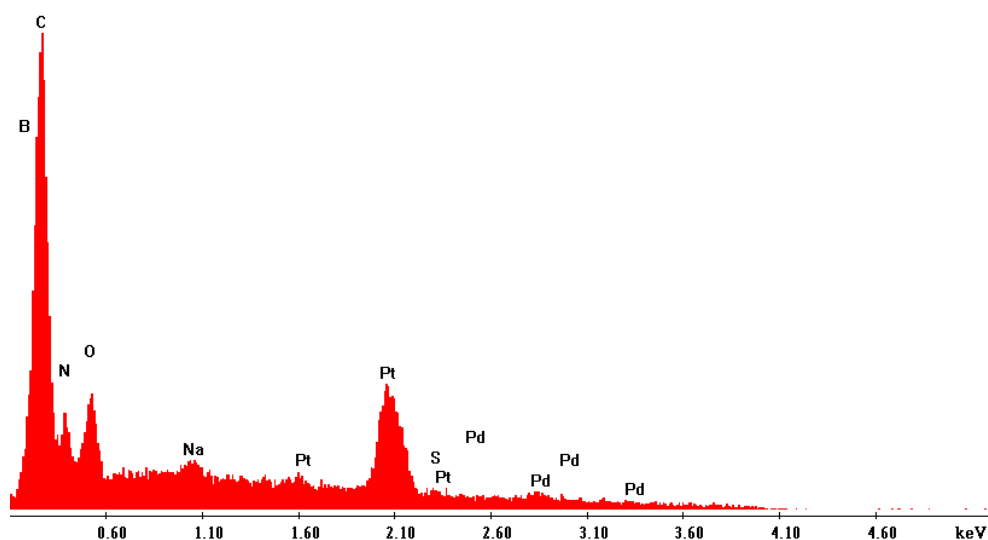


Figure 4.151 EDX spectrum from polymer substrate shown in figure 4.149 - sample 70

An additional peak is also observed between the carbon and oxygen - thought to be nitrogen. Perhaps the DMF had reacted with the NaBH_4 , forming a compound containing nitrogen. These particles are interesting as they have a particle size much lower than the original ground NaBH_4 particles. The size may have reduced when the polymer dispersion was agitated at the high shear rate or perhaps a dissolution has occurred, or reaction with the solvent to form a different species. The fact that these particles are present on the surface of the microcapsules emphasises that using 100% DMF to dissolve the PSF is not suitable for this project.

NMP and DMF Substituted by THF

This research indicates that problems have occurred trying to encapsulate NaBH_4 using a PSF polymer system when utilising either NMP or DMF as the solvent for the polymer.

PSF readily dissolves in NMP and DMF and most of the background work using non-metal hydride samples was developed using these two solvents. However, because of the issues seen to evolve when working with NaBH_4 , an alternative solvent was sourced. After some

initial literature searching, the new solvent decided upon for the dissolution of PSF was THF (Abdelhamid, 2021) as this has minimal solubility issues with NaBH_4 (Brown et al., 1982).

PSF in THF – NaBH_4 Dispersion in 100%-Acetonitrile - Sample 62

Using the procedure as given in method 16, a new batch of PSF- NaBH_4 dispersion was generated - substituting NMP by THF.

Using THF for the PSF solvent generated a slightly cloudy solution when following the same experimental procedure outlined in method 16, unlike the clear solutions observed when using NMP or DMF. Following the procedure outlined in method 18, the dispersion droplets were introduced to 100% acetonitrile using a Microlance 3 20G (0.9mmx40mm) needle connected to a 1ml syringe. The resultant microcapsules were dried under nitrogen overnight. For simplicity, to view if the experiments had worked at this stage, the microcapsules were examined quickly using the FEI Quanta 250.

The SEM micrographs, figure 4.152, represent both low and high magnified areas of the cross-sectioned microcapsule, obtained after slicing open with a razor blade.

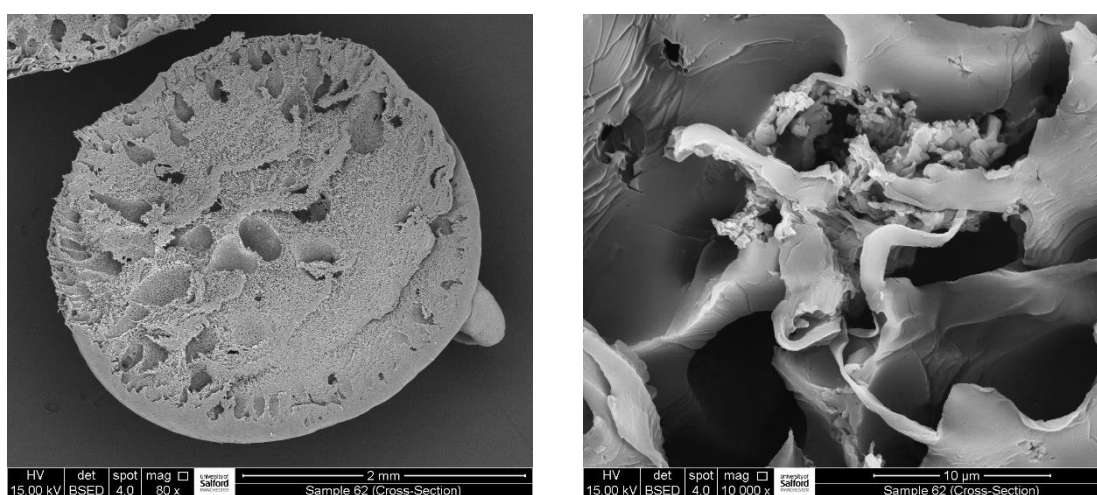


Figure 4.152 SEM micrograph of internal structure - sample 62

The low magnified micrograph obtained with a system magnification of 80x illustrates that the internal structure exists as a tight, honeycomb morphology. This is thought to be the

result of using 100% acetonitrile. The addition of chloroform to the non-solvent often improves the internal porosity. NaBH_4 is soluble in chloroform, so for this experiment it was decided to use only acetonitrile as the non-solvent.

The higher magnified micrograph obtained using a system magnification of 10,000x shows a cluster of small, irregular-shaped particles. When the small particles were examined using EDX analysis, the resulting spectrum (figure 4.153) shows the presence of sodium. As a result of the reduced particle size, the spectrum picked up elements associated with the supporting polymer due to scattering or penetration as explained from the analysis of many previous samples.

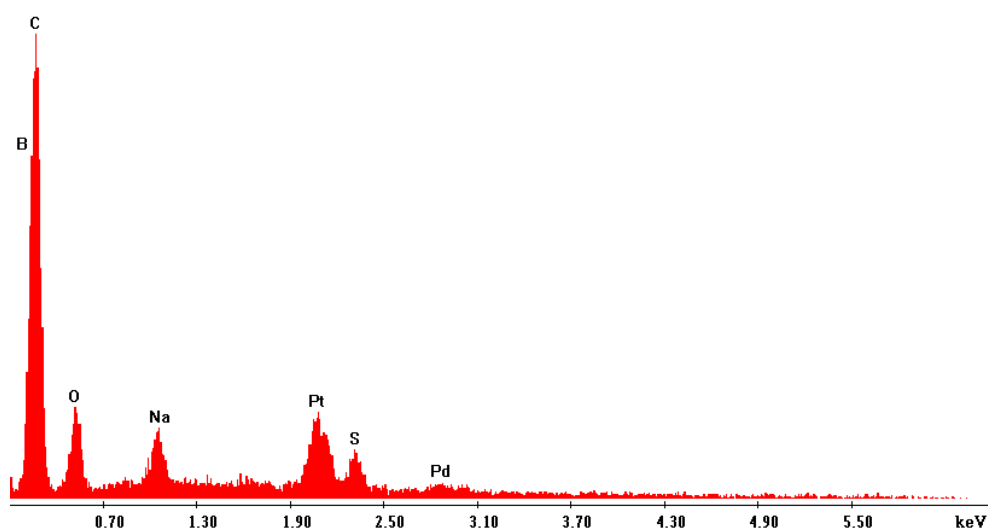


Figure 4.153 EDX spectrum from particles shown in figure 4.152 - sample 62

The EDX spectrum obtained from the polymer substrate, figure 4.154, displays similar levels of carbon, oxygen and sulfur, suggesting that the NaBH_4 particles may have remained unchanged during the encapsulation process.

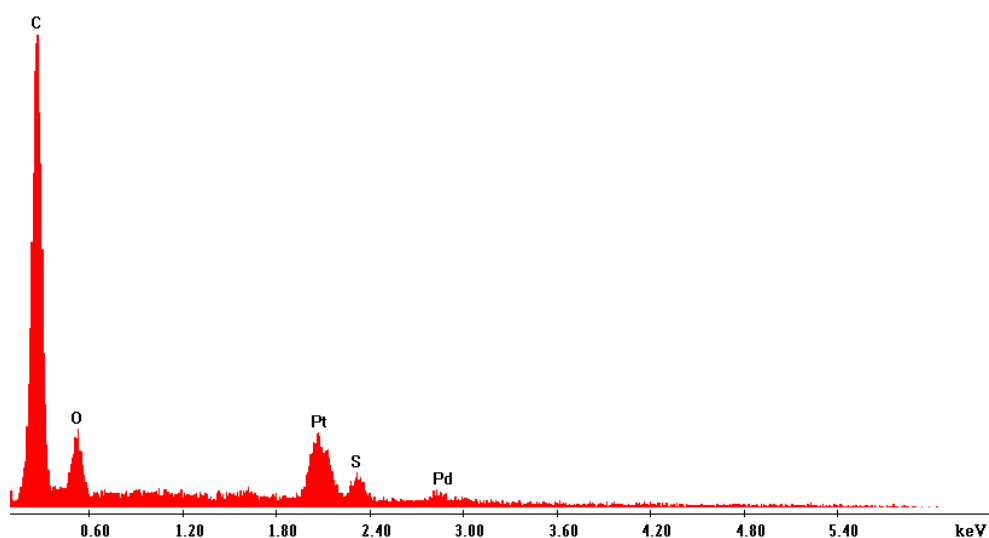


Figure 4.154 EDX spectrum from polymer substrate figure 4.152 - sample 62

Figure 4.155 shows a cluster of particles to be present in a different region of the same microcapsule cross-section.

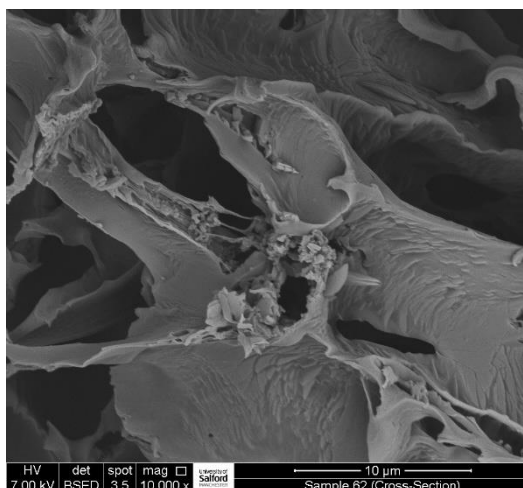


Figure 4.155 SEM micrograph of internal structure - sample 62

The particles, when examined using EDX, generated the corresponding spectrum figure 4.156 - showing a slight increase in the oxygen peak. This result could suggest that the NaBH_4 particles have only just started to hydrolyse.

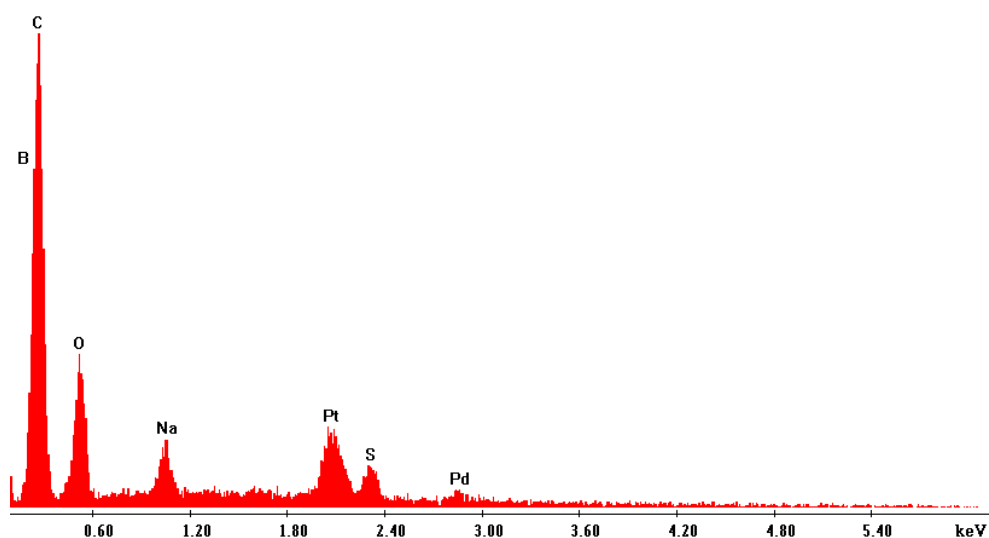


Figure 4.156 EDX spectrum from particles figure 4.155 - sample 62

The issue when using 100% acetonitrile is that the internal porosity of the generated microcapsules is seen to be reduced. As demonstrated in figure 4.152, the overall porosity is compromised, existing as a honeycomb structure. This internal morphology is not as good as previous samples generated using a small quantity of chloroform in the non-solvent mix.

PSF in THF – NaBH₄ Dispersion in 12% Chloroform / 88%-Acetonitrile - Sample 63

To increase the internal porosity, the non-solvent blend was changed to 3ml chloroform and 22ml acetonitrile. An additional micro-spatula of NaBH₄ was added to the dispersion within the nitrogen glove box to increase the concentration. The SEM micrographs shown at figure 4.157 are a low magnified micrograph obtained using a system magnification of 80x and a higher magnified area obtained at 10,000x respectively.

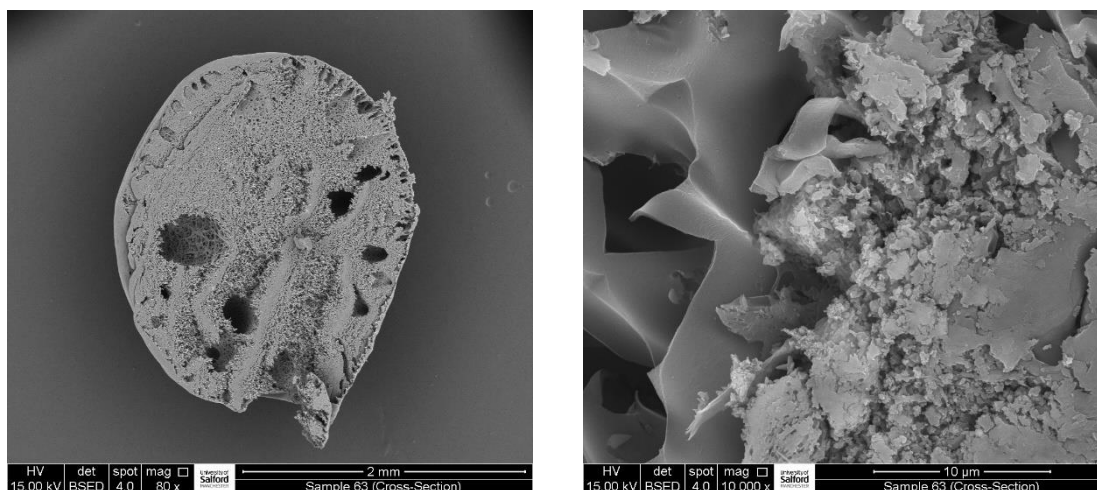


Figure 4.157 SEM micrograph of internal structure - sample 63

As predicted, the internal porosity is seen to have increased slightly using 12% chloroform in the non-solvent blend. The particles as shown in the higher magnified area were examined using EDX analysis. The resulting EDX spectrum (figure 4.158) shows high levels of oxygen, suggesting that NaBH_4 has hydrolyzed.

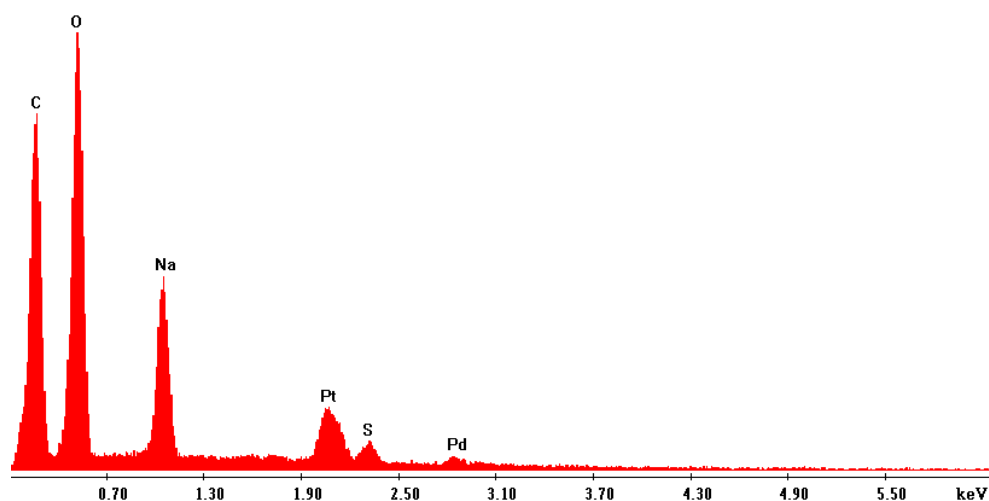


Figure 4.158 EDX spectrum from particles figure 4.157 - sample 63

These results would suggest that the chloroform could be causing issues with the experimental procedure.

PSF in THF – NaBH₄ Dispersion in 4% Chloroform / 96%-Acetonitrile - Sample 64

To investigate the presumption of the effect of chloroform, droplets of the same PSF-NaBH₄ dispersion used for sample 63 were introduced slowly into a non-solvent blend of 4% chloroform and 96% acetonitrile using a Microlance 3 20G (0.9x40mm) needle connected to a 1ml syringe.

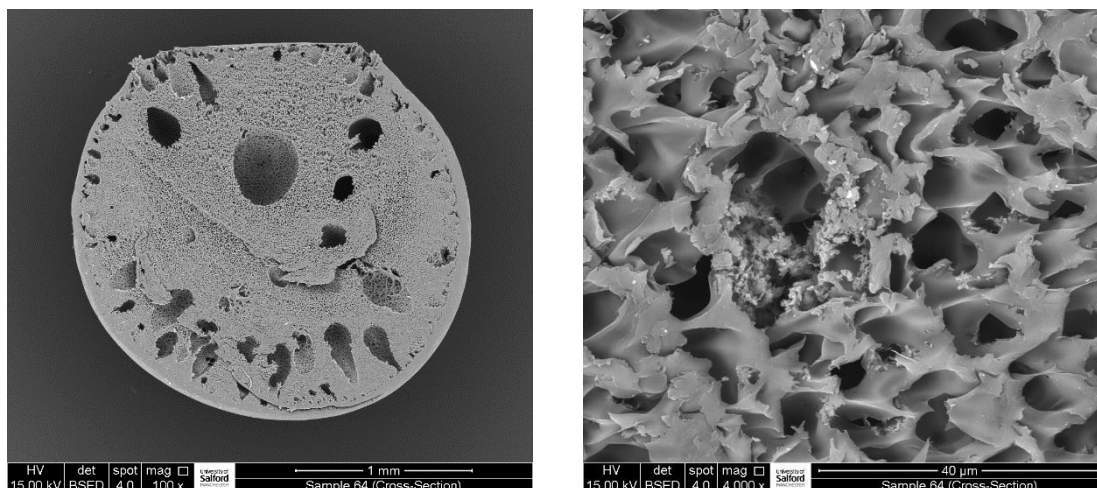


Figure 4.159 SEM micrograph of internal structure - sample 64

The SEM micrographs shown in figure 4.159 were obtained after the microcapsules were cut open using a razor blade. The micrographs suggest that the addition of 4% chloroform had some effect on improving the porosity of the internal structure. The higher magnified micrograph shows a cluster of small particles. When these particles were examined using EDX analysis, the resulting EDX spectrum (figure 4.160) displayed an increased oxygen level, suggesting that the NaBH₄ particles had hydrolyzed.

These results would suggest that the addition of a lower concentration of chloroform to the non-solvent still improved the porosity of the internal structure of the generated microcapsules. However, with both samples, the resulting EDX spectra obtained from the NaBH₄ particles suggest hydrolysis had occurred.

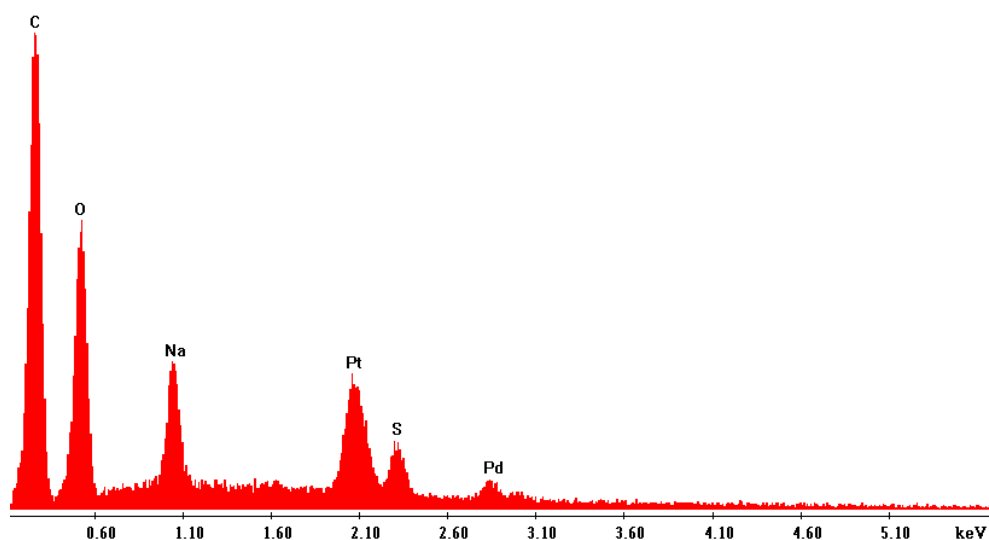


Figure 4.160 EDX spectrum from particles figure 4.159 - sample 64

PSF in THF – NaBH₄ Dispersion in 100% Acetonitrile - Sample 66

An extra micro-spatula of NaBH₄ was added to the same PSF-NaBH₄ dispersion utilised to generate the microcapsules of sample 64. The dispersion was then introduced to 100% acetonitrile as the non-solvent, following the procedure as outlined in method section 18 except for the agitation being left at 8 for 1 hour.

The generated microcapsules were cut open at room temperature then quickly transferred to the FEI Quanta 250 after coating with 4nm of platinum/palladium using the Cressington 208 sputter coating unit.

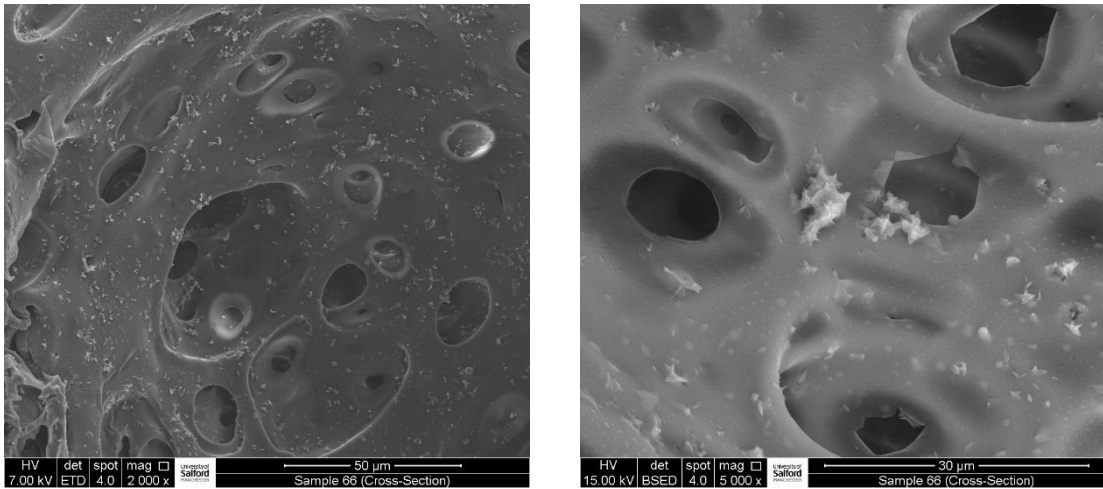


Figure 4.161 SEM micrograph of internal structure - sample 66

The SEM micrographs in figure 4.161 were obtained using a system magnification of 2000x and 5000x respectively. They show that irregular-shaped, small particles have completely covered the internal surface of the cross-sectioned microcapsule. These are quite unique and appear different from most particles seen to exist within previously examined microcapsules.

The larger particle, present in the SEM micrograph with a system magnification of 5000x, was examined using EDX analysis, and the results are interesting. The EDX spectra overlay below, figure 4.162, represents the results from both the particle and corresponding polymer substrate.

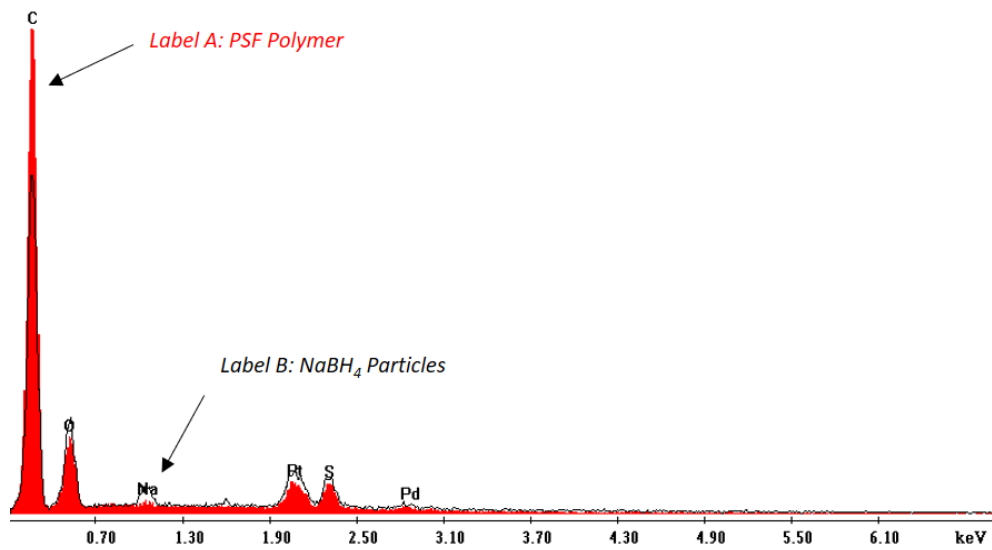


Figure 4.162 EDX spectra overlay PSF polymer against particles figure 4.161 - sample 66

The EDX results from the larger particle would suggest that the NaBH₄ particle has not changed as the oxygen levels are similar to the background polymer.

However, the micrograph shown in figure 4.163 was obtained using a system magnification of 8000x. It represents a different region within the internal structure of the same microcapsule, showing the presence of many small crystallites.

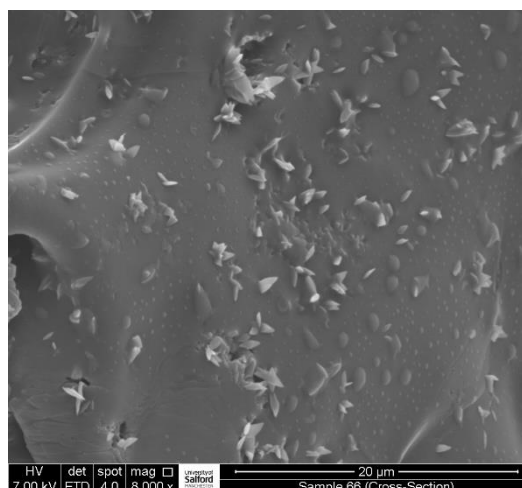


Figure 4.163 SEM micrograph of internal structure - sample 66

These are not thought to represent particles of NaBH_4 as they appear as small crystallites rather than ground irregular-shaped particles.

However, when examined using EDX analysis, the small crystallites gave the corresponding spectrum, figure 4.164, showing the presence of high levels of carbon with lower levels of oxygen, sodium and sulfur. These results are interesting as they suggest that the NaBH_4 has hydrolyzed, generating particles of a completely different morphology.

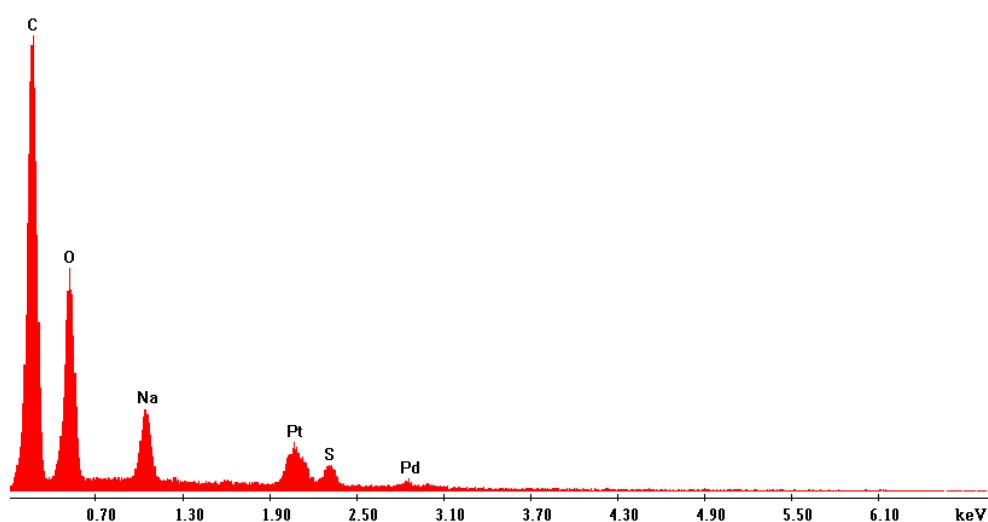


Figure 4.164 EDX spectrum from crystallites figure 4.163 - sample 66

The oxygen peak height is significantly higher than the level obtained from the background PSF polymer - figure 4.165.

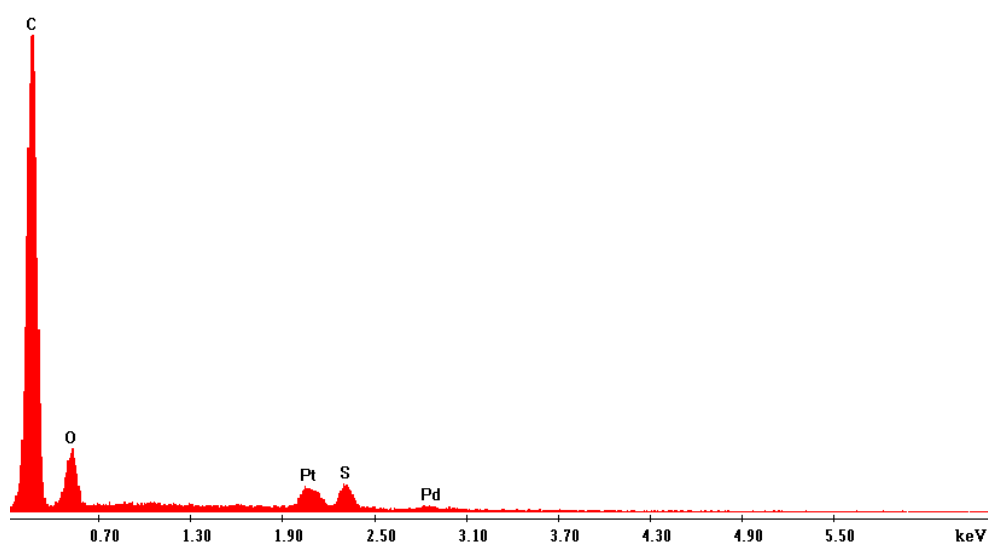


Figure 4.165 EDX spectrum from polymer substrate figure 4.158 - sample 66

PSF in THF – NaBH₄ Dispersion in 100% Acetonitrile - Sample 68

The PSF-NaBH₄ dispersion used for sample 66 was the same initial batch of dispersion produced for sample 62. Changes to this dispersion had involved the addition of extra NaBH₄ for previous samples, so it was extremely well used and perhaps the crystallites were an indication that the dispersion required changing. However, for interest, the very viscous dispersion used for sample 66 was diluted by the addition of a small amount of THF and the dispersion was re-agitated.

Microcapsules were generated by introducing droplets of the dispersion into 100% acetonitrile following the conditions as outlined in method 18, using a slightly higher shear rate of 10 for 10 minutes, then reducing to 4 for 1 hour in an attempt to increase the internal porosity of the microcapsules.

The microcapsules were initially examined using the Quanta 250, then later examined using the XL30 interfaced to the preparation chamber.

The SEM micrographs are interesting as the increased agitation speed, with the increased dilution, has helped create an improved internal porosity as shown in the 100x magnified micrograph, figure 4.166.

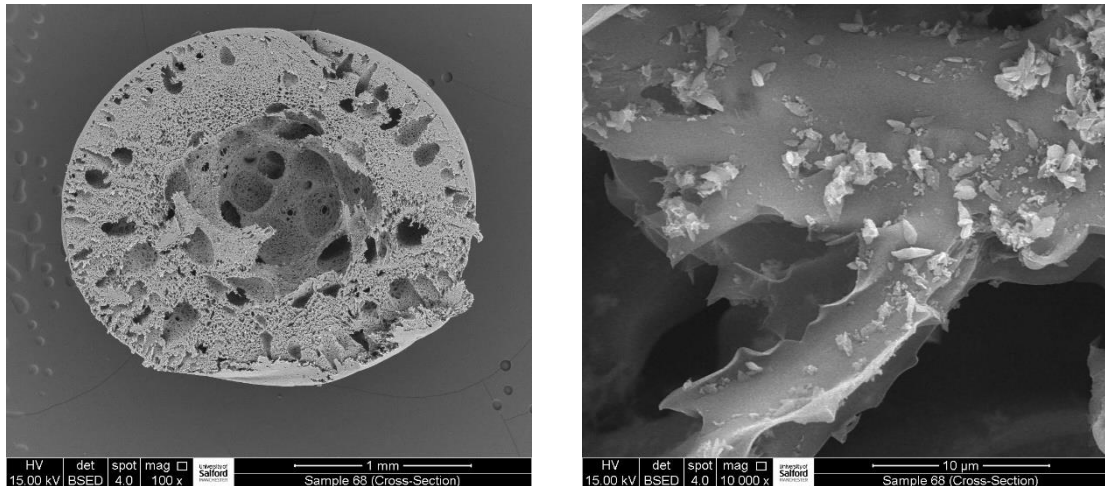


Figure 4.166 SEM micrograph of internal structure - sample 68

The SEM micrograph obtained with the higher magnification of 10,000x displays a coating of irregular-shaped particles. When these particles were examined using EDX analysis at 15kV, the resultant spectrum (figure 4.167) indicates that they represent NaBH_4 particles that have not changed. The oxygen level from the particles is similar to the spectrum obtained from the background PSF substrate - figure 4.168.

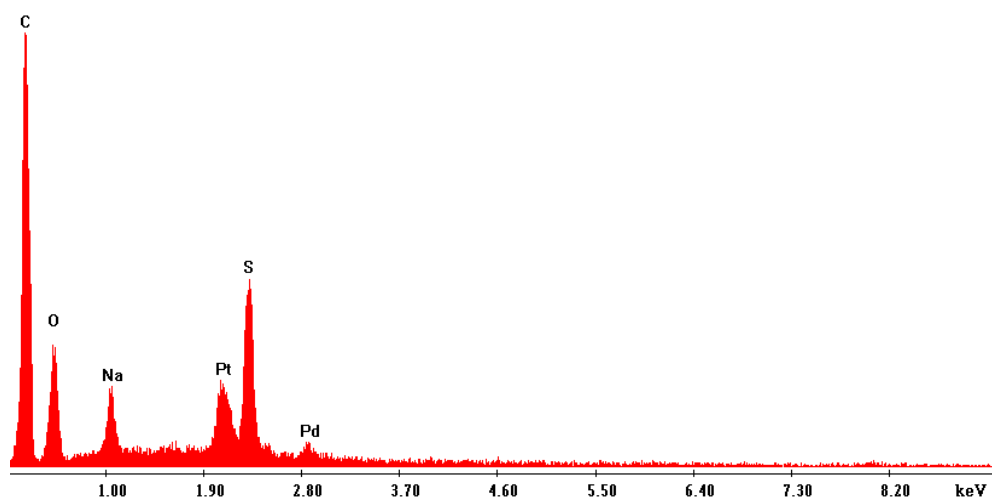


Figure 4.167 EDX spectrum from particles figure 4.166 - sample 68

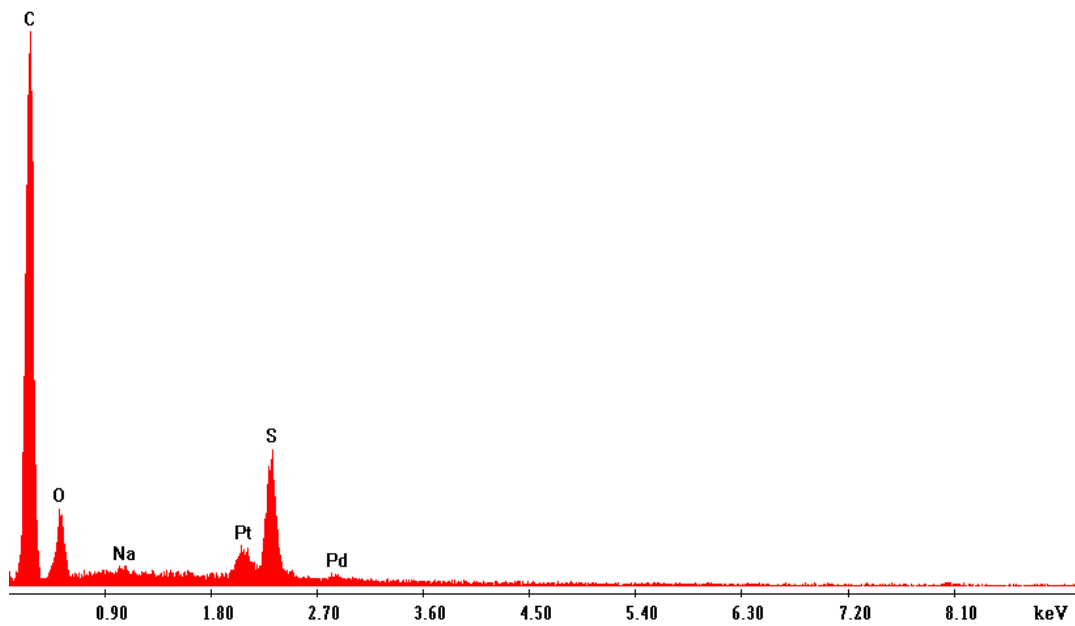


Figure 4.168 EDX spectrum from polymer substrate figure 4.166 - sample 68

Figure 4.169 shows an SEM micrograph obtained from a different cross-sectioned microcapsule from the same batch of sample 68. This micrograph represents an area from the internal structure, showing a mixture of different particle morphologies. Some have the appearance of the small crystallites as seen to exist in figure 4.163.

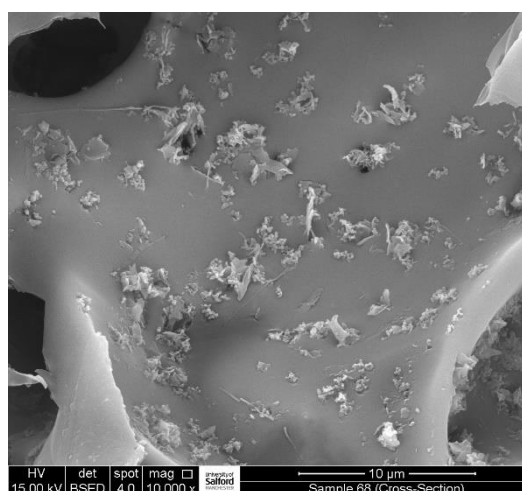


Figure 4.169 SEM micrograph of internal structure - sample 68

When a representative particle was examined using EDX analysis, the corresponding spectrum, figure 4.170, shows higher levels of oxygen, suggesting that the NaBH_4 had hydrolyzed.

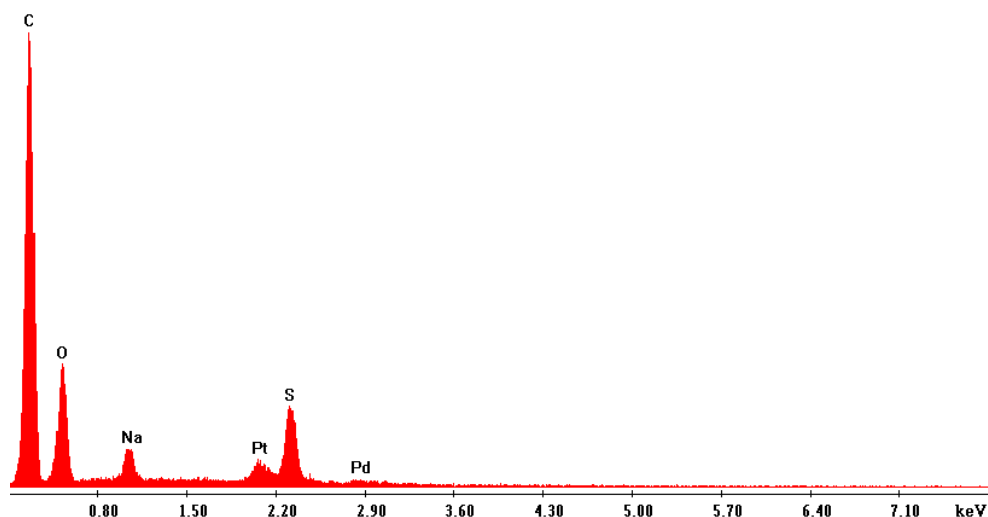


Figure 4.170 EDX spectrum from particles - sample 68

The differences seen from the various particles examined could have been the result of the polymer dispersion going off over time or perhaps it could represent a direct result of the preparation technique. Moisture from the air may have reacted with the encapsulated NaBH_4 particles after the microcapsules had been prepared in the open lab.

It is still difficult to discern that the formation of boron oxides is directly related to the use of chloroform in the non-solvent mix, as seen in previous sample 63. These results also show the presence of the oxide in some areas of the microcapsule even though the non-solvent was 100% acetonitrile.

Sample 68 was examined using the XL30 SFEF interfaced to the preparation chamber. A microcapsule was glued onto a rivet using rapid-setting Araldite and examined after cross-sectioning in the preparation chamber under vacuum. The resulting SEM micrograph given

in figure 4.171 displays small irregular-shaped particles that are present within the internal structure of the microcapsule.

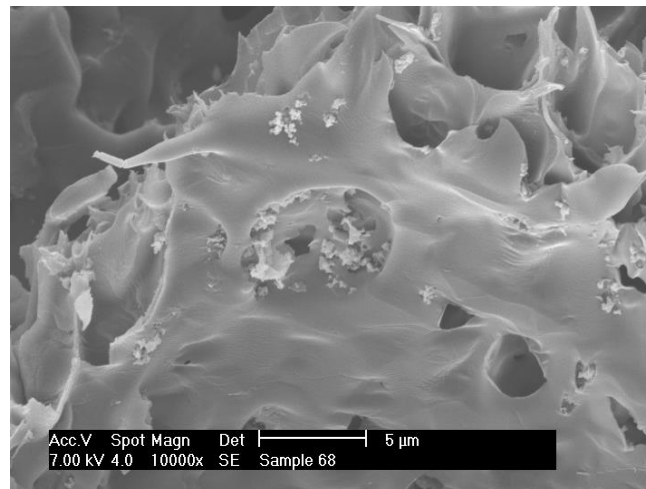


Figure 4.171 SEM micrograph of internal structure-XL30 - sample 68

The small particles were examined using EDX and the resulting spectrum overlay, figure 4.172, shows the presence of sodium with similar oxygen levels to those obtained from the polymer substrate.

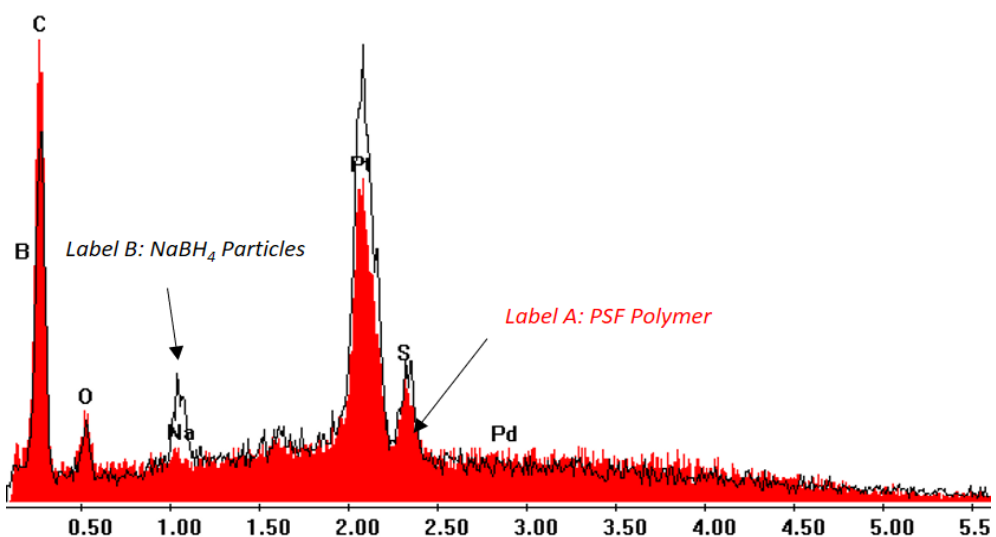


Figure 4.172 EDX spectra overlay PSF polymer against NaBH₄ particles - sample 68

The SEM micrographs, figure 4.173, represent a different region within the cross-sectioned microcapsule. The micrographs were obtained using system magnifications of 5000x and 20,000x respectively. The particles show a mixed morphology, with some particles having a similar appearance to the crystallites observed in figure 4.169.

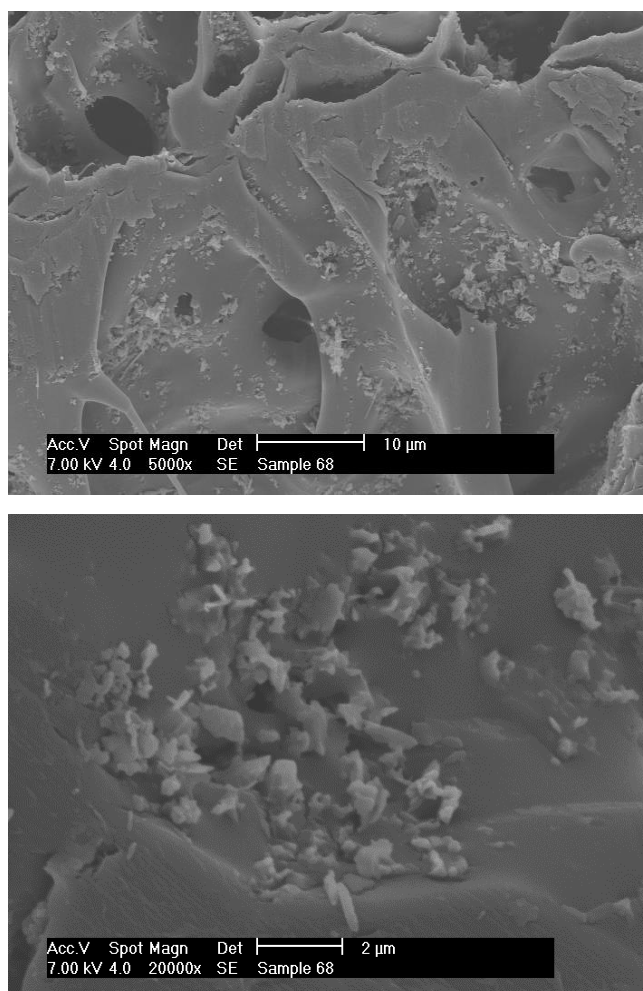


Figure 4.173 SEM micrographs of particles from internal structure-XL30 - sample 68

When examined using EDX analysis, these particles produced the corresponding EDX spectrum overlay, figure 4.174, showing sodium with oxygen levels slightly higher than the background polymer, implying that the NaBH_4 particles had started to hydrolyse.

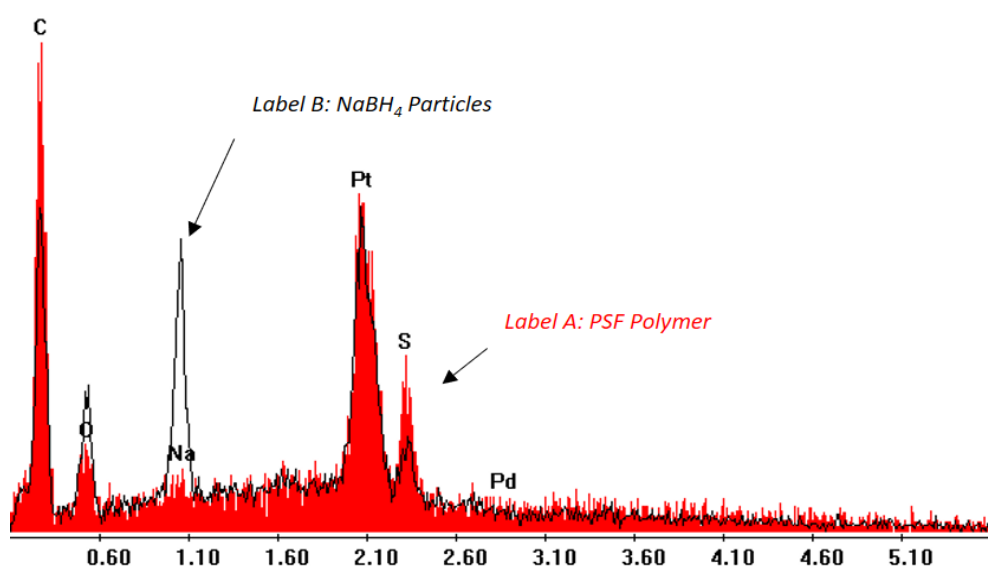


Figure 4.174 EDX spectra overlay PSF polymer against NaBH₄ particles - sample 68

These results are promising as, when using THF, the NaBH₄ particles are shown to be encapsulated within the internal structure of the microcapsules. The morphology of some of the particles, shown in figure 4.173, is more consistent with what would be expected from the mortar-and-pestle-ground NaBH₄ used in the preparation.

PSF in THF – NaBH₄ Dispersion in 100% Acetonitrile - Sample 69

In order to understand if the crystallites associated with samples 66 and 68 were related to the NaBH₄ particles changing in the dispersion and forming the oxide due to the age and continuous use of the dispersion, a new dispersion was generated using THF as the polymer solvent - following the procedure outlined in method 16.

An observation was made that the PSF solution looked cloudy even after the polymer had been heated and stirred over a long time. This was concerning as these observations made it difficult to know if the THF had fully dissolved the PSF polymer. After the addition of NaBH₄ to generate the dispersion, droplets were slowly introduced to 25ml of acetonitrile using a Microlance 3 20G (0.9x40mm) needle connected to a 1ml syringe, following the procedure as outlined in method 18.

The generated microcapsules were examined using the XL30 SFEF interfaced to the sample preparation chamber.

Little evidence was available from the study of the internal cross-sectional area of these microcapsules to demonstrate the presence of the crystallites previously seen. This would suggest that the small crystallites seen in samples 66 and 68 were the result of using a dispersion that had aged, and the NaBH_4 particles had changed to form the oxides.

The SEM micrograph below, figure 4.175, was obtained using BSE detection with a system magnification of 10,000x. Small, irregular-shaped particles can be seen to be present within the polymer cross-section.

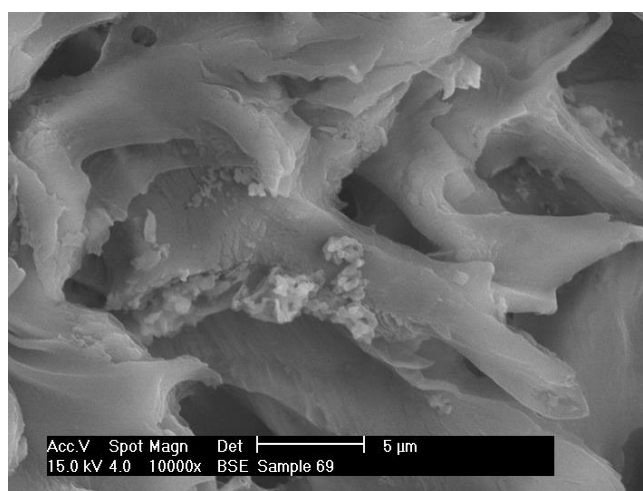


Figure 4.175 SEM micrograph of particles from internal structure-XL30 - sample 69

The particles were examined using EDX analysis with an acceleration voltage of 15kV and a spot size of 4. Figure 4.176 represents the EDX spectrum obtained from the small particles together overlaid against a spectrum obtained from the polymer substrate.

When comparing the peak heights, it is thought that the oxygen peak is slightly higher from the particles. This is not a fully quantitative measurement but can provide a qualitative evaluation. If the NaBH_4 had completely changed forming the oxide, the oxygen levels would have been significantly higher.

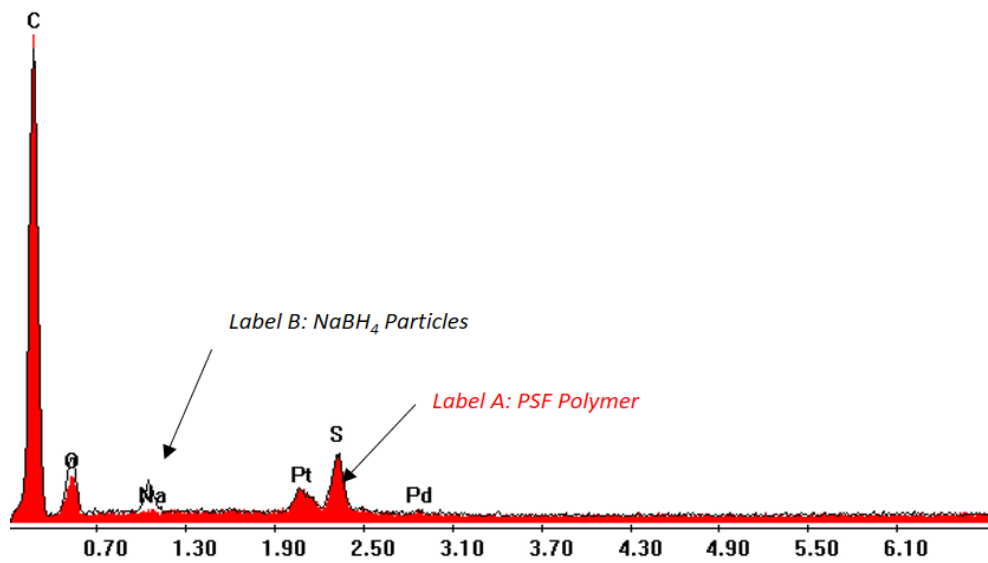


Figure 4.176 EDX spectrum from particles - sample 69

A second chosen area from the cross-sectioned microcapsule is shown in figure 4.177. The SEM micrograph was obtained using a system magnification of 10,000x. A cluster of irregular-shaped particles can be seen to be present within the pores of the PSF polymer.

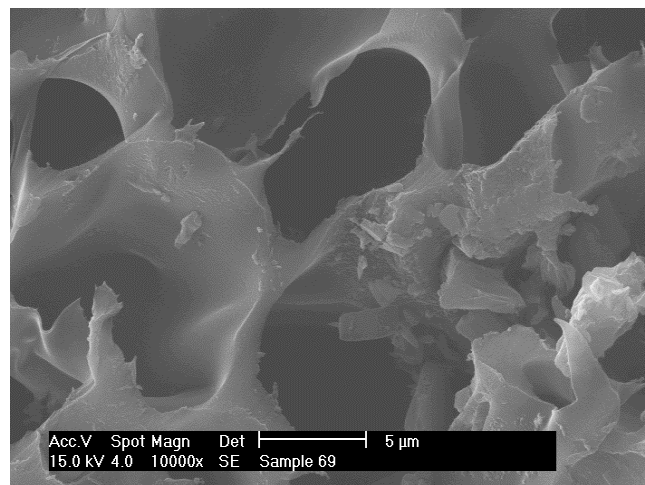


Figure 4.177 SEM micrograph of particles from internal structure-XL30 - sample 69

The particles, when studied using EDX analysis, produced the corresponding spectrum as shown in figure 4.178.

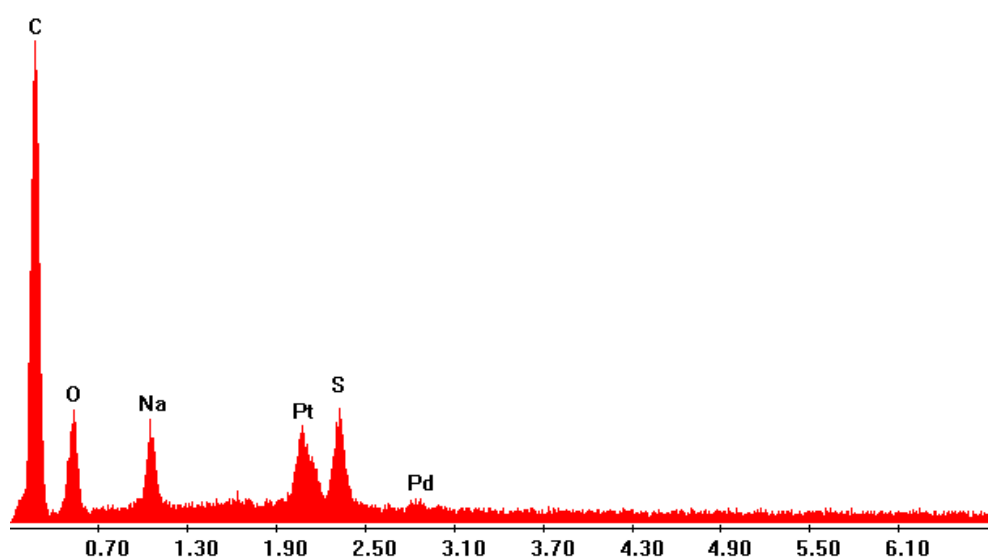


Figure 4.178 EDX spectrum from particles figure 4.177 - sample 69

These results suggest that the NaBH_4 particles have not formed the oxide as the counts from oxygen are very similar to those obtained from the polymer substrate.

PSF in THF – NaBH_4 Dispersion in 100% Acetonitrile - Sample 73

A new batch of the PSF- NaBH_4 polymer dispersion was produced, following a similar procedure to that outlined in method 19. The difference involved leaving the 2g of PSF in 10ml of THF overnight, rather than heating and stirring. This change generated a colourless, clear polymer solution. The NaBH_4 was added under nitrogen to the clear polymer solution, forming a slightly cloudy dispersion. It was believed that the cloudy appearance implies that the NaBH_4 had not dissolved but simply dispersed throughout the polymer solution.

Droplets of the dispersion were delivered to 25ml of 100% anhydrous acetonitrile following the procedure given in method 18. The Scuba-Seal was positioned onto the top neck and the droplets were introduced using a Microlance 3 20G (0.9mmx40mm) needle connected to a 1ml syringe. The non-solvent was agitated using the speed setting number 10.

It was observed that the created microcapsules appeared to stick together after forming a sphere in the acetonitrile.

The analysis from this sample again produced mixed results. The SEM micrograph, figure 4.179, was obtained with a system magnification of 10,000x and BSED detection.

The micrograph displays a cluster of irregular particles present within a pore of the PSF polymer.

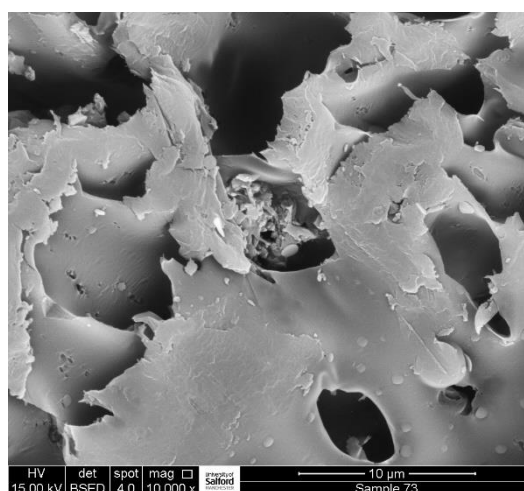


Figure 4.179 SEM micrograph of particles from internal structure - sample 73

The analysis from the particles within the pore is promising, generating the EDX spectrum shown in figure 4.180. The spectrum shows the presence of sodium together with background elements associated with the polymer substrate.

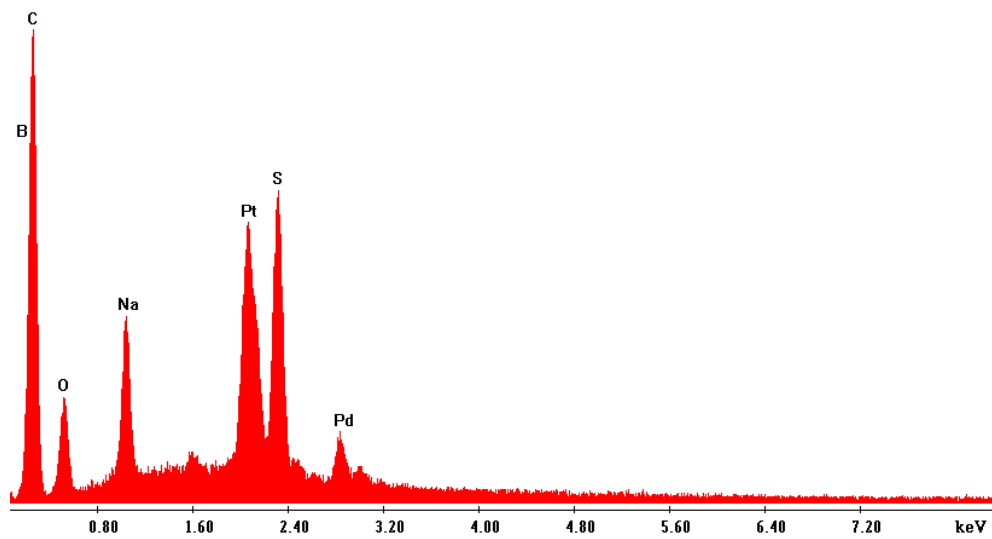


Figure 4.180 EDX spectrum from particles figure 4.179 - sample 73

The oxygen levels from the particle are seen to be consistent with the background polymer. The SEM micrograph given in figure 4.181 represents a different region from within the cross-sectional area. The micrograph displays an area showing particles that have the appearance of a separate phase, rather than irregular-shaped particles.

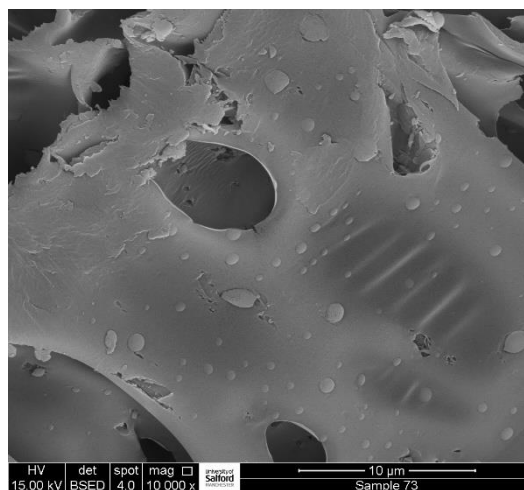


Figure 4.181 SEM micrograph of particles/phase from internal structure - sample 73

The resulting EDX spectrum, figure 4.182, was obtained from a typical particle and revealed the presence of sodium together with carbon, oxygen and sulfur associated with the

background polymer. The oxygen levels, however, are significantly higher than the concentration associated with the polymer.

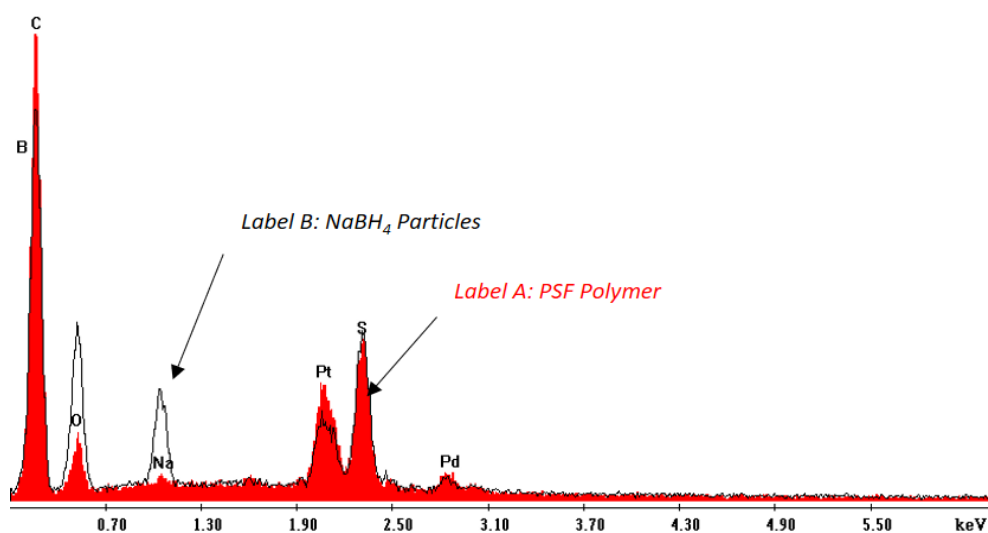


Figure 4.182 EDX spectrum from particles figure 4.181 - sample 73

These results would suggest that the NaBH₄ particles have started to hydrolyse.

PSF in THF – NaBH₄ Dispersion in 100% Acetonitrile - Sample 75

This sample represents a re-run of sample 73, which generated microcapsules that were seen to stick together after formation. One possible reason for the sticking of microcapsules is that the PSF-NaBH₄ dispersion was introduced into the non-solvent acetonitrile from the top reaction flask neck. This experiment utilises the same dispersion except that this time the droplet addition was from the side neck and the agitation speed was reduced to 8. The syringe needle was a Microlance 3 20G (0.9mmx40mm) connected to a 1ml syringe.

The results were very interesting as the microcapsules did not stick together after formation. It is difficult to fully understand if the issues associated with sample 73 were directly related to either the agitation speed or the method used for introducing the droplets or a combination of the two.

Figure 4.183 represents SEM micrographs obtained from the internal microcapsule structure after it had been cross-sectioned using a razor blade. The micrographs show particles to exist both within the area obtained using a 10,000x system magnification and within the area captured at 20,000x magnification.

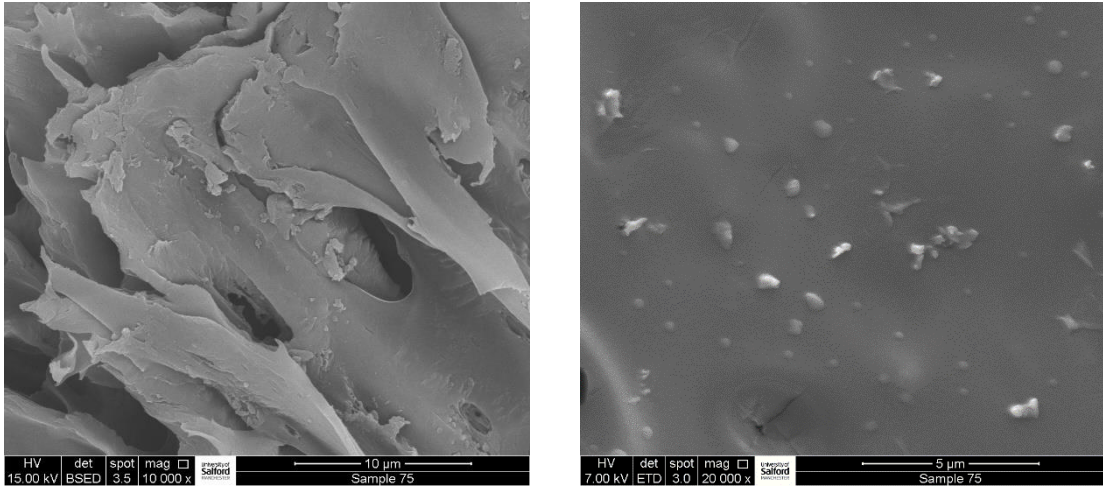


Figure 4.183 SEM micrograph of particles from internal structure - sample 75

EDX analysis was performed on both areas and the results were seen to be consistent. EDX spectrum figure 4.184 signifies the results from a spot probe of the small particles shown in the SEM micrograph, obtained using a system magnification of 20,000x. These particles are small, existing around 1µm in size, thus analysis would always pick up the corresponding elements associated with the background polymer. The spectrum obtained using 15kV displays high levels of carbon with lower levels of oxygen, sodium and sulfur.

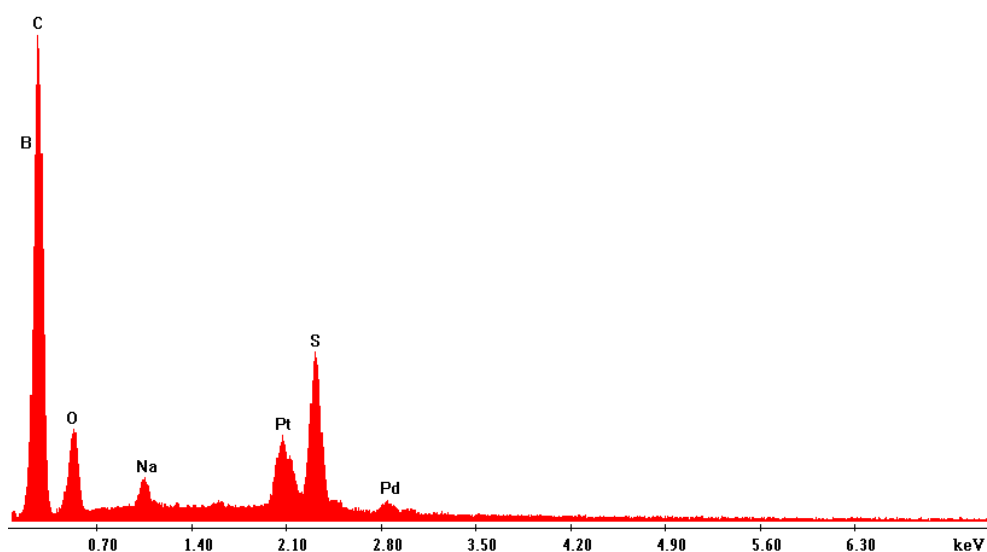


Figure 4.184 EDX spectrum from particles figure 4.183 - sample 75

The EDX spectrum figure 4.185 represents analysis of the polymer substrate very close to the particles examined. This is not a quantitative assessment, but the general comparison of peak heights of oxygen against sulfur are seen to be similar for both particles examined and the PSF polymer substrate. These results suggest that the small NaBH_4 particles are stable within the microcapsule.

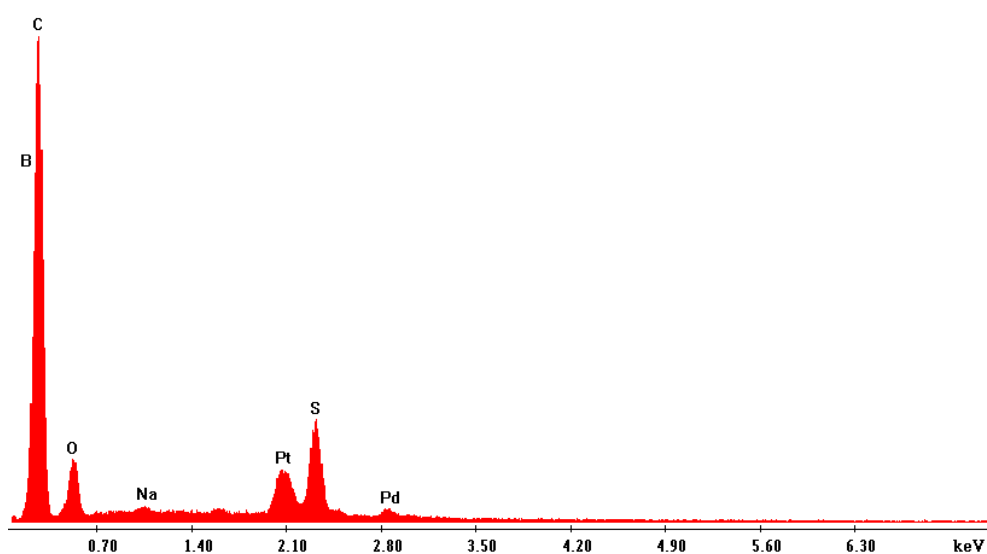


Figure 4.185 EDX spectrum from polymer substrate near particles - sample 75

The solvent THF used for this project was purchased from Fisher Scientific and was thought to be pure. However, the solvent was examined using the Bruker 400 MHz NMR based at the University of Salford. The NMR spectrum figure 4.186 shows the resulting ^1H NMR of THF in $\text{CDCl}_3 + \text{TMS}$ (Byjus, 2021).

The spectrum has many chemical shifts that were interpreted by Kirit Amin - an expert in NMR spectroscopy at the University of Salford. The chemical shifts indicate that the THF contained water and small amounts of aldehyde, and aliphatic ether or ester as demonstrated in table 4.1.

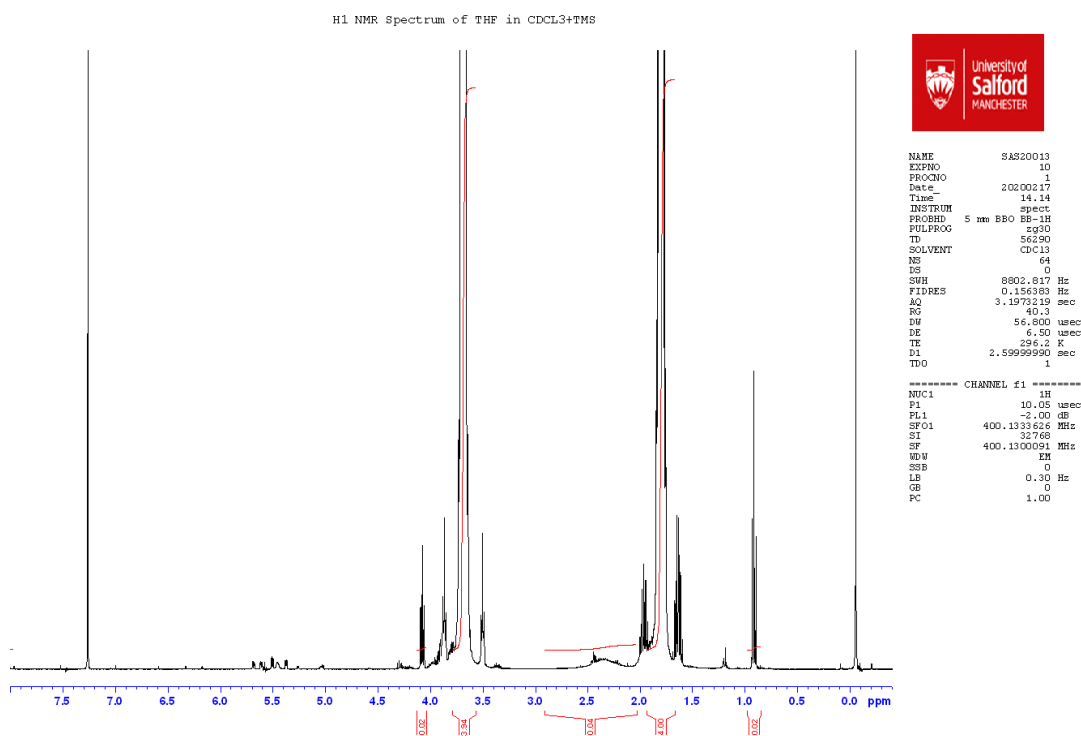
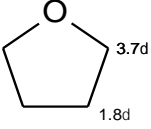
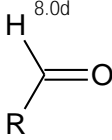
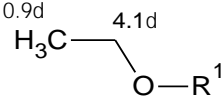
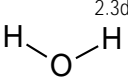


Figure 4.186 NMR spectrum obtained from THF solvent ex Fisher

Interpretation of these chemical shifts is explained in detail in table 4.1.

Table 4.1 NMR results from THF analysis

Structure - Proton Shift (δ)ppm	Assignment
	THF
	Unknown Aldehyde
	Unknown Ether or Ester
	Water

The water was a major concern as this would react with the NaBH_4 , triggering a reaction to form the oxide. Perhaps this explains why some microcapsules show NaBH_4 particles that have undergone a reaction forming the oxide and other particles have remained stable.

A new supply of THF (Anhydrous 99.9%) was purchased from Sigma-Aldrich.

PSF in Anhydrous THF – NaBH_4 Dispersion in 100% Anhydrous Acetonitrile - Sample 76

This experiment is based on the same conditions used for the previous sample 75, except that the THF purchased from Fisher Scientific¹ was substituted by THF (anhydrous 99.9%) ex Sigma-Aldrich.

The PSF polymer and THF solvent were left overnight for the polymer to fully dissolve. The following morning, the polymer solution looked slightly opaque but appeared to be a solution - as seen from many previous samples. To change the polymer solution to clear would have probably required further addition of THF. However, the concentration of

polymer solution must remain high for the microcapsules to form as demonstrated from previous studies earlier in this thesis.

Using the glovebox, a micro-spatula ~0.1g of ground NaBH_4 was added to the polymer solution and the dispersion was agitated as outlined in method 19.

Using a BD Precision Glide Needle G21 (0.8mmx50mm) connected to a 1ml syringe, droplets of the polymer dispersion were slowly introduced into anhydrous acetonitrile following the procedure as defined in method 18.

Analysis involved initially fixing a generated polymer microcapsule onto a rivet using rapid-setting Araldite, followed by cross-sectioning under vacuum within the preparation chamber connected to the Philips XL30 SFEG.

The SEM micrograph, figure 4.186, shows that the internal structure of the microcapsule is honeycomb, displaying some areas of increased porosity. Little evidence could be found to suggest the presence of NaBH_4 particles existing within the cross-sectioned particle.

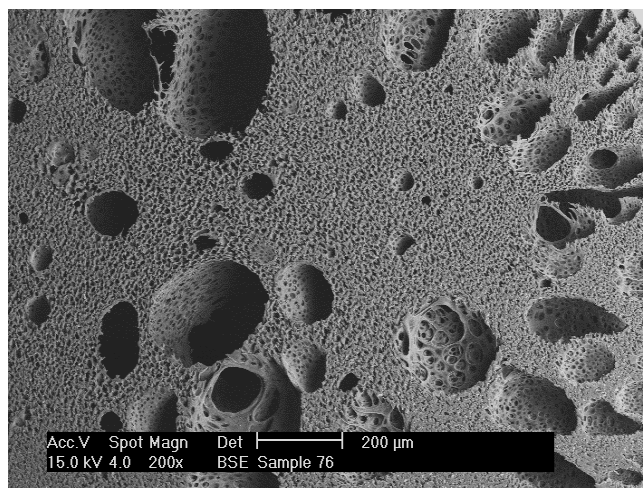


Figure 4.187 SEM micrograph of particles from internal structure - sample 76

The preparation procedure involving gluing a microcapsule onto a rivet is relatively time consuming. Further analysis of extra microcapsules from the same batch of sample 76 were examined using the Quanta 250 after the microcapsules had been quickly cut open in

the open lab. The SEM micrographs, figure 4.188, show that the generated microcapsule has a good internal structure, but only limited regions of encapsulated particles were located.

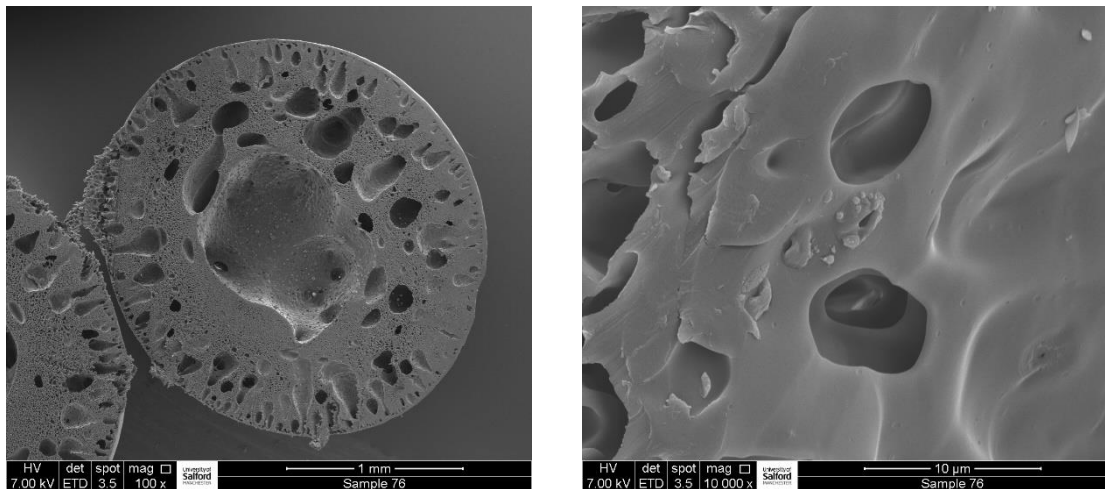


Figure 4.188 SEM micrograph of particles from internal structure - sample 76

The particles displayed in the high magnified SEM micrograph were examined using EDX analysis with an accelerating voltage of 7kV. The resultant spectrum, figure 4.189, suggests that the NaBH_4 particles have started to hydrolyse - based on the observed increased levels of oxygen.

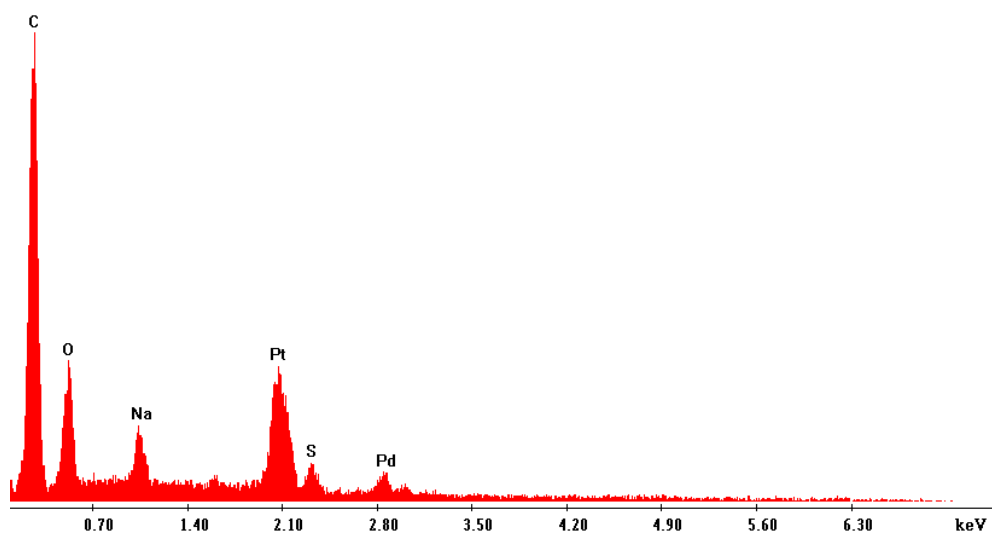


Figure 4.189 EDX spectrum from particles figure 4.188 - sample 76

EDX spectrum figure 4.190 obtained from the polymer near the particles displays reduced levels of oxygen.

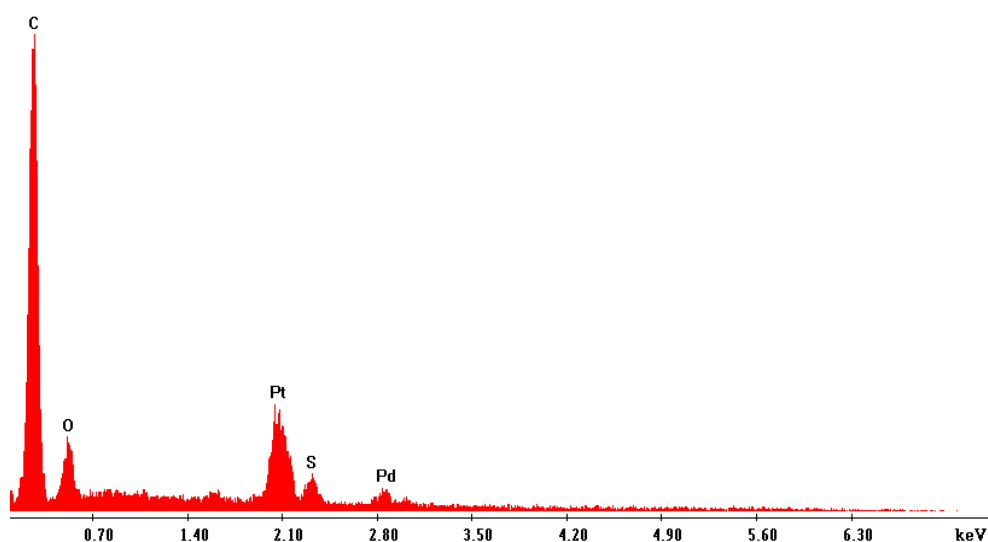


Figure 4.190 EDX spectrum from polymer substrate near particles - sample 76

PSF in Anhydrous THF – NaBH₄ Dispersion in 100% Anhydrous Acetonitrile - Sample 77

A new batch of the PSF-NaBH₄ dispersion was produced following the same experimental procedure as used for sample 76. The PSF-NaBH₄ dispersion was introduced to the dry acetonitrile using a BD Precision Glide Needle G21 (0.8mmx50mm) connected to a 1ml syringe.

To evaluate the reduced levels of encapsulated NaBH₄ particles observed from the previous sample 76, the surface of this sample was examined using the Quanta 250 SEM.

The SEM micrographs, figure 4.191, represent low and high magnified regions of the surface of the generated microcapsules.

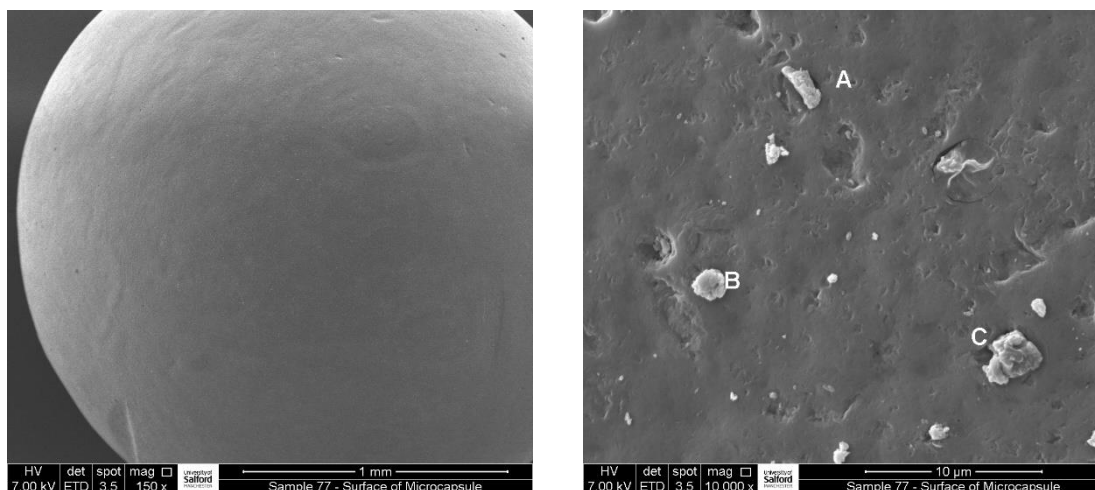


Figure 4.191 SEM micrograph of particles from the outer surface - sample 77

The low magnified micrograph obtained with a system magnification of 150x shows that the shape and morphology of the microcapsule is very good. The higher magnified micrograph obtained with a system magnification of 10,000x demonstrates that the microcapsule has a non-porous outer surface, but particles can be seen - thought to be NaBH_4 .

The particles on the surface of the microcapsule exist in different shapes and sizes. Three separate particles on the micrograph were annotated A, B and C. Each particle was then individually examined using EDX analysis.

The EDX spectra overlay, figure 4.192, represents each individual spectrum obtained from the 3 annotated particles. Each particle produced the same EDX spectrum, showing the presence of carbon, oxygen, sodium, aluminium, silicon and sulfur together with possible traces of magnesium and potassium. Carbon, sulfur, and oxygen are thought to be from the polymer substrate. However, the oxygen levels are significantly higher. These particles are not from surface NaBH_4 but are thought to represent small fragments from the aluminosilicate molecular sieve drying agent from either THF or acetonitrile.

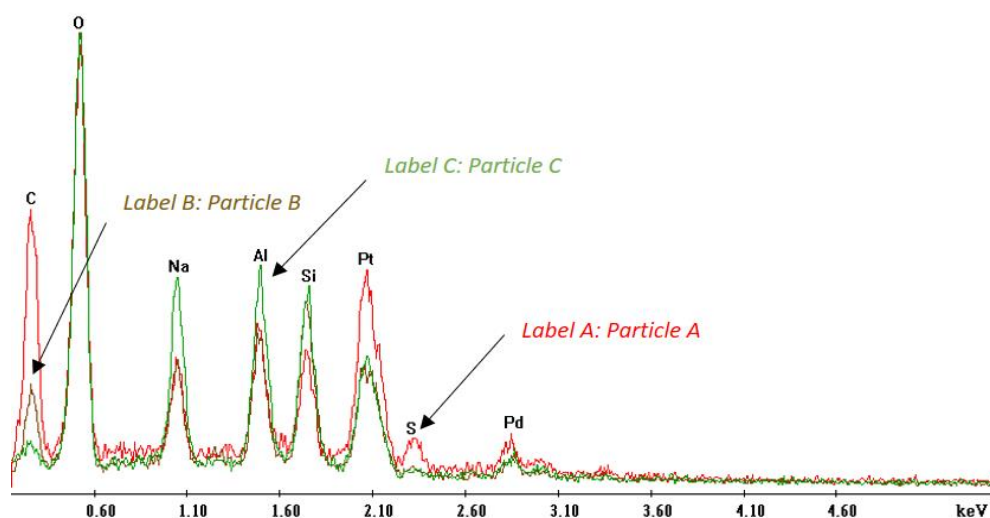


Figure 4.192 EDX spectra overlay from surface particles - sample 77

The 99.9% extra dry acetonitrile was dried over a molecular sieve. For interest, a small particle was extracted from the solvent and allowed to dry overnight.

The SEM micrographs, figure 4.193, represent both a low magnified micrograph obtained using a system magnification of 100x together with a higher magnified micrograph obtained with a system magnification of 2,500x. The area seen at high magnification is relatively porous, making it possible for fragments to have been dislodged using the high shear agitation procedure.

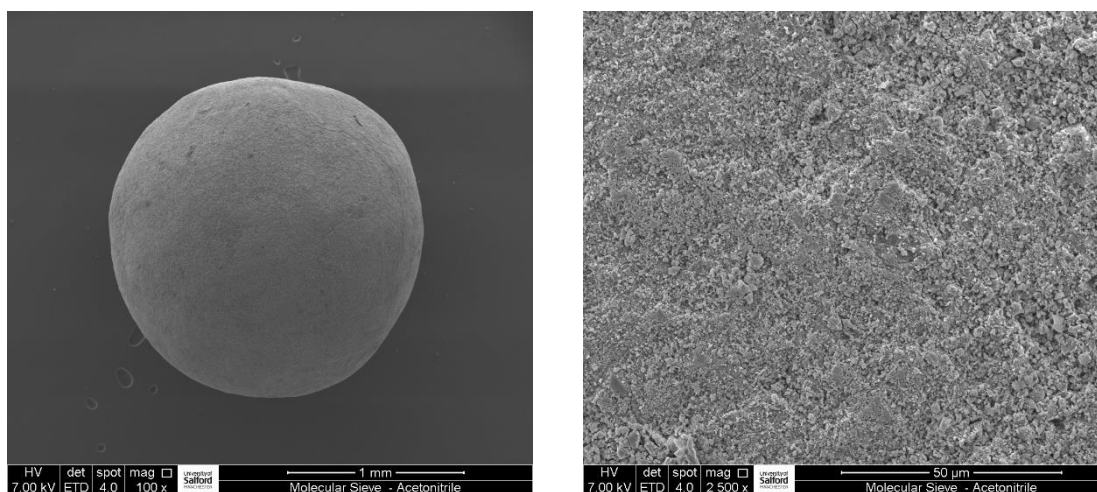


Figure 4.193 SEM micrograph of molecular sieve particle - ex acetonitrile

EDX analysis from the particle produced the corresponding spectrum, figure 4.194, which shows high levels of oxygen with lower levels of sodium, aluminium, silicon, sodium, magnesium, and potassium. These elements are comparable with those elements associated with the small particles present on the surface of sample 77.

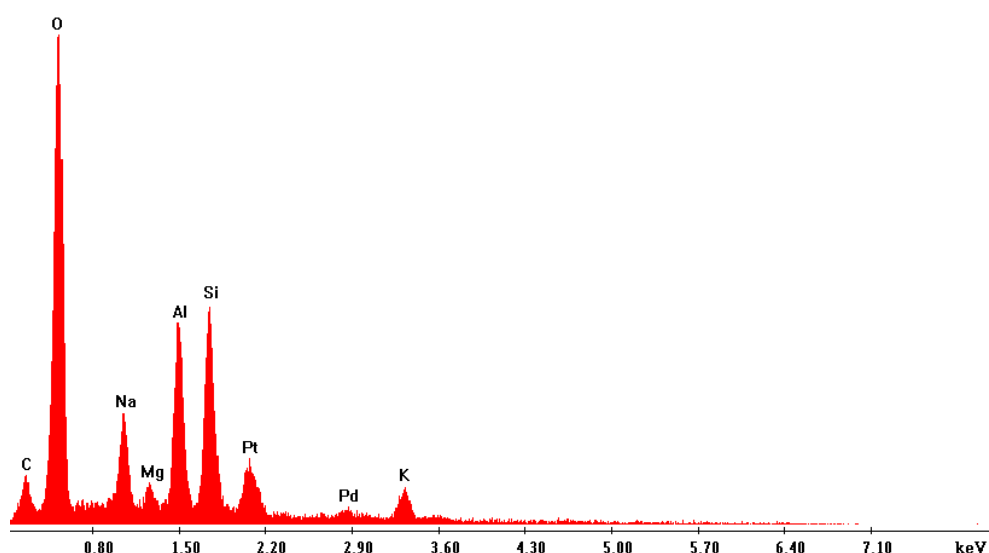


Figure 4.194 EDX spectrum from molecular sieve particle - ex acetonitrile

PSF in Anhydrous THF – NaBH₄ Dispersion in 100% Anhydrous Acetonitrile - Sample 78

This sample was prepared on the same day as sample 77, following identical conditions except for the use of 2 micro-spatulas of NaBH₄ rather than 1 as used for sample 77.

Several of the generated microcapsules were fixed onto rivets using rapid-setting Araldite. After obtaining a suitable cross-section within the preparation chamber, the internal structure was examined using the Philips XL30 SFEG.

The SEM micrograph, figure 4.195, shows the presence of small irregular-shaped particles within the internal structure of the cross-sectioned microcapsule.

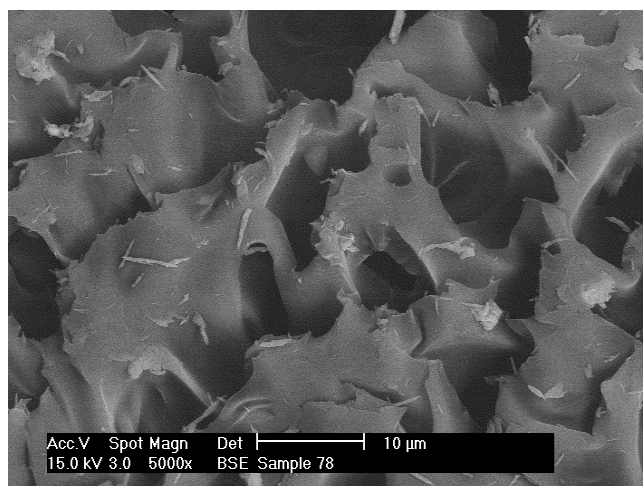


Figure 4.195 SEM micrograph of particles from internal structure - sample 78

When examined using EDX analysis, utilising a microscope beam accelerating voltage of 15kV, a particle produced the corresponding spectrum as shown in figure 4.196.

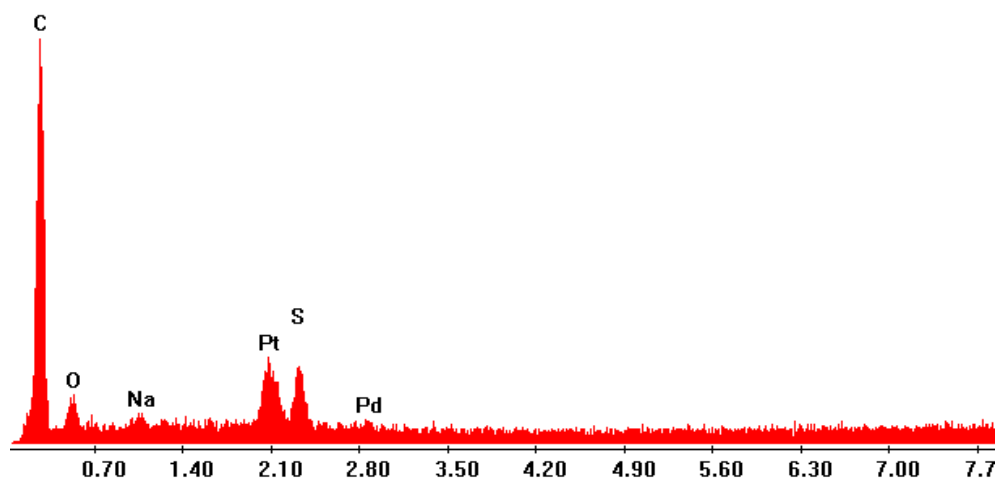


Figure 4.196 EDX spectrum from particles figure 4.195 - sample 78

The EDX spectrum, figure 4.197, represents the polymer substrate close to the particle initially examined in figure 4.196. Examination of the oxygen levels against the sulfur would suggest that the NaBH_4 has remained unchanged.

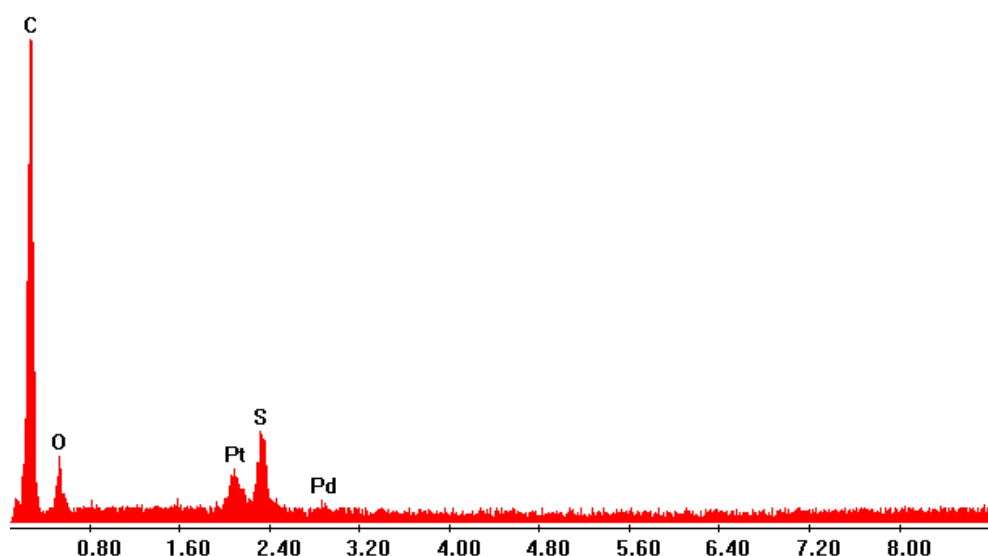


Figure 4.197 EDX spectrum from polymer substrate near particles - sample 78

PSF in Anhydrous THF – NaBH₄ Dispersion in 100% Anhydrous Acetonitrile - Sample 79

The results so far are promising, but the generated microcapsules are not displaying a high loading of NaBH₄ within the cross-sectioned microcapsules. This could indicate that perhaps the NaBH₄ particles are not dispersing well within the PSF/THF solution. In an effort to improve the dispersion, a small drop of Tween 80 - non-ionic surfactant polyoxyethylene (20) sorbitan monooleate (Croda, 2021) - was added to the PSF-NaBH₄ dispersion. To prevent any foaming, a single drop of the anti-foaming agent Simethicone, a mixture of polydimethylsiloxane (PDMS) and silica gel (Brečević et al., 1994), was also added to the dispersion.

Following the procedure given in method 18, the dispersion was slowly added to 25ml of dry acetonitrile using a precision glide 21G (0.8mmx50mm) needle connected to a 1ml syringe. The microcapsules produced were dried overnight under nitrogen.

When the microcapsules were cut open using a razor blade, it was observed that the inner area of the microcapsule was wet, as a liquid phase was released.

It was decided that rather than continue with this sample, it would be better to prepare a new batch of microcapsules as something had clearly occurred during the drying procedure.

PSF in Dry THF – NaBH₄ Dispersion in 92% Dry Acetonitrile 8% Dry Chloroform - Sample 80

This sample represents a scale-up of the NaBH₄ together with utilising 8% of dry chloroform to widen the internal pores of the microcapsules.

These microcapsules were produced following the procedure outlined in method 19. Some changes to the procedure included adding an extra micro-spatula of NaBH₄ to the polymer dispersion used to generate sample 79, together with substituting the Fisher Scientific THF for anhydrous 99.9% THF.

Following experimental procedure 18, the polymer dispersion was slowly dripped into a blend of 23ml anhydrous acetonitrile ex Acros Organics and 2ml 99.9% extra dry chloroform ex Acros Organics using a Precision Glide 21G (0.8mmx50mm) needle connected to a 1ml syringe.

The SEM micrographs shown in figure 4.198 represent high magnified areas of the internal structure of a microcapsule obtained using a system magnification of 20,000x. The left-hand micrograph displayed was obtained using secondary electron detection. The right-hand micrograph displayed was obtained using back scattered electron detection, demonstrating contrast variation between the polymer and the NaBH₄ particles. The micrograph shows that the soft polymer had smeared during the cut, resulting in particles being pushed towards the edge of the microcapsule.

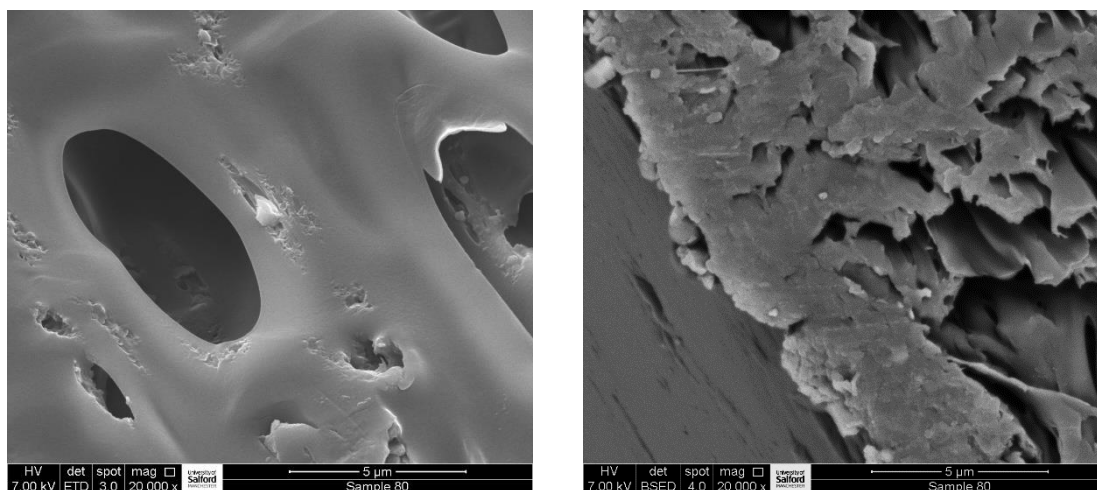


Figure 4.198 SEM micrograph of particles from internal structure - sample 80

The particles from both SEM micrographs were examined using EDX analysis utilising an electron beam acceleration voltage of 7kV. The results are positive - indicating that the NaBH_4 had not changed.

The EDX results from the small particle present on the left hand-side micrograph shows the presence of sodium together with elements associated with the polymer substrate. The spectrum overlay, figure 4.199, represents the particle against polymer substrate. This is not quantitative but indicates that the oxygen levels are similar - suggesting that the NaBH_4 particle had not hydrolyzed.

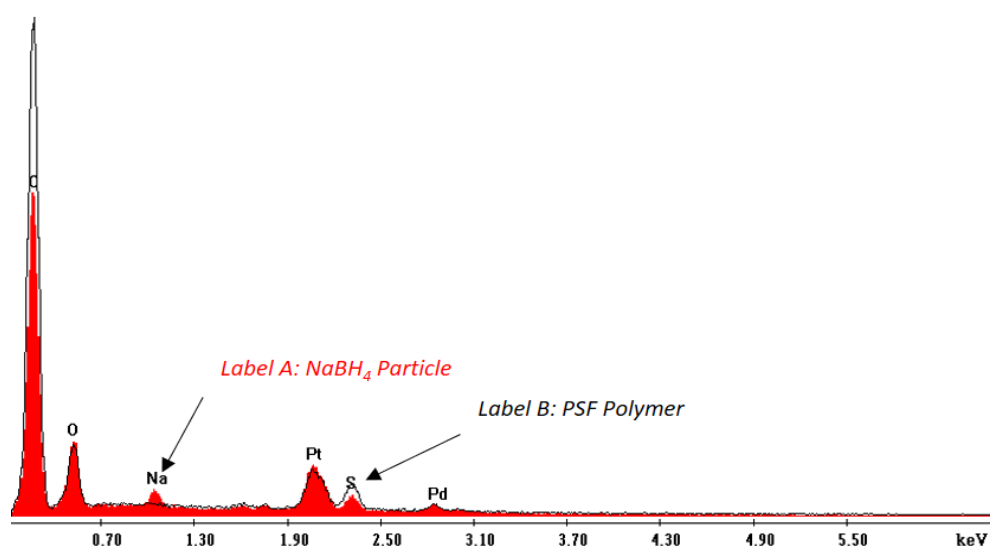


Figure 4.199 EDX spectrum from particle figure 4.198 - sample 80

The EDX spectrum, figure 4.200, symbolises the results from a spot probe of the larger particle present towards the lower region of the right-hand-side micrograph in figure 4.198. The spectrum shows that the particle contains high levels of sodium with carbon, oxygen and sulfur present at the same levels as the background polymer. Trace levels of silicon, aluminium and chlorine were also detected, thought to be impurities.

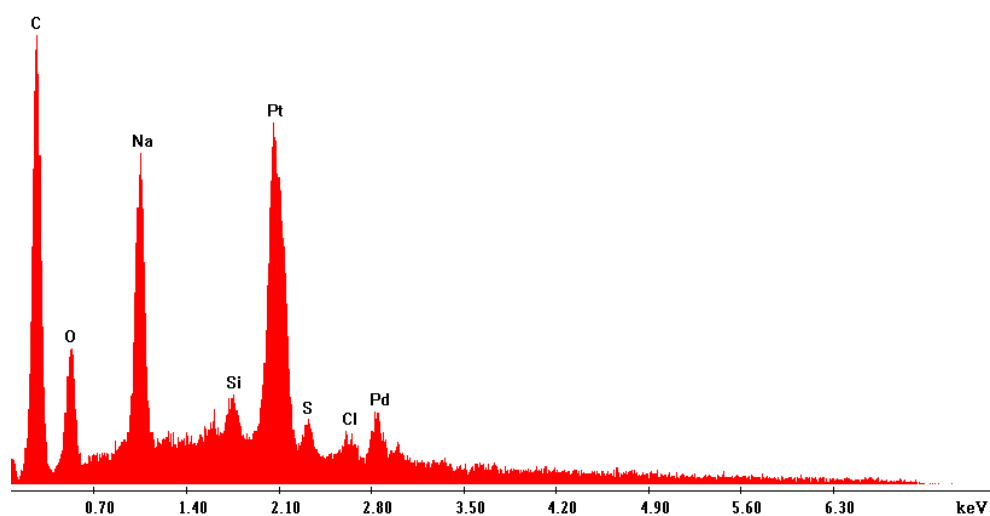


Figure 4.200 EDX spectrum from particle figure 4.194 - sample 80

These results demonstrate that NaBH₄ particles have been encapsulated within the generated PSF microcapsules with minimum change to the structure. However, the loading of NaBH₄ particles is still not enough to allow other techniques (such as X-Ray Diffraction) to characterise the metal hydride particles (Bunaciu et al., 2015).

X-Ray Diffraction would be an excellent technique to confirm the composition of the encapsulated NaBH₄ particles. This technique would also be suitable to try to monitor the stability of the NaBH₄ within the polymer microcapsule. A time study would be of interest to monitor the transformation of the hydride eventually forming the oxide after exposure to moisture.

For X-ray Diffraction to generate dependable data, the concentration of encapsulated NaBH₄ particles must be increased.

PSF in Dry THF – NaBH₄ Dispersion in 92% Dry Acetonitrile 8% Dry Chloroform - Sample 81

In a further attempt to increase the loading of encapsulated NaBH₄ within the microcapsules, an additional quantity (2x micro-spatulas) of NaBH₄ was added to the same dispersion used for sample 80. The NaBH₄ was freshly ground using a pestle and mortar within the nitrogen glove box.

The SEM micrographs shown in figure 4.201 display that a good porous internal structure has been achieved, with evidence of particles existing within the internal structure.

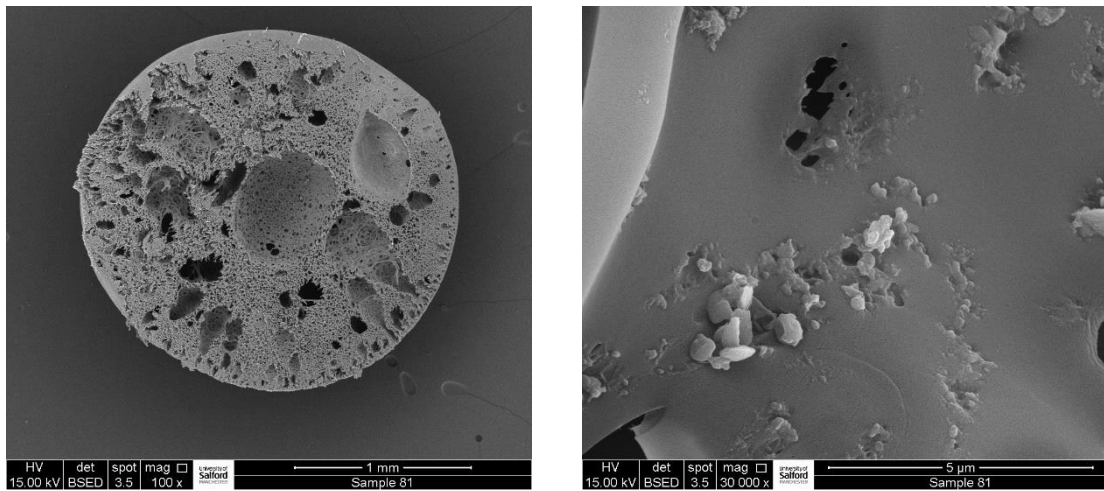


Figure 4.201 SEM micrograph of particles from internal structure - sample 81

When examined using EDX analysis at 15kV, the particles produced spectrum figure 4.202. When compared directly against the spectrum from the surrounding polymer (figure 4.203), there is validation that little change has occurred to the NaBH_4 particles.

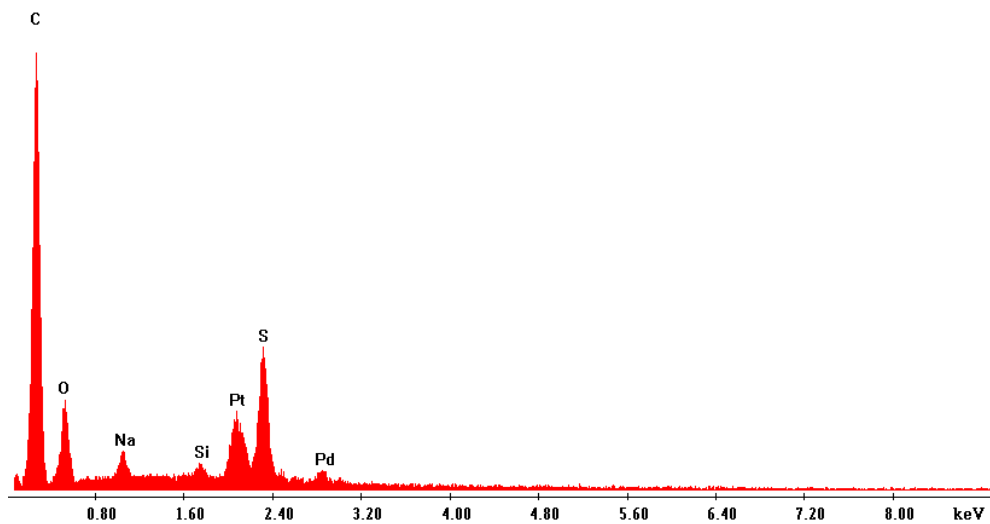


Figure 4.202 EDX spectrum from particle figure 4.197 - sample 81

The spectrum also shows low levels of silicon. This could be from a drying agent, as very small particles are seen to be present as clusters; alternatively, it could be associated with the Simethicone.

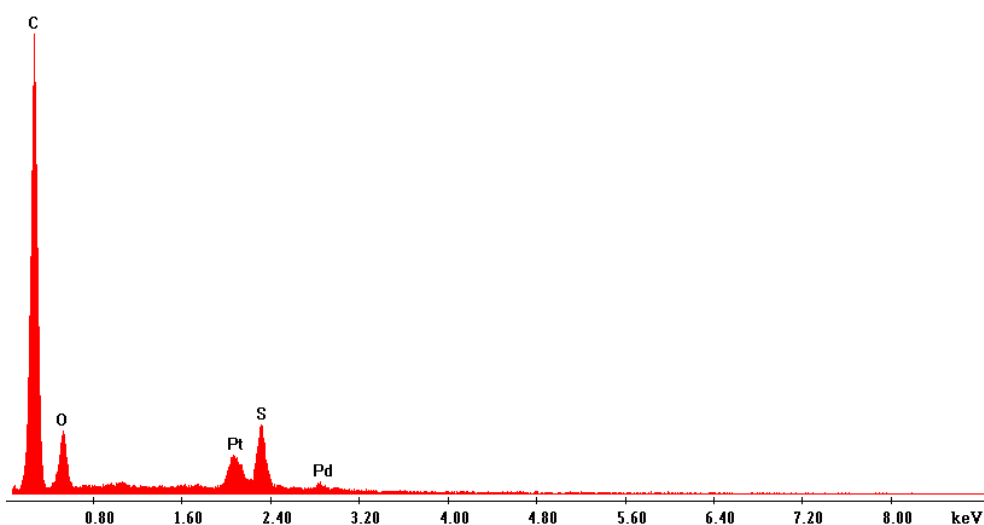


Figure 4.203 EDX spectrum from polymer substrate near particles - sample 81

PSF in Dry THF – NaBH₄ Dispersion in 92% Acetonitrile 8% Dry Chloroform - Sample 82

Sample 82 was prepared with the aim of investigating the nature of the silicon as detected in the previous sample. It used the same dispersion generated for sample 81, but the droplets of the PSF-NaBH₄ dispersion were introduced into a non-solvent blend of acetonitrile that hadn't been dried over a molecular sieve. The acetonitrile was the same as used in many previous experiments - 99.8% for HPLC purchased from Acros Organics.

The procedure was identical except for the substitution of acetonitrile.

The SEM micrographs given in figure 4.204 represent different regions of the internal structure of a generated microcapsule. The micrograph obtained with a system magnification of 25,000x shows the presence of many large irregular-shaped particles.

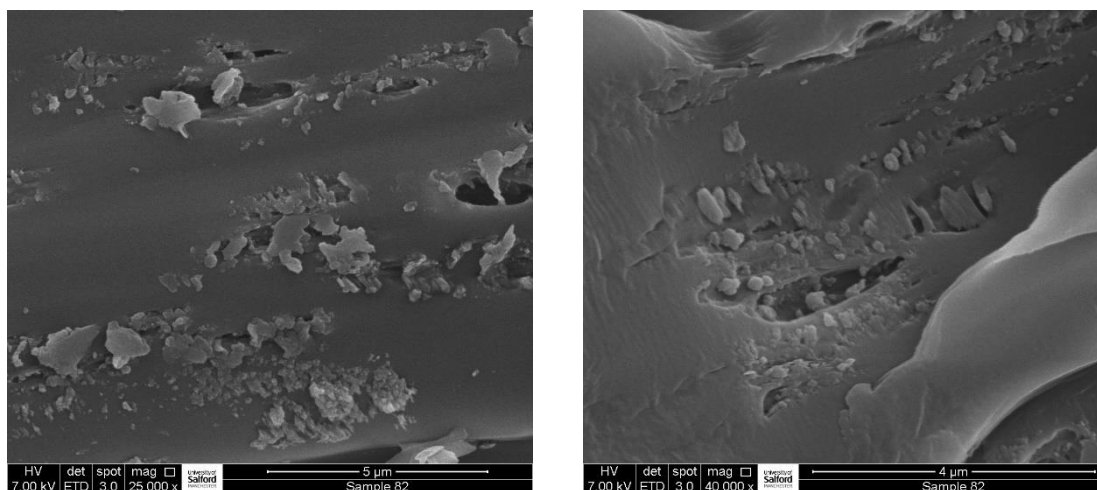


Figure 4.204 SEM micrograph of particles from internal structure - sample 82

When examined using EDX analysis, the larger particles all produced similar spectra - showing the presence of sodium with elements associated with the supporting PSF polymer represented in figure 4.205. No evidence is available to suggest that the NaBH_4 particles had hydrolyzed. The elements from the supporting PSF polymer are shown in figure 4.206. When comparing the levels of oxygen from the supporting polymer against those seen from the spectrum from the particles, it is thought to be similar.

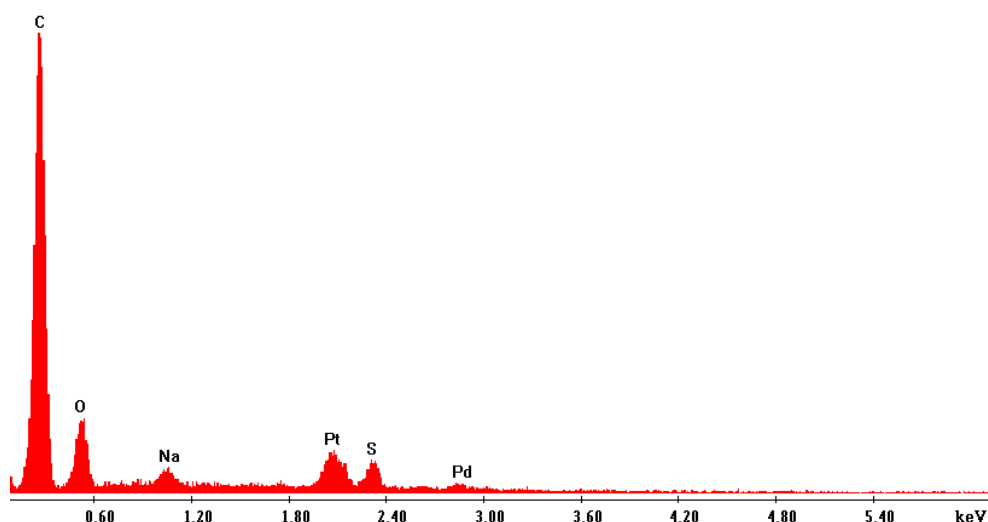


Figure 4.205 EDX spectrum from large particle figure 4.204 - sample 82

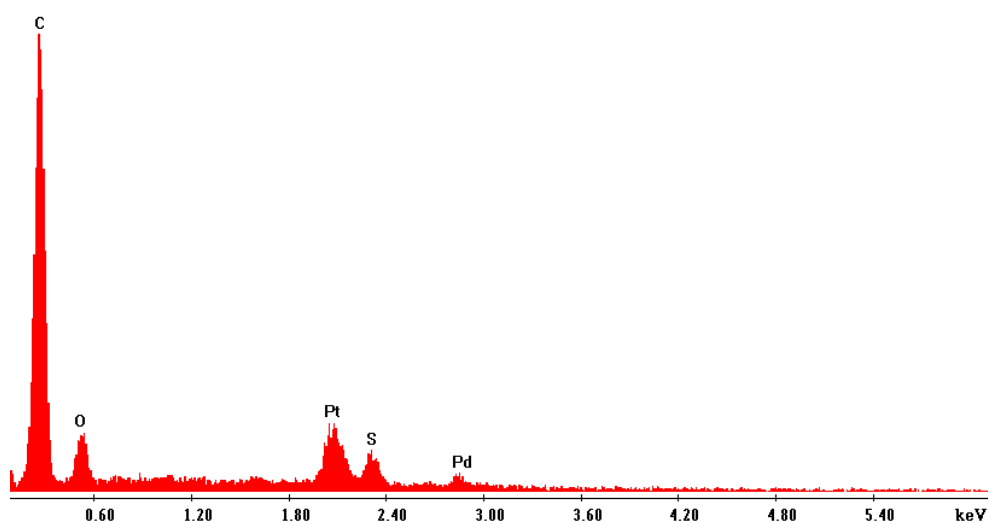


Figure 4.206 EDX spectrum from polymer substrate near the particles - sample 82

The smaller particles seen to exist towards the lower area of the same micrograph produced the EDX spectrum figure 4.207, showing high levels of carbon with lower levels of oxygen, sodium, silicon, and sulfur. These results prove that the silicon previously seen in sample 81 is not associated with the acetonitrile. These results would suggest that the silicon is either from a colloidal drying agent from the chloroform or the Simethicone as this contains silicon within the structure of the polydimethylsiloxane which is mixed with silica gel. Many commercial antifoaming formulations exist as a mixture of PDMS oil and hydrophobically treated silica particles (Bergeron et al., 1997). The small particles shown in figure 4.204 could signify the presence of colloidal silica particles - accounting for the raised oxygen levels.

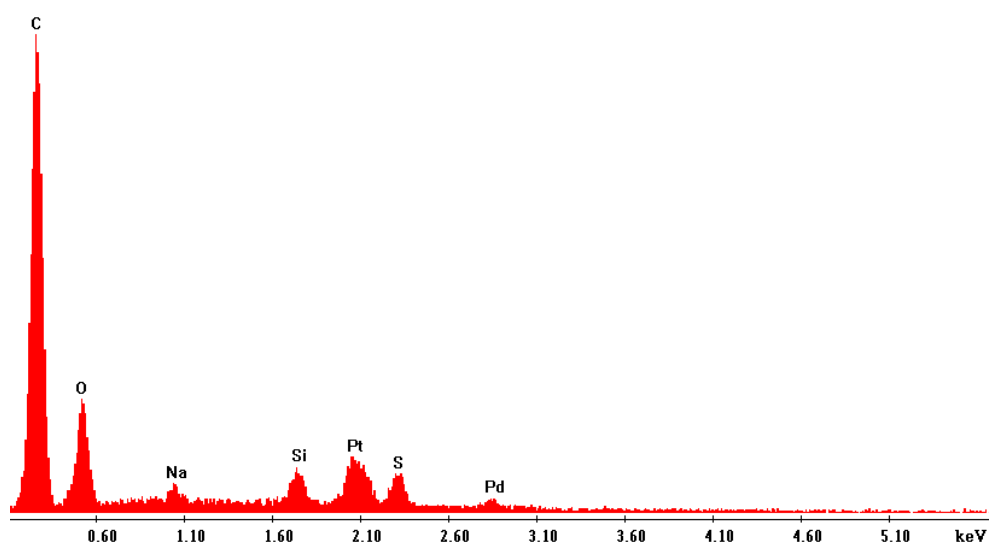


Figure 4.207 EDX spectrum from small particle figure 4.200 - sample 82

PSF in 100% Dry THF – NaBH₄ Dispersion in 100% Acetonitrile - Sample 83

This preparation was to evaluate if a new, fresh batch of concentrated PSF-NaBH₄ would show a reasonable quantity of NaBH₄ particles to exist within the cross-sectional area of a microcapsule. The Simethicone and Tween 80 did not improve the loading properties and caused issues with potential silicon-based impurities, so they were removed from this new dispersion. In addition, to try to understand whether the small silicon particles seen to exist within the polymer from previous samples was associated with the drying agent of the chloroform or Simethicone, the chloroform was removed from the non-solvent.

A new batch of PSF-NaBH₄ dispersion was produced, following the procedure outlined in method 19, using dry THF. Once the PSF polymer had fully dissolved, 3x micro-spatulas of NaBH₄ were added to the polymer, using a glove box, to produce a suitable dispersion.

The PSF-NaBH₄ dispersion was slowly released into 100% HPLC grade acetonitrile following the procedure given in method 18.

The created microcapsules were initially cross-sectioned, and the internal structure was examined thoroughly for the presence of NaBH_4 particles. Little evidence was available to show the presence of encapsulated NaBH_4 particles.

The surface SEM micrographs, figure 4.208, were obtained using system magnifications of 1000x and 4000x respectively. The micrographs clearly demonstrate that the surface has a coating of spherical-shaped particles existing below $10\mu\text{m}$ in size.

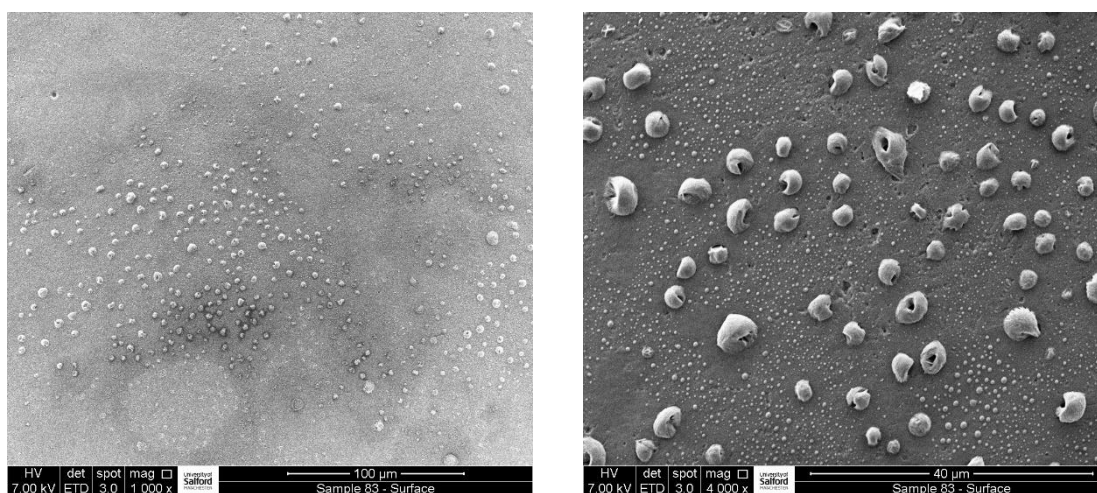


Figure 4.208 SEM micrographs of surface particles - sample 83

The surface particles do not share the same morphology associated with the ground crystalline NaBH_4 particles. Many of the spheres comprise of a hollow-centre arrangement.

When examined using EDX analysis, the larger particles produced the spectrum as shown in figure 4.209, indicating the presence of carbon, oxygen, sodium and sulfur. The sodium is seen to have a similar peak height to the oxygen. These results are interesting, as the different morphology of the particles would suggest that the NaBH_4 has started to hydrolyse.

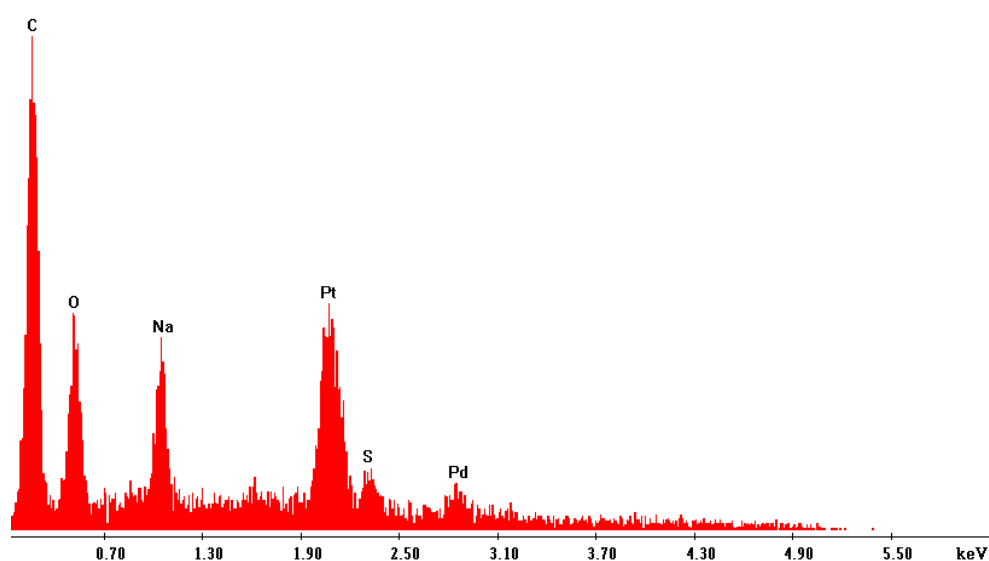


Figure 4.209 EDX spectrum from surface of large particles figure 4.208 - sample 83

The reason for the surface deposit of NaBH_4 on the outer surface of the microcapsules could be related to an issue with the reaction chamber or the conditions of analysis. The levels of metal hydride were high, as 3x micro-spatulas of NaBH_4 were used to generate the dispersion. This may have influenced the results.

PSF in 100% Dry THF – NaBH_4 Dispersion 87% Acetonitrile/17% Chloroform - Sample 84

To further understand the results observed from the previous sample 83, this experiment involved using the same PSF- NaBH_4 dispersion but utilising a different non-solvent. The non-solvent was changed from 100% acetonitrile to 25ml of dry acetonitrile and 5ml of dry chloroform. The same procedure as outlined for sample 83 was followed, and the resulting microcapsules were dried under nitrogen.

The created microcapsules were initially cross-sectioned using a razor blade in the open lab and introduced to the Quanta 250 SEM after sputter-coating with 4nm of platinum/palladium using the Cressington 208 unit.

The SEM micrographs displayed in figure 4.210 represent different system magnifications obtained at 15,000x and 50,000x respectively. They display clusters of irregular-shaped particles that would be consistent with the morphology expected from ground NaBH_4 particles.

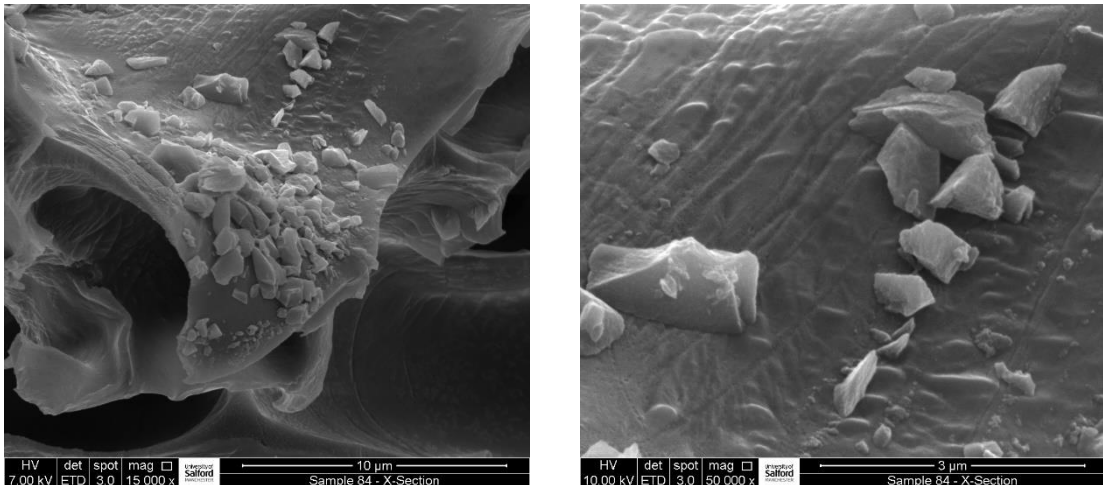


Figure 4.210 SEM micrograph of particles from internal structure - sample 84

The larger irregular-shaped particles were examined using EDX analysis. The results from the spectra overlay, figure 4.211, representing a spectrum obtained from a particle against background polymer, verify that the NaBH_4 particles have not changed.

The EDX spectra overlay, figure 4.211, is not quantitative, but when comparing peak heights, the oxygen levels from the particle are observed to be similar to the background polymer substrate.

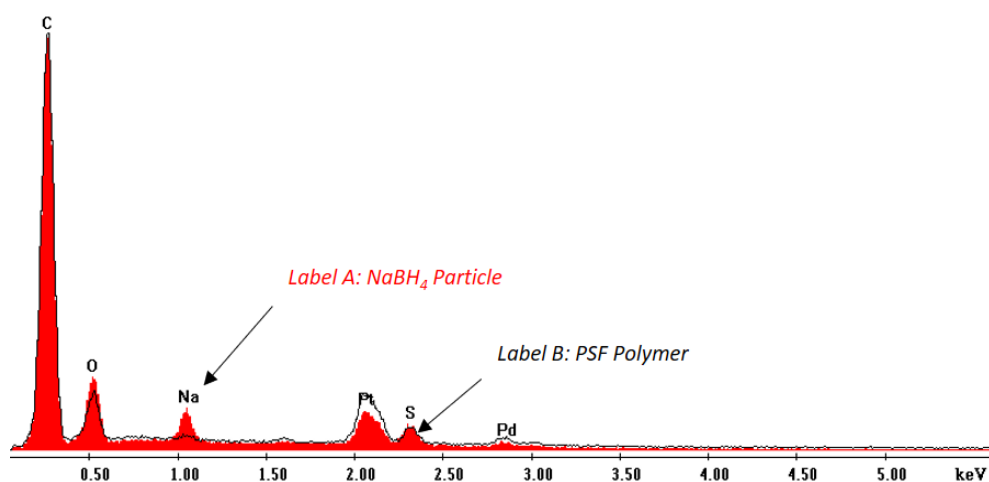


Figure 4.211 EDX spectrum overlay from internal particle/ PSF figure 4.210 - sample 84

Figure 4.212 represents a second area obtained from the same cross-sectioned microcapsule. The SEM micrograph was obtained with a system magnification of 40,000x and reveals irregular-shaped particles.

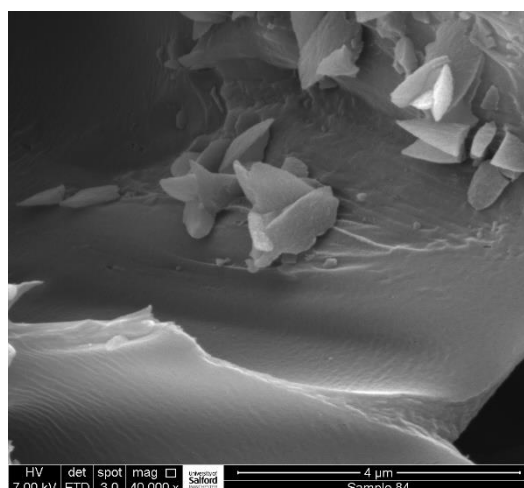


Figure 4.212 SEM micrograph of particles from internal structure - sample 84

When examined using EDX analysis, the particles gave a similar spectral overlay, figure 4.213, showing that the oxygen levels are comparable to the background polymer.

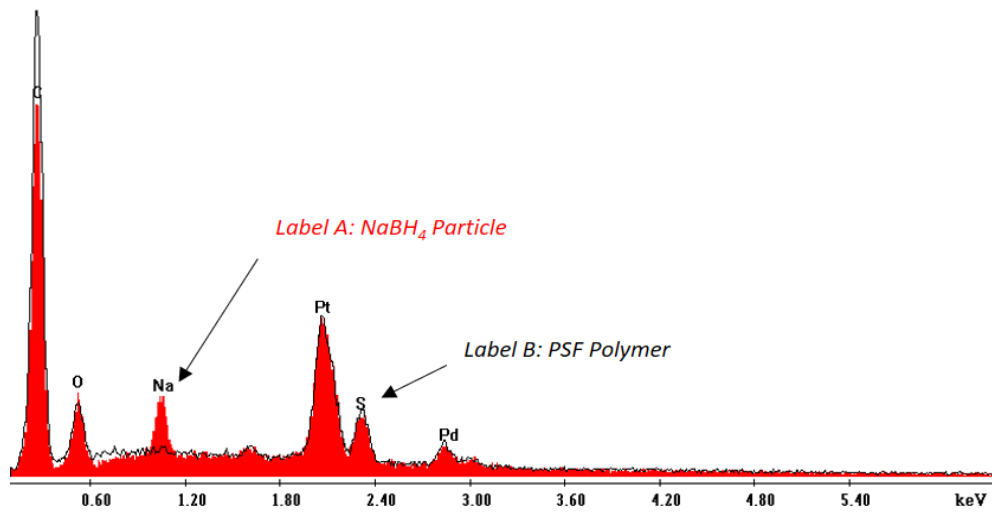


Figure 4.213 EDX spectrum overlay from internal particle/ PSF figure 4.212 - sample 84

Surface Analysis of Microcapsules

Close examination of the surface of the generated microcapsules using high resolution SEM demonstrates some evidence of surface particles. The SEM micrographs shown in figure 4.214 represent system magnifications of 1000x and 10,000x respectively.

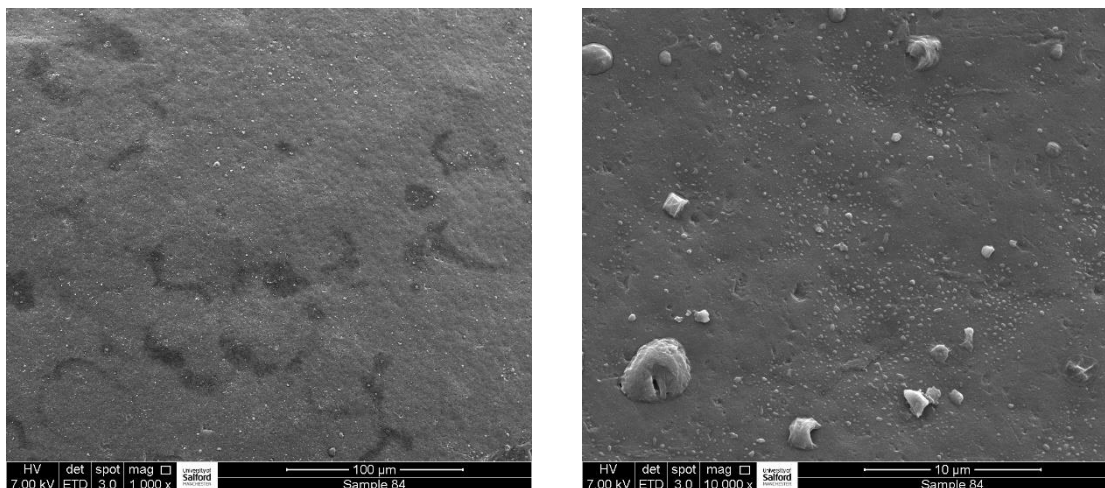


Figure 4.214 SEM micrographs of surface particles - sample 84

A fine distribution of particles is seen to exist in scattered regions on the surface of the microcapsule examined. The SEM micrograph obtained with a system magnification of 1000x shows that the degree of particles present at the surface are considerably lower than those observed from the previous sample 83. The higher magnified micrograph demonstrates that the surface particles exist as a mixture of different shapes and sizes. Some particles appear slightly irregular and crystalline, but others appear as spherical droplets significantly smaller than those observed in sample 83.

EDX analysis performed on a typical particle produced the spectrum figure 4.215, displaying high levels of sodium and oxygen with lower levels of carbon and sulfur. These results would indicate that the NaBH_4 particles have started to hydrolyse.

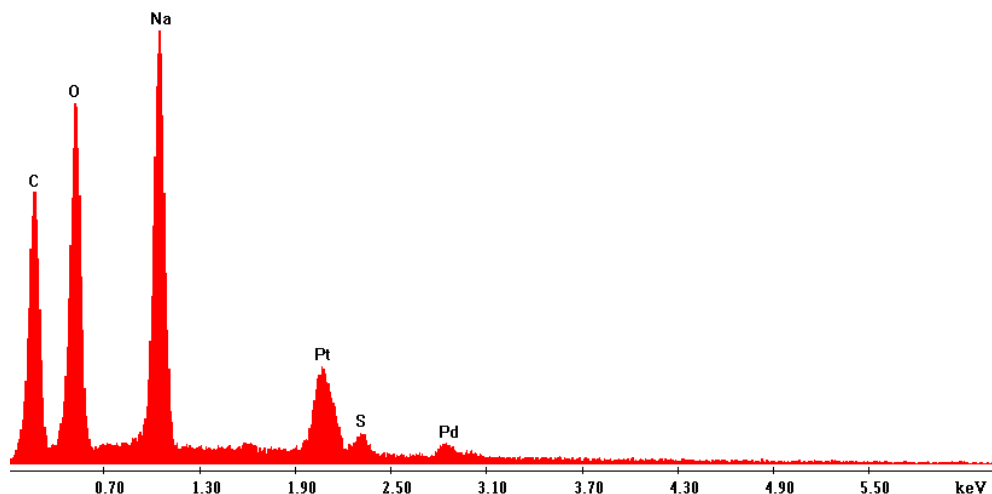


Figure 4.215 EDX spectrum from surface particles figure 4.214 - sample 84

These results would imply that the aim of encapsulating a high concentration of NaBH_4 particles within the PSF microcapsule caused some particles to be present at the outer surface. The presence of NaBH_4 on the outer edge of the microcapsules would have contributed to particles sticking together, as seen from previous experiments.

PSF 80% THF/20% DMF – NaBH₄ Dispersion 87% Acetonitrile/17% Chloroform - Sample 85

This sample represents a further attempt to improve the loading of NaBH₄ into the microcapsules. Some changes were made to the experimental conditions in an attempt to improve the dispersion properties of NaBH₄ within THF.

A new batch of PSF-NaBH₄ dispersion was created following the procedure outlined in method 19, however a small quantity of DMF was added to the initial solvent used to dissolve the PSF. The 100% THF was changed to 80% Dry THF and 20% DMF.

Once the polymer had completely dissolved, 3x micro-spatulas of NaBH₄ were added to the solution polymer under nitrogen within a glove box. The sample was then agitated to generate a suitable dispersion.

The microcapsules were generated following the same experimental conditions as for sample 84, using 5ml of dry chloroform and 25ml of dry acetonitrile as the non-solvent.

The microcapsules created were dried over the weekend under nitrogen. The dried microcapsules were stuck together, and a white deposit was present under the polymer microcapsules. This would suggest that the NaBH₄ particles had deposited on the outer edge of the microcapsules, causing them to stick together.

To investigate this presumption, the microcapsules were fixed onto a standard SEM stub using a carbon adhesive pad. After coating with platinum/palladium, the microcapsules were introduced to the Quanta 250 SEM. The surface structure of these created microcapsules was examined in detail. The SEM micrographs at figure 4.216 were obtained using system magnifications of 1000x and 10,000x respectively. They demonstrate that the outer surface of the microcapsule is coated in a residue.

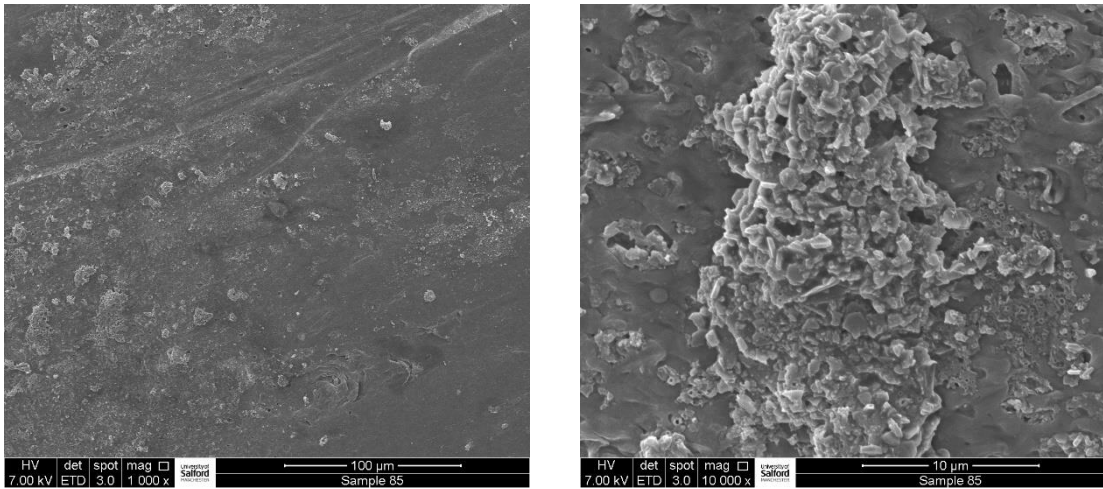


Figure 4.216 SEM micrographs of surface particles - sample 85

Figure 4.217 represents the corresponding EDX spectrum obtained from the surface residue. The spectrum shows high levels of oxygen with lower levels of sodium and traces of carbon, chlorine and sulfur.

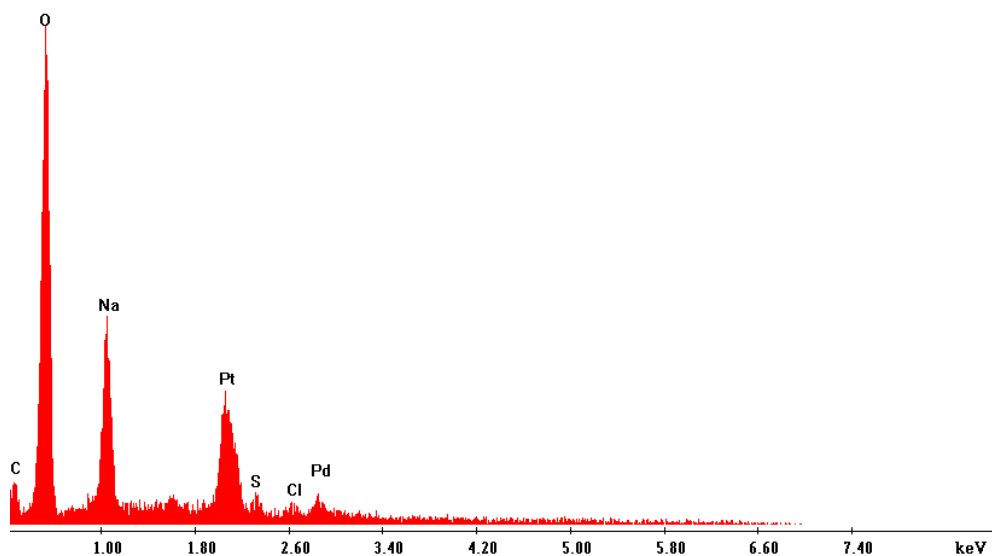


Figure 4.217 EDX spectrum from surface particles figure 4.213 - sample 85

These results would imply that the surface of the microcapsules created must have been coated in NaBH_4 particles. Over the weekend, during the drying process, the NaBH_4 particles have hydrolyzed.

One issue that may have caused the particles to not encapsulate fully into the polymer microcapsule is excess pressure from nitrogen within the 100ml round bottomed flask used to deliver the droplets of PSF-NaBH₄ dispersion. Delivery of nitrogen into the 100ml reaction flask was introduced later in the project as the 3-neck reaction flask replaced the 2-neck round-bottomed flask. Perhaps using a tight-fitting Scuba-Seal on one of the necks restricted excess pressure from escaping.

This is only an inference, as the bubble meter within the fume cupboard did indicate that nitrogen was flowing through the reaction flask and then escaping. The degree of nitrogen going through the experiment was always set at a reduced rate as the bubbles seen to pass through the oil were always slow. Using the two necks on the reaction flask is thought to form an equilibrium between the gas coming in and going out to the bubble monitor. Even though the bubble indicator showed that nitrogen was flowing through the reaction flask, using both necks of the flask may simply have been too much pressure for the NaBH₄ particles to be driven into the centre of the microcapsule upon impact with the non-solvent system. Another theory is that the NaBH₄ particles could have migrated to the outer surface of the capsule before the polymer hardened. Perhaps using 20% DMF caused problems as previous experiments demonstrated that particles were seen to exist on the surface, rather than existing within the microcapsules.

However, this research has demonstrated that some samples examined were proven to have encapsulated and stabilised NaBH₄ within the microcapsules. Perhaps these later results simply outline that it is difficult to achieve a high loading of the NaBH₄.

This assumption needs time in a further project that may follow on from this PhD.

4.6 An Investigation into the Stability of Sodium Borohydride (NaBH_4)

Sodium borohydride (NaBH_4) is known to react with moisture from the atmosphere, sometimes violently, forming oxides such as sodium metaborate (NaBO_2), (Lo et al., 2007). The research described below was aimed at demonstrating the conversion from the hydride to the oxide using SEM.

Figure 4.218 represents SEM micrographs obtained from the ground NaBH_4 particles using the Quanta 250 SEM. Preparation involved dusting the particles onto a cover glass that had been fixed onto an SEM stub using a carbon adhesive pad. Using the Cressington 208 sputter coating unit, the particles were coated with 4nm of platinum/palladium to avoid unnecessary charging issues when exposed to the electron beam.

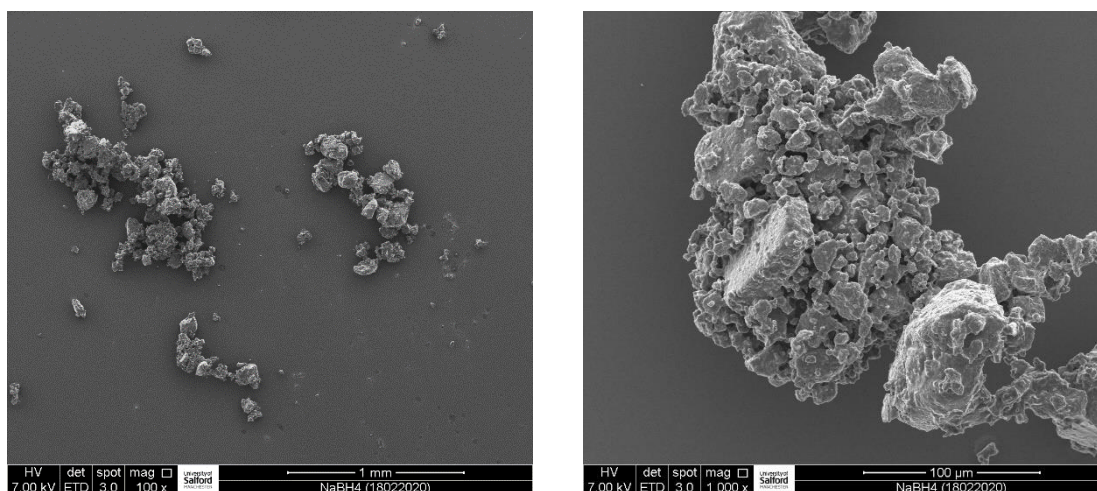


Figure 4.218 SEM micrographs of NaBH_4 after grinding under nitrogen

When examined using EDX analysis, the particles gave the spectrum figure 4.219, displaying high levels of sodium with lower levels of oxygen and boron. The platinum and palladium peaks are from the preparation.

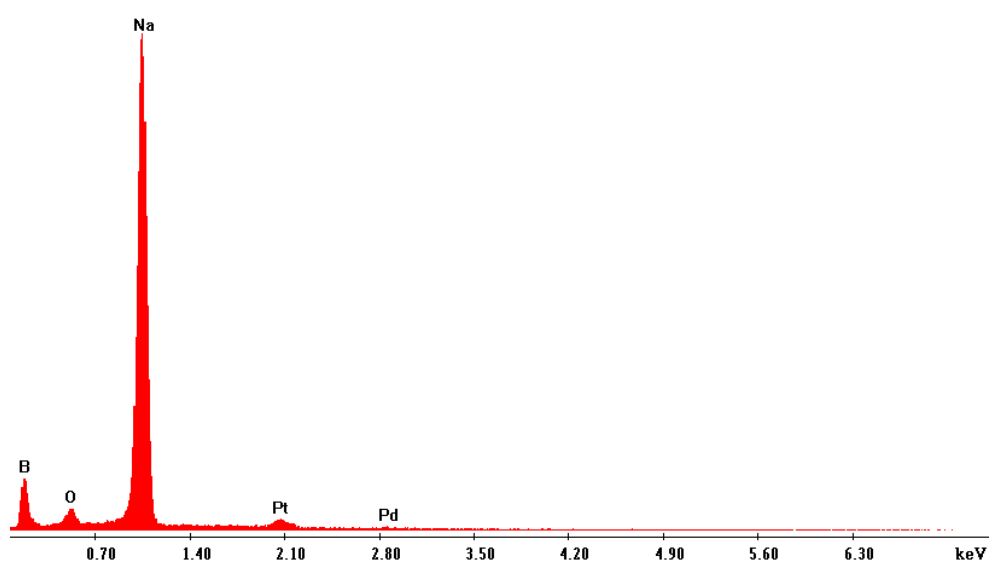


Figure 4.219 EDX spectrum obtained from NaBH_4 particles shown in figure 4.222

Figure 4.220 symbolises the NaBH_4 particles after they had been left overnight in air. Even though the particles were coated in platinum/palladium, the morphology of the particles is seen to have completely changed. The low magnified micrograph obtained with a system magnification of 100x shows that the clusters of particles have dissolved, with some areas forming amorphous regions. The micrograph obtained with a system magnification of 1000x shows crystalline particles to be present up to $50\mu\text{m}$ in size within the dissolved regions. Some particles are seen to have formed an hexagonal structure and others appear lath-shaped.

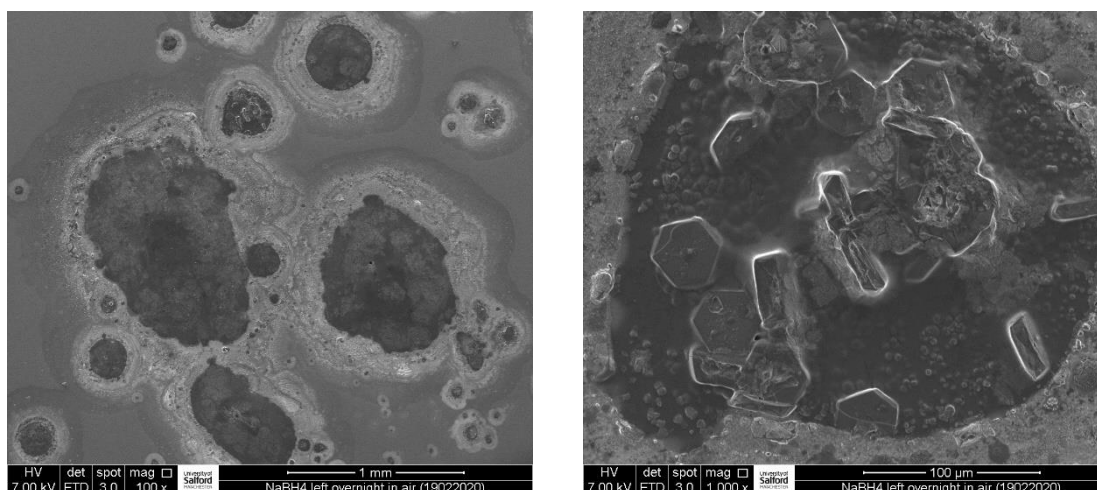


Figure 4.220 SEM micrographs of NaBH_4 particles left overnight in air

EDX analysis of a hexagonal particle produced the resulting spectrum figure 4.221 displaying the presence of sodium with significantly higher levels of oxygen.

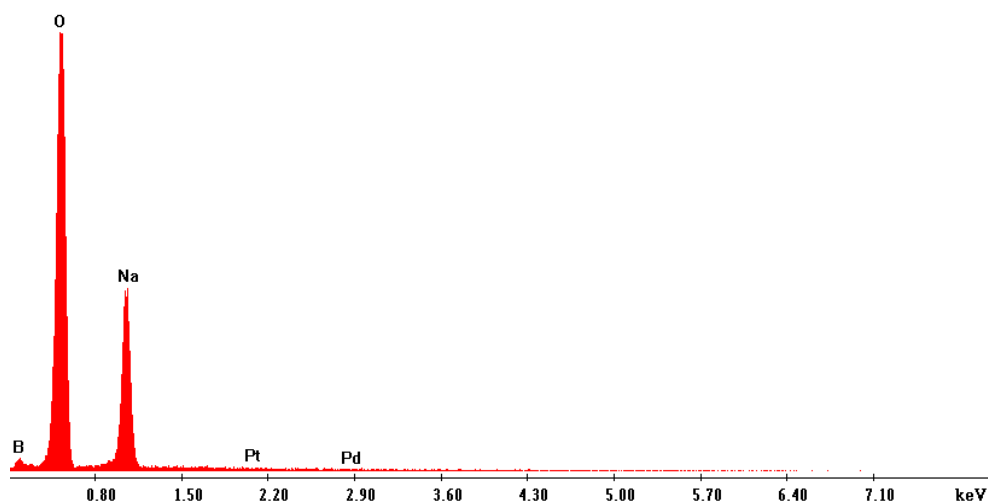


Figure 4.221 EDX spectrum obtained from hexagonal particle shown in figure 4.224

A similar study was performed on ground NaBH_4 particles using high resolution SEM to demonstrate the changes in morphology over a shorter period of time.

The preparation involved dusting a small amount of ground NaBH_4 onto cleaved silicon that had been fixed onto an SEM stub using a carbon adhesive pad.

To allow greater exposure to moisture in the air, the sample was not coated with platinum/palladium. This, however, had the effect of reducing the quality of the resulting micrographs.

Figure 4.222 represents an SEM micrograph obtained (at 8.27am) using a system magnification of 200x. The micrograph displays that the NaBH_4 particles have an irregular shape and show variations in particle size as a direct result of the grinding process.

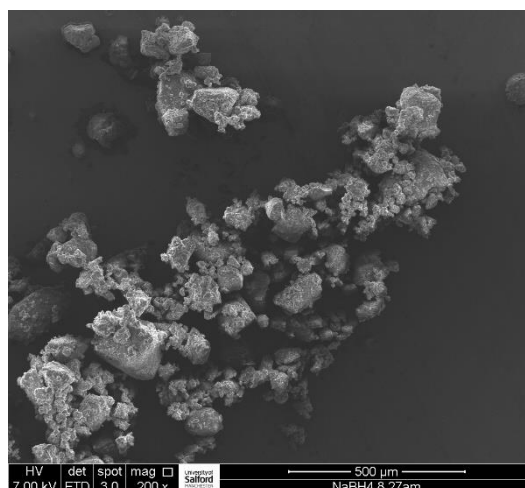


Figure 4.222 NaBH_4 particles uncoated - 8.27am

The sample was then left on the bench in the open lab, exposed to air and moisture from the atmosphere. The SEM micrographs shown in figure 4.223 symbolise the same low magnified area, together with a higher magnified micrograph showing the particle morphology. These micrographs were acquired at 11.45am (approximately 3 hours later) and demonstrate a significant change had occurred to the morphology of the particles.

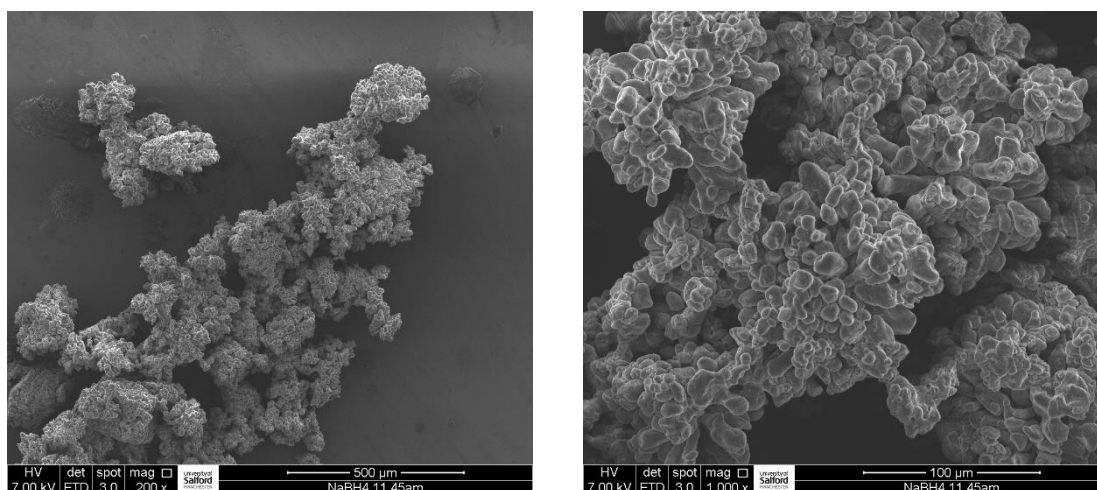


Figure 4.223 NaBH_4 particles uncoated - 11.45am

The larger irregular-shaped particles have changed morphology over time to form clusters of smaller particles existing with a uniform structure. The particles show only a slight variation in particle size, and most of the individual particles have a smooth-edged appearance. This morphology is completely different from the initial particles examined at 8.27am.

The final SEM micrograph, figure 4.224 (taken at 3.45 μm), illustrates that the morphology of the particles has changed again. The particles have merged together, forming a continuous structure as opposed to the individual primary particles displayed in figure 4.222.

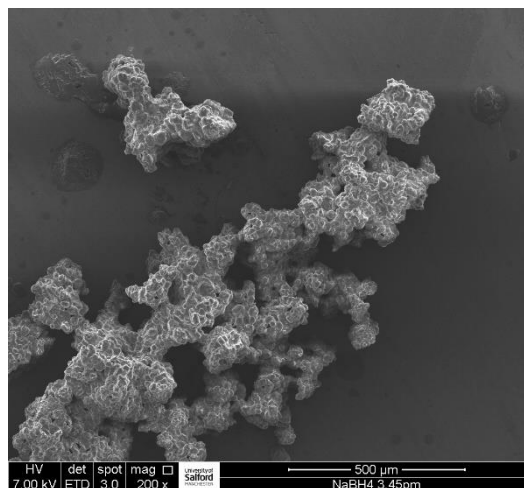


Figure 4.224 NaBH_4 particles uncoated at 3.45 μm

The EDX results verify the changes seen from the particle morphology when the ratios of sodium and oxygen are compared. Figure 4.225 represents the spectrum obtained from the NaBH_4 particles examined at 8.27 μm . The spectrum displays high levels of sodium with very low levels of oxygen and boron. The trace silicon peak is associated with the silicon substrate used in the sample preparation.

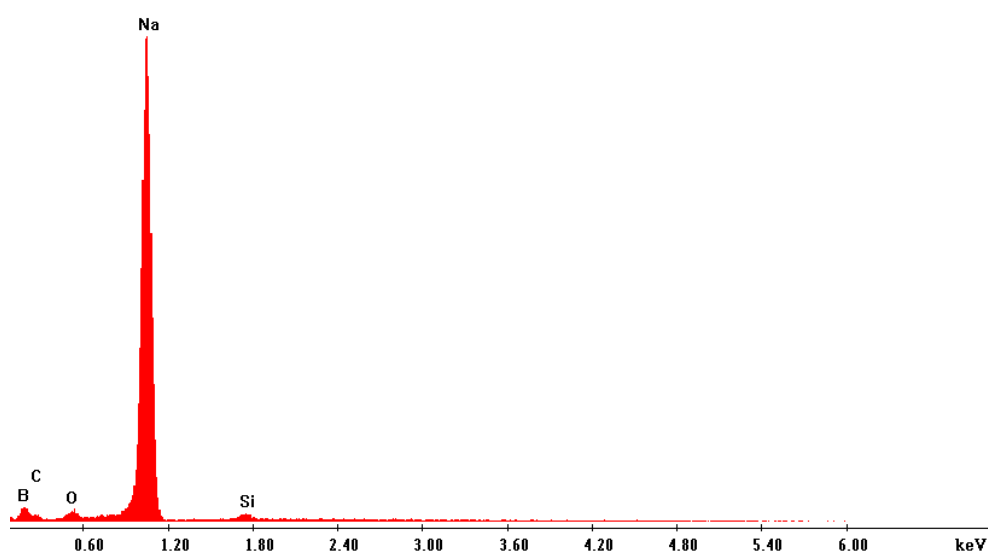


Figure 4.225 EDX spectrum obtained from NaBH_4 particle at 8.27am

The resulting EDX spectrum figure 4.226, obtained from the particle examined at 3.45pm, demonstrates that the oxygen levels had increased considerably when compared against the peak height of sodium. Interestingly, the ratio of sodium to boron had also changed. These results are not quantitative but show that the NaBH_4 had undergone a transformation throughout the day.

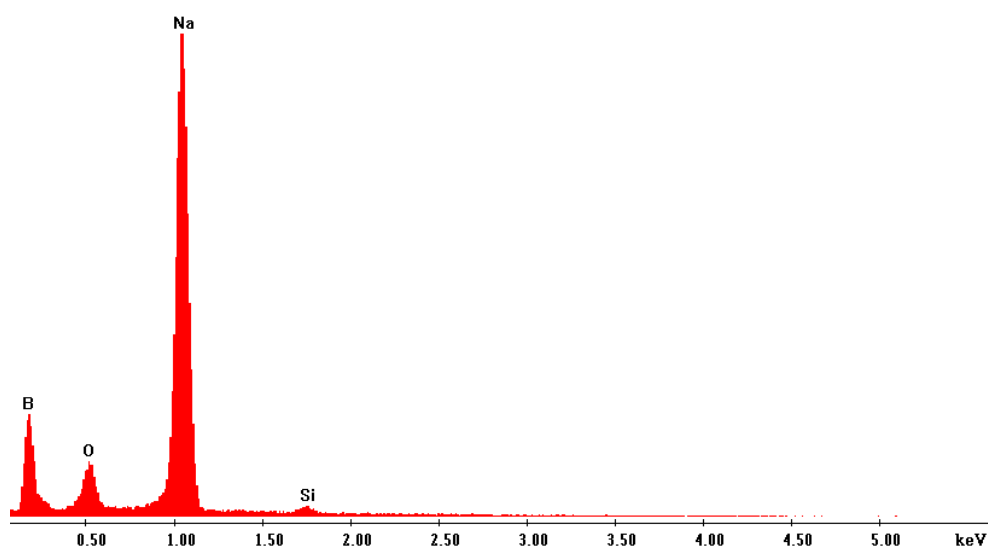


Figure 4.226 EDX spectrum obtained from NaBH_4 particle at 3.45 pm

These results are interesting as they demonstrate the changes in morphology to the NaBH_4 particles after exposure to moisture from the atmosphere (Chen et al., 2017). The results from leaving the particles overnight revealed hydrolysis had occurred due to the changes to the particle morphology and a significant increase to the oxygen levels as revealed in EDX spectrum figure 4.221.

The shorter exposure time showed some fascinating changes to the particle morphology throughout the day.

5 Conclusions and Future Work

This research involved developing a suitable polymer microcapsule that would allow the safe handling of moisture-sensitive metal hydride nanoparticles for characterisation.

It was necessary that the microcapsule design prevented exposure of the metal hydride nanoparticles to moisture from the atmosphere, helping to retard unwanted vigorous reactions. In addition, it was vital that the microcapsule allowed a mechanism for easy access to the encapsulated nanoparticles, permitting a study of the primary particle morphology using high-resolution Scanning Electron Microscopy.

The process of developing a suitable polymer microcapsule was not straight forward as metal hydrides react violently with water and other protic solvents, together with amine and hydroxide groups.

Initially, to understand the process of creating microcapsules, a method utilising Cellulose Acetate Phthalate (CAP) polymer for the encapsulation of paracetamol was modified. The initial experimental conditions were analogous to those outlined in the non-solvent addition technique, as described in the encapsulation of Paracetamol (Nokhodchi and Farid, 2002). Paracetamol was substituted by nanoparticles of TiO_2 . After adjusting the concentration ratios of TiO_2 and the CAP polymer, a method was designed that produced spherical microcapsules containing nanoparticles of TiO_2 within the inner core of the microcapsule, demonstrating that the available equipment and techniques were suitable for preparing encapsulated materials. However, CAP is unsuitable as a material for encapsulation since metal hydrides react with hydroxyl groups and so a more suitable polymer for generating the microcapsules was sought.

The CAP polymer was replaced by Polysulfone (PSF) as this polymer contained no reactive groups that could cause potential issues for the encapsulation of metal hydride particles.

The initial design of the experimental conditions had to be significantly changed as the method utilised for the generation of CAP microcapsules did not produce suitable microcapsules. The technique for generating microcapsules was changed, and a new robust method was devised, allowing the generation of microcapsules using a PSF polymer system.

After accomplishing a suitable methodology for the process of encapsulating nanoparticles of TiO_2 , the microcapsules were cross-sectioned and the distribution of the TiO_2 nanoparticles was demonstrated using SEM.

The TiO_2 nanoparticles were substituted for non-reactive lithium salts with similar properties to lithium amide. Initially, suitable methods were designed for the encapsulation of both Li_2CO_3 and Li_3PO_4 into PSF microcapsules. The experimental design for the encapsulation of each different lithium salt into PSF required enhanced development work to the procedure for each separate salt. Methods had to be tweaked for the different salts, indicating that a universal method for lithium salts was not possible. These changes included adjustments to the agitation rate of the non-solvent, together with modifications to the non-solvent blend. Subtle changes to the method seemed to noticeably improve the internal morphology of the created microcapsules. At each stage of this research aimed at improving the encapsulation of the lithium salts into microcapsules, it was necessary to continually examine the internal morphology of cross-sectioned microcapsules using SEM to validate the suitability of the encapsulation process. This initial development work led to the generation of excellent spherical microcapsules.

Once sufficient expertise had been developed to understand the efficacy of the various parameters (speed, concentration, ratio of non-solvents) to generate the necessary microcapsules, the lithium salts were subsequently exchanged for reactive lithium amide which necessitated working under an inert atmosphere. The cross-sectional analysis using SEM generated micrographs showing the presence of LiNH_2 nanoparticles. However, the corresponding EDX analysis from the encapsulated particles produced spectra showing a large oxygen peak, suggesting that the LiNH_2 had formed the hydroxide. One issue at this stage of the research project was that microcapsules had to be cut open in the open lab. After fixing to an SEM stub, the cross-sections had to be transferred to the preparation

sputter coating unit, before entering the microscope. In this time, moisture could have reacted with the LiNH_2 , yielding the hydroxide. Another hypothesis could be that the LiNH_2 had already reacted to form the hydroxide before the encapsulation process, as the particles were ex Sigma-Aldrich.

In an attempt to develop a more robust preparation technique to allow the study of the internal structure of the generated microcapsules, a cryo-preparation chamber was borrowed and fixed onto the high vacuum porthole of the Philips XL30 SFEG. This technique allowed the microcapsules to be cross-sectioned under vacuum with an additional option of an argon gas purge. This hopefully would provide an ideal method for the preparation of air/moisture-sensitive materials to be examined using the high-resolution SEM, utilising microcapsules as the transfer vehicle.

It may have been a useful exercise to revisit the LiNH_2 microcapsules to check this theory. However, because of the limitations for detection of lithium with the equipment available for this project, it was decided to encapsulate a different metal hydride which contained elements more suitable for detection using EDX analysis.

The final phase of this research project involved encapsulating NaBH_4 into a PSF polymer microcapsule. Samples of NaBH_4 purchased from Sigma-Aldrich and Acros Organics were seen to be irregular in shape, having a particle size up to $200\mu\text{m}$. These particles appeared as a fine powder, but ideally a much smaller particle size was desired for encapsulation within a polymer microcapsule. To reduce the particle size, the NaBH_4 was ground using a pestle and mortar within a glove box under a flow of nitrogen. The technique was successful - producing irregular-shaped particles with an average size around $30\mu\text{m}$.

From the preliminary experimental studies using lithium salts, NMP was the preferred solvent for the dissolution of PSF. The generated microcapsules had an excellent morphology, which demonstrated encapsulation of primary particles within the polymer shell. However, when switching to NaBH_4 , the PSF/NMP system produced remarkably shaped microcapsules with a good internal porosity. Unfortunately, the SEM micrographs presented evidence that suggested the NMP had solubility issues with NaBH_4 . The

cross-sectioned micrographs obtained from many different encapsulation experiments exhibited a mixture of unchanged NaBH_4 , together with hydrolyzed material. In addition, some microcapsules gave evidence that the encapsulated NaBH_4 particles had re-crystallised to a needle-shaped morphology. From these findings, it was evident that the ground NaBH_4 particles were too soluble in NMP.

The initial experiments undertaken with DMF generated microcapsules that appeared ideal, based on the outer and internal morphology. However, the SEM micrographs obtained from each cross-sectioned microcapsule revealed a low concentration of encapsulated particles. When examined using EDX analysis, the particles produced mixed results with some spectra revealing that the NaBH_4 particles were unchanged, and others had hydrolyzed. The SEM micrographs demonstrated that the surface was covered in particles which gave a corresponding EDX spectrum, suggesting hydrolyzed NaBH_4 from the high levels of oxygen seen in the EDX spectrum.

This research indicates that problems have occurred trying to encapsulate NaBH_4 using a PSF polymer system when utilising either NMP or DMF as the solvent for the polymer.

PSF is readily soluble in NMP and DMF, and most of the background work using non-metal hydride particles was developed using these two solvents. However, due to possible incompatibilities with NaBH_4 , an alternative solvent was sourced.

Both solvents were replaced by THF, as this appeared to dissolve the PSF. Using THF sometimes produced a cloudy polymer solution, but on other occasions the solution was clear. However, after some experimental changes such as working with dry THF for the PSF solvent, and dry acetonitrile and chloroform for the non-solvent, the methodology did generate interesting results. The SEM micrographs from the cross-sectioned microcapsules demonstrate that it was possible to encapsulate ground irregular-shaped particles of NaBH_4 , as shown in the examples given in figures 4.201 and 4.210 respectively. These micrographs show that the irregular-shaped particles have not changed from the grinding process. This confirms that it is possible to encapsulate reactive NaBH_4 within a PSF polymer microcapsule, allowing the particle morphology to be studied.

However, it proved difficult to increase the loadings of NaBH_4 . The example given in figure 4.214 displays the outer surface of a generated microcapsule. At 1000x magnification, the surface appears relatively clean, however the micrograph obtained with a system magnification of 10,000x displays a fine dusting of NaBH_4 particles which had started to hydrolyse. Surface particles can cause the microcapsules to stick together within the non-solvent. The concentration for these samples was based on using 3x micro-spatulas of NaBH_4 as opposed to the usual 1x micro-spatula loading.

This initial research could be continued by additional researchers, as it would be useful to investigate the issues around increasing the concentration of encapsulated material. Perhaps the experimental design could be modified, and any surface deposits could be removed by a simple wash at the final stage of the procedure. As the average size of the ground NaBH_4 was approximately $30\mu\text{m}$, this could have hindered the quality of the polymer dispersion. If the particle size were reduced further, it may have improved the degree of encapsulated particles. It would be interesting for further projects to see if alternative research could demonstrate the encapsulation of additional metal hydride materials such as the binary metal hydride NaH or a slightly more complex ternary metal hydride, for example NaAlH_4 . In addition to encapsulation of different metal hydrides, it would be interesting to investigate the possibility of incorporating a second external shell layer onto the surface of the microcapsules. Using an additional coating would hopefully provide increased stability for the encapsulated metal hydride particles, delaying unwanted reactions and therefore expanding the duration of safe storage. It would be interesting to compare the use of different polymers to generate the extra shell coating.

References

- Abdelhamid, H.N., 2021. A review on hydrogen generation from the hydrolysis of sodium borohydride. *International Journal of Hydrogen Energy*, 46(1), pp.726–765.
- Ahmad, S.U. et al., 2021. Recent advances in microencapsulation of drugs for veterinary applications. *Journal of Veterinary Pharmacology and Therapeutics*, 44(3), pp.298–312.
- Alonso, M.L. et al., 2013. Pesticides microencapsulation. A safe and sustainable industrial process. *Journal of Chemical Technology & Biotechnology*, 89(7), pp.1077–1085.
- Arenas-Jal, M., Suñé-Negre, J.M. & García-Montoya, E., 2020. An overview of microencapsulation in the food industry: opportunities, challenges, and innovations. *European Food Research and Technology*, 246(7), pp.1371–1382.
- Ashraf, M.A. et al., 2015. Effectiveness of silica based sol-gel microencapsulation method for odorants and flavors leading to sustainable environment. *Frontiers in Chemistry*, 3.
- Askew, K., 2021. EU E171 ban set for 2022: 'the safety of our food is not negotiable'. *foodnavigator.com*. Available at: <https://www.foodnavigator.com/Article/2021/10/11/EU-E171-ban-set-for-2022-The-safety-of-our-food-is-not-negotiable>.
- Baldissin, G. et al., 2013. Synthesis of Pure Lithium Amide Nanoparticles. *European Journal of Inorganic Chemistry*, 2013(12), pp.1993–1996.
- Beckman, 2021. Coulter Principle, Counting and Sizing Particles - Beckman Coulter. *Beckman.hk*. Available at: <https://www.beckman.hk/resources/technologies/flow-cytometry/history/coulter-principle>.
- Bell, D.C. & Garratt-Reed, A.J., 2003. *Energy-dispersive X-ray analysis in the electron microscope* 1st ed., London: Garland Science.
- Bergeron, V. et al., 1997. Polydimethylsiloxane (PDMS)-based antifoams. *Colloids and Surfaces A: Physicochemical and Engineering Aspects*, 122(1-3), pp.103–120.
- Bewernitz, M.A., Lovett, A.C. & Gower, L.B., 2020. Liquid–solid core-shell microcapsules of calcium carbonate coated emulsions and liposomes. *Applied Sciences*, 10(23), p.8551.
- Blaznik, U. et al., 2021. Use of food additive titanium dioxide (E171) before the introduction of regulatory restrictions due to concern for genotoxicity. *Foods*, 10(8), p.1910.

- Borodina, T. et al., 2010. Hydrogen storage materials protected by a polymer shell. *J. Mater. Chem.*, 20(8), pp.1452–1456.
- Bourgeois, N. et al., 2017. Systematic First-Principles Study of Binary Metal Hydrides. *ACS Combinatorial Science*, 19(8), pp.513–523.
- Brečević, L., Bošan-Kilibarda, I. & Strajnar, F., 1994. Mechanism of antifoaming action of simethicone. *Journal of Applied Toxicology*, 14(3), pp.207–211.
- Broens, L. et al., 1980. Asymmetric membrane structures as a result of phase separation phenomena. *Desalination*, 32, pp.33–45.
- Brown, H.C., Narasimhan, S. & Choi, Y.M., 1982. Selective reductions. 30. effect of cation and solvent on the reactivity of Saline Borohydrides for reduction of carboxylic esters. improved procedures for the conversion of esters to alcohols by metal borohydrides. *The Journal of Organic Chemistry*, 47(24), pp.4702–4708.
- Bunaciu, A.A., Udriștioiu, E.gabriela & Aboul-Enein, H.Y., 2015. X-ray diffraction: Instrumentation and applications. *Critical Reviews in Analytical Chemistry*, 45(4), pp.289–299.
- Byjus, 2021. NMR Spectroscopy. *BYJUS*. Available at: <https://byjus.com/chemistry/nmr-spectroscopy/>.
- Chen, S.-H. et al., 2007. Effect of the polarity of additional solvent on membrane formation in polysulfone/N-methyl-2-pyrrolidone/water ternary system. *European Polymer Journal*, 43(9), pp.3997–4007.
- Chen, W. et al., 2017. Hydrolysis and regeneration of sodium borohydride (NaBH₄) – A combination of hydrogen production and storage. *Journal of Power Sources*, 359, pp.400–407.
- Chescoe, D. & Goodhew, J., 1990. *The Operation of Transmission Electron Microscopy* 1st ed., Royal Microscopical Society.
- Childs, M., 2020. The role of hydrogen in our future | Policy and insight. *Friends of the Earth / Policy and insight*. Available at: <https://policy.friendsoftheearth.uk/insight/role-hydrogen-our-future>.
- Choudhury, N., Meghwal, M. & Das, K., 2021. Microencapsulation: An overview on concepts, methods, properties and applications in foods. *Food Frontiers*, 2(4), pp.426–442.
- Cressington, 2021. Specification - 208HR High Resolution Sputter Coater. *Cressington.com*. Available at: https://www.cressington.com/spec_208hr.html.
- Croda, 2021. ECO Tween™ 80 | Smart Materials. *Crodasmartmaterials.com*. Available at: https://www.crodasmartmaterials.com/en-gb/product-finder/product/1428-ECO_1_Tween_1_80.

- Delgado, A.V. et al., 2007. Measurement and interpretation of electrokinetic phenomena. *Journal of Colloid and Interface Science*, 309(2), pp.194–224.
- Demirci, U.B. et al., 2010. Sodium Borohydride Hydrolysis as Hydrogen Generator: Issues, State of the Art and Applicability Upstream from a Fuel Cell. *Fuel Cells*, 10(3), pp.335–350.
- Dobbins, T., Kamineni, V. & Lvov, Y., 2007. Nanoarchitecture of Protective Coatings for Air-Sensitive Metal Hydrides. *Material Matters*, 2(2), p.19.
- D'onofrio, G.P., Oppenheim, R.C. & Bateman, N.E., 1979. Encapsulated microcapsules. *International Journal of Pharmaceutics*, 2(2), pp.91–99.
- Douma, M., 2021. Pigments through the Ages - History - Titanium white. *Webexhibits.org*. Available at: <http://www.webexhibits.org/pigments/individ/history/titaniumwhite.html>.
- Dréno, B. et al., 2019. Safety of titanium dioxide nanoparticles in cosmetics. *Journal of the European Academy of Dermatology and Venereology*, 33(S7), pp.34–46.
- Eqbal, M.D. & Gundabala, V., 2017. Controlled fabrication of multi-core alginate microcapsules. *Journal of Colloid and Interface Science*, 507, pp.27–34.
- Fakioğlu, E., Yürüm, Y. & Veziroğlu, T., 2004. A review of hydrogen storage systems based on boron and its compounds. *International Journal of Hydrogen Energy*, 29(13), pp.1371–1376.
- Fei, C. et al., 2005. Preparation and adsorption ability of polysulfone microcapsules containing modified chitosan gel. *Tsinghua Science and Technology*, 10(5), pp.535–541.
- Feng, B. et al., 2021. Development of chlorantraniliprole and Lambda Cyhalothrin double-loaded nano-microcapsules for synergistical pest control. *Nanomaterials*, 11(10), p.2730.
- Fernandes, V.R., Pinto, A.M.F.R. & Rangel, C.M., 2010. Hydrogen production from sodium borohydride in methanol–water mixtures. *International Journal of Hydrogen Energy*, 35(18), pp.9862–9868.
- Fischer Scientific, 2021. Summary of Key Physical Data for Solvents. *Fishersci.co.uk*. Available at: <https://www.fishersci.co.uk/gb/en/scientific-products/technical-tools/summary-key-physical-data-solvents.html>.
- Galli, S. et al., 2010. Development of a compact hydrogen generator from sodium borohydride. *International Journal of Hydrogen Energy*, 35(14), pp.7344–7349.
- Gatan, 2021. TEM Imaging & Spectroscopy | Gatan, Inc. *Gatan.com*. Available at: <https://www.gatan.com/products/tem-imaging-spectroscopy>.

- Ghayempour, S. & Montazer, M., 2016. Micro/nanoencapsulation of essential oils and fragrances: Focus on perfumed, antimicrobial, mosquito-repellent and medical textiles. *Journal of Microencapsulation*, 33(6), pp.497–510.
- Gislon, P., Monteleone, G. & Prosini, P., 2009. Hydrogen production from solid sodium borohydride. *International Journal of Hydrogen Energy*, 34(2), pp.929–937.
- Goldstein, D. & Duchi, S., 2019. Using microencapsulation to unlock resveratrol's commercial potential in skincare. *cosmeticsdesign-europe.com*. Available at: <https://www.cosmeticsdesign-europe.com/Headlines/Promotional-Features/Using-microencapsulation-to-unlock-resveratrol-s-commercial-potential-in-skincare>.
- Goldstein, J. et al., 1992. 33. *Scanning Electron Microscopy and X-ray Microanalysis* 2nd ed.,
- Gong, X. et al., 2008. Preparation of polysulfone microcapsules containing 1-octanol for the recovery of Caprolactam. *Journal of Microencapsulation*, 26(2), pp.104–110.
- Gong, X.C. et al., 2006. Separation of organic acids by newly developed polysulfone microcapsules containing triethylamine. *Separation and Purification Technology*, 48(3), pp.235–243.
- Guegan, A.P., 2010. Cheminform Abstract: A survey of binary and ternary metal hydride systems. *ChemInform*, 26(50).
- Guillen, G.R. et al., 2013. Direct microscopic observation of membrane formation by nonsolvent induced phase separation. *Journal of Membrane Science*, 431, pp.212–220.
- Guo, J. et al., 2020. Microencapsulation of curcumin by spray drying and freeze drying. *LWT*, 132, p.109892.
- Horiba, 2021. Fundamental Principles of Laser Diffraction - HORIBA. *Horiba.com*. Available at: <https://www.horiba.com/cn/scientific/products/particle-characterization/technology/laser-diffraction/fundamentals-of-diffraction/>.
- Hořda, A.K. & Vankelecom, I.F.J., 2014. Integrally skinned PSF-based srnf-membranes prepared via phase inversion—part B: Influence of low molecular weight additives. *Journal of Membrane Science*, 450, pp.499–511.
- Hořda, A.K. & Vankelecom, I.F.J., 2015. Understanding and guiding the phase inversion process for synthesis of solvent resistant nanofiltration membranes. *Journal of Applied Polymer Science*, 132(27).
- Huang, B. et al., 2018. Advances in targeted pesticides with environmentally responsive controlled release by nanotechnology. *Nanomaterials*, 8(2), p.102.
- Ilitchev, A., 2019. How Do You Make an Electron Beam? *Accelerating Microscopy*. Available at: <https://www.thermofisher.com/blog/microscopy/electron-source-fundamentals/>.

- Jacobsen, H., 2008. Hydrogen and dihydrogen bonding of transition metal hydrides. *Chemical Physics*, 345(1), pp.95–102.
- Jeannot, L. et al., 2018. Internal structure of matrix-type multilayer capsules templated on porous vaterite CaCO_3 crystals as probed by staining with a fluorescence dye. *Micromachines*, 9(11), p.547.
- JEOL, 2021. JEM-2100 Electron Microscope. *Jeol.co.jp*. Available at: <https://www.jeol.co.jp/en/products/detail/JEM-2100.html>.
- Kang, S. et al., 2015. Core–shell polymeric microcapsules with superior thermal and solvent stability. *ACS Applied Materials & Interfaces*, 7(20), pp.10952–10956.
- Keller, J. & Klebanoff, L., 2012. Metal Hydride Storage Materials. *Energy.gov*. Available at: <https://www.energy.gov/eere/fuelcells/metal-hydride-storage-materials>.
- Kim, J.Y., Lee, H.K. & Kim, S.C., 2000. Liquid-liquid phase separation during polysulfone membrane preparation. *Korean Journal of Chemical Engineering*, 17(5), pp.564–569.
- Kulkarni, V.S., 2015. *Essential chemistry for formulators of semisolid and liquid dosages*, Academic Press Inc.
- Kwon, S.-mo, Kang, S. & Kim, T., 2019. Development of NaBH_4 -Based Hydrogen Generator for Fuel Cell Unmanned Aerial Vehicles with Movable Fuel Cartridge. *Energy Procedia*, 158, pp.1930–1935.
- Leckey, J.H., Nulf, L.E. & Kirkpatrick, J.R., 1996. Reaction of Lithium Hydride with Water. *Langmuir*, 12(26), pp.6361–6367.
- Li, H. et al., 2016. Preparation of high thermal stability polysulfone microcapsules containing lubricant oil and its tribological properties of epoxy composites. *Journal of Microencapsulation*, 33(3), pp.286–291.
- Li, N. et al., 2021. Advances in Controlled-Release Pesticide Formulations with Improved Efficacy and Targetability. *Journal of Agricultural and Food Chemistry*, 69(43), pp.12579–12597.
- Liu, Y., Li, H.-W. & Huang, Z., 2020. Editorial: Metal Hydride-Based Energy Storage and Conversion Materials. *Frontiers in Chemistry*, 8.
- Lo, C.-ting F., Karan, K. & Davis, B.R., 2007. Kinetic Studies of Reaction between Sodium Borohydride and Methanol, Water, and Their Mixtures. *Industrial & Engineering Chemistry Research*, 46(17), pp.5478–5484.
- Luz, C. & Wenyan, L., 2006. pH Sensitive Microcapsules for Delivery of Corrosion Inhibitors. *ECS Meeting Abstracts*.

- Ma, X. et al., 2011. Preparation of novel polysulfone capsules containing zirconium phosphate and their properties for Pb²⁺ removal from aqueous solution. *Journal of Hazardous Materials*, 188(1-3), pp.296–303.
- Maldonado-Lopez, L.E., Fimbres-Weihs, G.A. & Escobar-Barrios, V.A., 2021. Structural modification of Polysulfone/NMP membranes: Effect of chloroform as co-solvent. *Polymer Bulletin*.
- Malvern, 2021. Laser Diffraction Particle Size Analysis. *Malvernpanalytical.com*. Available at: <https://www.malvernpanalytical.com/en/products/technology/light-scattering/laser-diffraction>.
- Malvernpanalytical, 2021. Dynamic Light Scattering DLS. *Malvernpanalytical.com*. Available at: <https://www.malvernpanalytical.com/en/products/technology/light-scattering/dynamic-light-scattering>.
- Mankar, S.D. & Shaikh, S.B., 2020. Microencapsulation: Is an advance Technique of Drug formulation for Novel Drug Delivery System. *Research Journal of Science and Technology*, 12(3), p.201.
- McClements, D.J., 2017. Recent progress in hydrogel delivery systems for improving nutraceutical bioavailability. *Food Hydrocolloids*, 68, pp.238–245.
- Mishra, M., 2016. *Handbook of encapsulation and controlled release*, Boca Raton: Taylor & Francis, CRC Press.
- Mulder, M., 2010. *Basic principles of membrane technology* 2nd ed., Dordrecht: Kluwer Acad. Publ.
- Nanakoudis, A., 2019. What is SEM? Scanning Electron Microscopy Explained. *Accelerating Microscopy*. Available at: <https://www.thermofisher.com/blog/microscopy/what-is-sem-scanning-electron-microscopy-explained/>.
- Newey-Keane, L., 2021. Resonant mass measurement as an analytical tool. *Manufacturingchemist.com*. Available at: https://www.manufacturingchemist.com/technical/article_page/Resonant_mass_measurement_as_an_analytical_tool/90290.
- Nokhodchi, A. & Farid, D., 2002. Microencapsulation of paracetamol: By various emulsion techniques using cellulose acetate phthalate. *Pharmaceutical Technology*, 26, pp.54–60.
- Oberoi, K. et al., 2019. Microencapsulation: An overview for the survival of probiotic bacteria. *Journal of Microbiology, Biotechnology and Food Sciences*, 9(2), pp.280–287.
- Orimo, S.-ichi et al., 2007. Complex Hydrides for Hydrogen Storage. *ChemInform*, 38(51).

- Pasha, A., Utekar, S. & Ghosh, R., 2021. Recent Advances in Microencapsulation Technology and their Applications. *The Bombay Technologist*, 68(1).
- Peanparkdee, M. et al., 2016. Microencapsulation: A review of applications in the food and pharmaceutical industries. *Reviews in Agricultural Science*, 4, pp.56–65.
- Pena, B. & Gumi, T., 2013. State of the Art of Polysulfone Microcapsules. *Current Organic Chemistry*, 17(1), pp.22–29.
- Peña, B. et al., 2012. Preparation and characterization of polysulfone microcapsules for perfume release. *Chemical Engineering Journal*, 179, pp.394–403.
- Pinto Reis, C. et al., 2006. Nanoencapsulation I. Methods for preparation of drug-loaded polymeric nanoparticles. *Nanomedicine: Nanotechnology, Biology and Medicine*, 2(1), pp.8–21.
- Pinto, A. et al., 2006. Hydrogen generation and storage from hydrolysis of sodium borohydride in batch reactors. *International Journal of Hydrogen Energy*, 31(10), pp.1341–1347.
- Poe, S.L., Kobašlija, M. & McQuade, D.T., 2007. Mechanism and Application of a Microcapsule Enabled Multicatalyst Reaction. *Journal of the American Chemical Society*, 129(29), pp.9216–9221.
- Pongpaibul, Y. & Whitworth, C.W., 1986. Microencapsulation by Emulsion Non-Solvent Additive Method. *Drug Development and Industrial Pharmacy*, 12(14), pp.2387–2402.
- Ranner, R. & DeRose, J., 2022. Introduction to Ultramicrotomy. *Leica-microsystems.com*. Available at: <https://www.leica-microsystems.com/science-lab/brief-introduction-to-ultramicrotomy/>.
- Salaün, F., 2016. Microencapsulation technology for Smart Textile Coatings. *Active Coatings for Smart Textiles*, pp.179–220.
- Sanderson, J.B., 2019. *Understanding light microscopy*, Hoboken, NJ: Wiley.
- Scher, H.B., Rodson, M. & Lee, K.-S., 1998. Microencapsulation of pesticides by interfacial polymerization utilizing isocyanate or aminoplast chemistry†. *Pesticide Science*, 54(4), pp.394–400.
- Schueth, F., Bogdanovic, B. & Felderhoff, M., 2005. Light Metal Hydrides and Complex Hydrides for Hydrogen Storage. *ChemInform*, 36(2).
- Shima, T. et al., 2011. Molecular heterometallic hydride clusters composed of rare-earth and d-transition metals. *Nature Chemistry*, 3(10), pp.814–820.

- Singh, M.N. et al., 2010. Research in Pharmaceutical Sciences, 2010. Microencapsulation: a promising technique for controlled drug delivery. *Research in Pharmaceutical Sciences*, 5(2), pp.65–77.
- Sprockel, O.L. & Prapaitrakul, W., 1990. A comparison of muencapsulation by various emulsion techniques. *International Journal of Pharmaceutics*, 58(2), pp.123–127.
- Sriamornsak, P. et al., 2008. Cryo-scanning electron microscopy (cryo-SEM) as a tool for studying the ultrastructure during bead formation by ionotropic gelation of calcium pectinate. *International Journal of Pharmaceutics*, 352(1-2), pp.115–122.
- Tekin, R., Bac, N. & Erdogmus, H., 2013. Microencapsulation of Fragrance and Natural Volatile Oils for Application in Cosmetics, and Household Cleaning Products. *Macromolecular Symposia*, 333(1), pp.35–40.
- Thermo Fisher Scientific, 2021. EDX Analysis with a Scanning Electron Microscope (SEM). *Thermofisher.com*. Available at: <https://www.thermofisher.com/uk/en/home/global/forms/industrial/edx-analysis-sem.html>.
- Torras, C. et al., 2006. Novel polymeric membrane structures: Microcapsules. *Desalination*, 200(1-3), pp.12–14.
- Tsuji, K., 2001. Microencapsulation of pesticides and their improved handling safety. *Journal of Microencapsulation*, 18(2), pp.137–147.
- Vasisht, N., 2014. Factors and mechanisms in microencapsulation. *Microencapsulation in the Food Industry*, pp.15–24.
- Veillard, A., Daniel, C. & Rohmer, M.M., 1990. Cobalt tetracarbonyl hydride and cobalt tricarbonyl hydride revisited: structure and electronic states through ab initio calculations. *The Journal of Physical Chemistry*, 94(14), pp.5556–5559.
- Wang, J. et al., 2021. Hydroboration reaction and mechanism of carboxylic acids using $\text{NaNH}_2(\text{BH}_3)_2$, a hydroboration reagent with reducing capability between NaBH_4 and LiAlH_4 . *The Journal of Organic Chemistry*, 86(7), pp.5305–5316.
- Ward, D.E. & Rhee, C.K., 1989. Cheminform abstract: Chemoselective reductions with sodium borohydride. *ChemInform*, 20(47).
- Washington, C., 1992. *Particle Size Analysis In Pharmaceutics And Other Industries*, CRC Press; 1st edition (June 30, 1992).
- Wienk, I.M. et al., 1996. Recent advances in the formation of phase inversion membranes made from amorphous or semi-crystalline polymers. *Journal of Membrane Science*, 113(2), pp.361–371.

- Yang, M. et al., 2022. Isothermal Kinetics Model for Solid–Solid Reaction of Powders Through Surface Area and Size Distribution of Particles. *Metallurgical and Materials Transactions B*.
- Yu, F. et al., 2021. Preparation of Polyurea Microcapsules by Interfacial Polymerization of Isocyanate and Chitosan Oligosaccharide. *Materials*, 14(13), p.3753.
- Zeiss , 2021. Zeiss Stereo V8. *Zeiss.com*. Available at:
<https://www.zeiss.com/microscopy/int/products/stereo-zoom-microscopes/stereo-discovery-v8.html>.